Engineering Guide for Estimating Material Pyrolysis Properties for Fire Modeling

Mihyun Esther Kim
and
Nicholas Dembsey

WPI

Project Final Report 28 September 2012

Acknowledgement

The authors greatly appreciate the funding support from NIST Award Number 60NANB8D8106 (Federal Program Officer Dr. Kevin McGrattan). Additionally, the authors appreciate the valuable background information provided by Dr. Marc Janssens of Southwest Research Institute. Dr. Janssens' information made a significant contribution to Chapters 3 and 4, and the related appendices as well as making a useful contribution to Chapter 5 and the related Appendix.

The following persons should be recognized as they contributed to the development of this Guide by participating in pyrolysis modeling round robins and/or providing valuable comments on various drafts of the Guide.

The names are listed in alphabetical order: Nicolas Bal, Marcos Chaos, Craig Hofmeister, Simo Hostikka, Chris Lautenberger, Jamie Lord, Anna Matala, Alex Morgan, Haejun Park, Eduardo Puente, Guillermo Rein, Stanislav Stoliarov, Robert Webster, Christopher Wood, and Young-Geun You.

Table of Contents

Acknowledgement. 2

CHAPTER 1 – INTRODUCTION 8
Background 9
Purpose 11
Organization of the Guide 11
References. 12

CHAPTER 2 – DETERMINE MODEL TYPE. 13
Pyrolysis of Materials 14
Pyrolysis Models 16
Process of Choosing Pyrolysis Model. 17

CHAPTER 3 – EMPIRICAL MODELS 21
Understanding Model. 22
General Description of Models 22
Governing Equations 22
Model Parameters and Measurement Methods 23
Virtual Material 23
Model Parameter Table. 23
Model Parameter Measurement Methods 23
Uncertainty Analysis 26
Parameter Estimation Process 27
Example Cases Overview 29
Case 1: Burning Object. 30
General Model Parameter Table 30
Example 3.1 Modeling Sofa 30
Case 2: Burning Flat Surfaces 34
General Model Parameter Table 34
Example 3.2 Modeling PMMA 34
Example 3.3 Modeling Corrugated Cardboard. 36
Example 3.4 Modeling Fire Retarded FRP Composite 38
Example 3.5 Modeling Plywood 40
References. 43

CHAPTER 4 – SIMPLE ANALYTICAL MODELS. 44
Understanding Model. 45
General Description of Models 45
Governing Equations 45
Model Parameters and Measurement Methods 48
Virtual Material 48
Model-Parameter Table 49
Model-Parameter-Measurement Methods 49
Uncertainty Analysis. 58
Ignition Data Analysis 58
Burning-Rate Data Analysis 60
Parameter-Estimation Process. 61
Example Cases Overview 63
Case 1: Thermally-Thick, Inert at Pre-Ignition with Steady Burning at Post-ignition 64
Virtual Microstructure of Virgin Material. 64
General Model-Parameter Table 64
Example 4.1 Modeling Poly(methylmethacrylate), PMMA 65
Example 4.2 Modeling Corrugated Cardboard. 69
Example 4.3 Modeling Fire Retarded FRP Composite 72
Example 4.4 Modeling Plywood 75
Case 2: Thermally-Thin, Inert at Pre-Ignition with Steady Burning at Post-ignition 79
Virtual Microstructure of Virgin Material. 79
General Model-Parameter Table 79
Example 4.5 Modeling Sandwich Composite – GRP Skin with Balsawood Core 79
Example 4.6 Modeling Thin FRP Composite 83
References. 88

CHAPTER 5 – COMPREHENSIVE MODELS 89
Understanding Model. 90
General Description of Models 90
Brief Description of Typical Pyrolysis Models Available in the Fire Community 91
Governing Equations 92
Model Parameters and Measurement Methods 96
Virtual Microstructure of Virgin Material and Decomposition Kinetics Type 96
Model-Parameter Table 98
Model-Parameter Measurement Methods. 99
Parameter-Estimation Process. 113
Sensitivity Analysis 117
Example Case 1 and 2. 117
Example Case 3 (Global Sensitivity Analysis: Morris Method) 117

Uncertainty Analysis. . . . 119
Optimization 121
Example Cases Overview 124
Case 1: Single-Step Decomposition Reaction without Residue Production 125
Virtual Microstructure of Virgin Material 125
Decomposition Kinetics Type 125
General Model-Parameter Table 125
Example 5.1 Modeling Poly(methylmethacrylate), PMMA 126
Case 2: Single-Step Decomposition Reaction With Residue Production 135
Virtual Microstructure of Virgin Material 135
Decomposition Kinetics Type 135
General Model Parameter Table 135
Example 5.2 Modeling Triple-layered Corrugated Cardboard 136
Case 3: Two-Step Decomposition Reaction With Residue Production 144
Virtual Microstructure of Virgin Material 144
Decomposition Kinetics Type 144
General Model Parameter Table 144
Example 5.3 Modeling FRP Composite with Modified Acrylic Resin with High-charring Inorganic Additive 145
Example 5.4 Modeling Plywood 159
References 169

CHAPTER 6 – CONCLUSIONS 172
Conclusions 173

APPENDIX A – UNCERTAINTY ANALYSIS 174
Uncertainty Analysis 175
Type A Uncertainty 177
Type B Uncertainty 178
References 179

APPENDIX B – EXAMPLE SOLUTIONS FOR CHAPTER 3 180
Example 3.1 Modeling Sofa 181
Obtain Parameters via Experiment 181
Validation and Commentary 183
Example 3.2 Modeling PMMA 186
Obtain Parameters via Experiment 186
Validation and Commentary 188
Example 3.3 Modeling Corrugated Cardboard 189
Obtain Parameters via Experiment 189
Validation and Commentary 192

Example 3.4 Modeling Fire Retarded FRP Composite 193
Obtain Parameters via Experiment. 193
Validation and Commentary 196
Example 3.5 Modeling Plywood 197
Obtain Parameters via Experiment. 197
Validation and Commentary 199
References. 200

APPENDIX C – EXAMPLE SOLUTIONS FOR CHAPTER 4 201
Example 4.1 Modeling PMMA 202
Measure Parameters 202
Obtain Parameters via Data Analysis 204
Validation 213
Commentary 218
Example 4.2 Modeling Corrugated Cardboard. 219
Measure Parameters 219
Obtain Parameters via Data Analysis 220
Validation 229
Commentary 232
Example 4.3 Modeling Fire-Retarded FRP Composite 233
Measure Parameters 233
Obtain Parameters via Data Analysis 234
Validation 243
Commentary 247
Example 4.4 Modeling Plywood 248
Measure Parameters 248
Obtain Parameters via Data Analysis 249
Validation 259
Commentary 262
Example 4.5 Modeling GRP with Balsa Wood Core Sandwich Composite 263
Measure Parameters 263
Obtain Parameters via Data Analysis 265
Validation 274
Commentary 277
Example 4.6 Modeling Thin FRP Composite Sheet 278
Measure Parameters 278
Obtain Parameters via Data Analysis 280
Validation 289
Commentary 292
References. 293

APPENDIX D – EXAMPLE SOLUTIONS FOR CHAPTER 5 294
Example Solutions for Chapter 5 295
Example 5.1 Modeling PMMA 295
Measure Parameters 295
Obtain Parameters via Numerical Optimization 299
Validation 303
Example 5.2 - Modeling Corrugated Cardboard 310
Measure Parameters 310
Obtain Parameters via Numerical Optimization 312
Validation 318
Commentary 322
Example 5.3 Modeling Modified Acrylic FRP Composite 325
Measure Parameters 326
Obtain Parameters via Numerical Optimization 332
Validation 338
Commentary 345
Example 5.4 Modeling Plywood 348
Measure Parameters 348
Obtain Parameters via Numerical Optimization 351
Validation 355
Commentary 360
References 362

CHAPTER 5 – SUPPLEMENT – MORRIS' OAT METHOD 364
Supplement – Morris' OAT Method 365
References 367

LIST OF TABLES (Divider) 368
List of Tables 369

LIST OF FIGURES (Divider) 373
List of Figures 374

Chapter 1
Introduction

Background 9
Purpose 11
Organization of the Guide 11
References 12

Background

The use of fire models in Fire Protection Engineering (FPE) is widespread, and as a tool these models are vital to the practicing engineer especially in performance-based design. Typical classes of fire models are algebraic,[1] zone, [2] and field/CFD.[3] The input data required for these models can be generally characterized as gas phase (combustion and radiation sub-models) and solid phase (heating and pyrolysis sub-models). A significant challenge for the practicing engineer is compiling and developing input data consistent with model assumptions, as FPE is yet to develop standard input databases.

Recognizing this absence of input databases, a standard guide on creating model input data has been developed as ASTM E 1591,[4] which was developed for zone models. The standard describes the input data required by a model mathematically and presents guidelines to obtain the data. The existence of this guide has enabled users to develop input data in a consistent manner for zone models. Similarly, this new guide will enable the users to develop input data in a consistent manner for different pyrolysis models and various materials.

Among fire-model inputs, in general, gas-phase input is readily available to the practicing engineer, as a range of standard information for certain materials can be found in the combustion literature. In contrast, solid-phase input for heating and thermal decomposition of materials is rarely available. Some standard information on heating may be found in the heat transfer literature for certain materials. However, this information is significantly limited compared to the needs of practitioners. Hence, other practical methods are necessary to estimate model parameters to conduct fire modeling.

In search of a method for estimating parameters, over the past few decades numerous approaches have been developed to extract solid-phase pyrolysis parameters from bench-scale fire test data for computer model input. Examples of early research involving ignition temperature and steady burning are the work performed by Tewarson,[5] and Quintiere and Harkleroad.[6] These approaches consider only the aggregate behavior of solids (time-to-ignition and MLR) but not details of the decomposition of the solids. Parameter estimation is accomplished via slope-based plotting techniques of the bench scale data. Field/CFD models[3,7] use essentially the same thermal model as described in these references, but field/CFD models do not have any built-in parameter estimation method, like the slope based techniques. These pyrolysis models have shown good success at providing meaningful parameters for thermoplastic solids. Charring solids and other complex systems (composites: thin linings over substrates, fiber-reinforced polymers, plywood, etc.) have not shown as good success. Flame-spread models[8,9] based on this approach have been created that have demonstrated some degree of success.

Building on this work, development of pyrolysis (ignition) temperature based solid integral pyrolysis models[10,11,12,13,14] that address certain details of the decomposition of solids have been undertaken. The key detail of decomposition included in these models is propagation of a regression or charring front through the solid. Each of these models has an associated bench-scale testing

procedure to develop data needed for the associated parameter-estimation procedure using the model. The model of Theuns et al.[12,13] has been coupled to a field/ CFD model. These models have shown good success with thermoplastic-type solids and classic charring solids (wood). Complex systems have not been shown to be successful.

Recently, pyrolysis modeling focusing on details of solid decomposition, including "microstructure" and (multi-step) kinetics, have been developed with accompanying procedures to estimate parameters.[15,16,17,18,19] Parameter estimation is accomplished via optimization routines. These models have the potential to handle complex solids that need to have "micro structure" explicitly detailed as well as multi-step kinetics.

These pyrolysis models are relatively new and have not yet been extensively evaluated against a range of solids, including complex ones. Initial assessment of the models shows promise. An interesting observation of the above high quality work is that the focus has been on the important tasks of developing pyrolysis models and parameter-estimation routines as well as showing their potential with "limited" data comparison. As the work has been incorporated into the body of FPE knowledge, the assumptions and limitations of the models have not in general been clearly identified, accepted, and followed by practitioners. Accepted methods for comparing the models and estimated parameters, as well as guidance on how to use the parameters correctly in flame spread and other models, are also lacking. This points to the equally important tasks of interfacing these "theoretical" tools with proper empirical techniques to develop data strictly consistent with the assumptions and limitations of the models. Additionally the "robustness" and utility of the parameters needs to be assessed so as to allow comparison and proper use of the parameters.

In recent years, there has been a high demand for conducting Computational Fluid Dynamics (CFD) simulations in the fire community. The importance of accurate pyrolysis data for the continued use and development of CFD fire models becomes quite clear, especially given that none of the models has a pyrolysis-parameter database, and users are required to develop their own parameters. The current state of the art in procedures for development of model input data, ASTM E 1591[4], is out-of-date, as it focuses only on zone models and does not address solid-phase pyrolysis. This situation sets the stage for development of a standard guide for estimation of pyrolysis parameters for various types of fire pyrolysis models based on the current knowledge about solid pyrolysis models and parameters, and proper empirical techniques to develop "robust" pyrolysis parameters for fire models.

Purpose

With this *Guide*, standardized procedures for obtaining material parameters for input into fire-pyrolysis models are presented, such as empirical, simple analytical, and comprehensive pyrolysis models.

Organization of the Guide

The following section (Chapter 2) offers guidance to show what pyrolysis models are available for modelers and what may be appropriate for their modeling needs. To provide standardized procedures for obtaining material-pyrolysis parameters for input into fire models, pyrolysis models are grouped into three categories based on their modeling characteristics, understanding that most of the model-input unknowns are related to the solid phase during thermal decomposition. The three categories are Empirical Models (Chapter 3), Simple Analytical Models (Chapter 4), and Comprehensive Models (Chapter 5). For each model category the following information is provided:

- A brief description of its modeling approach and assumptions applied to simplify the problem.
- A typical mathematical formulation with identification of model parameters in the equations.
- Methods of estimating the unknown parameters either by independent measurements or numerical optimization in pair with the model.

Using this information, example cases are introduced for better understanding of the parameter-estimation procedure described for each model category. Additionally, the Appendix provides thorough explanation of example solutions from different chapters.

References

1 Walton, W.D.; and Thomas, P.H., "Estimating Temperatures in Compartment Fires," In SFPE Handbook of Fire Protection Engineering, 3rd ed., NFPA, Quincy, MA, USA (2002) Chapter 3-6.

2 Walton, W.D., "Zone Computer Fire Models for Enclosures," In *SFPE Handbook of Fire Protection Engineering*, 3rd ed., NFPA, Quincy, MA, USA (2002) Chapter 3-7.

3 Cox, G.; and Kumar, S., "Modeling Enclosure Fires Using CFD," In *SFPE Handbook of Fire Protection Engineering*, 3rd ed., NFPA, Quincy, MA, USA (2002) Chapter 3-8.

4 Standard Guide for Obtaining Data for Deterministic Fire Models, ASTM E 1591, ASTM International, West Conshohocken, PA, USA (2000).

5 Tewarson A.,"Generation of Heat and Chemical Compounds in Fires," In *SFPE Handbook of Fire Protection Engineering*, 3rd ed., NFPA, Quincy, MA, USA (2002) Chapter 3-4.

6 Quintiere, J.G.; and Harkleroad, M., "New Concepts for Measuring Flame Spread Properties." in Fire Safety Science and Engineering, ASTM STP 882, ASTM International, West Conshohocken, PA, USA (1985) 239-267.

7 McGrattan, Kevin; Hostikka, Simo; Floyd, Jason; Baum, Howard; Rehm, Ronald; Mell, William and McDermott, Randall, Fire Dynamics Simulator (Version 5) Technical Reference Guide, NIST Special Publication 1018-5, October 29, 2010.

8 Quintiere, J.G., "A Simulation Model for Fire Growth on Materials Subject to a Room-Corner Test," Fire Safety Journal, 20 (1993) 313-339.

9 Lattimer B.Y.; Hunt, S.P.; Wright, M.; and Sorathia, U., "Modeling Fire Growth in a Combustible Corner," *Fire Safety Journal*, 38 (2003) 771-796.

10 Hopkins, D.; and Quintiere, J.G., "Material Fire Properties and Predictions for Thermoplastics," Fire Safety Journal, 26 (1996) 241-268.

11 Chen, Y.; Delichatsios, M.A.; and Motevalli, V., "Material Pyrolysis Properties, Part I: An Integral Model for One-Dimensional Transient Pyrolysis of Charring and Non-Charring Materials," Combustion Science and Technology, 88 (1993) 309-328.

12 Theuns, E.; Merci, B.; Vierendeels, J.; and Vandevelde, P., "Extension and Evaluation of the Integral Model for Transient Pyrolysis of Charring Materials," Fire and Materials, 29 (2005) 195-212.

13 Theuns, E.; Merci, B.; Vierendeels, J.; and Vandevelde, P., "Critical Evaluation of an Integral Model for the Pyrolysis of Charring Materials," Fire Safety Journal, 40 (2005) 121-140.

14 Delichatsios, M.; Paroz, B.; and Bhargava, A., "Flammability Properties for Charring Materials," Fire Safety Journal, 38:3 (2003) 219-228.

15 Lautenberger, C.W.; Rein, G.; and Fernandez-Pello, A.C., "The Application of a Genetic Algorithm to Estimate Material Properties for Fire Modeling from Bench-Scale Fire Test Data," Fire Safety Journal, 41 (2006) 204-214.

16 Rein, G.; Lautenberger, C.; Fernandez-Pello, A.C.; Torero, J.L.; and Urban, D.L., "Application of Genetic Algorithms and Thermogravimetry to Determine the Kinetics of Polyurethane Foam in Smoldering Combustion," Combustion and Flame, 146 (2006) 95-108.

17 Ferriol, M.; Gentilhomme, A.; Cochez, M.; Oget, N.; and Mieloszynski, "Thermal Degradation of Poly(methylmethacrylate) (PMMA): Modelling of DTG and TG curves," Polymer Degradation and Stability, 79 (2003) 271-181.

18 Lautenberger, C.W.; and Fernandez-Pello, A.C., "A Generalized Pyrolysis Model for Simulating Charring, Intumescent, Smoldering, and Noncharring Gasification," Combustion Processes Laboratories, Fire Science, UC Berkeley, eScholarship Repository (2006), http://repsoitories.cdlib.org/cpl/fs/LautenbergerGenPyro.

19 Lefebvre, J., et al., "Thermal Stability and Fire Properties of Conventional Flexible Polyurethane Foam Formulations," Polymer Degradation and Stability, 88:1 (2005) 28-34.

Chapter 2
Determine Model Type

Pyrolysis of Materials 14
Pyrolysis Models 16
Process of Choosing Pyrolysis Model. 17

In this chapter, guidance is given to the modeler to help her/him to select certain types of pyrolysis models by considering processes involved in pyrolysis, characteristics of typical materials, and the models available today that incorporate various assumptions. For more information about each model type in terms of mathematical expressions and application, see the following chapters: Chapter 3 – Empirical Models, Chapter 4 – Simple Analytical Models, and Chapter 5 – Comprehensive Models.

Pyrolysis of Materials

Pyrolysis refers to the thermal decomposition of porous or non-porous solid-phase materials caused by heating during exposure to fire conditions. Pyrolysis is a complicated phenomenon, which is a combination of the following interactive processes: heat transfer through materials from fire exposure; thermal decomposition that produces combustible or non-combustible pyrolyzates in gas, liquid or solid form; and mass transfer of oxygen from ambient and those pyrolyzates.

Materials subject to pyrolysis can be first categorized into one of two groups depending on the geometry of interest: an object or a flat surface (see Figure 2-1). The object covers situations where the material's geometry is non-flat or complex in its fire behavior. Whether materials are considered an object or a flat surface, their physical structure may or may not remain stable during pyrolysis. When changes in structural stability do occur, those are typically due to melting, flowing and/or dripping, expanding, popping due to steam expansion, collapsing, etc. When materials maintain their structural stability throughout pyrolysis, further categorization can be applied depending on the location of thermal decomposition sites – Is thermal decomposition occurring near the surface or surface and at in-depth?

Examples of each material group are as follow: (1) Objects: furniture, boxed products, products in pressurized containers, electronics, and more; (2) Flat surfaces that experience structural instability during pyrolysis: flowing and/or dripping thermoplastics due to low melting and glass transition points, intumescent materials, plastic foams that liquefy, phenolic resin that pops, etc; (3) Flat surfaces that maintain their structural stability during pyrolysis and have decomposition occurring mostly on surface: non-flowing thermoplastics, etc; and (4) Flat surfaces that maintain their structural stability during pyrolysis and have decomposition occurring near surface and at in-depth: wood, highly cross-linked thermosets, plastics with charring additives, etc.

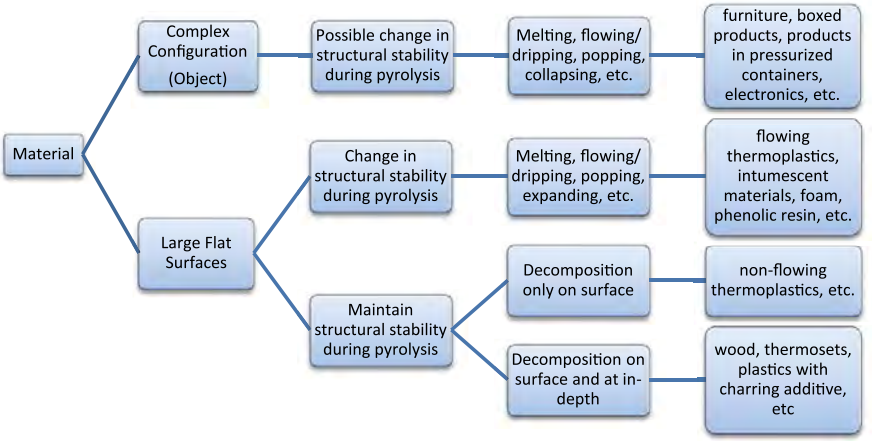

Figure 2-1. Material category: Depending on material's characteristics, material can be grouped into 4 categories and examples for each category is given.

Pyrolysis Models

As aforementioned, pyrolysis is a complicated phenomenon and is a combination of heat transfer, thermal decomposition, and mass transfer. When pyrolysis is modeled, various approaches can be taken by approximating the three processes of pyrolysis. Note that the goal of conducting pyrolysis modeling in fire engineering is to simulate the mass-loss rate per unit area as a result of decomposition of a solid-phase material under fire conditions. This information can be then used as input parameters for pyrolysis sub-models in a zone or CFD model.

The simplest approach of modeling pyrolysis is utilizing empirical data from calorimetry experiments: Empirical Models. Heat transfer, thermal decomposition, and mass-transfer effects are confounded assuming that the difference between testing and modeling conditions are negligible at all times. Another simple approach but more sophisticated than Empirical Models is using analytical solutions to describe pyrolysis: Simple Analytical Models. This approach analytically solves for heat transfer of pyrolyzing materials at the pre-ignition stage by assuming materials as inert and semi-infinite or lumped. Thermal decomposition is modeled by having an ignition criterion, ignition temperature (T_{ig}) at surface. At the post-ignition stage, steady-state burning is assumed. Any mass-transfer effects on pyrolysis are neglected.

The most complex approach available for fire problems is directly solving for the three processes using conservation equations: Comprehensive Models. In this approach, heat transfer is modeled using conservation of energy, which allows the most flexibility in specifying boundary conditions for front and back surfaces, i.e., in specifying heating and cooling at material boundaries. Thermal decomposition is modeled by using conservation of mass and either a pyrolysis criterion, pyrolysis temperature (T_p), or defining a finite reaction rate through kinetic modeling. This approach may also account for mass-transfer effects; however, in this *Guide*, Comprehensive Models will be considered without modeling mass-transfer effects on pyrolysis due to the lack of current understanding of these effects.

Empirical Models can be used for any kind of materials from any of the four material groups discussed previously. Simple Analytical Models can be used only for flat surfaces that maintain their structural stability during pyrolysis. Additionally, strictly, due to model assumptions these models should be applied to thermally-thick or thermally-thin behaving flat surface materials that have decomposition occurring mostly at the surface and resulting in steady-state burning after ignition. Despite this limitation, some modeling work has been conducted on charring materials such as wood by conducting analysis with data that has a short pre-ignition period followed by a quasi-steady burning. These behaviors allow the assumptions of thermally-thick or thermally-thin behavior and inert at the pre-ignition stage followed by steady-state burning at post-ignition stage to be applied. Comprehensive Models can be used to model all materials that are flat surfaces that maintain their structural stability during pyrolysis. However, caution should be used for modeling materials that have mass transfer of pyrolyzates and gas-phase reactants that significantly affect pyrolysis given the lack of knowledge in this area.

Process of Choosing Pyrolysis Model

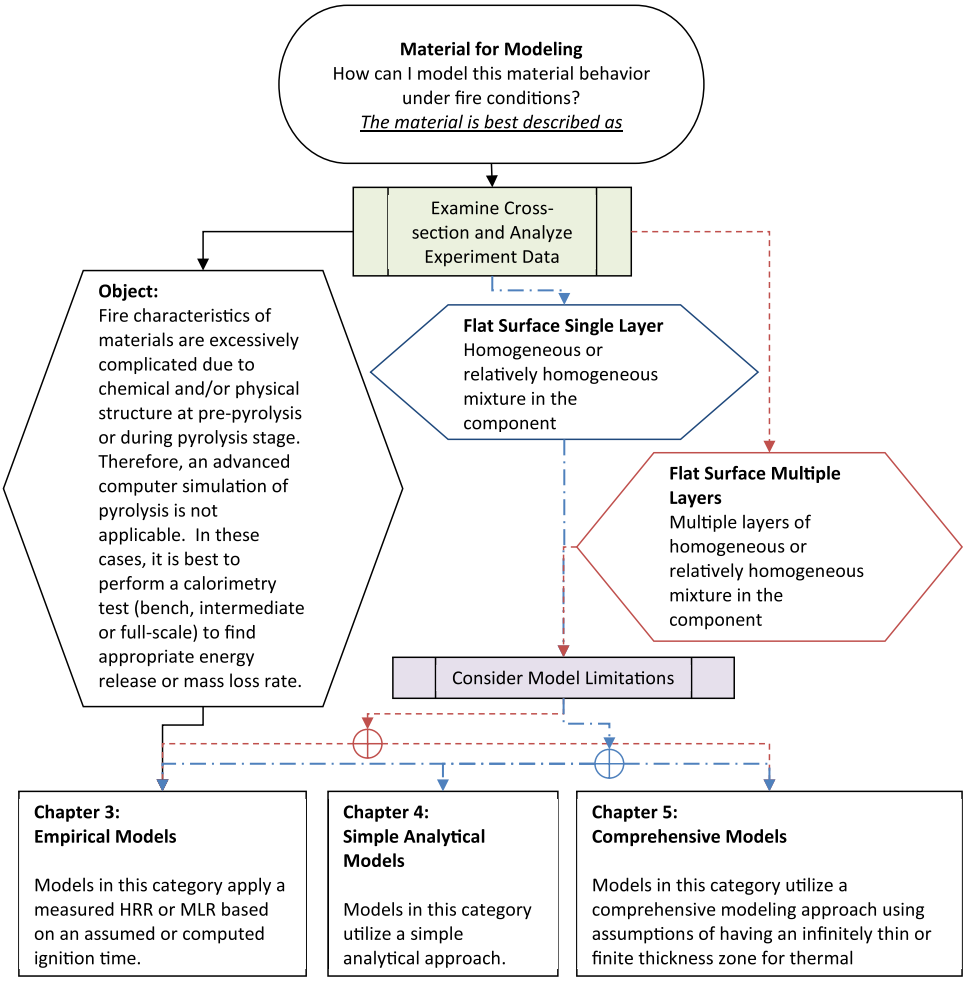

Figure 2-2. Model selection flowchart: By examining the cross-section of material and analyzing experiment data that presents its fire behavior, modeler may determine the material's virtual microstructure and appropriate pyrolysis models available for its specific use.

A flow chart is shown above (see Figure 2-2) to describe the process of model selection. As shown in this chart, a material's virtual microstructure is decided through "Examine Cross-section and Analyze Experiment Data." The virtual microstructure can be **Object, Flat Surface Single Layer**, or **Flat Surface Multiple Layers**.

Object is for materials without homogeneous or relatively homogeneous mixture layers based on this guide at the pre-pyrolysis stage or during pyrolysis stage, i.e., material geometry that cannot be considered one-dimensional knowing that typically pyrolysis models assume a one-dimensional geometry.

Flat Surface Multiple Layers is for materials that satisfy the following three conditions:

(1) Distinctive homogeneous or relatively homogeneous mixture layers based on visual inspection

(2) Experiment data, such as Heat Release Rate or Mass Loss Rate, from a bench-scale test that identify any effects of having multiple layers on material's thermally decomposing or burning characteristics

(3) That those effects found from analyzing data with consideration of the assumed microstructure are important for modeling purposes, and therefore multiple layers microstructure is necessary, although it adds more complexity to modeling

Flat Surface Single Layer is for materials either with one homogeneous or relatively homogeneous mixture layer, or with multiple homogeneous or relatively homogeneous mixture layers but does not satisfy all three conditions listed above for Flat Surface Multiple Layers.

The modeler now can select the model of his/her interest from the three model categories – **Empirical Models, Simple Analytical Models,** and **Comprehensive Models** – depending on its assumed microstructure (Object, Flat Surface Single Layer, or Flat Surface Multiple Layers) and each model's limitations ("Consider Model Limitations"). Note that the complexity of the model increases as model category changes from Empirical Models to Comprehensive Models. This means that the number of parameters that need to be estimated increases as well.

Empirical Models can be used for modeling materials with any microstructure discussed previously – Object, Flat Surface Single Layer, or Multiple Layers. The advantage of utilizing this approach is that it is simple, i.e., unknown model parameters are minimal and easy to obtain through various scale calorimetry experiments. Typically, these models are for materials that have excessively complicated fire behaviors due to either material geometry/structural stability at pre-pyrolysis stage (e.g., sofa, chair, bookshelf, etc.) or burning behavior during pyrolysis stage (e.g., melting, dripping, non-uniform expanding, etc.). The disadvantage of using models in this category is that, because empirical data such as the heat-release rate or mass-loss rate from a certain test is directly applied to modeling, effects of variation in fire conditions (e.g., ignition scenario, environment, etc.) of the fire scenario from a standard test condition is not considered. See Chapter 3 – Empirical Models for more description. There are five different materials considered as example cases in this chapter (see Table 2-1).

Table 2-1. Example materials in Chapter 3 – Empirical Models: materials are either considered as a burning object or flat surface in modeling

	Burning Object	Burning Flat Surfaces			
Example Materials	Sofa	PMMA	Corrugated Cardboard	Fire-Retarded FRP Composite	Plywood

Simple Analytical Models are for materials that have Flat Surface Single Layer geometry only. The advantage of considering models in this category is that, due to the simplicity of model, only a few unknown model parameters exist, and they are easily estimated typically using bench-scale test results. The disadvantage of using models in this category is that pyrolysis conditions under fire environment need to be applicable to many assumptions used in developing the model – material is considered to be homogeneous, thermally-thick or thermally-thin behavior, and results in steady burning after ignition. See more details on model assumptions and description in Chapter 4 – Simple Analytical Models. There are six different materials considered as example cases in this chapter (see Table 2-2).

Table 2-2. Example materials in Chapter 4 – Simple Analytical Models: materials are considered either thermally-thick and inert at pre-ignition with steady burning at post-ignition, or thermally-thin and inert at pre-ignition with steady burning at post-ignition in modeling

	Thermally-thick and Inert at Pre-ignition, Steady Burning at Post-ignition				Thermally-thin and Inert at Pre-ignition, Steady Burning at Post-ignition	
Example Materials	PMMA	Corrugated Cardboard	Fire Retarded FRP Composite	Plywood	Vinyl Ester GRP and Balsa Wood Core Sandwich Panel	Class C FRP Composite Sheet

Comprehensive Models are for materials that have either Flat Surface Single Layer or Multiple Layers geometry. The advantage of utilizing these models is that the modeler has much flexibility in setting up the pyrolysis problem mathematically. Generally, these models explicitly solve for heating of material during pyrolysis and account for weight loss due to thermal decomposition by conserving mass and energy. Some models even track mass transfer effects such as interactions between pyrolysis products, diffusion of oxygen from surface, etc. The disadvantage of using these models is that significant effort may be needed to estimate unknown model parameters, knowing that the number of unknowns can dramatically increase with respect to increasing modeling complexity. It can range from less than 10 unknowns up to 100 or even more. See Chapter 5 – Comprehensive Models for more description. There are four different materials considered as example cases in this chapter (see Table 2-3).

Table 2-3. Example materials in Chapter 5 – Comprehensive Analytical Models: materials are considered to decompose with single or multiple reaction(s) with or without residue production in modeling

	single-step decomposition RxN w/o residue	single-step decomposition RxN w/ residue	two-step decomposition RxN w/ residue	drying and sinlge-step decomposition RxN w/ residue
Example Materials	PMMA	Corrugated Cardboard	Fire Retarded FRP Composite	Plywood

Chapter 3
Empirical Models

Understanding Model 22
General Description of Models 22
Governing Equations 22
Model Parameters and Measurement Methods 23
Virtual Material 23
Model Parameter Table 23
Model Parameter Measurement Methods 23
Uncertainty Analysis 26
Parameter Estimation Process 27
Example Cases Overview 29
Case 1: Burning Object 30
General Model Parameter Table 30
Example 3.1 Modeling Sofa 30
Case 2: Burning Flat Surfaces 34
General Model Parameter Table 34
Example 3.2 Modeling PMMA 34
Example 3.3 Modeling Corrugated Cardboard 36
Example 3.4 Modeling Fire Retarded FRP Composite 38
Example 3.5 Modeling Plywood 40
References 43

Understanding Model

General Description of Models

This chapter focuses on empirical methods to estimate the pyrolysis rate of **Objects** (complex geometry) and **Flat Surfaces** materials in a fire scenario, typically in a compartment-fire situation. These methods are referred to as "Empirical Models." This is the easiest approach to estimate the burning rate of an object or flat surfaces, where heat release and mass loss rate data measured in a test is directly applied to describe a material's pyrolysis behavior. Data for burning of an object can be obtained through full-scale test with various ignition sources and locations, e.g., furniture calorimeter test. For flat surfaces, data can be obtained through intermediate/bench-scale calorimeter test at a specified heat flux.

The principle assumption is that the ignition scenario and exposure conditions in the fire are comparable to those used in the laboratory. In addition, Empirical Models for flat surfaces assume that (1) heat and mass transfer is one-dimensional, i.e., perpendicular to the exposed surface; (2) edge effects in material testing are not included; and (3) applied heat-flux level during testing is representative average (over space and time) for the fire scenario that is being modeled.[1]

Governing Equations

Mathematically the model for estimating the onset (ignition) and subsequent rate of pyrolysis can be described as follows:

$$(t_{ig})_{mod} = (t_{ig}) \qquad \text{Eq.3-1}$$

and

$$(\dot{Q}'')_{mod} = (\dot{Q}'')_{exp} = \Delta h_{c,eff}\ (m'')_{exp} \qquad \text{Eq.3-2}$$

where

$(t_{ig})_{mod}$ = ignition time used in the pyrolysis model (s)
$(t_{ig})_{exp}$ = ignition time measured in the calorimeter (s)
$(\dot{Q}'')_{mod}$ = heat release rate used in the compartment fire model (kW/m^2)
$(\dot{Q}'')_{exp}$ = heat release rate measured in the calorimeter (kW/m^2)
$(\dot{m}'')_{exp}$ = mass loss rate measured in the calorimeter (g/ m^2·s)
$\Delta h_{c,eff}$ = effective heat of combustion of the fuel (kJ/g)

Note that heat-release and mass-loss rates measured in a small- and intermediate-scale calorimeter are usually expressed as rate per unit exposed area (hence the double prime). However, for data obtained in a full-scale calorimeter experiment are typically expressed as rate.

Model Parameters and Measurement Methods

Virtual Material

The virtual material is an energy source releasing heat to the gas phase expressed in terms of heat-release rate or mass-loss rate and effective heat of combustion without certain geometry, whether the material is an object or a flat surface.

Model Parameter Table

The following table (see Table 3-1) summarizes model parameters that need to be estimated:

Table 3-1. Model parameter table: summary of model parameters required to conduct pyrolysis modeling

<table>
<tr><td>Ignition Parameters</td><td colspan="2">t_{ig}</td><td colspan="2">Time-to-Ignition</td></tr>
<tr><td rowspan="3">Burning-Rate Parameters</td><td colspan="2">Using HRR</td><td colspan="2">Using MLR and HoC</td></tr>
<tr><td rowspan="2">$\dot{Q}''(t)$</td><td rowspan="2">Heat-Release Rate</td><td>$\dot{m}''(t)$</td><td>Mass-Loss Rate</td></tr>
<tr><td>$\Delta h_{c,eff}$</td><td>Effective Heat-of-Combustion</td></tr>
</table>

Model Parameter Measurement Methods

1. Time to Ignition

For burning of an object with a complex geometry, full-scale tests such as Furniture (maximum capacity of 1 MW) or Larger (maximum capacity of 40 MW) Calorimeters are conducted. Various ignition sources are used in these tests and they are placed at certain locations for some specified time at the start of each test. Typically, due to this testing procedure, ignition time is at the start of the test. A number of ASTM standards have been tabulated below for full-scale calorimeter tests (see Table 3-2):

Table 3-2. Ignition sources specified in standard fire tests

Test Method	Specimen	Gas Burner Ignition Source			Location of Application
		No.	Type	Heat Output	
ASTM E 603	Various	1	Square	Various	Various
ASTM E 1537 CAL TB 133	Single chair	1	Square	19 kW for 80 s	Horizontal seating surface
ASTM E 1822	Stacked chairs	1	Line	18 kW for 80 s	Bottom chair front edge
ASTM E 1590	Mattress (set)	1	Line	18 kW for 180 s	Front bottom edge
CAL TB 603 16 CFR 1633	Mattress (set)	2	Line Line	19 kW for 70 s 10 kW for 50 s	Top surface Vertical along side
NFPA 286	Wall / Ceiling Lining	1	Square	40 kW for 300 s 160 kw for 600 s	Room corner

For burning of a flat surface material, an intermediate/bench-scale calorimeter test(s) is conducted at a specified heat flux. In these tests, an apparatus that consists of a radiant panel that exposes the specimen to a preset irradiance is used to measure the ignition time. The heat source can be a gas panel or consist of one or several electrical heating elements. A small flame, electric spark or hot wire is usually present in the gas phase above the specimen surface (horizontal specimen orientation) or at the top edge of the specimen (vertical or inclined surface). Time of ignition is typically determined on the basis of visual observations. This can be tricky when the material exhibits extensive flashing before sustained flaming. An alternative method based on the second time derivative of the mass of the specimen has been suggested to alleviate this problem.[2] Ignition criteria based on a critical mass loss rate of 1 $g/m^2 \cdot s$ or a critical heat-release rate of 24 kW/m^2 have also been proposed.[3] A number of ASTM standards have been tabulated below (see Table 3-3) for measuring the time to ignition of a material exposed to a specified level of incident radiant heat and intermediate/bench-scale calorimeter tests:

Table 3-3. ASTM standards for measurement of time-to-ignition of materials exposed to specified level of incident radiant heat source in intermediate/bench-scale calorimeter tests

Standard Test	Description
ASTM E 1321 – 09	*Standard Test Method for Determining Material Ignition and Flame Spread Properties*
ASTM E 1354 – 11b	*Standard Test Method for Heat and Visible Smoke Release Rates for Materials and Products Using an Oxygen Consumption Calorimeter*
ASTM E 2058 – 09	*Standard Test Methods for Measurement of Synthetic Polymer Material Flammability Using a Fire Propagation Apparatus (FPA)*

2. Heat-Release Rate or Mass-Loss Rate and Effective Heat of Combustion

HEAT RELEASE RATE

Heat-release rate is measured via calorimetry test in various scales. Two major methods used since the early 1980s are oxygen-consumption and carbon-oxides generation techniques. Oxygen-consumption method is based on test results of organic fuels showing a nearly constant net amount of heat, E, is released per unit mass of oxygen consumed for complete combustion.[4,5] Carbon-oxides generation method is based on the fact that the amount of heat released per mass unit of carbon dioxide and carbon monoxide generated is also relatively constant within a category of fuels or polymers. This method is particularly useful for oxidizers.[6] See section for measurement of Time to Ignition for a list of ASTM standards for calorimetry tests.

MASS-LOSS RATE

The energy release by material pyrolysis can also be expressed in terms of mass-loss rate and effective heat of combustion. Mass-loss rate is found from direct measurement of mass loss, as calorimeters are often equipped with a scale. The mass-loss rate of the specimen in a test is then determined by continuously weighing the specimen during the test and by subsequently calculating the time derivative of the mass vs. time curve.

EFFECTIVE HEAT OF COMBUSTION

The effective heat of combustion, $\Delta h_{c,eff}$, is equal to the net heat-release rate divided by the mass-loss rate measured in a calorimeter (see Eq.3-3):

$$\Delta h_{c,eff} \equiv \frac{\dot{Q}}{\dot{m}} = \frac{\dot{Q}''}{\dot{m}''} \qquad \text{Eq.3-3}$$

The effective heat of combustion at a particular time *t* can be calculated by substituting the values for $\dot{Q}$ (or $\dot{Q}''$) and $\dot{m}$ (or $\dot{m}''$) at that time as in above equation. The average effective heat of combustion over a specified time period is equal to the cumulative heat released over the specified period divided by the mass loss over the specified period. Theoretically it is possible to calculate $\Delta h^{c,eff}$ at every data scan. In practice, however, there are several challenges.

1. The heat-release rate and mass-loss rate measurements are not completely synchronized. This may result in significant errors, in particular at times when there is a rapid change in the burning rate.
2. Measurement errors are amplified during periods of slow burning, as both numerator and denominator in Eq.3-3 are small.
3. Even if a general math filter is used, calculated mass-loss rates can still be very noisy, resulting in fluctuations in the calculated effective heat of combustion values.

For this reason it usually better to report the average effective heat of combustion over a specified period of time, i.e., the cumulative heat released over the specified period divided by the mass loss over the specified period. It is very common to report the average effective heat of combustion over the entire test (see Eq.3-4):

$$\left(\Delta h_{c,eff}\right)_{avg} = \frac{Q_{tot}}{m_0 - m_f} \qquad \text{Eq.3-4}$$

where

$\left(\Delta h_{c,eff}\right)_{avg}$ = average effective heat of combustion over the entire test (kJ/g);
Q_{tot} = total heat released over the entire test duration (kJ);
m_0 = specimen mass at the start of the test (g); and
m_f = specimen mass at the end of the test (g).

Dillon et al. found the average effective heat of combustion over the peak burning period to be useful for predicting fire growth of wall linings (flat surfaces) in a room/corner test on the basis of Cone Calorimeter data.[7] The peak burning period was defined in this study as the time during which the heat release rate in the Cone Calorimeter is equal to or higher than 80% of the (first) peak heat release rate.

Uncertainty Analysis

An engineering fire safety analysis involving compartment fire modeling must take into account the uncertainty of the input data in order to determine the uncertainty of the results of the analysis. This process is referred to as "propagation of uncertainty." Some input data, such as the dimensions of the compartment, are relatively well known and their uncertainty can be neglected. Other input parameters, such as the heat release rate of an object, are significantly more variable and the uncertainty of these parameters must be accounted for. A distinction is made between two types of uncertainly: Type A and Type B. The former is uncertainty due to random variation, while the latter is due to lack of (complete) knowledge. A brief and general discussion of the two types of uncertainty can be found in Appendix A.

Considering that the model input parameters are time-to-ignition and heat-release rate directly found from certain tests, uncertainty in measurements from calorimetry tests in the literature are searched for. For a large-scale apparatus, a 3 MW quantitative HRR facility at NIST has been assessed to calculate the HRR uncertainty.[8] This work has taken into account the basic measurement inputs, which are the instrument voltages, thermocouple temperatures, and constant parameters used in calculations, and has showed that the relative uncertainties were ±7.5, ±5.3, and ±5.3% for HRR at 0.05, 0.65, and 2.7MW, respectively. There are studies that have addressed the uncertainty associated with the HRR calculation for bench-scale apparatuses – Cone Calorimeter and Fire Propagation Apparatus (FPA).[9,10] Enright and Fleischmann[9] have reported that the relative HRR uncertainty is about ±5.5% for the HRR in the range of 200–500kW/m^2. Zhao and Dembsey[10] have estimated the relative HRR uncertainties are 20 to 30%, 10% and 10% for 1 kW, 3 kW and 5 kW methane fires, respectively.

Parameter Estimation Process

To create a virtual material, these tasks must be considered:

- Create a list of model inputs, which needs to be determined
- Obtain model unknown inputs via measurement or literature search

When the above is done and every unknown has been estimated, validation work and commentary is needed to understand the performance of the estimated parameter set:

- Run model
- Analyze simulation quality with consideration of uncertainties in modeling outputs and data
- Add commentary

When presenting the parameter estimation results, three summary tables will be introduced: Model Parameter Table, Validation, and Commentary sections. Model Parameter Table includes the model parameters necessary to conduct pyrolysis modeling, their estimated values, and methods of estimating the unknowns. Validation work consists of the following information: description of modeling goal, pyrolysis model type and modeling approach used in the exercise, experiment type and its data used to empirically simulate material's heat release rate and uncertainty information of experimental data, and modeling outputs. Commentary section discusses any limitations of pyrolysis modeling conducted above, which has been summarized in Model Parameter and Validation Tables.

For better visualization of the problem, a flowchart is shown below (see Figure 3-1):

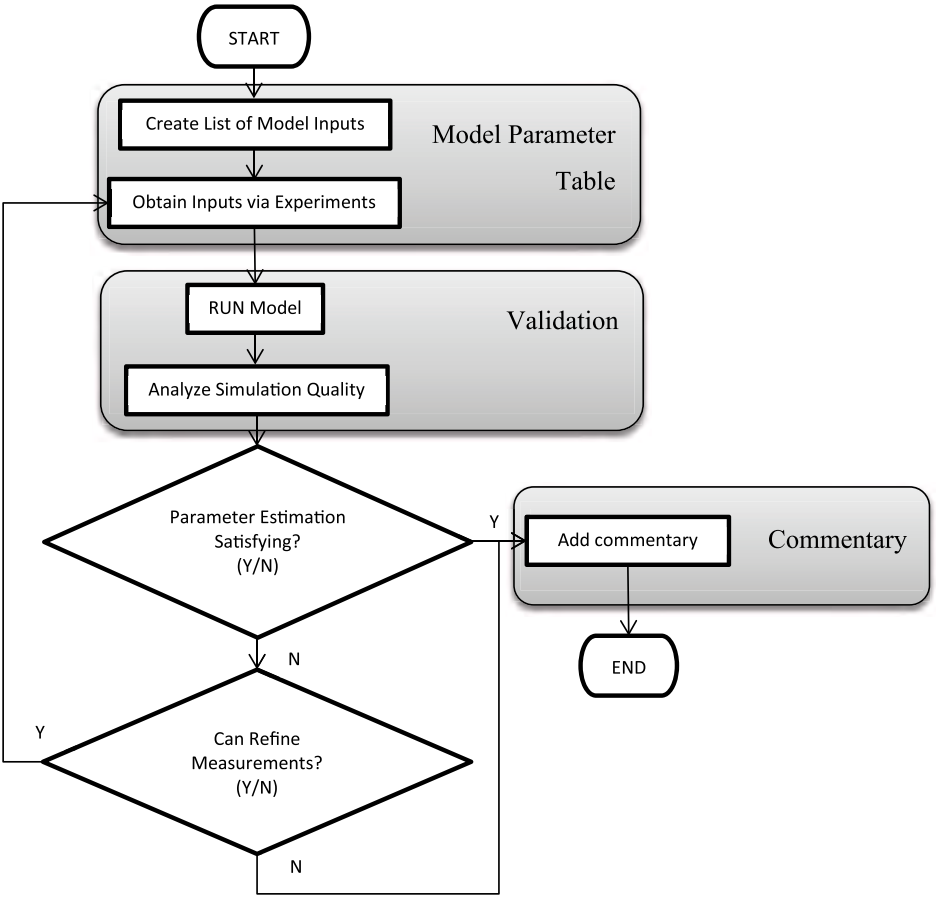

Figure 3-1. Flow chart of parameter estimation for empirical pyrolysis models

Example Cases Overview

Table 3-4. Overview of example cases using empirical pyrolysis models

Case	Description	Examples
1	Burning Objects	Sofa
2	Burning Flat Surfaces	PMMA
		Corrugated Cardboard
		Fire-Retarded FRP Composite
		Plywood

In the following, summarized results are shown for each example case. Detailed solutions of these example cases are given in Appendix B.

Case 1: Burning Object

General Model Parameter Table

Table 3-5. Model-parameter table for Case 1 examples

<table>
<tr><td>Ignition Parameters</td><td colspan="2">t_{ig}</td><td colspan="2">Time-to-Ignition</td></tr>
<tr><td rowspan="3">Burning-Rate Parameters</td><td colspan="2">Using HRR</td><td colspan="2">Using MLR and HoC</td></tr>
<tr><td rowspan="2">$\dot{Q}''(t)$</td><td rowspan="2">Heat-Release Rate</td><td>$\dot{m}''(t)$</td><td>Mass-Loss Rate</td></tr>
<tr><td>$\Delta h_{c,eff}$</td><td>Effective Heat-of-Combustion</td></tr>
</table>

Example 3.1 Modeling Sofa

3.1.1 Model Parameter Table

<table>
<tr><th colspan="2">Model Parameters</th><th>Unit</th><th>Estimated Values and Estimation Methods</th></tr>
<tr><td rowspan="2">Ignition Parameters</td><td rowspan="2">t_{ig}</td><td rowspan="2">s</td><td>80</td></tr>
<tr><td>Measurement,
Furniture Calorimeter</td></tr>
<tr><td rowspan="2">Burning-Rate Parameters</td><td rowspan="2">HRR</td><td rowspan="2">kW</td><td> 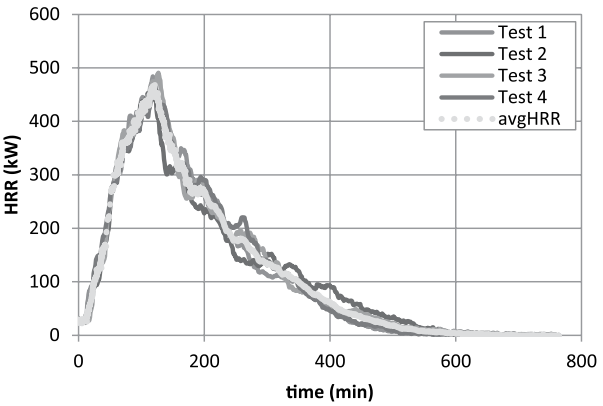
</td></tr>
<tr><td>Measurement,
Furniture Calorimeter</td></tr>
</table>

3.1.2 Validation

3.1.2.1 MODELING GOAL

Estimate model parameters for conducting modeling of pyrolysis of an object under well-ventilated condition.

3.1.2.2 MODEL TYPE

Empirical Pyrolysis Model

3.1.2.3 MODELING APPROACH

- Pre-ignition stage is:
  - Inert: decomposition before ignition is neglected
  - Always the same as in Furniture Calorimeter test
- Ignition scenario is the same as in Furniture Calorimeter experiment: time to ignition is the same in modeling as determined in experiment
- Post-ignition stage is:
  - Considered to have instantaneous release of volatiles from solid to gas phase: typically, an area is specified that can be correlated to the actual burning object where energy is released to the gas phase
  - Considered to be the same as in Furniture Calorimeter test in terms of heat-release rate or mass-loss rate

3.1.2.4 EXPERIMENT DESCRIPTION

Furniture Calorimeter test

3.1.2.5 DATA SET

Experiment data of a single-seat sofa mockup is found for pyrolysis modeling using Empirical Model. This sofa mockup was burned under a hood of a furniture calorimeter. The mockup consisted of a steel frame with untreated polyurethane foam cushions (80% of the combustible mass) and a cotton fabric (20% of the combustible mass). Total combustible mass was 3.93 kg. The test was performed according to *ASTM E 1537* and CAL TB 133. The ignition source consisted of a 0.25 m square tubular propane burner producing a 19 kW flame for 80 seconds applied to the top of the seat cushion.

3.1.2.6 UNCERTAINTY

Uncertainty in Experiment Data

- Data reproducibility is checked by repeating four identical sofa mockup tests
- Uncertainty of HRR is estimated by first calculating the confidence interval for 95% confidence level ($\alpha = 0.05$) assuming student t distribution with a sample size of 3 (four data sets) at each time step. Then an average confidence interval is calculated for the time interval of interest ($0 < t < 800$ min), which results in **± 20.4 kW.**
- Assume:
  - Uncertainties are comparable to those of similar objects pyrolyzing in a compartment fire

Uncertainty in Modeling Outputs

- Same as in experiment data

3.1.3 Commentary

When using the Empirical Model to simulate pyrolysis of a sofa, furniture calorimeter test data has been utilized to estimate the time to ignition from exposure to a propane burner and the energy released from burning. As noted in the Understanding Model part of the chapter, this approach is limited as follows in terms of the conditions being comparable to those found in the fire scenario of interest:

- Ignition scenario and exposure conditions

The basic assumption used in Empirical Models is that the ignition scenario and exposure conditions in the fire are comparable to those used in the laboratory. Therefore, any changes made in the ignition scenario and exposure conditions have to be accounted for by the model user when applying the data to Empirical Models. The furniture calorimeter experiment in this example is conducted under certain conditions: ignition is achieved by applying propane flame on the horizontal surface (seating cushion) for 80 s and sufficient supply of air is provided throughout its burning phase. To illustrate the effect of altering the conditions in HRR curves, two other HRR curves are shown below:

Effect of ignition source strength (see Figure 3-2): Two identical single-seat sofas were obtained for testing. In the first test the sofa was ignited with a 45 W butane gas flame applied to the center of the seat cushion for 20 s. In the second test 59 ml (2 oz) of gasoline was poured on the seat cushion to simulate an incendiary fire. The resulting heat-release rate measurements are shown below. In this case the use of the weaker ignition source delays the propagation to full involvement by approximately 170 s. For this case the effect of ignition source strength can relatively easily be accounted for, although in practice it may not be trivial to determine the exact time period over which to shift the HRR curve. The effect can be much more pronounced when the source strength is close to the level needed to obtain sustained burning.

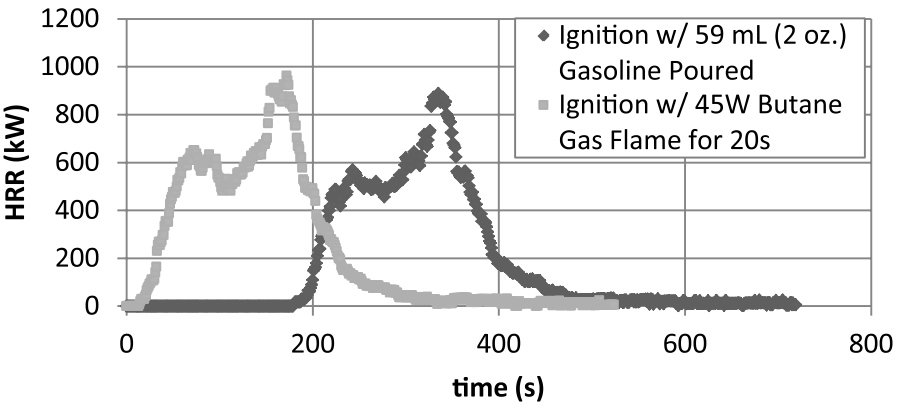

Figure 3-2. Effect of ignition source strength: single-seat sofas tested in furniture calorimeter test with different ignition sources – ignition with 59 mL gasoline poured (◆) or with 45 W butane gas flame (■)

Effect of ignition location (see Figure 3-3): Two tests were conducted on a steel-framed-seat sofa mockup according to the same procedure and using the same padding and fabric as in the tests described in the Example case. In the first test the burner flame was applied to the seat cushion on the right side. In the second test the burner was applied to the center seat cushion. The resulting HRR measurements are compared in Figure 3-3 below. In the first test the flames spread from the right side to the left side. When the flames reached the armrest on the left side, part of the material on the right side had already been consumed. This resulted in a relatively steady HRR that peaked slightly above 400 kW. In the second test the flames spread in two directions. As a result the heat rate continuously increased until the two armrests ignited and a peak heat-release rate of close to 1 MW was reached. This case illustrates that a seemingly small difference in the ignition scenario can have a surprisingly dramatic effect on fire growth.

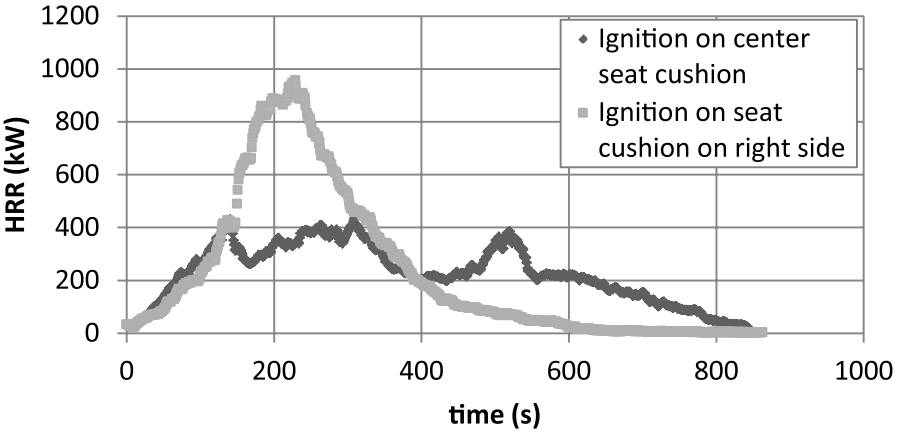

Figure 3-3. Effect of ignition location: steel-framed seat sofa mockups tested in furniture calorimeter test with different ignition locations – ignition on center seat cushion (◆) or seat cushion on right side (■)

- Heat and mass transfer

This is a multi-dimensional problem, and the dimensional effect is implicitly addressed in modeling by a single parameter – HRR or MLR and effective heat of combustion.

Case 2: Burning Flat Surfaces

General Model Parameter Table

Table 3-6. Model Parameter Table for Case 2 Examples

Ignition Parameters	t_{ig}		Time-to-Ignition	
Burning-Rate Parameters	Using HRR		Using MLR and HoC	
	$\dot{Q}''(t)$	Heat-Release Rate	$\dot{m}''(t)$	Mass-Loss Rate
			$\Delta h_{c,eff}$	Effective Heat-of-Combustion

Example 3.2 Modeling PMMA

3.2.1 Model Parameter Table

Model Parameters		Unit	Estimated Values and Estimation Methods
Ignition Parameters	t_{ig}	s	22 Measurement, Cone Calorimeter
Burning-Rate Parameters	MLR	g/s-m^2	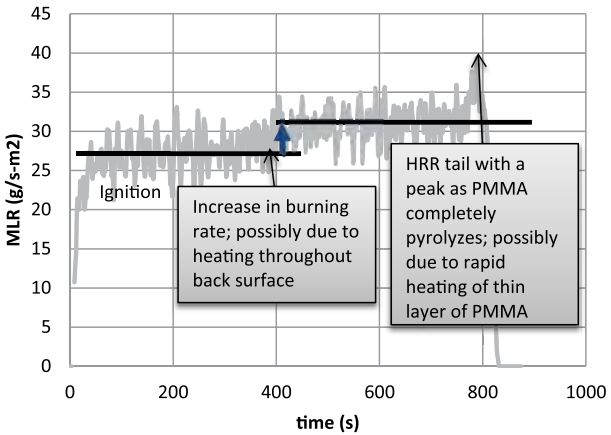 * Measurement is made at applied heat flux of 50 kW/m^2 in Cone Calorimeter. Measurement, Cone Calorimeter
	HoC	kJ/g	24.8 ± 0.1 Measurement, Cone Calorimeter

3.2.2 Validation

3.2.2.1 MODELING GOAL

Estimate model parameters for conducting modeling of pyrolysis of a flat surface under well-ventilated condition.

3.2.2.2 MODEL TYPE

Empirical Pyrolysis Model

3.2.2.3 MODELING APPROACH

- Pre-ignition stage is
  - Inert: decomposition with bubbling before ignition is neglected
  - Always the same as in Cone Calorimeter test with a specified heat flux impinging on material's surface (typically ~50 kW/m^2 is used)
- Ignition phenomenon is the same as in Cone Calorimenter experiment: time to ignition is the same in modeling as determined in experiment
- Post-ignition stage is
  - Considered to have instantaneous release of volatiles from solid to gas phase: bubbling layer is neglected and is considered as a surface phenomena
  - Considered to be the same as in Cone Calorimeter test in terms of heat-release rate or mass-loss rate per unit area

3.2.2.4 EXPERIMENT DESCRIPTION

Cone Calorimeter test

3.2.2.5 DATA SET

Cone Calorimeter test data of black PMMA with thickness of 18 mm, density of 1170 kg/m^3 and applied heat flux of 50 kW/m^2 is found.

3.2.2.6 UNCERTAINTY

Uncertainty in Experiment Data

- Uncertainty in time-to-ignition and mass-loss rate: From the experiment work done by Beaulieu and Dembsey[11] on thermally-thick behaving black PMMA using AFM apparatus, the experiment uncertainty in time-to-ignition and mass-loss rate at steady burning were determined as ± 2 s and ± 3 g/m^2s, respectively. The test results were compared with other literature values using different apparatuses such as Cone Calorimeter as well, which were considered as consistent.
- Assume:
  - Uncertainties are comparable to those of similar flat surfaces pyrolyzing under heating

Uncertainty in Modeling Outputs

- Same as in experiment data

3.2.3 Commentary

When using Empirical Model to simulate pyrolysis of PMMA, PMMA test data from a bench-scale Cone Calorimeter experiment at a set heat-flux level has been utilized to estimate the time-to-ignition from exposure to heating and the energy released from burning of PMMA. As noted in the Understanding Model part of the chapter, this approach is limited as follows in terms of the conditions being comparable to those found in the fire scenario on interest:

- Ignition scenario: piloted ignition with an electric sparker
- Exposure conditions: electrically heated coil uniformly heating PMMA with a set heat flux impinging on the front surface, where this applied heat-flux level during testing is assumed to be representative average (over space and time) for the fire scenario that is being modeled
- Heat and mass transfer: one-dimensional, i.e., perpendicular to the exposed surface
- Surface-burning data: edge effects in material testing are not included; therefore, data per unit area can be applied to simulate larger areas by simply multiplying by the material surface area involved in fire

Example 3.3 Modeling Corrugated Cardboard

3.3.1 Model Parameter Table

<table>
<tr><th colspan="2">Model Parameters</th><th>Unit</th><th>Estimated Values and Estimation Methods</th></tr>
<tr><td rowspan="2">Ignition Parameters</td><td rowspan="2">t_{ig}</td><td rowspan="2">s</td><td>32 ± 4</td></tr>
<tr><td>Measurement, Cone Calorimeter
(4 tests at 25 kW/m^2 average and 95% C.I. using student t distribution)</td></tr>
<tr><td rowspan="4">Burning-Rate Parameters</td><td rowspan="2">MLR</td><td rowspan="2">g/s-m^2</td><td> 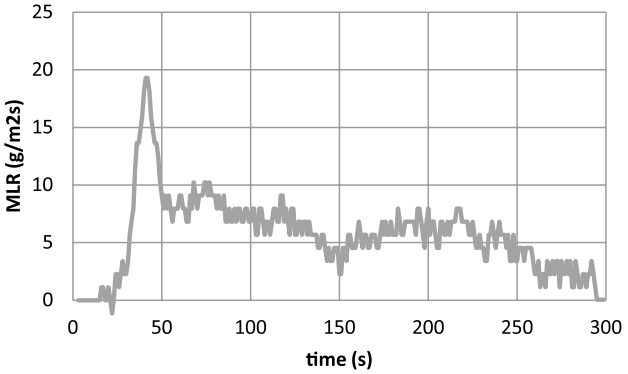

* Measurement is made at applied heat flux of 25 kW/m^2 in Cone Calorimeter.</td></tr>
<tr><td>Measurement, Cone Calorimeter</td></tr>
<tr><td rowspan="2">HoC</td><td rowspan="2">kJ/g</td><td>13.5 ± 0.5</td></tr>
<tr><td>Measurement, Cone Calorimeter
(2 tests at 25 kW/m2 average and 2 times standard deviation)</td></tr>
</table>

3.3.2 Validation

3.3.2.1 MODELING GOAL

Estimate model parameters for conducting modeling of pyrolysis of a flat surface under well-ventilated condition.

3.3.2.2 MODEL TYPE

Empirical Pyrolysis Model

3.3.2.3 MODELING APPROACH

- Pre-ignition stage is
  - Inert: non-uniform charring is considered to be evenly distributed
  - Always the same as in Cone Calorimeter test with a specified heat flux impinging on material's surface
- Ignition phenomenon is the same as in Cone Calorimenter experiment: time-to-ignition is the same in modeling as determined in experiment
- Post-ignition stage is
  - Considered to have instantaneous release of volatiles from solid to gas phase
  - Considered to be the same as in Cone Calorimeter test in terms of heat-release rate or mass-loss rate per unit area

3.3.2.4 EXPERIMENT DESCRIPTION

Cone Calorimeter test

3.3.2.5 DATA SET

Cone Calorimeter test data of triple-layer cardboard with thickness of 15 mm, density of 116 kg/m^3, and applied heat flux of 25 kW/m^2 is found.

3.3.2.6 UNCERTAINTY

Uncertainty in Experiment Data

- The uncertainty in the mass-loss rate data is estimated via statistical approach, taking the standard deviation (0.58 g/sm^2) from the mean of a steady burning of five identical PMMA tests conducted in a Cone Calorimeter[12]. The estimated uncertainty is 1.4 g/sm^2, which is found by calculating the 95% confidence interval applying student t distribution with a sample size of 5.
- The uncertainty in time to ignition data is estimated via statistical approach, taking four identical Cone Calorimeter test data at heat flux 25 kW/m^2 of this cardboard. 95% confidence interval is calculated for each heat-flux level assuming student t distribution.
- The uncertainty in effective heat-of-combustion is estimated by average heat-release rate divided by average mass-loss rate of two identical tests. Two times the standard deviation is used as its uncertainty band.
- Assume:
  - Uncertainties are comparable to those of similar flat surfaces pyrolyzing under heating

Uncertainty in Modeling Outputs

- Same as in experiment data

3.3.3 Commentary

When using Empirical Model to simulate pyrolysis of this triple-layer cardboard, test data from a bench-scale Cone Calorimeter experiment at a set heat-flux level has been utilized to estimate the time to ignition from exposure to heating and the energy released from burning of this cardboard. As noted in the Understanding Model part of the chapter, this approach is limited as follows in terms of the conditions being comparable to those found in the fire scenario of interest:

- Ignition scenario: piloted ignition with an electric sparker
- Exposure conditions: electrically heated coil uniformly heating sample with a set heat flux impinging on the front surface, where this applied heat-flux level during testing is assumed to be representative average (over space and time) for the fire scenario that is being modeled
- Heat and mass transfer: one-dimensional, i.e., perpendicular to the exposed surface
- Surface-burning data: edge effects in material testing are not included ; therefore, data per unit area can be applied to simulate larger areas by simply multiplying by the material surface area involved in fire

Example 3.4 Modeling Fire Retarded FRP Composite

3.4.1 Model Parameter Table

<table>
<tr><th colspan="2">Model Parameters</th><th>Unit</th><th>Estimated Values and Estimation Methods</th></tr>
<tr><td rowspan="2">Ignition Parameters</td><td rowspan="2">t_{ig}</td><td rowspan="2">s</td><td>175 ± 36</td></tr>
<tr><td>Measurement, Cone Calorimeter
(4 tests at 50 kW/m^2 average and 95% C.I. using student t distribution)</td></tr>
<tr><td rowspan="4">Burning-Rate Parameters</td><td rowspan="2">MLR</td><td rowspan="2">g/s-m^2</td><td> 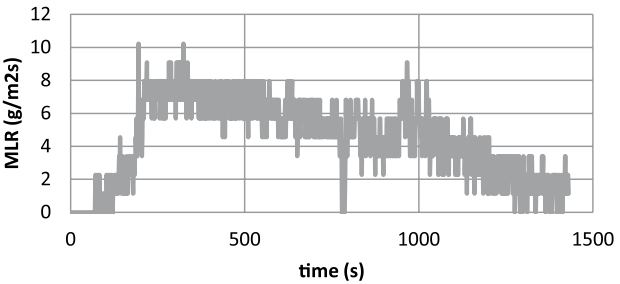

* Measurement is made at applied heat flux of 50 kW/m^2 in Cone Calorimeter.</td></tr>
<tr><td>Measurement, Cone Calorimeter</td></tr>
<tr><td rowspan="2">HoC</td><td rowspan="2">kJ/g</td><td>14.7 ± 3.8</td></tr>
<tr><td>Measurement, Cone Calorimeter
(4 tests at 50 kW/m2 average and 95% C.I. using student t distribution)</td></tr>
</table>

3.4.2 Validation

3.4.2.1 MODELING GOAL

Estimate model parameters for conducting modeling of pyrolysis of a flat surface under well-ventilated condition.

3.4.2.2 MODEL TYPE

Empirical Pyrolysis Model

3.4.2.3 MODELING APPROACH

- Pre-ignition stage is
  - Inert: non-uniform charring is considered to be evenly distributed
  - Always the same as in Cone Calorimeter test with a specified heat flux impinging on material's surface
- Ignition phenomenon is the same as in Cone Calorimenter experiment: time-to-ignition is the same in modeling as determined in experiment
- Post-ignition stage is:
  - Considered to have instantaneous release of volatiles from solid to gas phase
- Considered to be the same as in Cone Calorimeter test in terms of heat-release rate or mass-loss rate per unit area

3.4.2.4 EXPERIMENT DESCRIPTION

Cone Calorimeter test

3.4.2.5 DATA SET

Cone Calorimeter test data of FRP composite with thickness of 9.2 mm, density of 1900 kg/m^3, and applied heat flux of 50 kW/m^2 is found.

3.4.2.6 UNCERTAINTY

Uncertainty in Experiment Data

- The uncertainty in the mass loss rate data is estimated via statistical approach, taking the standard deviation (0.58 g/sm^2) from the mean of a steady burning of five identical PMMA tests conducted in a Cone Calorimeter.[12] The estimated uncertainty is 1.4 g/sm^2, which is found by calculating the 95% confidence interval applying student t distribution with a sample size of five.
- The uncertainty in time to ignition data is estimated via statistical approach, taking four identical Cone Calorimeter test data at heat flux 50 kW/m^2 of this cardboard. 95% confidence interval is calculated for each heat-flux level assuming student t distribution.
- The uncertainty in effective heat of combustion is estimated by average heat release rate divided by average mass loss rate of four identical tests. 95% confidence interval is calculated for each heat-flux level assuming student t distribution.
- Assume:
  - Uncertainties are comparable to those of similar flat surfaces pyrolyzing under heating

Uncertainty in Modeling Outputs

- Same as in experiment data

3.4.3 Commentary

When using Empirical Model to simulate pyrolysis of this fire retarded FRP composite, test data from a bench-scale Cone Calorimeter experiment at a set heat-flux level has been utilized to estimate the time to ignition from exposure to heating and the energy released from burning of this material. As noted in the Understanding Model part of the chapter, this approach is limited as follows in terms of the conditions being comparable to those found in the fire scenario of interest:

- Ignition scenario: piloted ignition with an electric sparker
- Exposure conditions: electrically heated coil uniformly heating sample with a set heat flux impinging on the front surface, where this applied heat flux level during testing is assumed to be representative average (over space and time) for the fire scenario that is being modeled
- Heat and mass transfer: one-dimensional, i.e., perpendicular to the exposed surface
- Surface-burning data: edge effects in material testing are not included; therefore, data per unit area can be applied to simulate larger areas by simply multiplying by the material surface area involved in fire

Example 3.5 Modeling Plywood

3.5.1 Model Parameter Table

<table>
<tr><th colspan="2">Model Parameters</th><th>Unit</th><th>Estimated Values and Estimation Methods</th></tr>
<tr><td rowspan="2">Ignition Parameters</td><td rowspan="2">t_{ig}</td><td rowspan="2">s</td><td>27 ± 9</td></tr>
<tr><td>Measurement, Cone Calorimeter
(3 tests at 50 kW/m^2 average and 95% C.I. using student t distribution)</td></tr>
<tr><td rowspan="4">Burning-Rate Parameters</td><td rowspan="2">MLR</td><td rowspan="2">g/s-m^2</td><td> 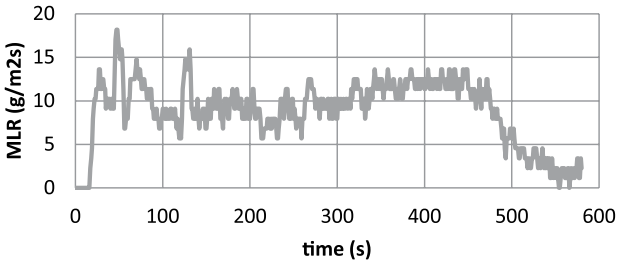

* Measurement is made at applied heat flux of 50 kW/m^2 in Cone Calorimeter.</td></tr>
<tr><td>Measurement, Cone Calorimeter</td></tr>
<tr><td rowspan="2">HoC</td><td rowspan="2">kJ/g</td><td>11.0 ± 0.3</td></tr>
<tr><td>Measurement, Cone Calorimeter
(2 tests at 50 kW/m2 average and 2 times standard deviation)</td></tr>
</table>

3.5.2 Validation

3.5.2.1 MODELING GOAL

Estimate model parameters for conducting modeling of pyrolysis of a flat surface under well-ventilated condition.

3.5.2.2 MODEL TYPE

Empirical Pyrolysis Model

3.5.2.3 MODELING APPROACH

- Pre-ignition stage is:
  - Inert: non-uniform charring is considered to be evenly distributed
  - Always the same as in Cone Calorimeter test with a specified heat flux impinging on material's surface
- Ignition phenomenon is the same as in Cone Calorimenter experiment: time to ignition is the same in modeling as determined in experiment
- Post-ignition stage is:
  - Considered to have instantaneous release of volatiles from solid to gas phase
  - Considered to be the same as in Cone Calorimeter test in terms of heat-release rate or mass loss rate per unit area

3.5.2.4 EXPERIMENT DESCRIPTION

Cone Calorimeter test

3.5.2.5 DATA SET

Cone Calorimeter test data of triple-layer cardboard with thickness of 11.1 mm, density of 542 kg/m^3 and applied heat flux of 50 kW/m^2 is found.

3.5.2.6 UNCERTAINTY

Uncertainty in Experiment Data

- The uncertainty in the mass loss rate data is estimated via statistical approach, taking the standard deviation (0.58 g/sm^2) from the mean of a steady burning of five identical PMMA tests conducted in a Cone Calorimeter.[12] The estimated uncertainty is 1.4 g/sm^2, which is found by calculating the 95% confidence interval applying student t distribution with a sample size of five.
- The uncertainty in time-to-ignition data is estimated via statistical approach, taking three identical Cone Calorimeter test data at heat flux 50 kW/m^2 of this cardboard. 95% confidence interval is calculated for each heat flux level assuming student t distribution.
- The uncertainty in effective heat of combustion is estimated by average heat release rate divided by average mass loss rate of two identical tests. Two times the standard deviation is used as its uncertainty band.
- Assume:
  - Uncertainties are comparable to those of similar flat surfaces pyrolyzing under heating

Uncertainty in Modeling Outputs

- Same as in experiment data

3.5.3 Commentary

When using Empirical Model to simulate pyrolysis of this plywood, test data from a bench-scale Cone Calorimeter experiment at a set heat-flux level has been utilized to estimate the time-to-ignition from exposure to heating and the energy released from burning of this material. As noted in the Understanding Model part of the chapter, this approach is limited as follows in terms of the conditions being comparable to those found in the fire scenario of interest:

- Ignition scenario: piloted ignition with an electric sparker
- Exposure conditions: electrically heated coil uniformly heating sample with a set heat flux impinging on the front surface where this applied heat-flux level during testing is assumed to be representative average (over space and time) for the fire scenario that is being modeled
- Heat and mass transfer: one-dimensional, i.e., perpendicular to the exposed surface
- Surface-burning data: edge effects in material testing are not included; therefore, data per unit area can be applied to simulate larger areas by simply multiplying the by material surface area involved in fire

References

1 Babrauskas, V., "Specimen Heat Fluxes for Bench-Scale Heat Release Rate Testing," *Fire and Materials*, 19 (1995) 243-252.

2 Khan, M.; and deRis, J., "Determination of Operator Independent Ignition for Polymeric Solids," in 9th *Fire and Materials Conference*, Interscience Co.mmunications, London, England., (2005) 11-22.

3 Lyon, R.; and Quintiere, J., "Criteria for Piloted Ignition of Combustible Solids," *Combustion and Flame*, 151 (2007) 551-559.

4 Thornton, W., "The Relation of Oxygen to the Heat of Combustion of Organic Compounds," *Philosophical Magazine and Journal of Science*, 33 (1917).

5 Huggett, C., "Estimation of the Rate of Heat Release by Means of Oxygen Consumption Measurements," *Fire and Materials*, 12 (1980) 61-65.

6 Buc, E., *Oxidizer Classification Research Project: Tests and Criteria*, Final Report, Fire Protection Research Foundation, Quincy, MA, (2009).

7 Dillon, S., *et al.*, "Determination of Properties and the Prediction of the Energy Release Rate of Materials in the ISO 9705 Room-Corner Test," National Institute of Standards and Technology, Gaithersburg, MD NIST-GCR-98-753, (1998).

8 Bryant, R.A.; Ohlemiller, T.J.; Johnsson, E.L.; Hammins, A.; Grove, B.S.; Guthrie, W.F.; Maranghides, A.; and Mulholland, G.W., The NIST 3 Megawatt quantitative heat release rate facility. NIST Special Publication 1007. NIST, Gaithersburg, MD, December (2003).

9 Enright, P.; and Fleischmann, C.; Uncertainty of heat release rate calculations of the ISO5660-1 Cone Calorimeter Standard Test Method", Fire Technology, 35:2 (1999) 153-169.

10 Zhao, L.; and Dembsey, N.A., "Measurement uncertainty analysis for calorimetry apparatuses", Fire and Materials, 32:1 (2008) 1-26.

11 Beaulieu, P.A.; and Dembsey, N.A., "Effect of Oxygen on Flame Heat Flux in Horizontal and Vertical Orientations," *Fire Safety Journal*, 43:6 (2008) 410-428.

12 Zhao, L., Bench Scale Apparatus Measurement Uncertainty and Uncertainty Effects on Measurement of Fire Characteristics of Material Systems, MS Thesis, Fire Protection Engineering, WPI, 2005-04-27, ETD-050105-182456.

Chapter 4
Simple Analytical Models

Understanding Model. 45
General Description of Models 45
Governing Equations 45
Model Parameters and Measurement Methods 48
Virtual Material 48
Model-Parameter Table 49
Model-Parameter-Measurement Methods 49
Uncertainty Analysis. 58
Ignition Data Analysis 58
Burning-Rate Data Analysis 60
Parameter-Estimation Process. 61
Example Cases Overview 63
Case 1: Thermally-Thick, Inert at Pre-Ignition with Steady Burning at Post-ignition 64
Virtual Microstructure of Virgin Material. 64
General Model-Parameter Table 64
Example 4.1 Modeling Poly(methylmethacrylate), PMMA 65
Example 4.2 Modeling Corrugated Cardboard. 69
Example 4.3 Modeling Fire Retarded FRP Composite 72
Example 4.4 Modeling Plywood 75
Case 2: Thermally-Thin, Inert at Pre-Ignition with Steady Burning at Post-ignition 79
Virtual Microstructure of Virgin Material. 79
General Model-Parameter Table 79
Example 4.5 Modeling Sandwich Composite – GRP Skin with Balsawood Core 79
Example 4.6 Modeling Thin FRP Composite 83
References. 88

Understanding Model

General Description of Models

In this model category, surface temperature of a material is solved based on the transient heat conduction equation using either the thermally-thick or thermally-thin assumption. When the thermally-thick assumption is used, the material is considered as a semi-infinite inert solid up until ignition from time-of-exposure to heating. The rate of surface-temperature increase is dependent upon the thermal inertia (kρc) of the material. The thermally-thin approach can be used for materials that are subject to heating under conditions of greater convective resistance between the solid and gas phase than conductive resistance within solid phase. This condition allows the material to be modeled with thermally-lumped analysis to calculate its temperature increase during the pre-ignition stage where any temperature gradient within the solid phase and mass loss is neglected. The rate of temperature increase is dependent upon the density multiplied by heat capacity (ρc) of the material. For both approaches, the material is assumed to ignite when its surface temperature reaches a material-dependent value (T_{ig}). Following ignition the mass-loss rate of the material is determined based on the net heat flux at the exposed surface and the heat of gasification (Δh_g). Finally the heat release rate is determined by multiplying the mass-loss rate by the effective heat of combustion ($\Delta h_{c,eff}$).

Principal assumptions are the same as those for Empirical Models for flat surfaces. In addition, the methods to obtain the two combustion properties ($\Delta h_{c,eff}$ and Δh_g) are based on the assumptions of steady burning on the material surface.

Governing Equations

Assuming that the material is a thermally-thick solid being heated on one side by applying a constant heat flux with the other side insulated (see Figure 4-1), conservation of energy with initial and boundary conditions can be written as below (see Eq. 4-1 through Eq. 4-4):

$$\rho c \frac{\partial T}{\partial t} = k \frac{\partial^2 T}{\partial x^2} \qquad \text{Eq. 4-1}$$

$$T_{t=0} = T_\infty \qquad \text{Eq. 4-2}$$

$$-k \left. \frac{\partial T}{\partial x} \right|_{x=0} = \dot{q}''_{net} \qquad \text{Eq. 4-3}$$

$$-k \left. \frac{\partial T}{\partial x} \right|_{x=\delta} = 0 \qquad \text{Eq. 4-4}$$

where

T	=	temperature (K);
x	=	distance from the exposed surface of the specimen (m);
δ	=	specimen thickness (m);
T_∞	=	ambient and initial temperature (K);
ε	=	surface emissivity/absorptivity;
h_c	=	convection coefficient (kW/m^2·K);
T_s	=	surface temperature (K); and
σ	=	Boltzmann constant (5.67·10^{-11} kW/K^4·m^2).

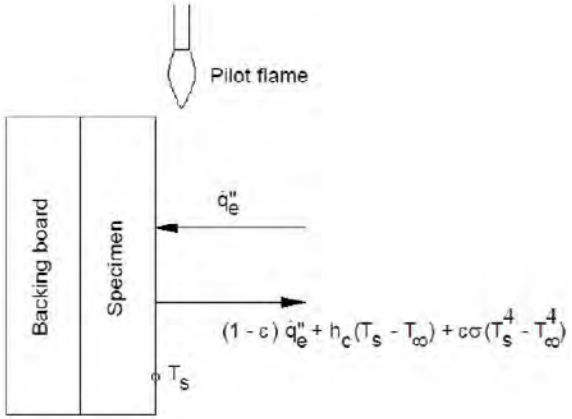

Figure 4-1. Schematic of a piloted ignition experiment

For the thermally-thin approach, the following governing equation is used (see Eq. 4-5 and Eq. 4-6):

$$\rho c \delta \frac{dT}{dt} = \dot{q}''_{net} \qquad \text{Eq. 4-5}$$

$$T_{t=0} = T_\infty \qquad \text{Eq. 4-6}$$

By assuming that the net heat flux is constant, time-to-ignition can be solved as below (see Eq. 4-7 and Eq. 4-8):

$$t_{ig} = \frac{\pi}{4} k\rho c \frac{\left(T_{ig} - T_\infty\right)^2}{\left(\dot{q}''_{net}\right)^2} \quad (thermally-thick) \qquad \text{Eq. 4-7}$$

$$t_{ig} = \rho c \delta \frac{\left(T_{ig} - T_\infty\right)}{\dot{q}''_{net}} \quad (thermally-thin) \qquad \text{Eq. 4-8}$$

where typically, $\dot{q}''_{net}$ impinging on the material surface for times prior to ignition in an intermediate or bench-scale calorimetry test can be expressed as below assuming the material is inert and opaque:

$$\dot{q}''_{net} = \varepsilon \dot{q}''_{e} - h_c (T_s - T_\infty) - \varepsilon\sigma(T_s^4 - T_\infty^4) \qquad \text{Eq. 4-9}$$

To determine whether the material of interest is acting thermally-thick or thermally-thin, one may examine the time-to-ignition data and plot them as $1/t_{ig}^{n}$ vs. applied heat flux and vary the exponent of t_{ig}, the n value from 0.5 to 1.0. When data gives its best fitness at n → 0.5, the material may be considered as thermally-thick behaving material. When data gives its best fitness at n → 1, the material can be considered as thermally-thin. Hence, careful examination of the ignition data should be done prior to parameter estimation for simple analytical pyrolysis modeling, because the model takes into account the material's thermal characteristics to simplify the model equations.

For both thermally-thick and -thin behaving materials, heat release at steady burning following ignition is calculated from Eq. 4-10:

$$\left(\dot{Q}(t)\right) = \begin{cases} 0 & for\ t < t_{ig} \\ \dfrac{\Delta h_{c,eff}}{\Delta h_g} \dot{q}''_{net}(t) & for\ t \geq t_{ig} \end{cases} \qquad \text{Eq. 4-10}$$

Model Parameters and Measurement Methods

Virtual Material

For modeling transient heating of an inert, semi-infinite homogeneous material and pyrolysis after ignition, the following set-up is used (see Figure 4-2):

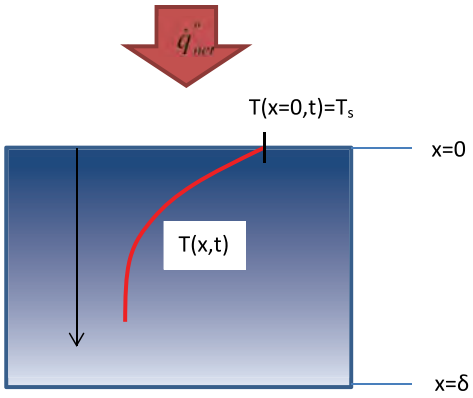

Figure 4-2. Pyrolysis modeling set-up used for thermally-thick materials

For modeling transient heating of an inert, thermally-thin homogeneous material and pyrolysis after ignition, the following set-up is used (see Figure 4-3):

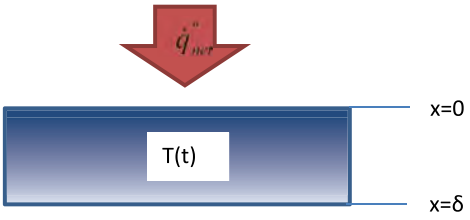

Figure 4-3. Pyrolysis modeling set-up used for thermally-thin materials

Model-Parameter Table

Table 4-1. Model-parameter table: summary of model parameters required to conduct pyrolysis modeling

Ignition Parameters	T_{ig}	Surface Temperature at Ignition
	$\dot{q}''_{cr}$	Critical Heat Flux for Ignition
	$k\rho c$	Thermal Inertia (Thermally-thick)
	$\rho c\delta$	Thermal Capacity (Thermally-thin)
Burning-Rate Parameters	$\Delta h_{c,eff}$	Effective Heat of Combustion
	Δh_g	Heat of Gasification
Parameters for Specifying Conditions	h_c	Convection Coefficient
	T_∞	Ambient Temperature
	ε	Surface Emissivity/Absorptivity
	Δt_{burn}	Burn Duration

Model-Parameter-Measurement Methods

1. Surface Temperature at Ignition

DIRECT MEASUREMENT

The most common approach for directly measuring surface temperature at ignition involves the use of fine thermocouples. The wire diameter has to be as small as possible to avoid having the thermocouple alter the material's response in the test. Although pre-welded type K unsheathed thermocouples are available with wire diameters down to 0.013 mm, it is extremely tedious to handle wires that are less than 0.25 mm in diameter. Butt-welded thermocouples are preferred because they have no bead. Since the smallest diameter of commercially available butt-welded thermocouples is 0.25 mm, it is recommended that these be used instead of 0.13-mm standard beaded wire thermocouples.

Thermocouples are installed on the surface by drilling two small holes through the specimen at 5–10 mm from opposite sides of its center. The wires are pulled through the holes and taped to the back side of the specimen, so that the thermocouple junction is in the middle between the holes and in contact with the specimen surface. It is beneficial to make a small incision between the holes so that the exposed part of the thermocouple wire is partially below the surface (see Figure 4-4(a)). It is critical to apply the right tension so that the wire is neither pulled into the material (see Figure 4-4(b)) nor loses contact with the surface (see Figure 4-4(c)).

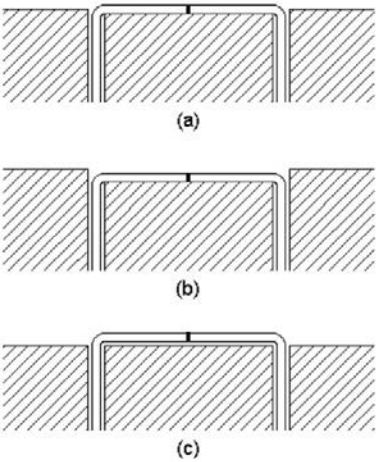

Figure 4-4. Measuring surface temperature with a thermocouple

It is very difficult and time-consuming to accurately measure the surface temperature of a specimen in a fire test with a thermocouple. The problems of this technique can be avoided by using a non-contact method that relies on an optical pyrometer or infrared camera. However, this approach is not without challenges either. First of all, it may not be possible to position the pyrometer or camera so that the instrument has a clear unobstructed view of the target surface. Often the radiant panel of the test apparatus is in the way and the pyrometer has to be positioned at an angle. Second, if the absorptivity of the target surface is less than unity, part of the incident heat flux from the radiant panel is reflected. The pyrometer or camera signal has to be corrected to account for this reflection. Finally, to accurately measure surface temperature with an optical pyrometer or infrared camera, the absorption of radiation, e.g., by CO_2 and water vapor,[1] in the space between the target and the sensor has to be accounted for. This presents a major challenge when measuring the surface temperature of a burning specimen due to the radiation from the flame and interference of the flame with the radiation from the surface. This challenge has been successfully addressed by using a narrow-band pyrometer that operates in the 8–10 μm range of the IR spectrum, i.e., outside the absorption/emission bands of carbon dioxide and water vapor.[2,3]

Investigators in Sweden have recently experimented with the use of thermographic phosphors to measure the surface temperature in fire tests.[4,5,6] This technique relies on the fact that the phosphorescence lifetime and spectral properties of UV laser-induced emissions from a thermographic phosphor applied to the surface of a test specimen are a function of the temperature of the phosphor. This method is still in its infancy, and more work is needed to demonstrate that it can be used for a wide range of materials and fire-test conditions.

The surface temperature at ignition of a thermoplastic is reasonably constant and independent of heat flux.[7,8] A number of investigators measured T_{ig} for a range of wood products.[9,10,11,12,13,14] Reasonably constant values were found for each material at heat fluxes ≥ 25 kW/m^2. All studies

reported a significant increase of T_{ig} at lower heat fluxes (50 °C–150 °C at 15 kW/m^2). This is due to the fact that pyrolysis and char formation at the surface are no longer negligible for ignition times exceeding 3 min. Under those conditions one of the basic assumptions of thermal-ignition theory, i.e., that the specimen behaves as an inert solid, is no longer valid.

A number of ASTM standards have been tabulated below for calorimeter tests that allow measurements of ignition and burning properties of materials (see Table 4-2):

Table 4-2. ASTM standards of calorimeter tests measuring ignition and burning properties of material

Standard Test	Description
ASTM D 1929 – 11	*Standard Test Method for Determining Ignition Temperature of Plastics*
ASTM E 1321 – 09	*Standard Test Method for Determining Material Ignition and Flame Spread Properties*
ASTM E 1354 – 11b	*Standard Test Method for Heat and Visible Smoke Release Rates for Materials and Products Using an Oxygen Consumption Calorimeter*
ASTM E 2058 – 09	*Standard Test Methods for Measurement of Synthetic Polymer Material Flammability Using a Fire Propagation Apparatus (FPA)*

IGNITION DATA ANALYSIS

Because it is very tedious to measure T_{ig} directly, it is much more common to determine ignition properties on the basis of an analysis of time-to-ignition data obtained over a range of heat fluxes. The analysis is usually based on a simple heat conduction model, which assumes that the solid is inert (negligible pyrolysis prior to ignition) and thermally-thick (heat wave does not reach the back surface prior to ignition) or thermally-thin (heat wave does reach the back surface prior to ignition; therefore, the temperature gradient can be neglected within the solid phase). It is important to understand that material properties obtained from such analyses are model parameters, which are not necessarily a good estimate of the real values.

Thermally-Thick Materials

Quintiere and Harkleroad developed a practical method for analyzing ignition data obtained with the LIFT apparatus.[15] The method is described in ASTM E 1321. The first step of the method consists of conducting ignition tests starting at a radiant heat-flux level near the maximum for the apparatus (60–65 kW/m^2). Time-to-ignition is obtained at heat-flux levels in descending order at intervals of 5 kW/m^2 to 10 kW/m^2, preferably with some replicates. When ignition time becomes sufficiently long (of the order of 10 min), data is obtained at heat-flux levels more closely together (1.5 kW/m^2 to 2 kW/m^2 intervals). At a certain level, ignition will no longer occur within the (arbitrary) maximum test duration of 20 min. The critical heat flux is taken to be slightly above this level. Usually, a few more tests are conducted around this level to confirm its value. Once the critical heat flux is known, T_{ig} can be calculated from a heat balance at the surface (see Figure 4-1) after very long exposure, since heat conduction into the specimen then becomes negligible (see Eq. 4-11):

$$\varepsilon \dot{q}''_{cr} = h_c (T_{ig} - T_\infty) + \varepsilon\sigma (T_{ig}^4 - T_\infty^4) \qquad \text{Eq. 4-11}$$

The same approach can be applied to estimate T_{ig} for thermally-thin materials.

2. Critical Heat Flux for Ignition

A quantity related to T_{ig} is the minimum heat flux for ignition, $\dot{q}''_{min}$. The minimum heat flux is just sufficient to heat the material surface to T_{ig} for very long exposure times (theoretically ∞). It is not a true material property, because it depends on the rate of convective cooling from the surface. This, in turn, depends primarily on the orientation, size, and flow field around the exposed surface. Since these are different in a small-scale test vs. a real fire, the minimum heat flux determined based on test data is an approximate value. To make the distinction, it is referred as the critical heat flux for ignition, $\dot{q}''_{cr}$ when measured directly. The critical heat flux may also vary between different small-scale test apparatuses due to differences in convective cooling. For example, Dietenberger obtained critical heat flux values of 14.3 kW/m^2 and 18.8 kW/m^2 for conditioned redwood in the Cone Calorimeter (*ASTM E 1354*) and Lateral Ignition and Flame spread Test (LIFT) apparatus (*ASTM E 1321*) respectively.[16]

The critical heat flux, $\dot{q}''_{cr}$, can be determined by bracketing, i.e., by conducting experiments at incrementally decreasing heat flux levels until ignition does not occur within a specified period (usually 10 or 20 min).

3. Thermal Inertia or Thermal Capacity per Unit Area

The thermal inertia, $k\rho c$, is a measure of how fast the surface temperature of a thermally-thick material rises when exposed to heat. A material with lower $k\rho c$ will ignite faster than a material with higher $k\rho c$ and the same T_{ig} exposed to the same heat flux. Similar to thermal inertia, for materials that are thermally-thin, thermal capacity per unit area, $\rho c\delta$, is a measure of how fast the material's lumped body temperature rises when exposed to heat.

DIRECT MEASUREMENT

This parameter can be determined by measuring thermal conductivity, density, and specific heat separately. Methods for measuring k, ρ, and c are described in the section on thermophysical parameters (see Chapter 5). Since k and c are temperature-dependent, the question is, at which temperature should these parameters be determined? A possible approach involves using average parameter values for the temperature range between ambient and T_{ig}.

IGNITION DATA ANALYSIS

Similar to measuring T_{ig} directly, direct measurement of $k\rho c$ or $\rho c\delta$ requires investment of time and financial commitment. Therefore, it is more common to determine this parameter on the basis of an analysis of time-to-ignition data obtained over a range of heat fluxes. The analysis is usually based on a simple heat-conduction model, which assumes that the solid is inert (negligible pyrolysis prior to ignition) and thermally-thick (heat wave does not reach the back surface prior to ignition) or thermally-thin (heat wave does reach the back surface prior to ignition; therefore, temperature gradient can be neglected within solid phase). It is important to understand that material properties obtained from such analyses are model parameters, which are not necessarily a good estimate of the real values.

Once the $\dot{q}''_{cr}$ and T_{ig} are known, the total heat-transfer coefficient at ignition, h_{ig}, can be calculated from a heat balance at the surface after very long exposure, since heat conduction into the specimen then becomes negligible (see Eq. 4-12):

$$\varepsilon \dot{q}''_{cr} = h_c (T_{ig} - T_\infty) + \varepsilon\sigma(T_{ig}^4 - T_\infty^4) \equiv h_{ig}(T_{ig} - T_\infty) \quad \text{Eq. 4-12}$$

where

h_{ig} = total heat transfer coefficient at ignition (kW/m²·K).

Surface temperature measurements under steady-state conditions for a number of inert materials and some combustible materials resulted in the following fit[15]:

$$\dot{q}''_{cr} = 0.015(T_{ig} - T_\infty) + \sigma(T_{ig}^4 - T_\infty^4) \equiv h_{ig}(T_{ig} - T_\infty) \quad \text{Eq. 4-13}$$

Thus, if specimens are heated for a sufficiently long time in the LIFT apparatus, it may be assumed that ε = 1 and that h_c = 15 W/m²·K. Once T_{ig} is calculated from the empirical value for $\dot{q}''_{cr}$ via Eq. 4-11, a total heat-transfer coefficient from the surface at ignition can be obtained by rearranging this equation as follows (see Eq. 4-14):

$$h_{ig} \equiv \frac{\dot{q}''_{cr}}{T_{ig} - T_\infty} = 0.015 + \sigma \frac{T_{ig}^4 - T_\infty^4}{T_{ig} - T_\infty} \quad \text{Eq. 4-14}$$

Based on approximate solutions of Eq. 4-1 through Eq. 4-4 with linearized heat losses from the exposed surface, the surface temperature at ignition for exposure to a constant radiant heat flux is approximated by (see Eq. 4-15):

$$T_{ig} = T_\infty + \frac{\dot{q}''_e}{h_{ig}} \mathrm{F}(t_{ig}) \quad with \quad \mathrm{F}(t) = \begin{cases} \dfrac{2\,h_{ig}\sqrt{t}}{\sqrt{\pi k\rho c}} & \text{small } t \\ 1 & \text{large } t \end{cases} \quad \text{Eq. 4-15}$$

where

t_{ig} = time to ignition at incident heat flux $\dot{q}''_e$ (s); and

F = function of time.

This leads to the following expression for correlation of piloted-ignition data (see Eq. 4-16):

$$\frac{\dot{q}''_{cr}}{\dot{q}''_e} = \mathrm{F}(t_{ig}) = \begin{cases} \dfrac{2\ h_{ig}\sqrt{t_{ig}}}{\sqrt{\pi k\rho c}} & t_{ig} \le t^* \\ 1 & t_{ig} > t^* \end{cases} \quad \text{Eq. 4-16}$$

where

t^* = time to reach steady conditions (s).

Thus, all data are plotted in a graph of $\dot{q}''_{cr} / \dot{q}''_e$ versus $\sqrt{t_{ig}}$. An "apparent" value for $k\rho c$ can be calculated from the slope of the line through zero that best fits the data. This line crosses $\dot{q}''_{cr} / \dot{q}''_e = 1$ at t*, the time needed to reach "steady-state" conditions. The functional form of Eq. 4-16

for small times is identical to that of the solution of the one-dimensional heat conduction equation for a semi-infinite solid exposed to a constant heat flux without heat losses from the surface. Consequently, *kρc* values obtained with this procedure are higher than actual average values. The same procedure can be used to analyze piloted-ignition data obtained with the Cone Calorimeter, provided an adjustment is made to h_c to account for the differences in convective cooling conditions.

Thermally-Thin Materials

Similar to what has been done for thermally-thick materials, ignition theory can be applied to thermally-thin materials. The only difference from the method introduced above is the F(t) function (see Eq. 4-17):

$$\frac{\dot{q}''_{cr}}{\dot{q}''_e} = \mathrm{F}(t_{ig}) = \begin{cases} \dfrac{h_{ig}\, t_{ig}}{\rho c \delta} & t_{ig} \le t^* \\ 1 & t_{ig} > t^* \end{cases} \qquad \text{Eq. 4-17}$$

where ρcδ is the thermal capacity per unit area. This parameter is comparable to thermal inertia in equations derived for thermally-thick behaving materials, which may be estimated from the slope of the line from linear regression.

4. Effective Heat of Combustion

See Chapter 3.

5. Heat-of-Gasification

The heat-of-gasification, Δh_g, is defined as the net heat flow into a specimen required to convert one mass unit of solid material to volatiles. The net heat flux can be obtained from an energy balance at the surface of the specimen. Typically, a specimen exposed in a small-scale calorimeter is heated by external heaters and by its own flame. Heat is lost from the surface in the form of radiation. A schematic of the heat balance at the surface of a burning specimen in the Cone Calorimeter (*ASTM E 1354*) is shown in Figure 4-5. Hence, Δh_g is defined as (see Eq. 4-18):

$$\Delta h_g \equiv \frac{\dot{q}''_{net}}{\dot{m}''} = \frac{\dot{q}_e'' + \dot{q}_f'' - \dot{q}_l''}{\dot{m}''} \qquad \text{Eq. 4-18}$$

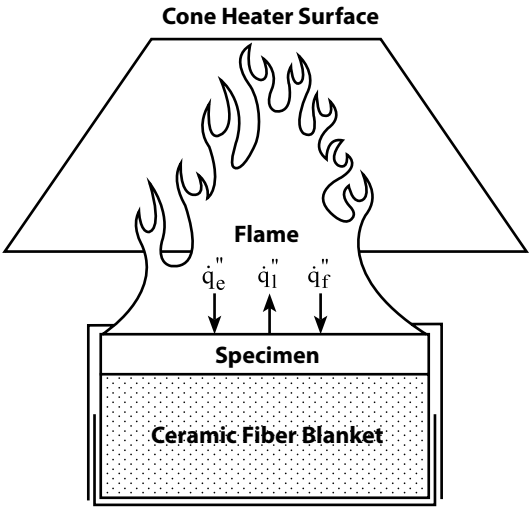

Figure 4-5. Heat balance at the surface of a burning cone calorimeter specimen

where

$\dot{q}''_{net}$ = net heat flux into the specimen (kW/m^2);

$\dot{q}''_e$ = heat flux to the specimen surface from external sources (kW/m^2);

$\dot{q}''_f$ = heat flux to the specimen surface from the flame (kW/m^2); and

$\dot{q}''_l$ = heat losses from the exposed surface (kW/m^2).

The heat of gasification is defined by Eq. 4-18. If the flame is approximated as a homogeneous grey gas volume, the heat flux from the flame can be expressed as follows (see Eq. 4-19):

$$\dot{q}''_f = \dot{q}''_{f,c} + \dot{q}''_{f,r} = h(T_f - T_s) + \sigma \varepsilon_f T_f^4 \qquad \text{Eq. 4-19}$$

where

$\dot{q}''_{f,c}$ = convective fraction of the flame flux (kW/m^2);

$\dot{q}''_{f,r}$ = radiative fraction of the flame flux (kW/m^2);

h^* = convection coefficient corrected for blowing (kW/m^2·K);

T_f = flame temperature (K);

T_s = surface temperature (K);

σ = Boltzmann constant ($5.67 \cdot 10^{-11}$ kW/m^2·K^4); and

ε_f = emissivity of the flame.

The flow of combustible volatiles emerging through the exposed surface of the specimen adversely affects the convective heat transfer between the flame and the surface. This effect is referred to as "blowing." The flame flux in a small-scale calorimeter is primarily convective, in particular in the vertical orientation, and flame absorption of external heater and specimen surface radiation can be neglected.

The heat losses from the surface can be expressed as Eq. 4-20:

$$\dot{q}_l'' = \sigma \varepsilon_s (T_s^4 - T_\infty^4) \qquad \text{Eq. 4-20}$$

where

ε_s = surface emissivity of the specimen; and

T_∞ = ambient temperature (K).

Some materials exhibit nearly steady mass-loss rates when exposed to a fixed radiant-heat flux. T_s for these materials reaches a steady value after a short initial transient period, and all terms in Eq. 4-20 are approximately constant. Δh_g can then be obtained by measuring steady mass-loss rates at different radiant-heat flux levels, and by plotting $\dot{m}''$ as a function of $\dot{q}_e''$. The reciprocal of the slope of a straight line fitted through the data points is equal to Δh_g. The intercept of the line with the abscissa is equal to $\dot{q}_l'' - \dot{q}_f''$. Tewarson et al.[17] and Petrella[18] have used this technique to obtain average Δh_g values for a large number of materials. Tewarson et al. also conducted tests in vitiated O_2/N_2 mixtures and found $\dot{q}_f''$ to decrease linearly with decreasing oxygen concentration. Analysis of these additional experiments made it possible to separate $\dot{q}_f''$ and $\dot{q}_l''$.

Many materials, in particular those that form an insulating char layer as they burn, take a long time to reach steady burning conditions or may never reach steady conditions. Eq. 4-18 is still valid for such materials, but the heat and mass fluxes and resulting Δh_g values vary with time. Tewarson and Petrella have used the method described in the previous paragraph to determine average Δh_g values for non-steady burning materials using average mass-loss rates. They found that average $\dot{m}''$ is still an approximately linear function of $\dot{q}_e''$. However, the average heat-of-gasification values obtained in this manner may not have any physical meaning. For example, Janssens demonstrated that the values based on average mass loss rates are too high for wood, and suggested a method to determine Δh_g as a function of char depth.

6. Convection Coefficient

The convection coefficient depends on the apparatus that was used to obtain the piloted ignition data. Table 4-3 summarizes recommended h_c values for different apparatuses.

Table 4-3. Recommended hc values for different test apparatuses

Apparatus	Orientation	h_c (kW/m^2·K)
ISO Ignitability Test	Horizontal	0.011
Cone Calorimeter	Horizontal	0.012
Cone Calorimeter	Vertical	0.016
LIFT	Vertical	0.015
Fire Propagation Apparatus	Horizontal	0.010

7. Ambient Temperature

Typically, ambient temperature is directly measured using a thermometer measuring room temperature located in the lab where testing is conducted.

8. Surface Emissivity / Absorptivity

The emissivity can be (1) obtained from the literature; (2) assumed to be equal to 1, or close to 1 (which is reasonable for many materials); or (3) measured according to a standard test method (see Table 4-4).

Table 4-4. ASTM standards for Measuring Emissivity

Standard Test	Description
ASTM C 835	*Standard Test Method for Total Hemispherical Emittance of Surfaces up to 1400°C*
ASTM C 1371	*Standard Test Method for Determination of Emittance of Materials Near Room Temperature Using Portable Emissometers*

9. Burn Duration

Burn duration is the time of burning, i.e., time of complete burnout minus time of ignition. This parameter can be calculated by considering steady burning rate after ignition and available amount of fuel mass to burn. At a certain level of applied heat flux, the modeler can estimate the burning rate from linear-regression plotting external applied heat flux, $\dot{q}_e''$ versus burning rate, $\dot{m}''$ (see Eq. 4-17). Burn duration can be estimated by Eq. 4-21:

$$\Delta t_{burn} = \frac{\rho\delta}{\dot{m}''} \qquad \text{Eq. 4-21}$$

Uncertainty Analysis

When a parameter is obtained via direct measurement, a statistical approach may be used to quantify the uncertainty. Use at least three identical measurements to analyze the confidence interval, assuming data is not biased due to inherent problems during data collection. When parameters are obtained via data analysis, uncertainty can be calculated using the Law of Propagation of Uncertainty. These are shown below:

Ignition Data Analysis

Thermally-thick Materials

ΔT_{IG}

This parameter is a function of $\dot{q}''_{cr}$, h_c, and T_∞. Knowing the uncertainty of $\dot{q}''_{cr}$, h_c and T_∞ uncertainty of T_{ig} can be estimated as below using the Law of Propagation of Uncertainty.

Recall the heat-balance equation at the front surface during steady burning (see Eq. 4-11). Using the Law of Propagation of Uncertainty, the following mathematical expression is found (see Eq. 4-22):

$$\delta\dot{q}''_{cr} = \sqrt{\left(\frac{\partial\dot{q}''_{cr}}{\partial\varepsilon}\delta\varepsilon\right)^2 + \left(\frac{\partial\dot{q}''_{cr}}{\partial h_c}\delta h_c\right)^2 + \left(\frac{\partial\dot{q}''_{cr}}{\partial T_\infty}\delta T_\infty\right)^2 + \left(\frac{\partial\dot{q}''_{cr}}{\partial T_{ig}}\delta T_{ig}\right)^2} \qquad \text{Eq. 4-22}$$

Therefore, the uncertainty of T_{ig} becomes (see Eq. 4-23):

$$\delta T_{ig} = \left(\frac{\partial\dot{q}''_{cr}}{\partial T_{ig}}\right)^{-1}\sqrt{\left(\delta\dot{q}''_{cr}\right)^2 - \left(\left(\frac{\partial\dot{q}''_{cr}}{\partial\varepsilon}\delta\varepsilon\right)^2 + \left(\frac{\partial\dot{q}''_{cr}}{\partial h_c}\delta h_c\right)^2 + \left(\frac{\partial\dot{q}''_{cr}}{\partial T_\infty}\delta T_\infty\right)^2\right)} \qquad \text{Eq. 4-23}$$

where

$$\frac{\partial\dot{q}''_{cr}}{\partial T_{ig}} = \frac{h_c + 4\varepsilon\sigma T_{ig}^3}{\varepsilon}$$

$$\frac{\partial\dot{q}''_{cr}}{\partial\varepsilon} = \frac{-\dot{q}''_{cr} + \sigma(T_{ig}^4 - T_\infty^4)}{\varepsilon}$$

$$\frac{\partial\dot{q}''_{cr}}{\partial h_c} = \frac{T_{ig} - T_\infty}{\varepsilon}$$

$$\frac{\partial\dot{q}''_{cr}}{\partial T_\infty} = \frac{-h_c - 4\varepsilon\sigma T_\infty^3}{\varepsilon}$$

$\Delta(K\rho C)$

This parameter is a function of estimated slope of the best-fit line that represents the relationship between $\dot{q}''_{cr} / \dot{q}''_e$ and $\sqrt{t_{ig}}$ and h_{ig} where h_{ig} is a function of ε, $\dot{q}''_{cr}$, T_{ig} and T_∞.

Recall $k\rho c = \dfrac{4\ h_{ig}^2}{\pi\cdot(slope)^2}$ and $\varepsilon\dot{q}''_{cr} \equiv h_{ig}(T_{ig} - T_\infty)$.

By substituting h_{ig}, thermal inertia can be rearranged to Eq. 4-24:

$$k\rho c = \frac{4}{\pi \cdot (slope)^2}\left(\frac{\varepsilon \dot{q}''_{cr}}{T_{ig} - T_{\infty}}\right)^2 \qquad \text{Eq. 4-24}$$

Therefore, using the Law of Propagation of Uncertainty, the following mathematical expression is found (see Eq. 4-25):

$$\delta(k\rho c) = \sqrt{\begin{aligned}&\left(\frac{\partial(k\rho c)}{\partial(slope)}\delta(slope)\right)^2 + \left(\frac{\partial(k\rho c)}{\partial \varepsilon}\delta\varepsilon\right)^2 + \left(\frac{\partial(k\rho c)}{\partial \dot{q}''_{cr}}\delta\dot{q}''_{cr}\right)^2 \\ &+ \left(\frac{\partial(k\rho c)}{\partial T_{ig}}\delta T_{ig}\right)^2 + \left(\frac{\partial(k\rho c)}{\partial T_{\infty}}\delta T_{\infty}\right)^2\end{aligned}} \qquad \text{Eq. 4-25}$$

where

$$\frac{\partial(k\rho c)}{\partial(slope)} = \frac{-8}{\pi \cdot (slope)^3}\left(\frac{\varepsilon \dot{q}''_{cr}}{T_{ig} - T_{\infty}}\right)^2$$

$$\frac{\partial(k\rho c)}{\partial \varepsilon} = \frac{8}{\pi \cdot (slope)^2}\left(\frac{\dot{q}''_{cr}}{T_{ig} - T_{\infty}}\right)^2 \varepsilon$$

$$\frac{\partial(k\rho c)}{\partial \dot{q}''_{cr}} = \frac{8}{\pi \cdot (slope)^2}\left(\frac{\varepsilon}{T_{ig} - T_{\infty}}\right)^2 \dot{q}''_{cr}$$

$$\frac{\partial(k\rho c)}{\partial T_{ig}} = \frac{-8}{\pi \cdot (slope)^2}\left(\frac{\varepsilon \dot{q}''_{cr}}{T_{ig} - T_{\infty}}\right)^2 \frac{1}{T_{ig} - T_{\infty}}$$

$$\frac{\partial(k\rho c)}{\partial T_{\infty}} = \frac{8}{\pi \cdot (slope)^2}\left(\frac{\varepsilon \dot{q}''_{cr}}{T_{ig} - T_{\infty}}\right)^2 \frac{1}{T_{ig} - T_{\infty}}$$

Thermally-thin Materials

ΔT_{IG}

Uncertainty of this parameter is the same as in thermally-thick case.

$\Delta(\rho C \Delta)$

This parameter is a function of the estimated slope of the best-fit line that represents the relationship between $\dot{q}''_{cr} / \dot{q}''_{e}$ and t_{ig} and h_{ig} where h_{ig} is a function of ε, $\dot{q}''_{cr}$, T_{ig} and T_{∞}.

Recall $\rho c \delta = \frac{h_{ig}}{slope}$ and $\varepsilon \dot{q}''_{cr} \equiv h_{ig}(T_{ig} - T_{\infty})$.

By substituting h_{ig}, thermal capacity per unit area can be rearranged to Eq. 4-26:

$$\rho c \delta = \frac{1}{slope}\left(\frac{\varepsilon \dot{q}''_{cr}}{T_{ig} - T_{\infty}}\right) \qquad \text{Eq. 4-26}$$

Therefore, using the Law of Propagation of Uncertainty, the following mathematical expression is found as Eq. 4-27:

$$\delta(\rho c\delta)=\sqrt{\left(\frac{\partial(\rho c\delta)}{\partial(slope)}\delta(slope)\right)^2+\left(\frac{\partial(\rho c\delta)}{\partial\varepsilon}\delta\varepsilon\right)^2+\left(\frac{\partial(\rho c\delta)}{\partial\dot{q}_{cr}^{"}}\delta\dot{q}_{cr}^{"}\right)^2+\left(\frac{\partial(\rho c\delta)}{\partial T_{ig}}\delta T_{ig}\right)^2+\left(\frac{\partial(\rho c\delta)}{\partial T_{\infty}}\delta T_{\infty}\right)^2} \quad \text{Eq. 4-27}$$

where

$$\frac{\partial(\rho c\delta)}{\partial(slope)}=\frac{-1}{(slope)^2}\left(\frac{\varepsilon\dot{q}_{cr}^{"}}{T_{ig}-T_{\infty}}\right)$$

$$\frac{\partial(\rho c\delta)}{\partial\varepsilon}=\frac{1}{(slope)}\left(\frac{\dot{q}_{cr}^{"}}{T_{ig}-T_{\infty}}\right)$$

$$\frac{\partial(\rho c\delta)}{\partial\dot{q}_{cr}^{"}}=\frac{1}{(slope)}\left(\frac{\varepsilon}{T_{ig}-T_{\infty}}\right)$$

$$\frac{\partial(\rho c\delta)}{\partial T_{ig}}=\frac{-1}{(slope)}\left(\frac{\varepsilon\dot{q}_{cr}^{"}}{T_{ig}-T_{\infty}}\right)\frac{1}{T_{ig}-T_{\infty}}$$

$$\frac{(\rho c\delta)}{\partial T_{\infty}}=\frac{1}{(slope)}\left(\frac{\varepsilon\dot{q}_{cr}^{"}}{T_{ig}-T_{\infty}}\right)\frac{1}{T_{ig}-T_{\infty}}$$

Burning-Rate Data Analysis

Δh_g

This parameter is estimated by calculating the reciprocal of the slope of the best-fit line of $\dot{m}''$ versus $\dot{q}_e''$ using mass-loss rate data obtained from Cone tests at different heat-flux levels. Recall $\Delta h_g \equiv \frac{\dot{q}_{net}^{"}}{\dot{m}''}=\frac{\dot{q}_e''+\dot{q}_f''-\dot{q}_l''}{\dot{m}''}$ during steady burning and therefore $\dot{m}''=\frac{1}{\Delta h_g}\dot{q}_e''+\frac{\left(\dot{q}_f''-\dot{q}_l''\right)}{\Delta h_g}$.

The uncertainty of the slope (=1/Δh_g) can be estimated through calculating the standard error of the slope of the best-fit line. Knowing the uncertainty of the slope, calculation of uncertainty of Δh_g becomes possible by considering the boundary values.

Parameter-Estimation Process

To create a virtual material, these tasks must be considered:

- Create a list of model inputs, which needs to be determined
- Obtain model unknown inputs via measurement or literature search

When the above is done and every unknown has been estimated, validation work and commentary is needed to understand the performance of the estimated parameter set:

- Run model
- Analyze simulation quality with consideration of uncertainties in modeling outputs and data
- Add commentary

When presenting the parameter-estimation results, three sections will be introduced: Model-Parameter Table, Validation section, and Commentary section. The Model-Parameter Table includes the model parameters necessary to conduct pyrolysis modeling, their estimated values, and methods of estimating the unknowns. The Validation section consists of the following information: description of modeling goal, pyrolysis model type, and the modeling approach used in the exercise, experiment type and its data used to empirically simulate the material's heat-release rate and uncertainty information of experimental data and modeling outputs. The Commentary section discusses any limitations of pyrolysis modeling conducted above, which has been summarized in the Model Parameter Table and Validation sections.

For better visualization of the problem, a flowchart is shown below (see Figure 4-6):

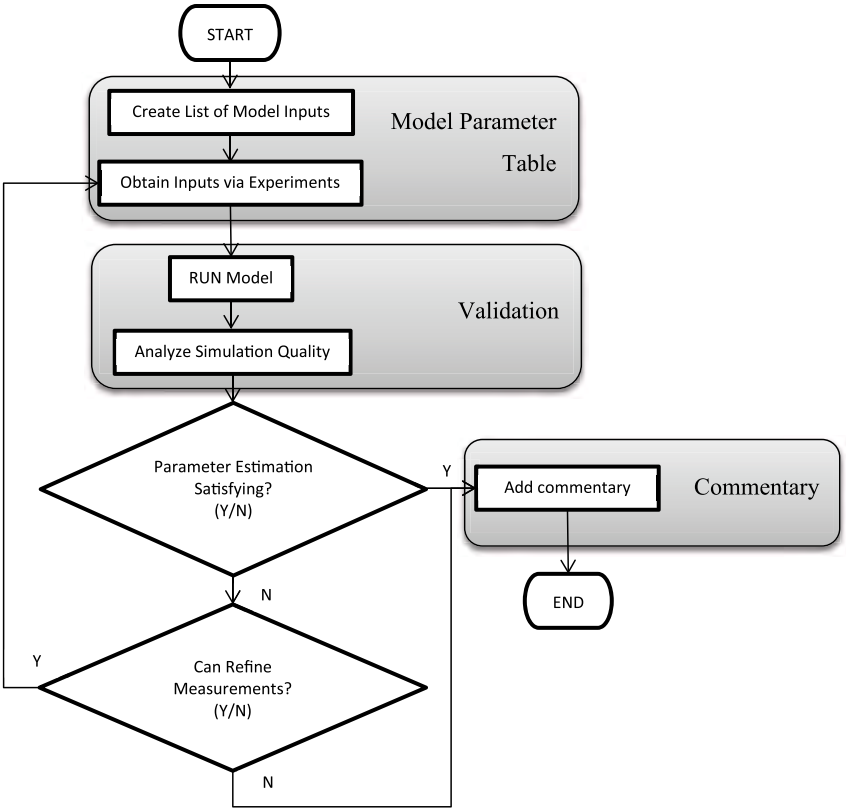

Figure 4-6. Flow chart of parameter estimation for simple analytical pyrolysis models

Example Cases Overview

Table 4-5. Overview of example cases using simple analytical pyrolysis models

Case	Description	Examples
1	Thermally-thick, inert at pre-ignition with steady burning at post-ignition	PMMA
		Corrugated Cardboard
		Fire-Retarded FRP Composite
		Plywood
2	Thermally-thin, inert at pre-ignition with steady burning at post-ignition	Sandwich Composite
		Thin FRP Composite

In the following, summarized results are shown for each example case. Detailed solutions of these example cases are given in Appendix C.

Case 1: Thermally-Thick, Inert at Pre-Ignition with Steady Burning at Post-ignition

Virtual Microstructure of Virgin Material

- Homogeneous flat surface single layer in horizontal position
- Pre-ignition stage: inert, semi-infinite thickness (i.e., thermally-thick)
- Post-ignition stage: steady burning

General Model-Parameter Table

- Ignition and burning-rate parameters are considered in this example
- Reduced Model Parameter Table (see Table 4-6):

Table 4-6. Model Parameter Table for Case 1 Examples

Ignition Parameters	T_{ig}	Surface Temperature at Ignition
	$\dot{q}''_{cr}$	Critical Heat Flux for Ignition
	$k\rho c$	Thermal Inertia (Thermally-thick)
Burning-Rate Parameters	$\Delta h_{c,eff}$	Effective Heat-of-Combustion
	Δh_g	Heat-of-Gasification
Parameters for Specifying Conditions	h_c	Convection Coefficient
	T_∞	Ambient Temperature
	ε	Surface Emissivity/Absorptivity
	Δt_{burn}	Burn Duration

Example 4.1 Modeling Poly(methylmethacrylate), PMMA

4.1.1 Model Parameter Table

Model Parameters		Unit	Estimated Values and Estimation Methods
Ignition Parameters	T_{ig}	°C	318 ± 4
			Ignition Data Analysis
	$\dot{q}''_{cr}$	kW/m^2	10.5 ± 0.5
			Measurement, Cone Calorimeter by bracketing
	kρc	kJ^2/m^{4}K^{2}s	0.649 ± 0.151
			Ignition Data Analysis
Burning-Rate Parameters	$\Delta h_{c,eff}$	g/s-m^2	24.6 ± 0.9
			Burning-Rate Data Analysis
	Δh_g	kJ/g	2.9 ± 1.0
			Burning-Rate Data Analysis
Parameters for Specifying Conditions	h_c	W/m^{2}K	12 ± 0.5
			Reference value for horizontal position in cone calorimeter
	T_∞	°C	20 ± 2
			Measurement
	ε	-	0.9 ± 0.09
			Approximated
	Δt_{burn}	s	$\frac{(1170)(18)}{0.351\dot{q}''_e + 8.896}$
			Burning-Rate Data Analysis

4.1.2 Validation

4.1.2.1 MODELING GOAL

Estimate model parameters for conducting modeling of pyrolysis of PMMA under various heating rates – heat-flux levels ranging up to ~ 100kW/m^2.

4.1.2.2 MODEL TYPE

Thermally-thick model for ignition analysis (Quintiere and Harkleroad, ASTM E 1321) and steady burning model

4.1.2.3 MODELING APPROACH

- Pre-ignition stage is
  - Inert: decomposition with bubbling before ignition is neglected
  - Thermally-thick: heat transfer does not reach back surface
- Post-ignition stage is
  - Considered to have instantaneous release of volatiles from solid to gas phase: bubbling layer is neglected and is considered as a surface phenomenon
  - Considered to have a constant thickness: regression of PMMA is neglected
  - Steady burning: heat loss equals heat gain at front surface

4.1.2.4 EXPERIMENT DESCRIPTION

Cone Calorimeter test

4.1.2.5 DATA SET

- Cone Calorimeter test data of black PMMA with thickness of 18 mm, density of 1170 kg/m^3 and applied heat-flux levels ranging from 10 to 75 kW/m^2 is found.
- For ignition data analysis, only time-to-ignition with respect to applied heat-flux data will be used.
- For burning-rate data analysis, data for the entire testing time duration at HF =25, 50, and 75 kW/m^2, mass loss and heat release during testing period with respect to applied heat flux will be used.
- PMMA AFM tests[19] conducted under 28.4 and 60 kW/m^2 are used to compare data with extrapolated modeling cases – time of ignition and MLR at steady burning stage.

4.1.2.6 UNCERTAINTY

Uncertainty in Experiment Data

- Uncertainty in time to ignition and mass loss rate: From the experimental work done by Beaulieu and Dembsey[19] on thermally-thick behaving black PMMA using AFM apparatus, the experiment uncertainty in time-to-ignition and mass-loss rate at steady burning were determined as ± 2 s and ± 3 g/m^{2}s, respectively. The test results were compared with other literature values using different apparatuses, such as Cone Calorimeter as well, which were considered as consistent.
- Assume:
  - Uncertainties are comparable to those of similar flat surfaces pyrolyzing under heating

Uncertainty in Modeling Outputs

- Uncertainty in t_{ig} and $\dot{m}''$ can be estimated from linear regression process and using the Law of Propagation of Uncertainty

4.1.2.7 MODELING OUTPUT: MASS LOSS RATE (MLR)

- Ignition and Burning-Rate Data Analysis

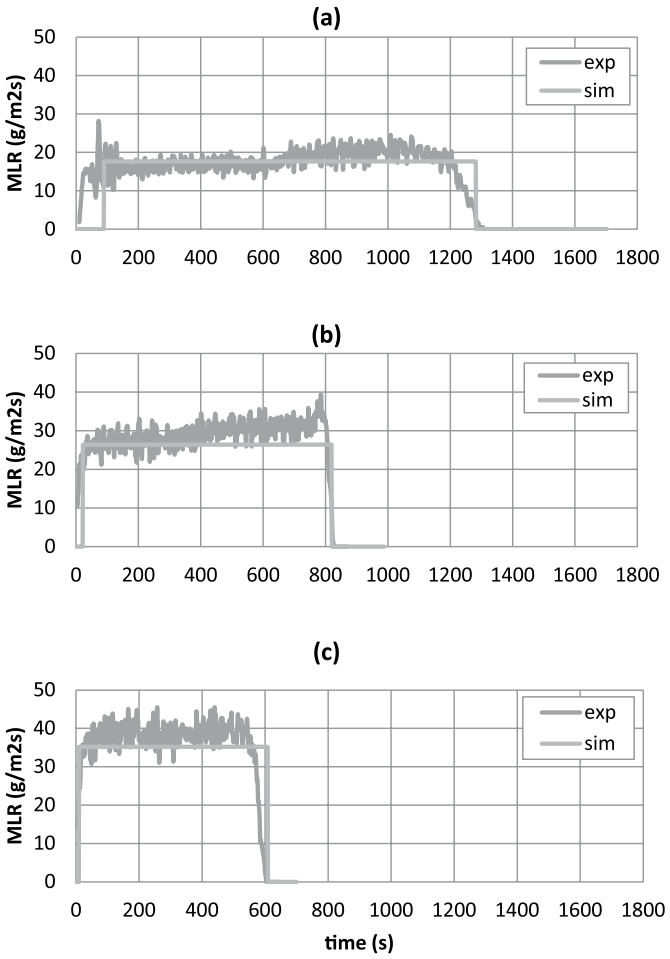

Figure 4-7. Mass-loss rate (MLR) comparisons for PMMA between actual MLR from experiment (exp) and modeled MLR (sim) at different applied heat-flux levels – (a) MLR at 25 kW/m²; (b) MLR at 50 kW/m²; and (c) MLR at 75 kW/m². Note that data shown were used to estimate model-parameter values.

- Extrapolation

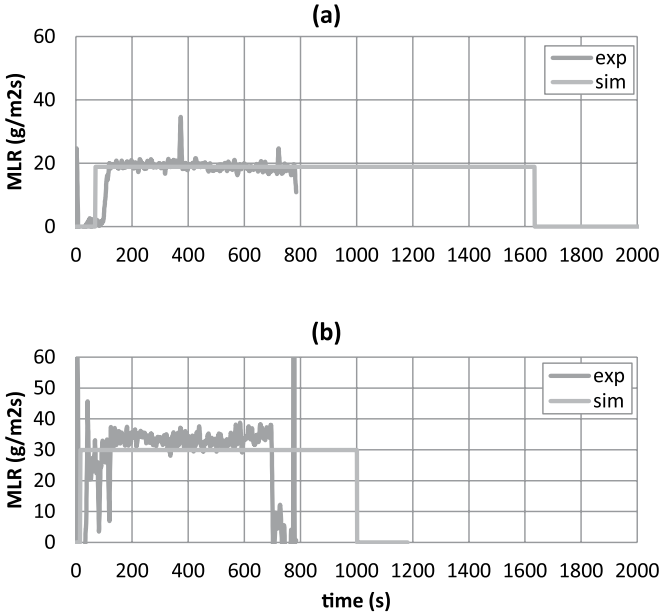

Figure 4-8. Mass-loss rate (MLR) comparisons for PMMA between actual MLR from experiment (exp) and modeled MLR (sim) at different applied heat-flux levels – (a) MLR at 28.4 kW/m²; and (b) MLR at 60 kW/m². Note that data shown were not included in the model-parameter-estimation process; hence, these two cases are considered as extrapolation cases.

4.1.3 Commentary

GENERAL COMMENTS ABOUT MLR

- Ignition and Burning-Rate Data Analysis at HF = 25, 50 and 75 kW/m²: Good agreement exists between experiment data and all modeling results
- Extrapolation at HF = 28.4 and 60 kW/m²: Generally, good agreement exists between MLR data and modeling results, except near ignition stage. In modeling time-to-ignition, the model's outputs are shorter than those from AFM tests for both heat-flux levels. This discrepancy can be explained by considering the in-depth absorption of radiation during heating of PMMA. The data from AFM tests, where IR lamps are used to heat the samples, possibly were subject to in-depth radiative absorption delaying ignition, knowing that the PMMA samples are somewhat transparent. However, this phenomenon is not accounted for in modeling assumptions and in parameter estimation process where Cone Calorimeter test data is used – in the Cone, radiation is absorbed mostly on the surface.

LIMITATION IN MODELING

- When using the Simple Analytical Model to simulate pyrolysis of black PMMA (density 1170 kg/m^3, thickness 18 mm), test data from a bench-scale Cone Calorimeter experiment at several heat flux levels have been utilized to estimate the time-to-ignition from exposure to heating and the mass-loss rate at steady-burning stage after ignition. The comparison between the model outputs (time- to-ignition and steady-burning rate) and the data from bench-scale experiment showed good agreement for both checking purposes, where the same heat flux levels (25, 50 and 75 kW/m^2) used in parameter estimation have been considered and extrapolation purposes where heat-flux levels (28.4 and 60 kW/m^2) not included in parameter estimation process have been considered.
- Although the modeling predictions of time-to-ignition and steady-burning rate in this example seem to be reasonable, limitations of Simple Analytical Modeling has been acknowledged in literature for modeling black PMMA at relatively high applied heat-flux levels. At high-heat flux levels, the assumption of having an inert condition during pre-ignition stage and neglecting thermal decomposition behavior- such as bubbling- cannot be made where these effects become more profound on temperature profile and ignition process of PMMA. Therefore, caution should be given when conducting modeling for cases with higher heat-flux levels.

Example 4.2 Modeling Corrugated Cardboard

4.2.1 Model Parameter Table

Model Parameters		Unit	Estimated Values and Estimation Methods
Ignition Parameters	T_{ig}	°C	293 ± 17
			Ignition Data Analysis
	$\dot{q}''_{cr}$	kW/m^2	9 ± 1
			Measurement, Cone Calorimeter by bracketing
	kρc	kJ^2/m^{4}K^{2}s	0.297 ± 0.101
			Ignition Data Analysis
Burning-Rate Parameters	$\Delta h_{c,eff}$	g/s-m^2	13.9 ± 1.3
			Burning-Rate Data Analysis
	Δh_g	kJ/g	21.6 ± 10.9
			Burning-Rate Data Analysis
Parameters for Specifying Conditions	h_c	W/m^{2}K	12 ± 0.5
			Reference value for horizontal position in Cone Calorimeter
	T_∞	°C	293 ± 17
			Ignition Data Analysis
	ε	-	0.9 ± 0.09
			Approximated
	Δt_{burn}	s	$\frac{(116)(15.1)}{0.046\dot{q}''_e + 5.530}$
			Burning-Rate Data Analysis

4.2.2 Validation

4.2.2.1 MODELING GOAL

Estimate model parameters for conducting modeling of pyrolysis of triple-layer corrugated cardboard under various heating rates – heat flux levels ranging up to ~ 75 kW/m^2.

4.2.2.2 MODEL TYPE

Thermally-thick model for ignition analysis (Quintiere and Harkleroad, ASTM E 1321) and steady-burning model

4.2.2.3 MODELING APPROACH

- Pre-ignition stage is
  - Inert: non-uniform charring is considered to be evenly distributed
  - Thermally-thick: heat transfer does not reach back surface
- Post-ignition stage is
  - Considered to have instantaneous release of volatiles from solid to gas phase
  - Considered to have a constant thickness: exfoliation of surface layers is neglected
  - Steady burning: heat loss equals heat gain at front surface

4.2.2.4 EXPERIMENT DESCRIPTION

Cone Calorimeter test

4.2.2.5 DATA SET

- Cone Calorimeter test data of triple-layered corrugated cardboard with thickness of 15 mm, density of 116 kg/m^3 and applied heat-flux levels ranging from 8 to 75 kW/m^2 is found.
- For ignition-data analysis, only time-to-ignition with respect to applied heat-flux data will be used.
- For burning-rate data analysis, data for the entire testing time duration mass loss and heat release during testing period with respect to applied heat flux will be used.

4.2.2.6 UNCERTAINTY

Uncertainty in Experiment Data

- The uncertainty in the mass loss rate data used for comparison between data and model outputs is estimated via statistical approach, taking the standard deviation (0.58 g/sm^2) from the mean of a steady burning of five identical PMMA tests conducted in a Cone Calorimeter.[20] The estimated uncertainty is 1.4 g/sm^2, which is found by calculating the 95% confidence interval applying student t distribution with a sample size of 5.
- The uncertainty in time-to-ignition data used for comparison is estimated via statistical approach, taking two to four identical Cone Calorimeter test data at heat fluxes ranging from 25 to 75 kW/m^2 of this cardboard. A 95% confidence interval is calculated for each heat-flux level assuming student t distribution.
- Assume:
  - Uncertainties are comparable to those of similar flat surfaces pyrolyzing under heating

Uncertainty in Modeling Outputs

- Uncertainty in t_{ig} and $\dot{m}''$ can be estimated from a linear regression process and using the Law of Propagation of Uncertainty

MODELING OUTPUT: MASS LOSS RATE (MLR)

- Ignition and Burning-Rate Data Analysis

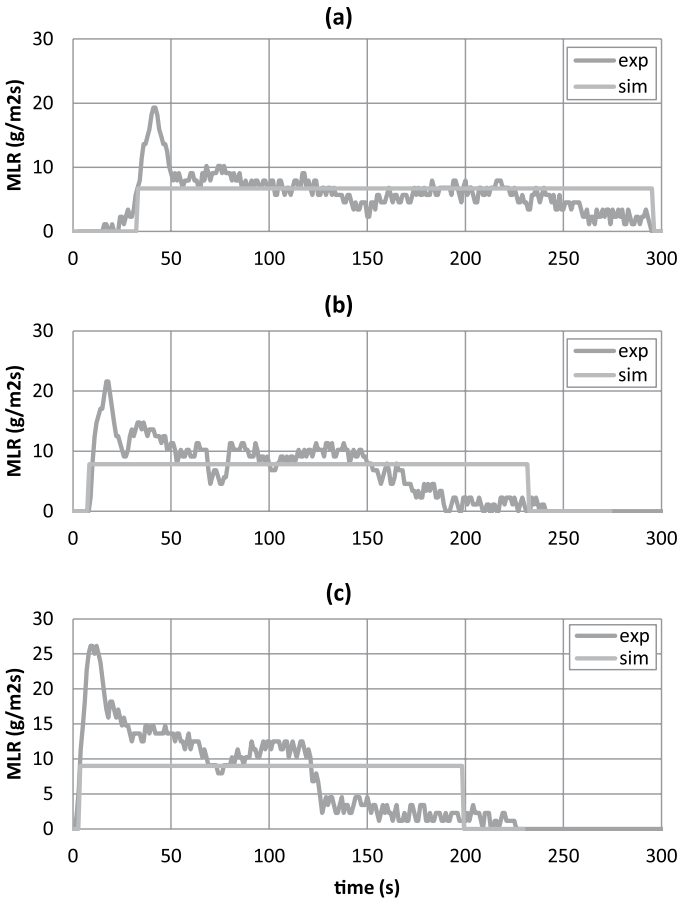

Figure 4-9. Mass-loss rate (MLR) comparisons for corrugated cardboard between actual MLR from experiment (exp) and modeled MLR (sim) at different applied heat-flux levels – (a) MLR at 25 kW/m²; (b) MLR at 50 kW/m²; and (c) MLR at 75 kW/m². Note that data shown were used to estimate model-parameter values.

4.2.3 Commentary

GENERAL COMMENTS ABOUT MLR

- Ignition and Burning-Rate Data Analysis at HF = 25, 50 and 75 kW/m²: Good agreement exists between experiment data and all modeling results
- The peaks are not captured in all cases, for averaged mass-loss rates have been used to estimate burning rate in the model.

LIMITATION IN MODELING

- When using the Simple Analytical Model to simulate pyrolysis of triple-layered corrugated cardboard (density 116 kg/m^3, thickness 15 mm), test data from a bench-scale Cone Calorimeter experiment at several heat-flux levels have been utilized to estimate the time-to-ignition from exposure to heating and the mass-loss rate at steady-burning stage after ignition. The comparison between the model outputs (time-to-ignition and steady-burning rate) and the data from bench-scale experiment showed good agreement for both checking purposes, where the same heat flux levels (25, 50, and 75 kW/m^2) used in parameter estimation have been considered.
- Although the modeling predictions of time-to-ignition and steady-burning rate in this example seems to be reasonable, limitation of this Simple Analytical Modeling should be noted, which is that the model is for thermally-thick-behaving materials and steady burning after ignition.

Example 4.3 Modeling Fire Retarded FRP Composite

4.3.1 Model Parameter Table

Model Parameters		Unit	Estimated Values and Estimation Methods
Ignition Parameters	T_{ig}	°C	523 ± 5
			Ignition Data Analysis
	$\dot{q}''_{cr}$	kW/m^2	29 ± 1
			Measurement, Cone Calorimeter by bracketing
	kρc	kJ^2/m^{4}K^{2}s	1.834 ± 0.408
			Ignition Data Analysis
Burning-Rate Parameters	$\Delta h_{c,eff}$	g/s-m^2	18.3 ± 6.7
			Burning-Rate Data Analysis
	Δh_g	kJ/g	13.7 ± 3.5
			Burning-Rate Data Analysis
Parameters for Specifying Conditions	h_c	W/m^{2}K	12 ± 0.5
			Reference value for horizontal position in Cone Calorimeter
	T_∞	°C	23 ± 3.45
			Measurement
	ε	-	0.9 ± 0.09
			Approximated
	Δt_{burn}	s	$\frac{(609)(8.9)}{0.073\dot{q}''_e + 0.830}$
			Burning-Rate Data Analysis

4.3.2 Validation

4.3.2.1 MODELING GOAL

Estimate model parameters for conducting modeling of pyrolysis of fire retarded FRP composite under various heating rates – heat-flux levels ranging up to ~ 75 kW/m^2.

4.3.2.2 MODEL TYPE

Thermally-thick model for ignition analysis (Quintiere and Harkleroad, ASTM E 1321) and steady burning model

4.3.2.3 MODELING APPROACH

- Pre-ignition stage is
  - Inert: non-uniform charring is considered to be evenly distributed
  - Thermally-thick: heat transfer does not reach back surface
- Post-ignition stage is
  - Considered to have instantaneous release of volatiles from solid to gas phase
  - Considered to have a constant thickness
  - Steady burning: heat loss equals heat gain at front surface

4.3.2.4 EXPERIMENT DESCRIPTION

Cone Calorimeter test

4.3.2.5 DATA SET

- Cone Calorimeter test data of FRP composite with thickness of 9.2 mm, density of 1900 kg/m3, and applied heat-flux levels ranging from 20 to 75 kW/m^2 is found.
- For ignition-data analysis, only time-to-ignition with respect to applied heat-flux data will be used.
- For burning-rate data analysis, data for the entire testing time duration mass loss and heat release during testing period with respect to applied heat flux will be used.

4.3.2.6 UNCERTAINTY

Uncertainty in Experiment Data

- The uncertainty in the mass-loss rate data used for comparison between data and model outputs is estimated via statistical approach, taking the standard deviation (0.58 g/sm^2) from the mean of a steady burning of five identical PMMA tests conducted in a Cone Calorimeter[20]. The estimated uncertainty is 1.4 g/sm^2, which is found by calculating the 95% confidence interval applying student t distribution with a sample size of five.
- The uncertainty in time-to-ignition data used for comparison is estimated via statistical approach, taking four to five identical Cone Calorimeter test data at heat fluxes ranging from 50 and 75 kW/m^2 of this cardboard. A 95% confidence interval is calculated for each heat-flux level assuming student t distribution.
- Assume:
  - Uncertainties are comparable to those of similar flat surfaces pyrolyzing under heating

Uncertainty in Modeling Outputs

- Uncertainty in t_{ig} and $\dot{m}''$ can be estimated from the linear-regression process and using the Law of Propagation of Uncertainty

4.3.2.7 MODELING OUTPUT: MASS LOSS RATE (MLR)

- Ignition and Burning-Rate Data Analysis

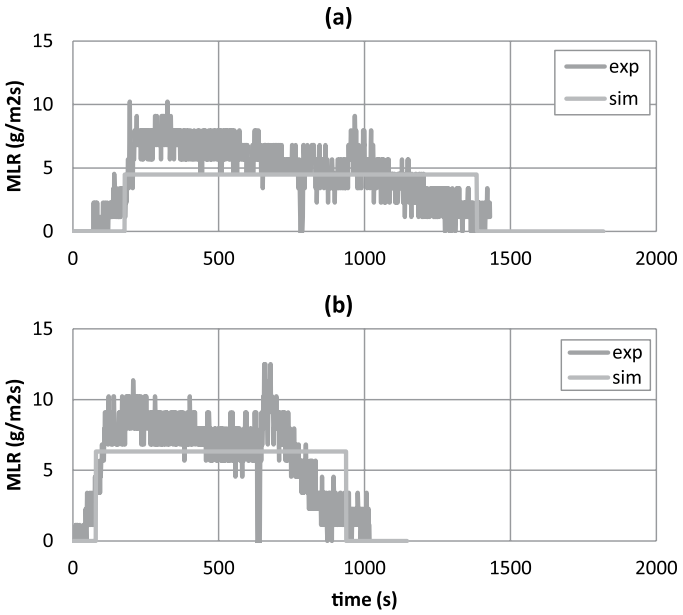

Figure 4-10. Mass-loss rate (MLR) comparisons for fire-retarded FRP composite between actual MLR from experiment (exp) and modeled MLR (sim) at different applied heat-flux levels – (a) MLR at 50 kW/m²; and (b) MLR at 75 kW/m². Note that data shown were used to estimate model-parameter values.

4.3.3 Commentary

GENERAL COMMENTS ABOUT MLR

- Ignition and Burning-Rate Data Analysis at HF = 25, 50, and 75 kW/m²: Good agreement exists between experiment data and all modeling results
- The peaks are not captured in all cases, for averaged mass-loss rates have been used to estimate burning rate in the model

LIMITATION IN MODELING

- When using the Simple Analytical Model to simulate pyrolysis of a fire-retarded fiberglass-reinforced polymer (FRP) composite (density 2100 kg/m³, thickness 8.9 mm, 71 wt% of composite remains as residue), test data from a bench-scale Cone Calorimeter experiment at several heat-flux levels have been utilized to estimate the time to ignition from exposure to heating and the mass-loss rate at steady-burning stage after ignition. The comparison between the model outputs (time-to-ignition and steady-burning rate) and the data from bench-scale experiment showed good agreement for both checking purposes- where the same heat-flux levels (50 and 75 kW/m²) used in parameter estimation have been considered.

- Although the modeling predictions of time-to-ignition and steady-burning rate in this example seems to be reasonable, limitation of this Simple Analytical Modeling should be noted, which is that the model is for thermally-thick-behaving materials and steady burning after ignition.

Example 4.4 Modeling Plywood

4.4.1 Model Parameter Table

Model Parameters		Unit	Estimated Values and Estimation Methods
Ignition Parameters	T_{ig}	°C	377 ± 11
			Ignition Data Analysis
	$\dot{q}''_{cr}$	kW/m^2	14.5 ± 1
			Measurement, Cone Calorimeter by bracketing
	kρc	kJ^2/m^{4}K^{2}s	0.501 ± 0.138
			Ignition Data Analysis
Burning-Rate Parameters	$\Delta h_{c,eff}$	g/s-m^2	14.4 ± 1.2
			Burning-Rate Data Analysis
	Δh_g	kJ/g	8.0 ± 1.1
			Burning-Rate Data Analysis
Parameters for Specifying Conditions	h_c	W/m^{2}K	12 ± 0.5
			Reference value for horizontal position in Cone Calorimeter
	T_∞	°C	20 ± 2
			Measurement
	ε	-	0.9 ± 0.09
			Approximated
	Δt_{burn}	s	$\frac{(542)(11.1)}{0.125\dot{q}''_e + 4.110}$
			Burning-Rate Data Analysis

4.4.2 Validation

4.4.2.1 MODELING GOAL

Estimate model parameters for conducting modeling of pyrolysis of plywood under various heating rates – heat-flux levels ranging up to ~ 100 kW/m^2.

4.4.2.2 MODEL TYPE

Thermally-thick model for ignition analysis (Quintiere and Harkleroad, ASTM E 1321) and steady-burning model

4.4.2.3 MODELING APPROACH

- Pre-ignition stage is
  - Inert
  - Thermally thick: heat transfer does not reach back surface

- Post-ignition stage is
  - Considered to have instantaneous release of volatiles from solid to gas phase: any mass transportation effect on pyrolysis is neglected and pyrolysis is considered as surface phenomenon only
  - Considered to have a constant thickness: shrinkage, regression and bending near the end is neglected
  - Steady burning: heat loss equals heat gain at front surface

4.4.2.4 EXPERIMENT DESCRIPTION

Cone Calorimeter test

4.4.2.5 DATA SET

- Cone Calorimeter test data of Douglas Fir plywood with thickness of 11.1 ± 0.1 mm, density of 542 ± 11 kg/m^3 and applied heat flux levels ranging from 14 to 100 kW/m^2 is found (student t distribution, $\alpha = 0.05$, sample size of 10).
- For ignition data analysis, only time-to-ignition with respect to applied heat-flux data will be used.
- For burning-rate data analysis, data for the entire testing time duration mass loss and heat release during testing period with respect to applied heat flux will be used.

4.4.2.6 UNCERTAINTY

Uncertainty in Experiment Data

- The uncertainty in the mass-loss rate data used for comparison between data and model outputs is estimated via statistical approach, taking the standard deviation (0.58 g/sm^2) from the mean of a steady burning of five identical PMMA tests conducted in a Cone Calorimeter[20]. The estimated uncertainty is 1.4 g/sm^2, which is found by calculating the 95% confidence interval applying student t distribution with a sample size of five.
- The uncertainty in time-to-ignition data used for comparison is estimated via statistical approach, taking three to four identical Cone Calorimeter test data at heat fluxes ranging from 25 to 75 kW/m^2 of this cardboard. A 95% confidence interval is calculated for each heat-flux level assuming student t distribution.
- Assume:
  - Uncertainties are comparable to those of similar flat surfaces pyrolyzing under heating

Uncertainty in Modeling Outputs

- Uncertainty in t_{ig} and $\dot{m}''$ can be estimated from linear regression process and using the Law of Propagation of Uncertainty

4.4.2.7 MODELING OUTPUT: MASS LOSS RATE (MLR)

- Ignition and Burning-Rate Data Analysis

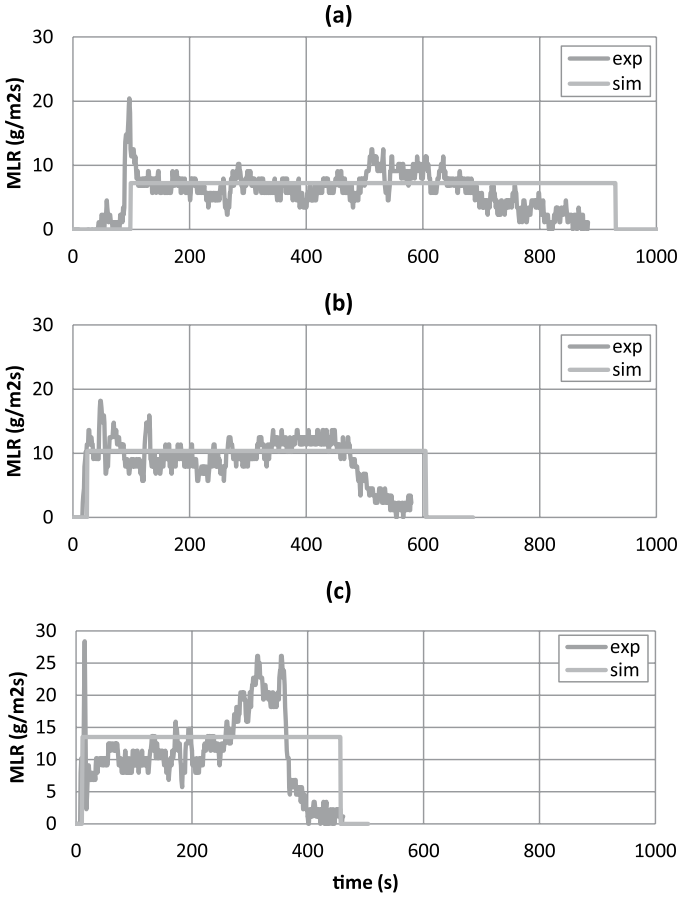

Figure 4-11. Mass-loss rate (MLR) comparisons for plywood between actual MLR from experiment (exp) and modeled MLR (sim) at different applied heat-flux levels – (a) MLR at 25 kW/m²; (b) MLR at 50 kW/m²; and (c) MLR at 75 kW/m². Note that data shown were used to estimate model-parameter values.

4.4.3 Commentary

GENERAL COMMENTS ABOUT MLR

- Ignition and Burning-Rate Data Analysis at HF = 25, 50 and 75 kW/m^2: Good agreement exists between experiment data and all modeling results

LIMITATION IN MODELING

- When using the Simple Analytical Model to simulate pyrolysis of Douglas Fir Plywood, test data from a bench-scale Cone Calorimeter experiment at several heat flux levels have been utilized to estimate the time-to-ignition from exposure to heating and the mass-loss rate at steady-burning stage after ignition. The comparison between the model outputs (time-to-ignition and steady-burning rate) and the data from bench-scale experiment showed good agreement for both checking purposes where the same heat-flux levels (25, 50 and 75 kW/m^2) used in parameter estimation have been considered.
- Although the modeling predictions of time-to-ignition and steady-burning rate in this example seems to be reasonable, limitation of this Simple Analytical Modeling should be noted, which is that the model is for thermally-thick-behaving materials and steady burning after ignition.

Case 2: Thermally-Thin, Inert at Pre-Ignition with Steady Burning at Post-ignition

Virtual Microstructure of Virgin Material

- Homogeneous flat surface single layer in horizontal position
- Pre-ignition stage: inert, thermally thin
- Post-ignition stage: steady burning

General Model-Parameter Table

- Ignition and burning-rate parameters are considered in this example
- Reduced Model Parameter Table (see Table 4-7):

Table 4-7. Model Parameter Table for Case 2 Examples

Ignition Parameters	T_{ig}	Surface Temperature at Ignition
	$\dot{q}''_{cr}$	Critical Heat Flux for Ignition
	$\rho c \delta$	Thermal Capacity (Thermally-thin)
Burning-Rate Parameters	$\Delta h_{c,eff}$	Effective Heat-of-Combustion
	Δh_g	Heat-of-Gasification
Parameters for Specifying Conditions	h_c	Convection Coefficient
	T_∞	Ambient Temperature
	ε	Surface Emissivity/Absorptivity
	Δt_{burn}	Burn Duration

Example 4.5 Modeling Sandwich Composite – GRP Skin with Balsawood Core

This material is composed of approximately 1 mm thickness of laminated glass-reinforced polymer (GRP) over approximately 25 mm thickness of resin-soaked balsa wood core as a skin layer (sandwich construction). The resin used in the GRP and with balsa wood is vinyl ester (VEX). The light weight core, balsa wood acts as an insulating layer for the thin GRP skin and allows the ignition data to behave thermally thin. This thermal behavior is examined by plotting $1/t_{ig}^n$ vs. applied heat flux where its best fitness of a linear regression occurs near n = 0.9.

4.5.1 Model Parameter Table

Model Parameters		Unit	Estimated Values and Estimation Methods
Ignition Parameters	T_{ig}	°C	350 ± 36
			Ignition Data Analysis
	$\dot{q}''_{cr}$	kW/m^2	12.5 ± 2.5
			Measurement, Cone Calorimeter by bracketing
	kρc	kJ^2/m^{4}K^{2}s	7.625 ± 19.1
			Ignition Data Analysis
Burning-Rate Parameters	$\Delta h_{c,eff}$	g/s-m^2	23.5 ± 2.1
			Burning-Rate Data Analysis
	Δh_g	kJ/g	8.7 ± 1.4
			Burning-Rate Data Analysis
Parameters for Specifying Conditions	h_c	W/m^{2}K	12 ± 0.5
			Reference value for horizontal position in Cone Calorimeter
	T_∞	°C	20 ± 5
			Measurement
	ε	-	0.9 ± 0.09
			Approximated
	Δt_{burn}	s	$\frac{(600)(1.3)}{0.129\dot{q}''_e + 7.415}$
			Burning-Rate Data Analysis

4.5.2 Validation

4.5.2.1 MODELING GOAL

Estimate model parameters for conducting modeling of pyrolysis of vinyl ester glass-reinforced polymer (GRP) skin with 1" thick resin soaked balsa wood core sandwich composite under various heating rates – heat-flux levels ranging up to ~ 90 kW/m^2.

4.5.2.2 MODEL TYPE

Thermally-thin model for ignition analysis and steady-burning model

4.5.2.3 MODELING APPROACH

- Pre-ignition stage is
  - Inert: decomposition with bubbling and changing color on surface before ignition is neglected
  - Thermally-thin GRP skin: heat transfer does reach back surface quickly and the surface layer (vinyl ester resin GRP) is considered to have uniform temperature throughout
  - Control volume for ignition analysis is the thermally-thin GRP skin layer on the front surface facing the heating source
- Post-ignition stage is
  - Considered to have instantaneous release of volatiles from solid to gas phase: any mass-transportation effect on pyrolysis is neglected and pyrolysis is considered as surface phenomenon only
  - Considered to have a constant thickness
  - Steady burning: heat loss equals heat gain at front surface
  - 30% of the GRP skin layer (density of 2000 kg/m^3) is consumed via burning, and this information is used to calculate the model's burnout time prediction

4.5.2.4 EXPERIMENT DESCRIPTION

Cone Calorimeter test

4.5.2.5 DATA SET

- Cone Calorimeter test data of this sandwich composite panel with thickness of 28 mm, density of 500 kg/m^3 and applied heat flux levels ranging from 15 to 90 kW/m^2 is found.
- For ignition data analysis, only time-to-ignition with respect to applied heat-flux data will be used.
- For burning-rate data analysis, data for the entire testing time duration mass loss and heat release during testing period with respect to applied heat flux will be used.

4.5.2.6 UNCERTAINTY

Uncertainty in Experiment Data

- The uncertainty in the mass-loss rate data used for comparison between data and model outputs is estimated via a statistical approach, taking the standard deviation (0.58 g/sm^2) from the mean of a steady burning of five identical PMMA tests conducted in a Cone Calorimeter.[20] The estimated uncertainty is 1.4 g/sm^2, which is found by calculating the 95% confidence interval applying student t distribution with a sample size of five.
- The uncertainty in time-to-ignition data used for comparison is estimated via a statistical approach, taking three to four identical Cone Calorimeter test data at heat fluxes ranging from 35 to 75 kW/m^2 of this cardboard. A 95% confidence interval is calculated for each heat-flux level assuming student t distribution.
- Assume:
- Uncertainties are comparable to those of similar flat surfaces pyrolyzing under heating

Uncertainty in Modeling Outputs

- Uncertainty in t_{ig} and $\dot{m}''$ can be estimated from a linear regression process and using the Law of Propagation of Uncertainty

4.5.2.7 MODELING OUTPUT: MASS LOSS RATE (MLR)

- Ignition and Burning-Rate Data Analysis

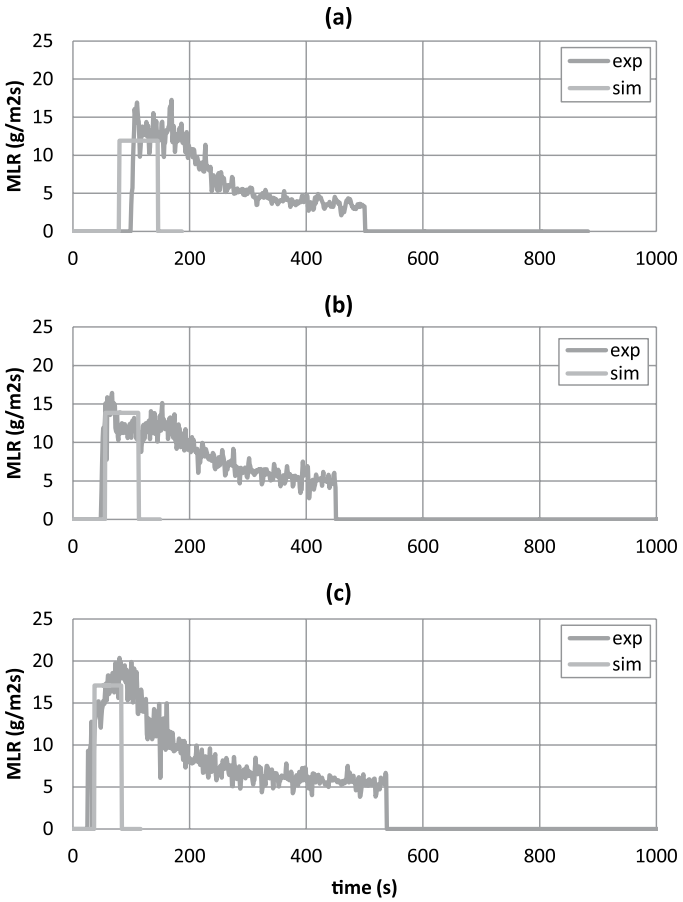

Figure 4-12. Mass-loss rate (MLR) comparisons for sandwich composite – GRP skin with balsawood core – between actual MLR from experiment (exp) of the composite and modeled MLR (sim) of GRP skin at different applied heat-flux levels – (a) MLR at 35 kW/m²; (b) MLR at 50 kW/m²; and (c) MLR at 75 kW/m². Note that data shown were used to estimate model-parameter values.

4.5.3 Commentary

GENERAL COMMENTS ABOUT MLR

- Ignition and Burning-Rate Data Analysis at HF = 35, 50 and 75 kW/m^2: Good agreement exists between experiment data and all modeling results

LIMITATION IN MODELING

- When using the Simple Analytical Model to simulate pyrolysis of Douglas Fir Plywood, test data from a bench-scale Cone Calorimeter experiment at several heat flux levels have been utilized to estimate the time-to-ignition from exposure to heating and the mass-loss rate at steady-burning stage after ignition. The comparison between the model outputs (time-to-ignition and steady-burning rate) and the data from bench-scale experiment showed good agreement for both checking purposes where the same heat-flux levels (35, 50 and 75 kW/m^2) used in parameter estimation have been considered.
- Although the modeling predictions of time-to-ignition and steady-burning rate in this example seem to be reasonable, limitation of this Simple Analytical Modeling should be noted, which is that the model is for thermally-thick-behaving materials and steady burning after ignition.

Example 4.6 Modeling Thin FRP Composite

The rigid FRP panel chosen for use in full-scale testing is commercially available and advertised for use as ceiling and wall linings (flat surfaces) in environments designed to be moisture- and mold-free. The panel has a Class C (ASTM E84) flame-spread rating. It consists of modified polyester copolymer and inorganic fillers as the resin base and reinforced with a weave of random chopped fiberglass. The panel's thickness is 0.09" (2.3 mm) nominal, with a smooth backface and a pebbled, embossed white front surface. When this material is tested for ignition in Cone Calorimeter test, thermally-thin behavior is observed. This thermal characteristic is examined by plotting $1/t_{ig}^{n}$ vs. applied heat flux where its best fitness of a linear regression occurs near n = 1.0.

4.6.1 Model Parameter Table

Model Parameters		Unit	Estimated Values and Estimation Methods
Ignition Parameters	T_{ig}	°C	397 ± 10
			Ignition Data Analysis
	$\dot{q}''_{cr}$	kW/m^2	16 ± 1
			Measurement, Cone Calorimeter by bracketing
	kρc	kJ^2/m^{4}K^{2}s	4.333 ± 4.369
			Ignition Data Analysis
Burning-Rate Parameters	$\Delta h_{c,eff}$	g/s-m^2	25.5 ± 1.8
			Burning-Rate Data Analysis
	Δh_g	kJ/g	16.3 ± 4.7
			Burning-Rate Data Analysis
Parameters for Specifying Conditions	h_c	W/m^{2}K	12 ± 0.5
			Reference value for horizontal position in Cone Calorimeter
	T_∞	°C	23 ± 3.45
			Measurement
	ε	-	0.9 ± 0.09
			Approximated
	Δt_{burn}	s	$\frac{(600)(2.0)}{0.061\dot{q}''_e + 1.194}$
			Burning-Rate Data Analysis

4.6.2 Validation

4.6.2.1 MODELING GOAL

Estimate model parameters for conducting modeling of pyrolysis of this Class C FRP composite under various heating rates – heat-flux levels ranging up to ~ 75 kW/m^2.

4.6.2.2 MODEL TYPE

Thermally-thin model for ignition analysis and steady burning model

4.6.2.3 MODELING APPROACH

- Pre-ignition stage is
  - Inert: decomposition with crackling sound and changing color on surface before ignition is neglected
  - Thermally thin: heat transfer does reach back surface quickly, and the entire layer is considered to have uniform temperature throughout
  - Control volume for ignition analysis is the thermally-thin GRP skin layer on the front surface facing the heating source
- Post-ignition stage is
  - Considered to have instantaneous release of volatiles from solid to gas phase: any mass-transportation effect on pyrolysis is neglected and pyrolysis is considered as a surface phenomenon only
  - Considered to have a constant thickness
  - Steady burning: heat loss equals heat gain at front surface
  - 40% of the FRP composite sheet (density of 1500 kg/m^3) is consumed via burning, and this information is used to calculate the model's burnout time prediction

4.6.2.4 EXPERIMENT DESCRIPTION

Cone Calorimeter test

4.6.2.5 DATA SET

- Cone Calorimeter test data of this sandwich composite panel with thickness of 2 mm, density of 1500 kg/m^3 and applied heat-flux levels ranging from 15 to 75 kW/m^2 is found.
- For ignition data analysis, only time-to-ignition with respect to applied heat-flux data will be used.
- For burning-rate data analysis, data for the entire testing time duration mass loss and heat release during testing period with respect to applied heat flux will be used.

4.6.2.6 UNCERTAINTY

Uncertainty in Experiment Data

- The uncertainty in the mass-loss rate data used for comparison between data and model outputs is estimated via a statistical approach, taking the standard deviation (0.58 g/sm^2) from the mean of a steady burning of five identical PMMA tests conducted in a Cone Calorimeter[20]. The estimated uncertainty is 1.4 g/sm^2, which is found by calculating the 95% confidence interval applying student t distribution with a sample size of five.
- The uncertainty in time-to-ignition data used for comparison is estimated via a statistical approach, taking two to three identical Cone Calorimeter test data at heat fluxes ranging from 25 to 75 kW/m^2 of this cardboard. A 95% confidence interval is calculated for each heat-flux level assuming student t distribution.
- Assume:
  - Uncertainties are comparable to those of similar flat surfaces pyrolyzing under heating

Uncertainty in Modeling Outputs

- Uncertainty in t_{ig} and $\dot{m}''$ can be estimated from a linear regression process and using the Law of Propagation of Uncertainty

4.6.2.7 MODELING OUTPUT: MASS LOSS RATE (MLR)

- Ignition and Burning-Rate Data Analysis

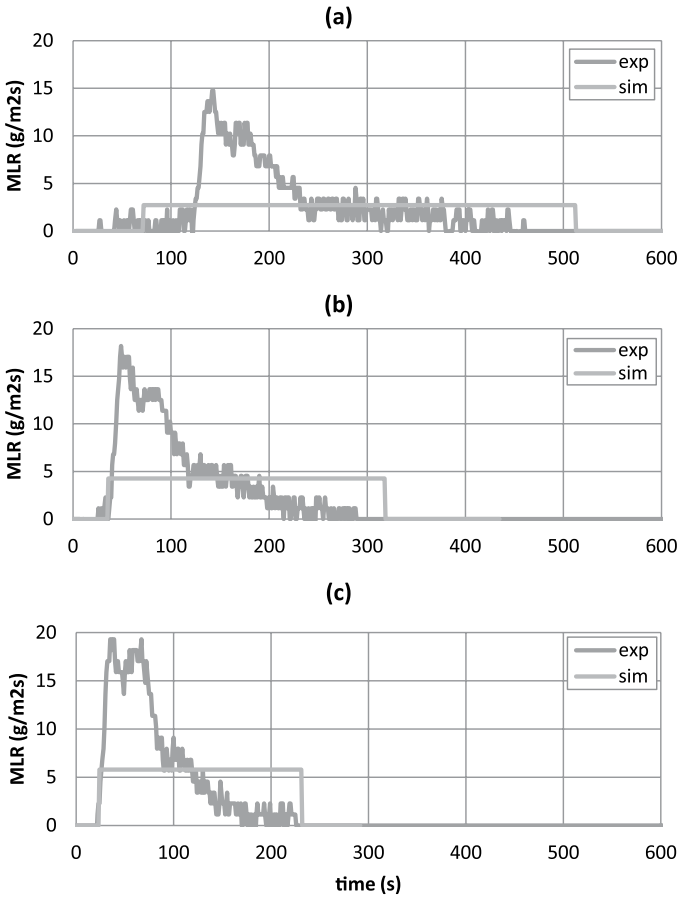

Figure 4-13. Mass-loss rate (MLR) comparisons for thin FRP composite between actual MLR from experiment (exp) and modeled MLR (sim) at different applied heat-flux levels – (a) MLR at 25 kW/m²; (b) MLR at 50 kW/m²; and (c) MLR at 75 kW/m². Note that data shown were used to estimate model-parameter values.

4.6.3 Commentary

GENERAL COMMENTS ABOUT MLR

- Ignition and Burning-Rate Data Analysis at HF = 25, 50 and 75 kW/m^2: Good agreement exists between experiment data and all modeling results
- The peaks are not captured in all cases, for averaged mass-loss rates have been used to estimate burning rate in the model

LIMITATION IN MODELING

- In this example, the Simple Analytical Model is used to simulate pyrolysis of thermally -thin-behaving FRP composite sheet. Test data from a bench-scale Cone Calorimeter experiment at several heat-flux levels have been utilized to estimate the time-to-ignition from exposure to heating and the mass-loss rate at steady-burning stage after ignition. The comparison between the model outputs (time-to-ignition and stead-burning rate) and the data from bench-scale experiment showed good agreement for both checking purposes where the same heat-flux levels (25, 50 and 75 kW/m^2) used in parameter estimation have been considered. To improve modeling results, one may consider taking the peak average of the mass-loss rate and the heat-release rates to estimate heat-of-gasification, for most of the burning occurs near the peak. The tail following the peak (MLR or HRR curve) extends for a longer period of time until flame-out, where smaller percentage of the combustible resin between fiber glass layers is burning off at in-depth.
- Although the modeling predictions of time-to-ignition and steady-burning rate in this example seems to be reasonable, limitation of this Simple Analytical Modeling should be noted, which is that the model is for thermally-thick-behaving materials and steady burning after ignition.

References

1 Fuss, S.; and Hamins, A., "An Estimate of the Correction Applied to Radiant Flame Measurements due to Attenuation by Atmospheric CO2 and H2O," *Fire Safety Journal*, 37 (2002) 181-190.

2 Urbas, J.; and Parker, W., "Surface Temperature Measurement in a Fire Environment Using an Infrared Pyrometer," in *Eighth International Symposium on Fire Safety Science*, Beijing, China, (2005) 1401-1412.

3 Urbas, J., *et al.*, "Surface Temperature Measurements on Burning Materials Using an Infrared Pyrometer: Accounting for Emissivity and Reflection Of External Radiation," *Fire and Materials*, 28 (2004) 33-53.

4 Omrane, A., *et al.*, "Surface Temperature Measurement of Flame Spread Using Thermographic Phosphors," in *Seventh International Symposium on Fire Safety Science*, Worcester, MA, (2003), 141-152

5 Göransson, U.; and Omrane, A., "Surface Temperature Measurements in the Cone Calorimeter Using Phosphorescence," in *10th Interflam Conference*, Edinburgh, Scotland, (2004), 1431-1442.

6 Omrane, A., *et al.*, "Surface Temperature of Decomposing Construction Materials Studied by Laser-Induced Phosphorescence," *Fire and Materials*, 29 (2005) 39-51.

7 Thomson, H.; and Drysdale, D., "Flammability of Plastics, I: Ignition Temperatures," *Fire and Materials*, 11 (1987) 163-172.

8 Thomson, H., *et al.*, "An Experimental Evaluation of Critical Surface Temperature as a Criterion for Piloted Ignition of Solid Fuels," *Fire Safety Journa*l, 13 (1988) 185-196.

9 Abu-Zaid, M., "Effect of Water on Ignition of Cellulosic Materials," Ph.D. Thesis, Michigan State University, East Lansing, MI, (1988).

10 Atreya, A., "Pyrolysis, Ignition and Fire Spread on Horizontal Surfaces of Wood," Ph.D. Thesis, Harvard University, Cambridge, MA, (1983).

11 Atreya, A., *et al.*, "Effect of Sample Orientation on Piloted Ignition and Flame Spread," in *First International Symposium on Fire Safety Science*, Gaithersburg, MD, (1985), 97-109.

12 Fangrat, J., *et al.*, "Surface Temprature at Ignition of Wooden Based Slabs," *Fire Safety Journal*, 27 (1996) 249-259.

13 Janssens, M., "Thermophysical Properties of Wood and their Role in Enclosure Fire Growth," Ph.D. Thesis, University of Ghent, Ghent, Belgium, (1991).

14 Yudong, L,; and Drysdale, D., "Measurement of the Ignition Temperature of Wood," *Fire Safety Science*, 1 (1992) 25-30.

15 Quintiere, J.; and Harkleroad, M., "New Concepts for Measuring Flame Spread Properties," in *Fire Safety: Science and Engineering*, ASTM STP 882, June 16-17, 1984, Denver, CO, (1985), 239-267.

16 Dietenberger, M., "Ignitability Analysis Using the Cone Calorimeter and LIFT Apparatus," in *Twenty-Second International Conference on Fire Safety*, Columbus, OH, (1996).

17 Tewarson, A.; and Pion, R., "Flammability of Plastics. I. Burning Intensity," *Combustion & Flame*, 26 (1976) 85-103.

18 Petrella, V., "The Mass Burning Rate of Polymers, Wood and Liquids," *Journal of Fire and Flammability*, 11 (1980) 3-21.

19 Beaulieu, P.A.; and Dembsey, N.A., Fire Safety Journal 43 (2008) 410-428

20 Zhao, Lei, Bench Scale Apparatus Measurement Uncertainty and Uncertainty Effects on Measurement of Fire Characteristics of Material Systems, MS Thesis, Fire Protection Engineering, WPI, 2005-04-27, ETD-050105-182456.

Chapter 5
Comprehensive Models

Understanding Model 90
General Description of Models 90
Brief Description of Typical Pyrolysis Models Available in the Fire Community 91
Governing Equations 92
Model Parameters and Measurement Methods 96
Virtual Microstructure of Virgin Material and Decomposition Kinetics Type 96
Model-Parameter Table 98
Model-Parameter Measurement Methods 99
Parameter-Estimation Process 113
Sensitivity Analysis 117
Example Case 1 and 2 117
Example Case 3 (Global Sensitivity Analysis: Morris Method) 117
Uncertainty Analysis 119
Optimization 121
Example Cases Overview 124
Case 1: Single-Step Decomposition Reaction without Residue Production 125
Virtual Microstructure of Virgin Material 125
Decomposition Kinetics Type 125
General Model-Parameter Table 125
Example 5.1 Modeling Poly(methylmethacrylate), PMMA 126
Case 2: Single-Step Decomposition Reaction With Residue Production 135
Virtual Microstructure of Virgin Material 135
Decomposition Kinetics Type 135
General Model Parameter Table 135
Example 5.2 Modeling Triple-layered Corrugated Cardboard 136
Case 3: Two-Step Decomposition Reaction With Residue Production 144
Virtual Microstructure of Virgin Material 144
Decomposition Kinetics Type 144
General Model Parameter Table 144
Example 5.3 Modeling FRP Composite with Modified Acrylic Resin with High-charring Inorganic Additive 145
Example 5.4 Modeling Plywood 159
References 169

Understanding Model

General Description of Models

Comprehensive pyrolysis models are models that account for physical and chemical responses of fire characteristics of a solid material.[1,2,3] These models utilize fundamental conservation equations to describe the changes in a material during pyrolysis. Typically, models are constructed to conserve mass and energy when the material is being heated and/or thermally decomposed. Numerical calculations are conducted using various methods – finite difference, finite element, or integral formats, where governing equations are transformed to system of ODEs instead of PDEs using simplifications – to determine mass loss and temperature profiles from the heat-exposed front surface to unexposed back surface with respect to increasing time.

The thermal-decomposition process in comprehensive pyrolysis modeling can be modeled by two different approaches: reactions that are infinitely fast or finite. When thermal decomposition is infinitely fast, the pyrolysis front becomes an infinitely thin reaction zone where reactants are consumed instantaneously into products with releasing or consuming reaction heat. In this case, heat transfer is considered as a limiting factor for modeling the pyrolysis problem. Typically, a pre-determined pyrolysis temperature is used to locate the pyrolysis front. When the thermal-decomposition reaction rate is modeled as finite, the pyrolysis front has a finite thickness. Whether the virgin material pyrolyzes completely (single solid-state case) or partially (multiple solid-state case) to fuel vapor, the assumption used in this approach allows the model to approximate the pyrolysis kinetics as well as the heat transfer throughout the solid fuel. When pyrolysis kinetics is explicitly considered in modeling, pyrolyzates can be produced at various locations within the pyrolysis front, which has a finite thickness. By performing numerical calculations in these comprehensive pyrolysis models, the temperature profile is obtained for a solid fuel, and, depending on the local temperature, the pyrolysis reaction(s) rate is calculated, allowing the reactants to be consumed to produce pyrolyzates or other types of solid phase materials with associated energy consumption. Typically, an Arrhenius-type expression is used for describing the pyrolysis kinetics. Some models of this kind consider mass and heat transfer of gases through a decomposed solid-phase product layer, which requires additional governing equations to be solved.

Although accounting for physical and chemical phenomena observed during pyrolysis explicitly is a merit for comprehensive models, difficulties arise when using these models due to the numerous unknown model parameters that the model user needs to estimate. The ability of modeling various aspects of the pyrolysis problem results in greater complexity of the model. Therefore, the number of parameters involved in the simulation can dramatically increase, which results in the need of extra effort in estimating the additional unknown parameters.

Brief Description of Typical Pyrolysis Models Available in the Fire Community

In this section, a brief discussion of well-known comprehensive pyrolysis models available to fire community is given. These include a pyrolysis model in Fire Dynamics Simulator (FDS) version 6[1], Thermakin[2], and GPYRO.[3] Typically, pyrolysis modeling is composed of modeling of mass, energy and momentum transfers, and decomposition kinetics within the decomposing material.

Pyrolysis Model in FDS version 6[1]

In FDS, mass transfer within a porous solid phase material is not modeled. The assumption is that, when decomposition reaction occurs, the volatiles from solid decomposition are released instantaneously into the gas phase. Additionally, condensation of gaseous products within the solid phase is assumed to be negligible. Energy transfer within a solid is described via a one-dimensional heat conduction equation for the solid phase, including the voids from the pores, which allows the model to track temperature changes of the solid phase with respect to time and space. This approach is allowed due to the local thermal equilibrium assumed between the solid and the volatiles at all times. In this equation, the heat-source term is included and it accounts for heat release or absorption due to chemical reactions, radiative absorption, and emission-in-depth. In-depth radiative absorption and emission is modeled as a "two-flux" model based on the Schuster-Schwarzschild approximation,[4] where the radiative intensity is assumed to be constant at the "forward" and "backward" hemispheres. At the front surface boundary, convective heat transfer is modeled via a combination of natural and forced convection correlation for horizontal or vertical surfaces. Momentum transfer is not solved for in the solid phase in this model. Decomposition kinetics are modeled using an Arrhenius type expression with an n^{th} order reaction model. This kinetic model allows decomposition of a single solid-phase component into another type of solid-phase component and/or volatiles to be modeled. The model can configure multiple layers with multiple reactions for decomposition.

Thermakin[2]

Thermakin models gas-phase mass transfer within a porous solid-phase material; however, the condense phase is immobile. The traveling of gases within the solid is governed by concentration gradients. Gases can be produced by chemical reactions and released to the gas phase. The model tracks the changes of gases in the volume. Transportation of energy is modeled by taking into account the conductive heat transfer through solids (the condensed phase in the porous solid) via Fourier's Law, convective heat transfer from one element to another due to the travel of gases and heat generation or consumption due to chemical reactions. Radiation transport within the condensed phase is modeled by considering a single element absorbing the external radiation via a maximum-absorption or random-absorption algorithm. For both cases, the external radiation is modeled to penetrate the material and behave in accordance with Beer-Lambert's law.[5] These approaches assume that the absorbing element also acts as a gray-body reflector and emitter. Convective heat transfer is modeled at the front surface boundary using a simple Newtonian heat-transfer equation, where the convection coefficient is a user-specified input parameter. Momentum transfer is not solved for in the solid phase in this model. Decomposition kinetics are

modeled using an Arrhenius-type expression with a first-order reaction model. This kinetic model allows decomposition of a single solid/liquid/gas phase component or two together into another type of a single or two solid/liquid/gas phase component(s) to be modeled. The model can configure multiple components with multiple reactions for decomposition.

GPYRO[3]

In GPYRO, the condensed phase and the gas phase within a porous solid material can be modeled separately. Transfer of condensed phase is prohibited by the model. Mass transfer of gases within the porous solid material is modeled by considering the convective transfer, where conversion of condensed phase mass to gas phase via chemical reactions is accounted for in the source term. Any changes in species mass due to reactions in condensed or gas phases are conserved. Transportation of energy in the condensed phase is modeled by considering heat transfer via conduction using Fourier's Law; source terms that account for volumetric rate of heat release (or absorption) due to condensed phase and volumetric rate of heat transfer from the condensed phase to the gas phase; and in-depth radiative heat transfer. In this model, in-depth radiative heat transfer accounts only for "one–way" radiation, meaning the penetration of radiation into the solid is calculated, but the emission from interior parts of the solid is not calculated. For energy transfer in the gas phase, conductive and diffusive heat transfers have been included in the model. For calculating the diffusive flux term, Fickian diffusion is applied, and all gases are assumed to have the same diffusion coefficient for simplification. Momentum transfer within the gas phase is conserved in this model by assuming a Darcian flow of the gases with buoyancy. For modeling of decomposition kinetics, an Arrhenius type expression with various reaction models is allowed to describe heterogeneous (gas phase – condensed phase) or homogeneous (gas phase – gas phase) reactions. The model can configure multiple layers with multiple reactions for decomposition.

The advantage of using GPYRO is that only this pyrolysis model comes with various numerical optimization algorithms, including Genetic Algorithm (GA), Shuffled Complex Evolution (SCE), and Stochastic Hill Climber (SHC). These algorithms can be used to estimate unknown model parameters by comparing modeling outputs to certain optimization targets, e.g., experiment data.

Governing Equations

Although the effect of the porous nature of the material can be simulated directly by considering the gas phase and the pore-free condense phase separately[3,6] in comprehensive pyrolysis modeling, a more simplified and general approach is to consider a single mixture of the two phases: gas and condense phase. By doing so, material porosity is accounted for indirectly.

In Table 5-1, the system of equations is given for a Comprehensive Model, where conservation equations are solved for a single, porous, condensed phase. Note that the equations are presented in a one-dimensional form in the z-direction, considering that typical pyrolysis modeling is conducted in 1D. Additionally, basic assumptions are the volume change of a cell is negligible ($\Delta z = const$), and gases produced from thermal decomposition leave the porous-condense phase instantaneously without any restriction. These equations are a simplified version of GPYRO's; hence, similarities in mathematical expression exist. See the technical[3] and user's guide[6] of GPYRO (http://code.google.com/p/gpyro) for more information.

The major difference in the system of equations between models in Comprehensive Models with finite-thickness pyrolysis fronts and those with infinitely thin pyrolysis fronts is the approach in mathematically describing the decomposition reaction in terms of its speed (finite or infinitely fast). In general, the location of the infinitely thin reaction zone is identified by a material-dependent temperature known as the pyrolysis temperature, T_p, that remains on the pyrolyzing surface for non-charring materials or propagates towards in-depth, leaving a char layer behind near the surface for charring materials. At this location, pyrolysis heat, ΔH_p, is consumed, and reaction reactants and products are consumed and released, respectively.

Table 5-1. General governing equations for comprehensive pyrolysis models

Governing Equations	Material Property Parameters
Condensed-phase mass conservation $\frac{\partial \bar{\rho}}{\partial t} = -\dot{\omega}'''_{fg}$ Condensed-phase species conservation $\frac{\partial (\bar{\rho} Y_i)}{\partial t} = \dot{\omega}'''_{fi} - \dot{\omega}'''_{di}$ Condensed-phase energy conservation $\frac{\partial (\bar{\rho}\bar{h})}{\partial t} = -\frac{\partial}{\partial z}\left(\underbrace{\dot{q}''}_{\substack{\text{Fourier's Law for cond.} \\ \therefore \dot{q}'' = -\bar{k}\frac{\partial T}{\partial z}}} \right) + \underbrace{\sum_{k=1}^{K} \dot{Q}'''_{s,k}}_{\substack{\text{sum of heat release / loss due to condense phase rxns, } \Delta H}} - \frac{\partial}{\partial z}\left(\underbrace{\dot{q}''_r}_{\substack{\text{in-depth rad heat transfer}}} \right) + \underbrace{\sum_{i=1}^{M} \left(\dot{\omega}'''_{fi} - \dot{\omega}'''_{di} \right) h_i}_{\substack{\text{sum of gas phase prod. sensible enthalpy}}}$ where $\bar{h} = \sum_{i=1}^{M} Y_i h_i = \sum_{i=1}^{M} \left(Y_i \left(\int_{T_d}^{T} \left(\underbrace{c_i(\theta)}_{\substack{\text{baseline and melting} (\Delta H_{m,i})}} \right) \mathrm{d}\theta \right) \right)$, $\bar{k} = \sum_{i=1}^{M} X_i k_i$, $\bar{c} = \sum_{i=1}^{M} Y_i c_i$ *Heterogeneous-reaction rate of the k^{th} gas-phase reaction for a general n^{th} order reaction when reaction zone is modeled with finite thickness (i.e., destruction rate of condensed-phase species A_k) $r_k = \dot{\omega}'''_{dA_k} = \underbrace{f(\alpha_{A_k})}_{=(1-\alpha_{A_k})^{n_k}} \frac{(\bar{\rho} Y_{A_k} \Delta z)_{\Sigma}}{\Delta z} Z_k \exp\left(-\frac{E_k}{RT} \right)$	$\bar{\rho}$, ρ_i $\bar{k}$, k_i ΔH_k $\bar{c}$, c_i $\Delta H_{m,i}$ n_k, Z_k, E_k

Initial and Boundary Conditions	Parameters for Specifying Conditions Related to Porous Solid Phase
Condensed-phase mass conservation $\bar{\rho}\big\|_{t=0} = \sum_{i=1}^{M} X_{i0}\rho_{i0}$ Condensed-phase species conservation $\bar{\rho}Y_i\big\|_{t=0} = \sum_{i=1}^{M}\left(X_{i0}\rho_{i0}\right)Y_{i0}$ Condensed-phase energy conservation $T^{\circ}\big\|_{t=0} = T_0 \quad \Rightarrow \bar{h}^{\circ}\big\|_{t=0} = \sum_{i=1}^{M}\left(Y_{i0}h_{i0}\left(T_0\right)\right)$ $-\bar{k}\left.\frac{\partial T}{\partial z}\right\|_{z=0} = \underbrace{\dot{q}''_{front\ surf.}}_{Specified\ flux\ at\ front\ surf.}$ $-\bar{k}\left.\frac{\partial T}{\partial z}\right\|_{z=\delta} = \underbrace{\dot{q}''_{back\ surf.}}_{Specified\ flux\ at\ back\ surf}$	X_{i0} Y_{i0} X_{j0} Y_{j0} $\bar{\varepsilon}$, ε_i

Nomenclature

Letters

c	Specific-heat capacity (J/kg–K)
E	Activation energy (kJ/mole)
h	Enthalpy (J/kg)
ΔH	Change in enthalpy (J/kg)
k	Thermal conductivity (W/m–K)
$\dot{m}''$	Mass flux (kg/m^2–s)
n	Exponent (reaction order)
$\dot{q}''$	Heat flux (W/m^2)
$\dot{Q}'''$	Volumetric rate of heat release or absorption (W/m^3)
r	Reaction rate (kg/m^3–s)
t	Time (s)
T	Temperature (K)
X	Volume fraction (–)
Y	Mass fraction (–)
z	Distance (m)
Z	Condensed-phase pre–exponential factor (s^{-1})

Greek symbols

δ	Thickness (m)
ε	Emissivity (–)
κ	In–depth radiation absorption coefficient (m^{-1})
ρ	Density (kg/m^3)
$\dot{\omega}'''$	Volumetric reaction rate (kg/m^3–s)

Subscripts

A	Species A
d	Destruction or datum
f	Formation
g	Gaseous, gas phase, or gasification
i	Condensed phase species i
k	Heterogeneous reaction k
m	Melting
p	Pyrolysis
0	Initial (as in T_0)
∞	Ambient

Superscripts

$\bar{(\,)}$	Weighted or averaged
$^\circ$	Value at present time

Model Parameters and Measurement Methods

Virtual Microstructure of Virgin Material and Decomposition Kinetics Type

When conducting parameter estimation for a material of interest, visual inspection should be conducted first to model its microstructure. Considering that typical pyrolysis models are available in one-dimension in the direction of the depth from the sample surface, the material's cross-section should be examined to determine whether the virtual microstructure should be considered as a **single layer of homogeneous material** or **multiple layers of homogeneous materials**. Note that, when the virtual microstructure is determined as a single layer of homogeneous material, the modeler has an option of utilizing models of either type of Comprehensive Model. However, when multiple layers of homogeneous materials are necessary to describe the material's microstructure, using Comprehensive Models with pyrolysis fronts of finite thickness are required.

Despite the increase in modeling complexity, multiple layers of homogeneous materials can be necessary. A rule of thumb of when to utilize multiple layers structure is as follows: (1) the virgin material is composed of several distinctive layers that bear significantly different pyrolyzing characteristics; (2) different pyrolyzing characteristics can be identified in experiment data, where layers exist in test samples; and (3) this effect is desired to be captured in the simulations.

The next step should be determining the decomposition kinetics type for each layer of homogeneous material identified above. In the following (see Table 5-2), typical decomposition thermograms observed from a Thermogravimetric Analysis (TGA) experiments are shown for fire problems, which will be dealt with in the example cases in this *Guide*. Based on the characteristics of the TGA curve, the modeler may choose the type of example case to consider for their problem. Note that decomposition kinetics should be identified for each layer of the specified microstructure or decomposable component of the material composing a layer. In the following table, different types of decomposition kinetics and the corresponding minimum number of elementary reactions to describe materials' full decomposition are shown based on TGA data (DTG) obtained from nitrogen and air environments. Conduct a minimum of three TGA experiments with heating rates lower than 10°C/min., sample sizes smaller than 10 mg, and various sample shapes, assuming that, with these conditions, chemical reaction becomes the decomposition kinetic controlling factor rather than diffusion.

Table 5-2. Various Types of Decomposition Kinetics

Type	Inert (solid, typically nitrogen) and Oxidative (dash, typically air) Environments	
0	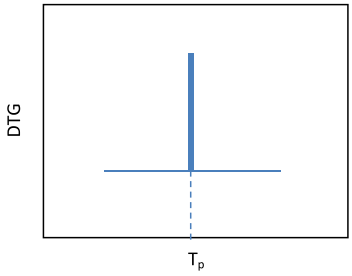	Weight-loss rate (DTG) with respect to temperature can be described with a single line independent of the testing environment (inert or oxidative) at pyrolysis temperature, T_p. **Minimum of 1 reaction**
1	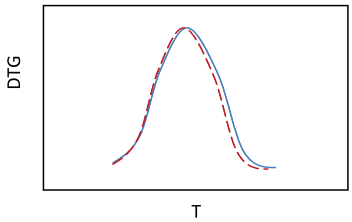	Weight-loss rate (DTG) with respect to temperature can be described with a single peak independent of the testing environment (inert or oxidative). In DSC experiments, endotherm is observed for tests conducted in both environments. **Minimum of 1 reaction**
2	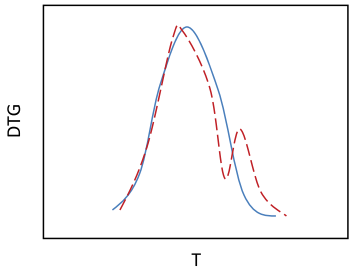	Weight-loss rate (DTG) with respect to temperature in inert environment can be described with a single peak. However, when sample is tested in oxidative environment (air), additional, secondary peak is observed at higher temperature range, typically considered as "char oxidation reaction." From DSC experiments, the first and second peak in TGA should correspond to an endothermic and exothermic peak, respectively. **Minimum of 2 reactions**
3	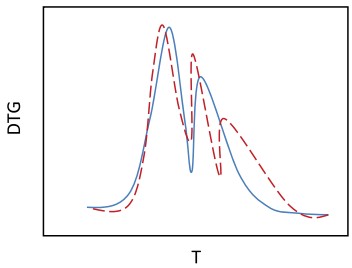	Weight-loss rate (DTG) with respect to temperature in inert environment should be described with multiple (*k*) peaks. When sample is tested in oxidative environment (air), additional peak is observed at higher temperature range, typically considered as "char oxidation reaction." From DSC experiments, the first few and last peak in TGA should correspond to endothermic and exothermic peaks, respectively. **Minimum of *k*+1 reactions**

Model-Parameter Table

With the virtual microstructure set and decomposition-kinetics type determined for each layer of the specified microstructure or decomposable component of the material composing a layer, the modeler is able to identify every species in the porous-condensed phase (*i*) and decomposition reactions involved in pyrolysis modeling.

To mathematically describe a pyrolyzing solid-phase material in comprehensive pyrolysis modeling in fire, a set of parameters are needed. Model parameters are related to heat transfer, mass transfer, and thermal-decomposition kinetics. Parameters consist of (1) **material properties** that are *intrinsic*, i.e., they depend on chemical and physical structure of the material or *effective* due to neglecting actual microstructure of the material and considering the material as homogeneous; (2) parameters related to modeling the **thermal-decomposition** process; and (3) **model-dependent fitting parameters**, which are not material properties but parameter constants that provide the best fitness of model output to experiment results. Typically, **material properties** can be considered in three groups: (1) thermo-physical properties – density, thermal conductivity, specific-heat capacity; (2) porous media characteristics – porosity, permeability; and (3) optical properties – absorption coefficient and emissivity. Parameters used in **thermal decomposition** modeling are pyrolysis onset temperature or kinetic parameters for applying infinitely thin or finite-thickness reaction zone assumptions, respectively, and reaction heats. An example of **model-dependent fitting parameters** can be exponent or constants used to describe temperature dependence of thermal conductivity, k: $k(T) = k_0 (T/T_r)^{n_k}$ or $k(T) = a + bT + cT^2 + dT^3$.

This allows the modeler to construct a model parameter table as below (see Table 5-3). Note that in this table only model-independent parameters are included. There can be other parameters related to material property in different models. For example, in GPYRO γT^3 term is used in the effective thermal conductivity to model radiative heat transfer through pores when the material is porous, where γ is a fitting parameter. These model-dependent parameters should be identified and obtained after setting up the problem in a model of choice in the validation section.

Table 5-3. Model parameter table: Summary of model parameters required to conduct pyrolysis modeling

		Condense Phase (*i*)	
Material Property		ρ_i	Density
		k_i	Thermal conductivity
		c_i	Specific-heat capacity
		κ_i	Absorption coefficient
Parameters for Specifying Conditions		X_{i0}	Volume fraction
		Y_{i0}	Mass fraction
		ε_i	Emissivity
		Heterogeneous RxN (*k*)	
Thermal Decomposition	Infinitely Thin Reaction Zone	T_p	
		ΔH_p	
	Finite Thickness Reaction Zone	n_k	Reaction order
		Z_k	Pre-exponential factor
		E_k	Activation energy
		ΔH_k	heat

Model-Parameter Measurement Methods

This section provides descriptions of how the model parameters identified above can be obtained via direct measurement using experiments. Relevant standard tests are listed when found. However, the most efficient approach for obtaining parameter values through independent measurements involves making contact with a commercial laboratory and consulting with them about the nature of your sample (brittle, soft, isotropic, melting, porous, etc.). Density, thermal conductivity and specific-heat capacity are thermophysical properties. Absorption coefficient and emissivity are optical properties. Kinetic parameters and heats are properties of thermal-decomposition kinetics. A modeler may search for test methods or labs that measure these properties.

1. Density

The bulk density of a porous solid material can be determined by measuring the mass of a representative specimen of the material and then dividing it by the measured volume of the specimen. Mass is generally measured with an analytical balance or scale. Volume can be determined, for example, by measuring the dimensions of the specimen or by submerging the specimen in a liquid and measuring the resulting displacement of the liquid. The bulk density of a material can also be determined on the basis of its specific gravity, i.e., the ratio of the density of the material to the density of a reference material. Although there are number of ASTM standards for measuring density or specific gravity at ambient temperature of specific materials, the typical approach in pyrolysis modeling is measuring the bulk density as noted above.

2. Thermal Conductivity

Various methods have been developed to measure the thermal conductivity of solids. In these methods the thermal conductivity is determined either under steady state or under transient conditions. The general principles of the two types of methods are summarized below.

STEADY-STATE METHODS

The one-dimensional heat-conduction equation based on Fourier's Law for a slab with infinitely large surface area and finite thickness, L- is as follows (see Eq.5-1):

$$\dot{q}'' = k\frac{\Delta T}{L} \qquad \text{Eq.5-1}$$

where $\dot{q}''$ = heat flux through the slab (W/m^2)
k = thermal conductivity of the slab material (W/m·K)
ΔT = temperature difference between two faces of the slab (K)
L = thickness of the slab (m)

Steady-state methods are based on the above equation and are classified into two categories: absolute and comparative. In absolute methods, ΔT and $\dot{q}''$ are measured, and k is determined from the equation. The test specimen (a slab of the material of which the thermal conductivity is to be determined) is sandwiched between a heater and a cooled plate. The temperature is measured on both faces of the specimen. To ensure one-dimensional heat transfer, guard heaters and insulation are used around the perimeter of the main heater and the specimen, respectively.

The main drawback of absolute methods is that it takes several hours to get to steady-state conditions with low thermal conductivity materials. Comparative methods were developed to reduce the test time (at the expense a slight reduction in accuracy). In comparative methods the heat flux is determined from the temperature gradient over a slab of a reference material with a known thermal conductivity. The specimen and reference material slabs are sandwiched between a heat source and a heat sink. The difference between the heat source and the heat sink is approximately 50-100K.

ASTM has standardized and published several steady-state methods (see Table 5-4). ASTM C 177 and ASTM E 1530 are absolute methods while the other two standards describe a comparative method.

Table 5-4. ASTM standards for measuring thermal conductivity using steady state methods

Standard Test	Description
ASTM C 177	*Standard Test Method for Steady-State Heat Flux Measurements and Thermal Transmission Properties by Means of the Guarded-Hot-Plate Apparatus*
ASTM C 518	*Standard Test Method for Steady-State Thermal Transmission Properties by Means of the Heat Flow Meter Apparatus*

TRANSIENT METHODS

The limitations of steady-state methods are: (1) it takes a long time to reach steady conditions (even when a comparative approach is used); (2) a relative large quantity of material is needed; and (3) it is not easy to perform measurements at elevated temperature. Transient methods are generally not as accurate, but they do not have the limitations of steady-state methods. Two well-known ASTM standards are shown in Table 5-5.

Table 5-5. ASTM standards for measuring thermal conductivity using transient methods

Standard Test	Description
ASTM C 1113	*Standard Test Method for Thermal Conductivity of Refractories by Hot Wire (Platinum Resistance Thermometer Technique)*
ASTM D 5930	*Standard Test Method for Thermal Conductivity of Plastics by Means of a Transient Line-Source Technique*

The hot-wire method is a typical example of a transient method. A fine metallic wire is placed at the center between two pieces of the material. The temperature of the wire is changed in step-wise fashion by incrementally increasing the current flowing through the wire. The generated heat flows in all radial directions and produces a temperature field in the material that increases with time. In most cases the wire itself serves as a temperature sensor as its resistance changes with temperature. The thermal conductivity of the material is a direct function of the heat dissipated in the wire and the rate at which its temperature rises. ASTM has developed standards that describe the use of the hot-wire method specifically for measuring the thermal conductivity of refractory materials and plastics.

Variations of the hot-wire method have been developed with different heat-source geometries (strip, plane, disc, or spiral) and an energy pulse instead of step-wise increases of the heat generated in the source. Adl-Zarrabi et al. used the Transient Plane Source (TPS) method to measure the thermal conductivity of concrete and wood at elevated temperatures and obtained reasonable agreement with literature values.[7] The TPS method was developed by Gustafsson and Long[8,9] and uses a heat source in the shape of a disc.

Bentz recently developed a transient method to determine the thermal conductivity of fire resistive materials.[10,11] The basic specimen configuration consists of a "sandwich," with a square central stainless-steel plate (slug) surrounded on two sides by a slab of the test material. This sandwich configuration provides an adiabatic boundary condition at the central axis of the slug plate, which greatly simplifies the analysis. The edges of the steel plate and specimens are insulated using a low thermal-conductivity fumed silica board. Two metal plates manufactured from a high-temperature alloy provide a frame for placing the entire sandwich specimen slightly in compression. The entire configuration is centrally placed at the bottom of an electrically heated box furnace, and the temperatures of the metal slug and exterior specimen surfaces are monitored during multiple heating and cooling cycles. Knowing the heat capacities and densities of the steel slug and the specimen material, an effective thermal conductivity can be estimated. The effective thermal conductivity of the specimen is influenced by its true thermal conductivity and by any endothermic or exothermic reactions or phase changes occurring within the specimens. The method is now standardized as ASTM E 2584.

3. Specific Heat Capacity

The enthalpy of a solid material is related to the kinetic energy of the particles in the solid. In the absence of chemical reactions or phase changes, the enthalpy of a solid material increases when it is heated. The rate at which it increases with respect to temperature is referred to as the specific-heat capacity. The specific-heat capacity for most solids varies with temperature.

Table 5-6. ASTM standard for measuring specific heat capacity

Standard Test	Description
ASTM E 1269	*Test Method for Determine Specific Heat Capacity by Differential Scanning Calorimetry*

Differential Scanning Calorimetry (DSC) is an accurate and convenient method to obtain specific heat capacities of solid materials at elevated temperatures. A standard procedure is described in ASTM E 1269 (see Table 5-6). In a DSC, a milligram-size sample and a reference are heated at a constant rate. The power required to increase the temperature of the sample and reference at the specified rate is proportional to their heat capacities. The sample heat capacity is determined on the basis of the power measured during the test, the baseline, and calibrations with a material with known heat capacity over the temperature range of interest (typically sapphire). The specific-heat capacity of the sample is then obtained by dividing the measured heat capacity by the sample mass. If the mass of the sample changes as a function of temperature, the heat capacity at a specified temperature should be divided by the sample mass at that same temperature. The latter can be obtained from TGA measurements performed under the same conditions, i.e., same heating rate, same purge gas, etc. DSC and TGA are often combined in a single instrument, which facilitates specific-heat capacity measurements.

As with TGA, DSC tests can be performed with different sample pans (aluminum, platinum or ceramic; open or sealed, with or without a pin hole), heating rates (typically between 1°C/min. and 60°C/min.), purge gases (typically air, nitrogen, or argon) and purge-gas rates. DSC tests are routinely performed at temperature ranging from ambient to 600°C. Many instruments can reach much higher temperatures.

4. Absorption Coefficient

With the absorption coefficient for radiation, a material's ability to allow penetration of thermal radiation in-depth can be quantified. Having a large radiative absorption coefficient means that the incident thermal radiation is attenuated quickly after passing through the material, i.e., the material is opaque and most of thermal radiation is absorbed near the surface. Having a lower value means that the material is more transparent; therefore, more in-depth radiation is occurring. Note that the absorption coefficient is strongly wavelength-dependent; therefore, some averaged value should be used to remove wavelength dependency. Additionally, it is known that obtaining accurate property data that characterizes the in–depth absorption (normally, the "gray" absorption coefficient) can be difficult.

5. Emissivity

Emissivity is a measure of a material's ability to emit energy by radiation at the surface. Although emissivity changes with respect to temperature, emission angle, wavelength, and more, a typical simplification made when determining this value is applying a grey body assumption, resulting in a wavelength- and temperature-independent constant. See Table 5-7 for relevant standard tests for measuring emissivity.

Table 5-7. ASTM standards for measuring emissivity

Standard Test	Description
ASTM C835 - 06	*Standard Test Method for Total Hemispherical Emittance of Surfaces up to 1400°C*
ASTM E 408-71	*Standard Test Methods for Total Normal Emittance of Surfaces Using inspection-Meter Techniques*

6. Parameters Related to Thermal Decomposition

INFINITELY-THIN REACTION-ZONE CASE

Assuming that the ignition temperature of a material is comparable to its pyrolysis temperature, this parameter can be directly measured using experiments or estimated using Ignition Data Analysis. See Chapters 3 and 4 for details.

REACTION ZONE WITH A FINITE-THICKNESS CASE

Mass as a function of temperature is most conveniently measured through thermogravimetric analysis (TGA). A TGA apparatus consists of a high-precision balance with a pan (usually aluminum, platinum, or ceramic) loaded with the sample. The sample mass is typically of the order of one milligram. It is kept as small as possible (to ensure uniform temperature) and depends on the material that is tested. The sample pan is placed in a small computer-controlled furnace with a thermocouple to accurately measure the temperature. The atmosphere may be purged with an inert gas (e.g., nitrogen or argon) to prevent oxidation or other undesired reactions. During a test, the furnace temperature is either kept constant or increased at a fixed rate (typically between 1 and 60 °C/min.) to a predefined maximum temperature (routinely 1000°C or higher). The result consists of a plot of mass (percentage) as a function of time and/or temperature.

For TGA testing and comparison of data, one needs to consider heating rates and atmosphere when studying mass-loss data relevant for fire models. Heating rates will affect the rate of thermal decomposition of a polymer, but in TGA faster heating rates tend to push the mass-loss curves to higher temperatures. Therefore, one should not compare different polymers unless they were tested at the same heating rate.

Atmosphere has a very important effect on TGA data in that a polymer will decompose in different chemical pathways under inert and oxidizing atmospheres. These changes in polymer decomposition chemistry can result in very different mass-loss rate curves, and so data for the same polymer collected under inert vs. oxidizing atmospheres can be compared qualitatively but not quantitatively. Likewise data for two different polymers collected under different atmospheres should not be compared. Of final note, it is always good practice to conduct TGA experiment in

inert and oxidizing atmosphere to make comparison and understand the effect of the change in the environment. Generally, oxygen is known to affect only thermal decomposition prior to ignition. After the material ignites all oxygen is known to be consumed at the flame front. In this sense, TGA data collected under inert atmospheres tends to be far more useful for understanding polymer decomposition and pyrolysis behavior under fire conditions.[12] This is why NIST created its gasification apparatus to study mass loss pyrolysis behavior in the absence of flaming combustion.[13,14,15] However, there are cases when the availability of oxygen affects the burning rate of the material as well, e.g., PMMA, wood, etc. Therefore, a careful consideration of the effect of atmosphere on TGA data should be given prior to modeling. See Table 5-8 for ASTM standards related to using TGA for studying thermal decomposition kinetics.

Table 5-8. ASTM standards for thermogravimetry analysis (TGA)

Standard Test	Description
ASTM E 2550	*Standard Test Method for Thermal Stability by Thermogravimetry*
ASTM E 1641	*Standard Test Method for Decomposition Kinetics by Thermogravimetry*

In the following section, brief descriptions of estimating methods for kinetic parameters using TGA data (single- or multiple-rate data) are provided. In both cases, decomposition kinetics is represented by an Arrhenius expression as below (see Eq.5-2):

$$\frac{d\alpha}{dt} = k(T) f(\alpha) = \left[A \exp\left(-\frac{E_a}{RT} \right) \right] f(\alpha) \qquad \text{Eq.5-2}$$

where

- k(T) = temperature dependent rate constant
- f(α) = temperature independent kinetic function of conversion, α (typically, α = 1-m/m0) and this function is dependent upon the mechanism of decomposition
- A = pre-exponential factor
- E_a = activation energy

Estimation Based on Single Heating Rate TGA Data Using DTG Peak Values (T_{PEAK}, R_{PEAK})[16]

Assuming that every peak in the DTG thermogram from the iso-heating rate (dynamic) TGA experiment can be considered as a single reaction with first-order reaction model (i.e., $f(\alpha) = (1-\alpha)^1$), this approach models the kinetics as follows: a condense-phase reactant thermally degrades to fuel vapor directly or to a secondary condense phase, which may or may not degrade further, producing fuel vapor and releasing it to the gas phase.

Consider an arbitrary DTG curve shown as below (see Figure 5-1). There is a single peak in this thermogram. Based on this approach, the modeler can assume a reaction for modeling thermal decomposition of this material. Apply a constant heating rate of $\beta = dT/dt$ and first-order kinetic model to above Arrhenius expression for describing decomposition. Rearranging it results in Eq.5-3:

$$\frac{d\alpha}{dT} = \frac{A}{\beta} \exp\left(-\frac{E_a}{RT} \right) (1-\alpha) \qquad \text{Eq.5-3}$$

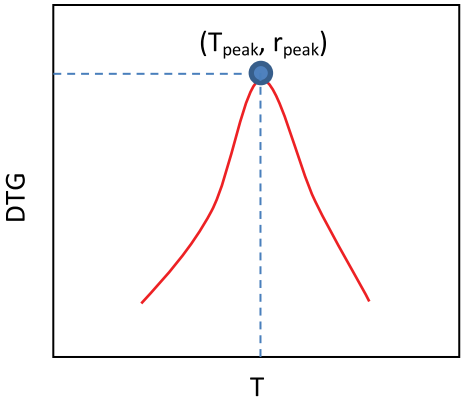

Figure 5-1. Typical DTG thermogram showing single peak

Assuming that, at each peak the second derivative of conversion, α, with respect to time is zero, and activation energy of each reaction is significantly greater than $2RT_p$ (i.e. $E_a >> 2RT_p$), estimation of A and Ea for each reaction can be done using the following equations (see Eq.5-4 and Eq.5-5):

$$E_a \approx \frac{RT_p^2}{\beta}\frac{er_p}{(1-\alpha_0)} \qquad \text{Eq.5-4}$$

$$A \approx \frac{er_p}{(1-\alpha_0)}\exp\left(\frac{E_a}{RT}\right) \qquad \text{Eq.5-5}$$

Estimation Based on Multiple Heating Rate TGA Data Using Iso-Conversional and Model Fitting Methods

Estimation of kinetic parameters based on multiple heating-rate data obtained from TGA experiments tries to take into account of any changes that may occur in thermally degrading behavior as the heating rate is changed. This approach requires a minimum of four iso-heating rate (dynamic) TGA data. The four heating rates should spread out in the range of less than 10 K/min. to above 40 K/min.

The Iso-conversional Method allows one to determine activation energy in terms of conversion with a minimum of four TGA tests with different heating rates without assuming the kinetic function. Two methods are introduced below:

Method of Ozawa, Flynn and Wall[17,18] (OFW)

Apply a constant heating rate β = dT/dt to the above Arrhenius expression for describing decomposition. Rearranging it results in Eq.5-6:

$$\ln(\beta) = \ln\left(\frac{dT}{dt}\right) = \ln\left(\frac{A\exp\left(-\frac{E_a}{RT}\right)f(\alpha)}{\frac{d\alpha}{dt}\Big/\beta}\right) = \ln\left(\frac{Af(\alpha)}{\frac{d\alpha}{dt}\Big/\beta}\right) - \frac{E_a}{RT} \qquad \text{Eq.5-6}$$

A plot of ln(β) versus 1/T should give a slope of $-E_a/R$ for a wide range of conversion, α. For example, at α = α*, four ln(β) values are found – $\ln(\beta_1)$, $\ln(\beta_2)$, $\ln(\beta_3)$ and $\ln(\beta_4)$ – at four different temperatures – T_1, T_2, T_3 and T_4 – when data from four iso-heating rate TGA tests are used as in the first figure below. These data points can be plotted in a ln(β) versus 1/T graph and the slope of the four points gives $-E_a/R$ at α = α* as shown in the second figure. This can be repeated for α ranging from 1 to 0, and the estimated E_a can be plotted with respect to alpha as in the last figure below (see Figure 5-2.)

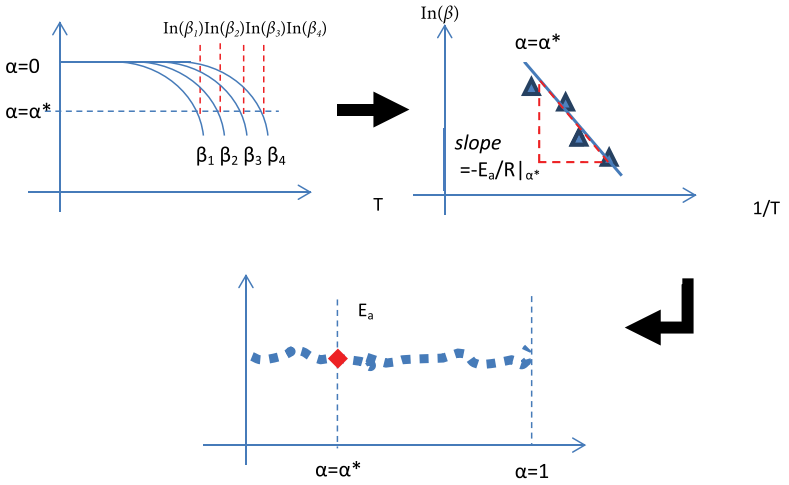

Figure 5-2. Schematic of conducting Ozawa, Flynn, and Wall Iso-conversional Method

Method of Friedmen[19,20] *(Friedmen)*

$$\ln\left(\frac{d\alpha}{dt}\right) = \ln\left(A\exp\left(-\frac{E_a}{RT}\right)f(\alpha)\right) = \ln\left(Af(\alpha)\right) - \frac{E_a}{RT} \qquad \text{Eq.5-7}$$

A plot of ln(dα/dt) versus 1/T is used to find the slope of $-E_a/R$ (see Eq.5-7). For example, at α = α*, four dα/dt values are found – $(d\alpha/dt)_{\beta 1}$, $(d\alpha/dt)_{\beta 2}$, $(d\alpha/dt)_{\beta 3}$ and $(d\alpha/dt)_{\beta 4}$ – at four different temperatures – T_1, T_2, T_3 and T_4 – when data from four iso-heating rate TGA tests are used as in the first figure below. These data points can then be plotted in a ln(dα/dt) versus 1/T graph and the slope of the four points gives $-E_a/R$ at α = α* as shown in the second figure. This can be repeated for α ranging from 1 to 0 and the estimated Ea can be plotted with respect to alpha as in the last figure below (see Figure 5-3).

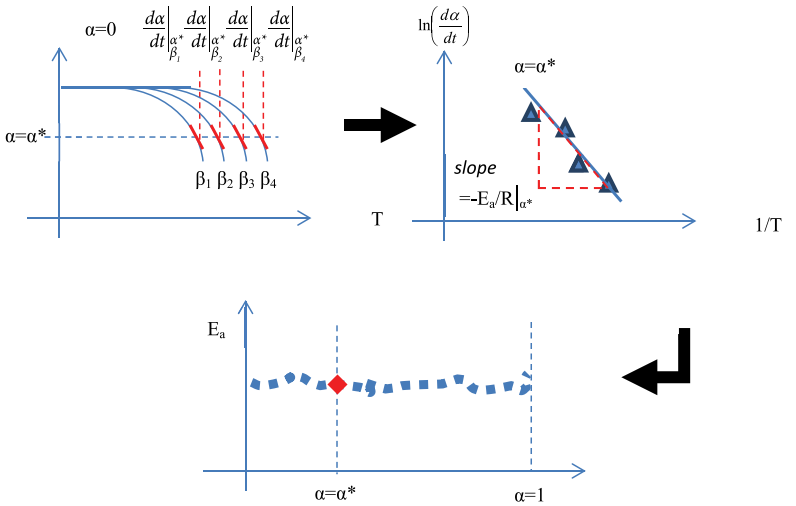

Figure 5-3. Schematic of conducting Friedmen's Iso-conversional Method

Interpreting Results from the Iso-conversional Method

When the E_a is found for the entire degradation process, the results provide insight for the minimum number of steps of elementary reactions needed to characterize the global reaction.[21] A global reaction composed of a single stage process will show no dependence of E_a on conversion, α. When the global reaction is a complex process, the E_a changes with respect to conversion, α. An increase in E_a with α typically indicates parallel reactions. A decrease in E_a with α suggests that either the process is reversible (concave shape) or there is a change in the rate determining step (convex shape). Therefore, by analyzing the shape of the curve plotted with E_a with respect to conversion, α, a minimum number of elementary reactions are suggested.

Model Fitting Method

Once the minimum number of reactions and their activation energies are estimated by conducting the Iso-conversional Method, other kinetic parameters to fully mathematically describe the decomposition of MA+A need to be estimated as well. This is done by conducting the model-fitting method with a kinetic model assumed. Typically, an nth order reaction model is used due to its flexibility in providing good fitness between the data and the model. Therefore, an nth order will be utilized in this example.

Based on the model-fitting method, estimation for weight-loss fraction (f), pre-exponential constant (A), and exponent in the nth order kinetic model (n) is conducted for each reaction. Note that the estimation has been done with a least-square method by comparing TGA data (TG and DTG from iso-heating rate tests) with the kinetic modeling's output. The kinetic modeling's output is a sum of properly scaled elementary reactions with the weight-loss fraction found for each reaction. Without scaling, every reaction results in 100% conversion. Each reaction is calculated by applying the Runge-Kutta 4th order method (ODE solving method) to decomposition and constant heating rate ODE equations: two dependent variables (α, T) with time (t) as the independent variable (see Eq.5-8 and Eq.5-9).

$$\frac{d\alpha(t)}{dt} = \left[A \exp\left(-\frac{E_a}{RT(t)} \right) \right] (1-\alpha(t))^n \quad \text{Eq.5-8}$$

$$\frac{dT(t)}{dt} = \beta \quad \text{Eq.5-9}$$

Weight-loss fraction (f): This parameter is for determining how much of the total weight of the entire sample (100%) is consumed by each reaction. Note that kinetic modeling is conducted in terms of conversion, α, and each reaction results in 100% conversion. Therefore, mathematically, weight loss ($d\alpha/dt$) should be properly scaled with the weight-loss fraction parameter (f) to have the summation of weight loss due to all elementary reactions and any solid-phase leftover (typically labeled as residue) at temperatures exceeding maximum temperature considered in TGA experiment to equal 100%. For this example, where two elementary reactions have been proposed, total weight loss (conversion) and weight-loss rate (derivative of conversion) can be expressed as follows (see Eq.5-10 and Eq.5-11).

$$\alpha_{Total} = f_R \alpha_R + f_{+A-R} \alpha_{+A-R} + f_{residue} \quad \text{Eq.5-10}$$

$$\frac{d\alpha_{Total}}{dt} = f_R \frac{d\alpha_R}{dt} + f_{+A-R} \frac{d\alpha_{+A-R}}{dt} \quad \text{Eq.5-11}$$

To optimize for this parameter (f), consider results from the Iso-conversional Method to find an initial guess.

Pre-exponential constant (A): This parameter, also known as the collision frequency, is originally from the Collision Theory[22] defined as the average number of collisions experienced by a reacting molecule with other molecules. However, in solid-state reactions, classical frequency factor becomes inappropriate, as reactions do not occur with molecules colliding but due to molecules being mostly stationary during solid-state decomposition. Although this parameter is different from that of Collision Theory, the A value can provide a measure of reactivity of the decomposition reaction.

When optimizing for this parameter, the modeler should be aware of the compensation effect[23] between the activation energy and pre-exponential constant, i.e., there are several sets of E_a and A that result in similar reaction rates. An increase in E_a can be compensated by a decrease in A and vice versa. Currently, no theory is accepted as explaining this effect, but it is well acknowledged that this exists. Therefore, it is important to estimate the activation energy value based on the Iso-conversional Method and optimize for A value using a model-fitting method.

Exponent in nth order kinetic model (n): Typically, n values considered for this reaction-order-type kinetic model (nth order) are between 0 and 3. Changing n value results in changes in the shape of DTG, i.e., an increase in n results in a lower peak in the DTG curve with wider temperature range as shown below (see Figure 5-4).

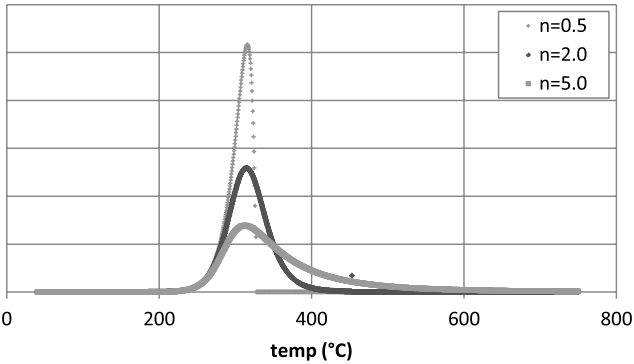

Figure 5-4. Change in DTG curve with respect to changes made in n values using nth order reaction model

Optimization: When optimizing for the parameters, an initial guess should be given for the weight fractions (*f*) for each reaction as the mid-values within the optimization range found via examining TGA and DSC data and results from the Iso-conversional Method. Additionally, an initial guess of the n value can be given as 1, where a first-order reaction model is the most simple and common model used to fit the data. The next step is to estimate the pre-exponential constants. Typically, the initial guess of this parameter can start from 10^{10}. The pre-exponential constant, A, for each reaction can be adjusted with other parameters set as their initial values to match the temperature range of the model's mass-loss rate peak (DTG) with the known temperature range found from analyzing the TGA and DSC data and results from the Iso-conversional Method. After this step, the n values can be optimized to match the peak of the mass-loss rate (DTG) from modeling to that of the data. As mentioned in the previous section, changing n value results in changes in the shape of DTG, i.e., increase in n results in lower peak in the DTG curve with wider temperature range. After going through these steps, manually each parameter can be optimized by comparing the kinetic modeling results (mass loss or mass loss rate, i.e., TG or DTG) to data from the TGA experiment. In general, a correlation coefficient can be calculated to evaluate the fitness of the estimation to actual data, e.g., as the square of the correlation coefficient (R^2) becomes close to 1 by optimizing each parameter, it reflects that a stronger linear relationship exists between the modeling results (x) and data (y). See Eq.5-12.

$$R = \frac{\sum(x-\bar{x})(y-\bar{y})}{\sqrt{\sum(x-\bar{x})^2 \sum(y-\bar{y})^2}} \qquad \text{Eq.5-12}$$

where $\bar{x}$ and $\bar{y}$ are sample means.

7. Heats

If the DSC sample goes through a transition, such as a phase change (e.g., evaporation of bound water) or a chemical reaction (e.g., pyrolysis), the associated enthalpy changes (e.g., the latent heat-of-vaporization or the heat-of-pyrolysis) will be recorded by the instrument. An example of decomposing polyurethane foam is shown in Figure 5-5.

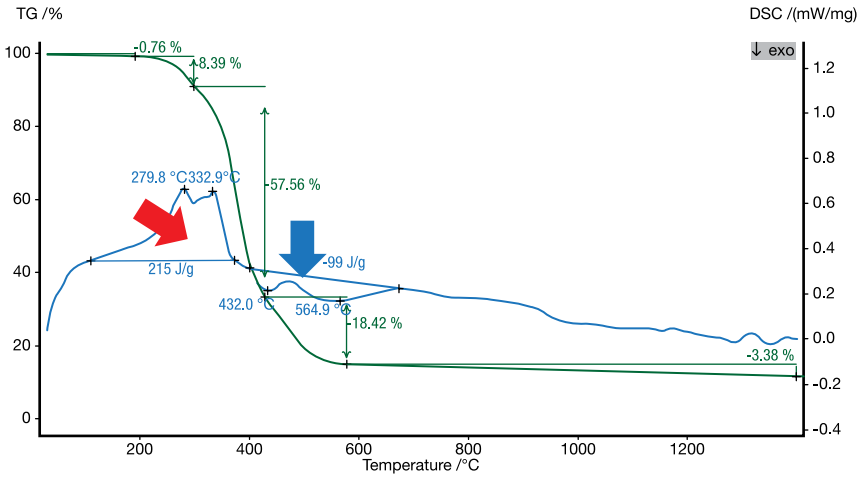

Figure 5-5. TG (weight loss) thermogram from TGA experiment (left) and heat-flow diagram from DSC experiment (right) for decomposition of a rigid-foam plastic

The polyurethane foam loses 85% of its mass between 100°C and 600°C. The thermal degradation is initially endothermic as the enthalpy rises above the baseline (see red arrow). Between 400°C and 600°C the enthalpy drops below the baseline, which is characteristic of exothermic reactions (see blue arrow). The heat-of-pyrolysis associated with the endothermic reactions is determined from the area under the peaks and is approximately 215 J/g. The heat-of-pyrolysis associated with the exothermic reactions is determined in a similar way and is equal to approximately -99 J/g (since heat is released in exothermic reactions, the enthalpy change is negative). The fact that there are two separate peaks indicates that there are two distinct endothermic reactions. Likewise, the two valleys imply that there are two distinct exothermic reactions. To model the thermal degradation of this material, the data suggest a four-step reaction scheme, which is not obvious from inspection of the TGA curve. The uncertainty of the baseline can result in significant errors of heat-of-transition values obtained with this method. ASTM D 3418 (see Table 5-9) provides some guidance on how to address this problem.

Table 5-9. ASTM standard for measuring reaction enthalpies

Standard Test	Description
ASTM D 3418	*Standard Test Method for Transition Temperatures and Enthalpies of Fusion and Crystallization of Polymers by Differential Scanning Calorimetry*

The main experimental parameter that can affect DSC results is the heating rate. Faster heating rates can cause some thermal events to disappear or blur together (such as glass transition temperatures and low-energy melting events) as well as shift the temperatures of events. An example of this is shown below for an engineering crystalline thermoplastic. As the heating rate is increased, the melting point shifts to lower temperature (see Figure 5-6). While the range of peak melt temperatures is not so large for this sample (332-335 °C), one should not assume that this is true for all materials. Therefore, some consideration needs to be given to the heating rate when selecting DSC data for different polymers in a model. Of particular importance is the effect of the heating rate on the onsets of thermal decomposition (an endothermic event) or potential exothermic events (such as cross-linking). So, DSC data on different polymers should only be compared to each other if the data was collected at the same heating rate. Note that the above-mentioned trend will not be seen in combined TGA/DSC experiments, as the loss of sample mass (evaporative cooling) will dominate the heat-transfer effects in the DSC measurements once the polymer begins to decompose. So one can argue that stand-alone DSC instruments are more accurate for measuring thermal events below thermal decomposition temperature, whereas TGA/DSC instruments are more accurate (or appropriate) for measuring thermal events where the polymer has begun to lose mass and is pyrolyzing/burning. However, in general TGA/DSC instruments are sufficient for fire pyrolysis modeling purposes, because more interest is given in the post-decomposition stage, where weight loss is considered in terms of heat being released.

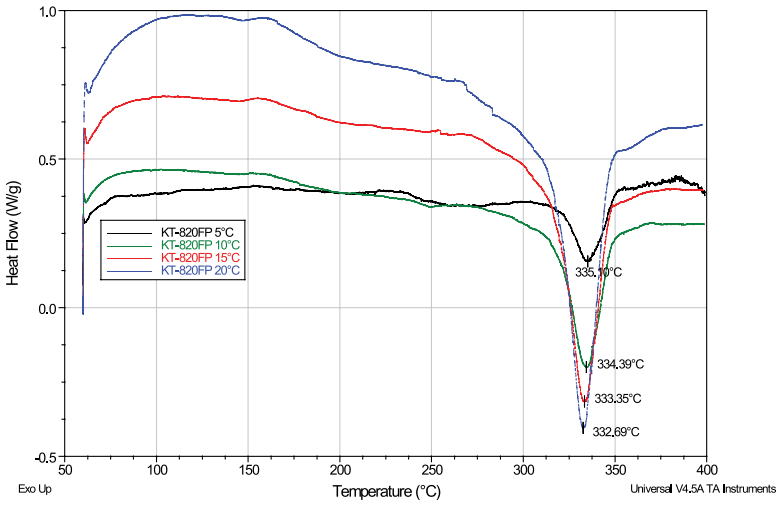

Figure 5-6. Melting points for a thermoplastic polymer as a function of DSC heating rates

Atmosphere choice in the DSC is typically not a parameter that gets changed, but some dual TGA/DSC units now commercially available can allow a material to have DSC data collected under oxidizing atmospheres while stand-alone DSC instruments are almost always tested under nitrogen. The atmosphere to which a polymer is exposed will affect its decomposition chemistry and therefore its kinetics of mass-loss rate. Likewise, a sample in a dual TGA/DSC unit will have very different behavior in nitrogen vs. air atmospheres (aerobic vs. anaerobic thermal decomposition). Therefore, any data from these types of units should only be compared to other polymer data on the same instrument if they are collected under the same atmosphere. Certainly, however, the results from the same polymer in air vs. nitrogen could be studied and compared, and this can be very useful in the above-mentioned TGA/DSC experiments. For standalone DSC instruments, which are closed-cell systems, it is highly recommended that the polymer not be taken to decomposition temperatures – and definitely not in air – so that the sensitive DSC heating cell is not damaged or contaminated with polymer-decomposition products. The reason for this is that these decomposition products will condense out into the cell and change the heat sensitivity/thermal conductivity of the cell over time.

Parameter-Estimation Process

If one does not know all the parameters required in modeling to create a virtual material, unknown parameters need to be estimated to perform actual calculations. This process is called parameter estimation. Parameter estimation for comprehensive pyrolysis modeling can be done using three different approaches: (1) measure each parameter via independent experiment; (2) search literature for measurement values on similar materials or use approximation; (3) conduct numerical optimization by pairing the pyrolysis model with an optimization routine. These approaches can be used alone or paired to estimate the entire unknown model-parameter set.

When the unknown parameters are estimated by measurement using independent experiment, typically small-scale experiments are used based on standard tests, such as ASTM or ISO. This approach only allows measurement of model parameters that are material properties and parameters related to modeling the thermal-decomposition process. It is noteworthy that material properties obtained through this approach are not always *intrinsic*, but in many cases are *effective*. Due to the limited sample size used in small-scale tests, material properties measured via independent experiment are generally accepted as *intrinsic*. However, in many cases for real-world heterogeneous materials, the material property measured becomes the *effective* property, as the small amount of sample used in these tests is also heterogeneous but treated as homogeneous by neglecting the heterogeneity nature of the material. Therefore, caution should be given to a common misconception of understanding that measurements always result in obtaining *intrinsic* material properties whereas often *effective* properties are measured. In general, applying this approach of conducting experiments to directly measure model parameters is challenging due to the following reasons: First, there may be a discontinuity in model parameter obtained in a small-scale experiment and in model parameter required in the pyrolysis model. For example, a naturally high-charring phenolic resin decomposing during a Thermogravimetric Analaysis (TGA) experiment in a powder form – a typical approach when conducting TGA experiment to reduce thermal lag effect – cannot represent decomposition of this same material in a bench-scale calorimeter test as a flat surface. This resin prepared in a powder form results in significantly large surface area (interface) exposed to the gas phase per unit mass or volume. On the other hand, resin prepared as a flat surface has relatively smaller surface area exposed to the gas phase per unit mass or volume compared to resin in powder form. This difference results in great deviation when comparing thermal decomposition of this material, because the smaller surface area per unit mass or volume is proportional to the formation of more thermally stable carbonatious char during decomposition. Therefore, for this case, obtaining kinetic parameters from a TGA experiment using powder-type sample and applying them to pyrolysis modeling to describe thermal decomposition occurring on a flat surface is not applicable. Second, material properties required in pyrolysis modeling that occurs while the material is decomposing cannot be measured via independent experiments. Typically, when measuring material properties in small-scale experiments, decomposition of the sample is not allowed, which makes it impossible to make measurements for

material properties of intermediate species involved in kinetic modeling. Third, measuring material properties and conducting thermal analysis for modeling thermal-decomposition kinetics through a commercial laboratory require significant financial investment.

Another approach to estimating model parameters is searching through literature for measurement values on similar materials or using certain approximations. Although using this approach is most practical because it is less time-consuming and inexpensive, caution should be given for the following: First, understanding of the material and its condition is essential. Certain polymers may have the same nomenclature, but depending on their polymer chain size, length and shapes, its character may vary.[24] The same material with moisture may show different thermal decomposition kinetics than that at dry state by water molecules chemically or physcially interfering in the process.[25,26,27,28] The same material with significant aging – e.g., scratches, cracks, etc. – may start to decompose at a lower temperature than that without aging.[29] These are some examples of how material and its conditions during experiments can affect the measurement results. Second, consideration to model parameter sensitivity and uncertainty is needed. In addition to the uncertainty reported for the measurement value in the literature, a greater uncertainty should be taken into account when using that value in pyrolysis modeling, for the two materials may have subtle differences physically or chemically as noted above. Also, when approximation is used to estimate certain model parameters for simplification of the problem, the modeler should be aware of the sensitivity of that parameter on modeling outputs of interest and check whether or not small changes to the approximated parameter value do not significantly alter the modeling results.

The third approach to estimating model parameters is by conducting numerical optimization by pairing the pyrolysis model with an optimization routine.[30,31,.32,33,34,35] To overcome the limitation in estimating parameters through measurements (first approach) or by literature search or approximations (second approach), the unknowns in pyrolysis modeling can be obtained by comparing modeling outputs with optimizing targets – experimental data such as mass-loss rate and temperature profiles from bench-scale test results – and finding the optimum parameter set that provides the best fitness to the target. When unknown parameters in a pyrolysis model are estimated using numerical optimization by comparing certain modeling outputs with a target, this is considered an inverse problem. These inverse problems in pyrolysis modeling are hard due to following reasons:[36] First, when the data contains noise or the mathematical model does not account for important physics and/or chemistry of the real problem, there may be no optimum that fits the data exactly, i.e., the solution to the problem may not exist (existence of solution). In other words, when data uncertainty is high enough to exert certain characteristics of a material through the acquired data and/or the model is too simplified, the model solution may not be determined through this process. For example, when model parameters are estimated by utilizing this approach for certain laminated fiberglass reinforced polymer (FRP) composites with relatively high glass content, successful optimization for the parameters separately for the two components of the composite, resin and fiberglass mats, may be unsatisfying, because the variation in mass-loss rate data used as targets generally do not show the effect of the alternating layers of resin and fiberglass mats in the composite.

Second, even when a solution is found, that may not be unique (uniqueness of solution). This occurs usually when the data used in solving the problem is significantly smoothed or biased. In resolving this problem, the typical approach is to reduce the total number of unknowns. This can be accomplished by fixing the unknown parameters to some values by utilizing approaches other than numerical optimization, as discussed previously.

Third, inverse problems are in most cases ill-posed, where a small change in a solution can lead to an enormous change in the modeling output, which is known as the instability problem of a solution (instability of solution). Therefore, effort should be given to always check the applicability of the solution upon extrapolation to other modeling conditions, which were not considered during numerical optimization, knowing that this may result in significant deviation from actual phenomena.

Fourth, the optimized parameters should be considered as a *linked* parameter set. Once numerical optimization is used, the optimized parameter value takes into account any assumptions used in pyrolysis modeling, all the intrinsic or effective parameter values with their uncertainty which were obtained through other means, etc. Hence, an optimized value for one parameter may not be used for other pyrolysis modeling cases, in general. Last, when applying this method, the estimation process can become confusing, and without a consistent approach it can lead to unsatisfying results.

This *Guide* is focused on presenting a process for estimating model parameters that allows modelers to conduct parameter estimation based on commonsense, consistency, and correctness. This process of creating a virtual material is composed of the three approaches discussed above: (1) measure each parameter via independent experiment; (2) search the literature for measurement values on similar materials or use approximation; (3) conduct numerical optimization by pairing the pyrolysis model with an optimization routine. In addition to these approaches, consideration is given to uncertainty of estimation of each model parameter and its propagation into pyrolysis modeling uncertainty, in the context of defining the criteria for satisfying or dissatisfying parameter estimation. Typically, estimation based on measurement of the maximum number of parameters possible will be considered first, then by literature review, as those can become practical constraints when conducting numerical optimization for solving unknowns. Therefore, estimation based on a numerical optimization routine in pair with pyrolysis modeling will be considered as the last option.

To create a virtual material, these tasks must be considered:

- Create microstructure of the virtual material
- Identify decomposition kinetics type
- Create a list of model inputs, which needs to be determined
- Obtain model unknown inputs via measurement or literature search

When the above is done and every unknown has been estimated, validation work is needed to understand the performance of the estimated parameter set:

- Run model
- Analyze simulation quality with consideration of uncertainties in modeling outputs and data
- Add commentary

When there are additional unknowns that need to be estimated, the modeler may conduct numerical optimization in pair with modeling. This process of obtaining unknowns via numerical optimization should be followed by validation work as well. Obtaining parameters using numerical optimization and validation should consist the following:

- Run model in pair with numerical optimization
- Analyze simulation quality with consideration of uncertainties in modeling outputs and data
- Validate simulation quality upon extrapolation
- Add commentary

When presenting the parameter estimation results, three sections will be introduced: Model Parameter Table, Validation section, and Commentary section. The Model Parameter Table includes the model parameters necessary to conduct pyrolysis modeling, their estimated values, and methods of estimating the unknowns. Validation consists of the following information: description of modeling goal, pyrolysis model type and modeling approach used in the exercise, experiment type and its data used to compare data to modeling outputs or numerically optimize for unknowns, and uncertainty information of experimental data and modeling outputs. Commentary discusses any limitations of pyrolysis modeling conducted above, which has been summarized in the Model Parameter Table and Validation sections.

For better visualization of the problem, a flowchart is shown below (see Figure 5-7):

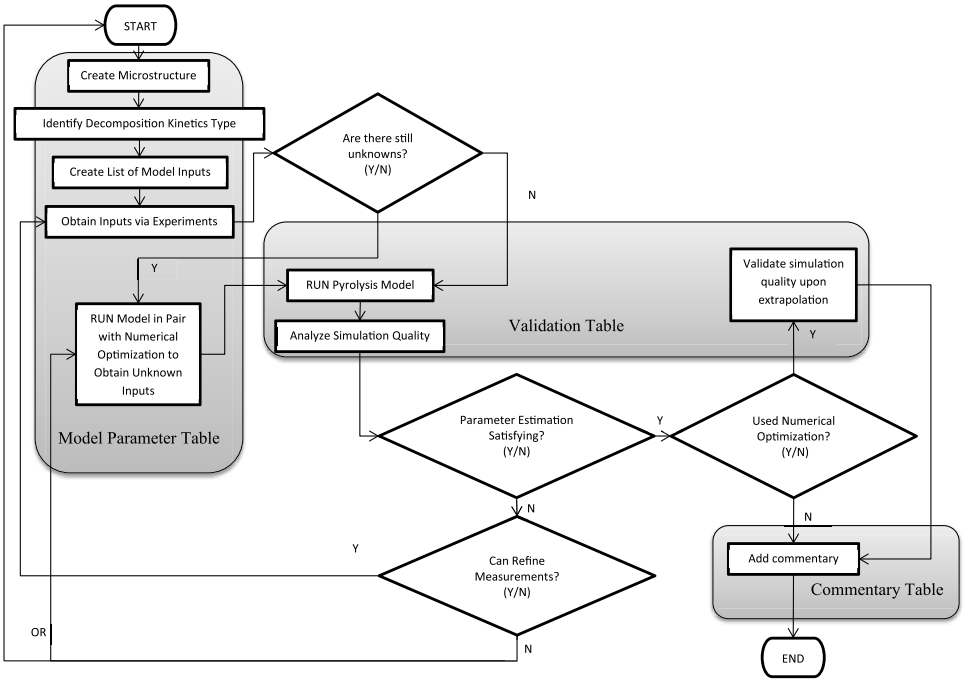

Figure 5-7. Flow chart of parameter estimation for comprehensive pyrolysis models

Example Case 1 and 2

For these example cases, less than a total of 20 parameters are necessary due to the single step thermal decomposition kinetic modeling applied in these problems. Therefore, extensive sensitivity analysis is not necessary to determine sensitive parameters on model outputs of interest, because work conducted by Stoliarov[37] and Chaos[38] for similar cases considers the effect of variation in material properties on the rate of burning. According to these papers, it was recognized that the knowledge of parameters related to emissivity of the virgin and char material and the decomposition reaction – Arrhenius pre-exponential factor, activation energy, heats, char yield – are significantly important for predicting the peak, average burning rates and surface temperatures. Based on this result, when determining the uncertainty of the model output, only these parameters will be considered where simulation quality is analyzed by comparing the model output with its uncertainty with experiment data with its uncertainty. Further details on sensitivity of each parameter can be found in this reference.[37,38]

Example Case 3 (Global Sensitivity Analysis: Morris Method)

For this example case, a greater number of parameters is involved in pyrolysis modeling. Therefore, a structured global sensitivity analysis technique is used to determine the sensitivity of model input parameters. Among various global analysis techniques, screening design is one of the simplest methods to identify important parameters.[39,40,41] Typical screening designs are one-at-a-time (OAT) experiments, where a value is changed and its impact is evaluated in turn. It is known that classical OAT experiments are less meaningful if the model of interest is affected by nonlinearities, which causes drastically different "sensitivities" when parameter changes around the "control" scenario, depending on the chosen "control" scenarios. To address this limitation, Morris (1991) has proposed a global OAT design method, by covering the entire space in which the parameters may vary independently of the specific initial "control" scenario with which one may commence the experiment. A global OAT design assumes that the model is characterized by a large number of parameters and/or is computationally expensive (regarding computational time and computational resources) to run.

Although originally the Morris method was used for unitless parameters, for these problems it was used for parameters with units. Because the Morris method allowed the user to interpret the effect of changes made in the inputs to the model outputs in terms of simulation variation observed in dimensional units (i.e., seconds for time, °C for temperature and g/m2-s for mass-loss rate), one was able to apply the significance level (see below) directly. This allows the user to rank the sensitivity of each parameter with a quantifiable variation.

To identify the sensitive parameters of a model via a sensitivity analysis, there needs to be a measure to determine the sensitivity. This measure, defined as the level of significance, should be able to distinguish which effects shown in the simulation results due to changes made in the inputs are significant and which are not. A typical sensitivity analysis allows the user to rank the input

parameters in terms of its sensitivity to model outputs. Defining the level of significance allows the user also to determine how many of the parameters from the top ranking should be set with caution, because those significantly affect the simulation results. The level of significance that defines the sensitivity of an input parameter should be predetermined by the user based on one's goal of conducting the simulation. When the best simulation accuracy is desired, the level of significance should be determined by the experimental uncertainty obtained by tests identical to the simulation set-up, such as the cone calorimeter tests. For example, if the ignition time has an uncertainty of +/- 20 sec. in the cone calorimeter tests, any changes in the model input that allows more than +/- 20 sec. in the model output should be considered as a "significant change." However, there are situations where low simulation accuracy is acceptable for one's simulation purposes. In these cases, the level of significance can be set by the modeler to be greater than the experimental uncertainty, and this approach results in less parameter being considered as sensitive to model outputs.

After identifying the necessary parameters for pyrolysis modeling with a model of choice and selecting the significance level, a sensitivity analysis is performed to identify sensitive input parameters to model output. To determine the region of experimentation for the Morris method, a minimum and maximum range for each parameter is selected by the user through common sense. Four levels, P1 through P4, are used in this *Guide* example cases ($p = \{0,1/3,2/3,1\}$) with an increment of $\Delta = p/[2(p-1)] = 2/3$ following the guide presented by Morris. Four cases are simulated in each example case, which results in four elementary effects for each parameter.

To calculate an elementary effect, first a baseline case needs to be constructed. The baseline is a group of the entire parameters with their values randomly chosen from **P1 or P2**. This is because there are four levels in this analysis, and when conducting the analysis, adding Δ should not exceed the region of experiment. Next, a random order should be created for each case, where this order is used to change the parameter value from its baseline by Δ one at a time. The effect of changing a parameter by Δ is evaluated by running the model and evaluating the changes made in the model output of interest. Using these four effects found from four cases for each parameter, the modeler now can calculate the mean and its standard deviation or variance of changes that occurred due to an increase/decrease made to a single parameter value by Δ. Any parameter resulting in a significant change in model outputs when changed by Δ (i.e., a large mean and/or standard deviation/variance for changes made in the modeling outputs) are considered to be "sensitive." Based on this analysis, when determining the uncertainty of the model output, only parameters that are "sensitive" will be considered, where simulation quality is analyzed by comparing the model output with its uncertainty versus experiment data with its uncertainty.

Uncertainty Analysis

To conduct uncertainty analysis for modeling outputs of interest, the uncertainty of each parameter value should be estimated first. When model parameters are estimated using experiment measurements or by literature search, the uncertainty of the measured value is typically estimated through the experiments. However, when numerical optimization is used to estimate unknown model parameters, estimating the uncertainties associated with those optimized values is nontrivial.

Assuming that the uncertainty of every parameter is known and each parameter can be considered as independent, the uncertainty propagated to pyrolysis modeling outputs of interest may be calculated via the Law of Propagation of Uncertainty. To conduct this calculation, first the sensitive parameters should be identified based on sensitivity analysis. Then those parameters are varied to their boundary values (minimum or maximum from representative values by considering parameter uncertainty) in modeling one at a time from its baseline case, which is the one modeled with all representative values for each parameter. The effect of variation is calculated by determining the modeling outputs of interest – e.g., peak heat-release rate, average heat-release rate, time-to-ignition, time to peak heat-release rate, etc. – and comparing the changes occurring from those in the baseline case. At the end, the overall summation of each maximum effect of changing one sensitive parameter at a time is calculated by the Law of Propagation of Uncertainty, which is used as a measure of the uncertainty in modeling results of interest.

When numerical optimization is utilized to estimate unknown parameters, one possible approach of addressing the uncertainty of those parameters is to use the near optimal parameter sets, or "best solutions," to generate a relatively large population of parameter sets. A multi-objective optimization algorithm such as Genetic Algorithm (GA) applied to pyrolysis modeling typically produces many near-optimal sets or "best solutions," which are a set of solutions that represent tradeoffs between many objective functions. Each parameter value from each set can be evaluated together to determine whether a near-optimal value of one parameter changes significantly from one set to another. Computing a histogram to understand the distribution of the optimized values and estimating uncertainty for each parameter would be a good practice.

Another possible approach for determining the uncertainty of optimized parameter values is using asymptotic methods.[32] This approach is conceptually appealing and easy to implement. However, when problems are highly nonlinear, they may be a poor representation of the actual uncertainties of optimized parameters, for they are calculated locally at the optimum point found by the optimization routine. Nevertheless, the uncertainties estimated can become a useful indication

of the reliability of the optimized parameters. At a certain optimum point, the standard error of the parameter estimates is approximated by a variance-covariance matrix based on the Jacobian of the model response. This matrix is then used along with the t-distribution at some desired confidence level to estimate the uncertainty. The set of equations shown below summarizes this approach:

$$\mathrm{COV}=\frac{\|\mathbf{f}(\hat{\boldsymbol{p}})\|_2^2}{n_d-n_p}(\mathbf{J}^T\mathbf{J})^{-1};\ f(\hat{\boldsymbol{p}})=y_{\exp\,i}-y_{\mathrm{mod}\,i}(\hat{\boldsymbol{p}});\ i=1,\cdots,n_d$$

$$\mathbf{J}=\begin{bmatrix}\left.\frac{\partial y_{\mathrm{mod}1}(\mathbf{p})}{\partial p_1}\right|_{\hat{\boldsymbol{p}}} & \cdots & \left.\frac{\partial y_{\mathrm{mod}1}(\mathbf{p})}{\partial p_{n_p}}\right|_{\hat{\boldsymbol{p}}}\\ \vdots & \ddots & \vdots\\ \left.\frac{\partial y_{\mathrm{mod}n_d}(\mathbf{p})}{\partial p_1}\right|_{\hat{\boldsymbol{p}}} & \cdots & \left.\frac{\partial y_{\mathrm{mod}n_d}(\mathbf{p})}{\partial p_{n_p}}\right|_{\hat{\boldsymbol{p}}}\end{bmatrix}$$

$$\hat{\boldsymbol{p}}=\hat{\boldsymbol{p}}\pm t^{-1}\,(CL;\ n_d-n_p)\,\sqrt{diag[\mathbf{COV}]}$$

Where $\hat{\boldsymbol{p}}$ is the optimum parameter vector (i.e., set of material properties), n_d is the number of data points used for optimization, n_p is the number of parameters (i.e., material properties), **COV** and **J** are the covariance and Jacobian matrices, respectively, **f** is the vector of differences between model results (y_{mod}) and experimental data (y_{exp}), and t-1 is the value of the inverse t-distribution at a given confidence level (CL) and degrees of freedom (n_d–n_p). The availability of the the Jacobian matrix further allows for the computation of the sensitivity of model responses to changes in input parameters.

Optimization

There are two types of optimization methods applied in this *Guide*: manual optimization or numerical optimization routines. The manual optimization can be done for simple cases, e.g., estimating unknown parameters for two solid-phase species involved in one-step thermal decomposition kinetics; however, it requires much trial and error. Rules-of-thumb for conducting manual optimization are as follows. Consider having optimization targets as experimental data from bench-scale tests, such as the mass loss rate and temperature at various depths, which is a typical case. First, conduct kinetic modeling independently to understand at what temperatures each species will exist. Assume that the decomposition reaction occurs at temperatures between T_a and T_b, where $T_a < T_b$. The person conducting parameter estimation needs to understand any changes made in parameters related to reactants should affect fire behaviors at temperature smaller than T_a, and any changes made in parameters related to products should affect behaviors at temperatures greater than T_b (see (a) in Figure 5-8). With this in mind, manual optimization can be done. Second, understand that any changes made in heat-of-reaction (HoR) affects the mass-loss rate peak. When HoR is reduced, the peak becomes taller (see (b) in Figure 5-8). Third, understand that thermal conductivity (k) affects the temperature gradient throughout the specimen thickness. Reducing k results in a wider spread between the surface and the back surface temperature profiles (see (c) in Figure 5-8). Fourth, understand that specific-heat capacity (c_p) determines how soon material heats up, i.e., increases its body temperature. Applying smaller c_p results in faster increase in temperature profiles throughout, from surface to back surface (see (d) in Figure 5-8). Last, for estimating optical properties, apply simple approximations, e.g., having emissivity equal to 1, for surfaces that are close to black or quickly become black after exposure to radiative heating. Knowing these tips help manual optimization for estimation of unknown model parameters.

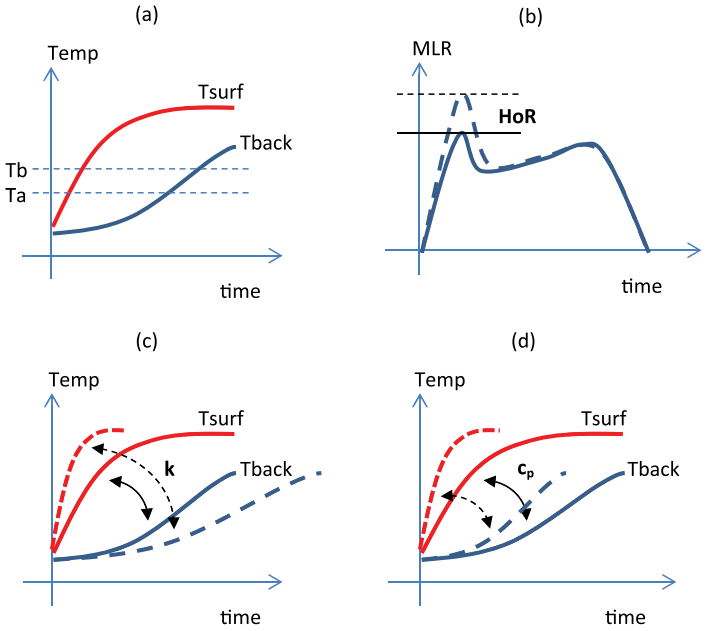

Figure 5-8. Understanding manual optimization: (a) For one-step thermal-decomposition kinetics that takes place within temperature range of $T_a < T < T_b$, the person conducting parameter estimation needs to understand changing parameters related to reactants should affect fire behaviors at temperatures below T_a, and changing parameters related to products should affect fire behaviors at temperatures above T_b; (b) Reducing HoR increases mass-loss rate peak; (c) Reducing thermal-conductivity results in wider spread between T_{surf} and T_{back}; (d) Reducing specific-heat capacity results in faster increase in temperature throughout. Note that results from greater parameter values are shown in solid lines, while those from smaller value are shown in dashed lines.

There are three types of numerical optimization routines that have been applied to fire pyrolysis modeling so far. In Table 5-11, these numerical optimization routines are introduced and compared. These are evolution-optimization schemes with high efficiency and robustness that allow multi-objective and multi-variable optimization under limited knowledge of the problem. All three optimization routines can be considered in terms of four processes: (1) Initialization of individuals, which refers to the set of initial guesses of unknown parameters; (2) Evolutionary process of selection and reproduction – selection from population for reproduction conducted for individuals with good fitness, i.e., better adaptation to their environment and reproduction resulting in new generation derived from a previous one while ensuring convergence, i.e., increase in fitness; (3) Termination of evolution at a user-defined termination condition.

Table 5-10. Three types of numerical optimization routines applied to comprehensive pyrolysis modeling in literature: Genetic Algorithm,[33,34] Shuffled Complex Evolution,[42,43,44] and Stochastic Hill-climber[35]

		Genetic Algorithm (GA)	Shuffled Complex Evolution (SCE)	Stochastic Hill-climber (SHC)
Process	Initialization	Initial traits of individuals are customarily randomly generated within a user-defined parameter space as many as the user-defined population size.	Random set of material properties is initial selected within the feasible parameter space (i.e., a population) and partitions it into several subsets or "complexes."	Initial traits of individuals are customarily randomly generated within a user-defined parameter space as many as the user-defined population size.
	Evolutionary Process of Selection and Reproduction	Probability of selection is customarily based on fitness. Reproduction occurs through the genetic processes of crossover (also called recombination) and/or mutation.	Each complex is allowed to evolve independently and, after a specified number of iterations, all points in each complex are combined back into a single population, ranked according to their objective function value, and then re-partitioned, i.e., shuffling the complexes. This procedure is iteratively repeated and allows for more extensive and freer exploration of the parameter space due to the partition of complexes. Shuffling enhances survivability by sharing information about the space gained independently by each complex.	Probability of selection is customarily based on fitness. Reproduction occurs through the genetic processes of random mutation only, i.e., same with genetic algorithm but without cross-mutation and a population of two - parent and child. The parents outlive the children if they are better adapted to the environment.
	Termination	The evolutionary process is continued until a user-defined termination condition is reached.	The evolutionary process is continued until a user-defined termination condition is reached.	The evolutionary process is continued until a user-defined termination condition is reached.
Computat-ional Expense		High	High	Low

Example Cases Overview

Table 5-11. Overview of example cases using comprehensive pyrolysis models

		Case 1	Case 2	Case 3	
Case Description		Single-step Decomposition RxN w/o Residue	Single-step Decomposition RxN w/ Residue	Two-step Decomposition RxN w/ Residue	Drying and sinlge-step decomposition RxN w/ residue
Material Example		PMMA	Corrugated Cardboard	Fire Retarded FRP Composite	Plywood
Estimation Approach	Mostly Non-optimization	Case 1 – A			
	Comparable Non-Optimization	Case 1 – B	Case 2 – B	Case 3 – B	
	Mostly Optimization	Case 1 – C	Case 2 – C		
	Manual Optimization				Case 3 – D

In the following, summarized results are shown for each example case. Detailed solutions for these example cases are given in Appendix D.

Case 1: Single-Step Decomposition Reaction without Residue Production

Virtual Microstructure of Virgin Material

- Homogeneous single layer

Decomposition Kinetics Type

- Type 0 or 1: fuel (solid) → pyrolyzates (gas)
- No solid-phase residue formed
- Weight-loss rate (DTG) with respect to temperature described with a single peak independent of the testing environment (inert or oxidative)

General Model-Parameter Table

- Virgin material is nonporous (no gas phase, only condense phase considered in modeling)
- Reduced-Model Parameter Table (see Table 5-12)

Table 5-12. Model-parameter table for Case 1 examples

		No	Condense Phase (*i=1*)	
Material Property		1	ρ_i	Density
		2	k_i	Thermal conductivity
		3	c_i	Specific heat capacity
		4	κ_i	Absorption coefficient
Parameters for Specifying Conditions		5	ε_i	Emissivity
			Heterogeneous RxN (*k=1*)	
Thermal Decomposition	Finite Thickness Reaction Zone	6	n_k	Reaction order
			Z_k	Pre-exponential factor
			E_k	Activation energy
		7	ΔH_k	heat
	Infinitely Thin Reaction Zone	6	T_p	Pyrolysis temperature
		7	ΔH_p	heat

Example 5.1 Modeling Poly(methylmethacrylate), PMMA

5.1.1 Model-Parameter Table

ID			A	B-GA	B-SCE	B-SHC	C-GA	C-SCE	C-SHC
Parameter		Unit	Measurement, Literature, or Approximation	Comparable Non-optimization and Optimization			Mostly Optimization		
Thermo-physical Property	ρ_i	kg/m^3	1200 ± 60	1200 ± 60			1200 ± 60		
			Measurement	Measurement			Measurement		
	k_i	W/m-K	0.18 ± 0.01	0.30 ± 0.01	0.21	0.33	0.29 ± 0.01	0.29	0.19
			Literature[45]	GA	SCE	SHC	GA	SCE	SHC
	c_i	J/kg-K	2.2 ± 0.1	1.8 ± 0.1	0.7	1.7	2.0 ± 0.1	1.1	1.7
			Literature[46,47]	GA	SCE	SHC	GA	SCE	SHC
Optical Property	κ_i	/m	2700 ± 1400	150000 ± 86000	1000000	3600000	2200 ± 500	790000	350000
			Literature[48]	GA	SCE	SHC	GA	SCE	SHC
	ε_i	-	0.85 ± 0.16	0.91 ± 0.01	0.66	0.89	0.66 ± 0.01	0.99	0.54
			Literature[48]	GA	SCE	SHC	GA	SCE	SHC
Thermal Decomposition Kinetics and Heats	n_k	-	1	1			0.5 ± 0.1	0.5	1.5
			Approximated	Approximated			GA	SCE	SHC
	Z_k	/s	(8.5 ± 4.3) x 10^{12}	(8.5 ± 4.3) x 10^{12}			(1.3 ± 0.6) x 10^{16}	3.3 x 10^{15}	5.3 x 10^{19}
			Model Fitting w/ multiple heating rate TGA data	Model Fitting with multiple heating rate TGA data			GA	SCE	SHC
	E_k	J/mol	(1.88 ± 0.06) x 10^5	(1.88 ± 0.06) x 10^5			(1.77 ± 0.01) x 10^5	2.27 x 10^5	2.43 x 10^5
			Model Fitting w/ multiple heating rate TGA data	Model Fitting with multiple heating rate TGA data			GA	SCE	SHC
	ΔH_k	kJ/kg	870 ± 130	870 ± 130			1100 ± 21	1300	520
			Literature[46]	Literature[46]			GA	SCE	SHC
Model Dependent Parameter	h_{crz}	W/m^2-K	0	12 ± 3	2	14	38 ± 4	3	-32
			Approximated adiabatic condition at back surface	GA	SCE	SHC	GA	SCE	SHC

*Note that GA, SCE and SHC refer to optimization routines – Genetic Algorithm, Shuffled Complex Evolution, and Stochastic Hill-climber. The GA's summarized parameter values are averaged values from near optimal parameter sets as sample population.

5.1.2 Validation

5.1.2.1 MODELING GOAL

Estimate model parameters for conducting modeling of pyrolysis of PMMA under various heating rates – heat-flux levels ranging up to ~ 100kW/m^2.

5.1.2.2 MODEL TYPE

GPYRO

5.1.2.3 MODELING APPROACH

- Instantaneous release of volatiles from solid to the gas phase
- Local thermal equilibrium between the solid and the volatiles
- No condensation of gaseous products
- No porosity effects

When conducting the GPYRO simulation for the cone calorimeter set-up, metal edge frame will be ignored, and backing is insulated. The ignition phenomenon is interpreted as the following in the simulations: at a known time-of-ignition (from experiment data), additional heat flux of 20 kW/m^2 is applied to the surface to simulate heat flux from the flame. This is the reference value found from the work of Beaulieu[49], where actual measurement of the flame heat flux of a black PMMA was conducted. The heat-of-combustion was determined using micro-scale combustion calorimeter[50] operating in following condition: pyrolysis in nitrogen atmosphere by heating samples (2 to 4 mg) at a fixed rate of 1 K/s from 373 to 1173 K. Value is normalized by initial sample weight: ΔH_c = 24100 kJ/kg

5.1.2.4 EXPERIMENT DESCRIPTION

Cone calorimeter test

5.1.2.5 DATA SET

- Cone calorimeter test data of thick PMMA (thickness, δ ranging from 24 ~ 29 mm) impinged with effective heat fluxes (EHF) of 23, 46, and 69 kW/m^2 is found to show the burning behavior under various heat-flux levels that are less than 100 kW/m^2. Data were reproduced from Stoliarov's paper[48], which are shown in Figure 5-9:

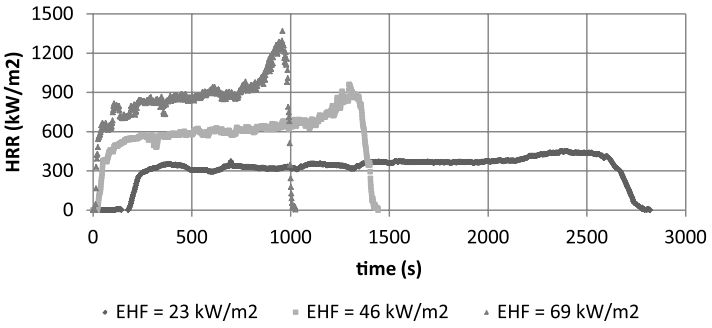

Figure 5-9. Cone calorimeter test data of thick PMMA (thickness, δ ranging from 24 ~ 29 mm) impinged with effective heat fluxes (EHF) of 23, 46, and 69 kW/m^2

- Surface temperature measured at steady burning during cone tests of black PMMA decomposing under various heat flux levels is found from Beaulieu's work[49] on black PMMA to be within 350 ± 50°C.

5.1.2.6 OPTIMIZATION TARGETS

MLR at EHF = 46 kW/m^2 with thick PMMA sample from cone calorimeter test

5.1.2.7 SENSITIVE PARAMETERS

ε_i, n_k, Z_k, E_k, ΔH_k

5.1.2.8 UNCERTAINTY

Uncertainty in Experiment Data

- Data reproducibility is checked by repeating 5 identical PMMA tests under 49 kW/m^2 heat flux level with medium thickness samples (thickness, δ ranging from 7.7 ~ 9.4 mm)
- Uncertainty of peak HRR, average HRR and time to peak HRR are estimated via taking 2 standard deviation of the difference and normalizing them by the mean of this parameter – 17%, 7% and 17%, respectively
- Assume:
  - Uncertainty of HRR is comparable to that of MLR
  - Uncertainties are comparable to those of thicker PMMA tested at various heat-flux levels
  - Data set found above is close to the averaged curves from multiple identical tests under same conditions
  - Uncertainty in surface temperature during steady burning is ±50°C

Uncertainty in Modeling Outputs

- Baseline case: HF = 46 kW/m^2, thickness = 29 mm
- Sensitive parameters varied one at a time from baseline to its max and min by considering uncertainty; however, due to compensation effect, pre-exponential factor and activation energy will be considered in pair to have max and min decomposition temperature
- Uncertainty is considered for GA optimization cases (B-GA, C-GA) only using 50 near-optimal parameter sets
- Integration of uncertainty is calculated by Law of Propagation of Uncertainty

5.1.2.9 TG / DTG PREDICTIONS AT 10 °C/MIN HEATING RATE USING ESTIMATED KINETIC PARAMETERS

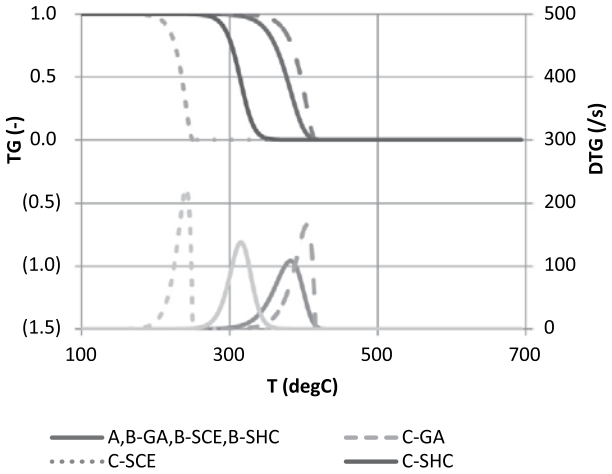

Figure 5-10. TG/DTG curves at 10°C/min heating rate with different estimation results for kinetic parameters for thermal decomposition of PMMA

5.1.2.10 COMPARISON BETWEEN DATA AND COMPUTED-MODELING OUTPUTS

- Modeling is conducted for case with HF = 46 kW/m^2, thickness = 29 mm

Table 5-13. Comparison between experiment data from cone calorimeter test and modeling outputs using estimated parameter values via either direct measurement, literature search, or approximation (A); measurements and numerical optimization (B-GA, B-SCE, B-SHC); or mostly numerical optimization (C-GA, C-SCE, C-SHC)

	Data	A	B-GA	B-SCE	B-SHC	C-GA	C-SCE	C-SHC
Peak MLR (g/m^{2}s)	36.9 ±6.3	45.1 ±10.6	40.9 ±5.3	32.6	39.3	27.5 ±0.7	34.4	67.0
Avg MLR (g/m^{2}s)	24.9 ±1.7	24.2 ±5.2	26.7 ±2.7	25.9	26.6	24.0 ±0.5	26.4	28.0
t to pMLR (s)	1310 ±223	1408 ±252	1285 ±123	1317	1284	1391 ±32	1297	1233
Ts (°c)	350 ±50	413 ±21	433 ±20	407	409	244 ±3	419	343

5.1.2.11 MODELING OUTPUT: MASS LOSS RATE (MLR)

- Case used in optimization process

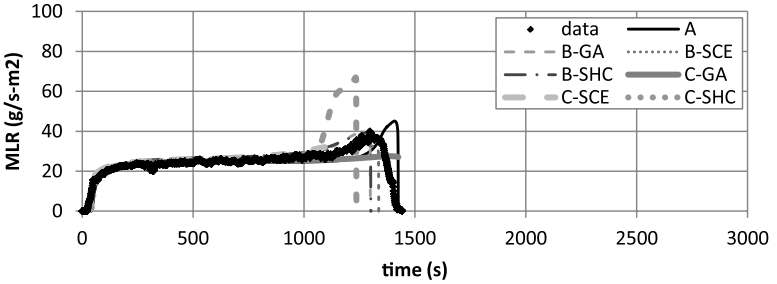

Figure 5- 11. Mass-loss rate (MLR) comparisons for PMMA between actual MLR from experiment (data) and modeled MLR (A, B-GA, B-SCE, B-SHC, C-GA, C-SCE, C-SHC) at applied heat flux of 46 kW/m². Note that data shown were used to estimate model-parameter values via numerical optimization using GA, SCE, or SHC routines.

- Extrapolation

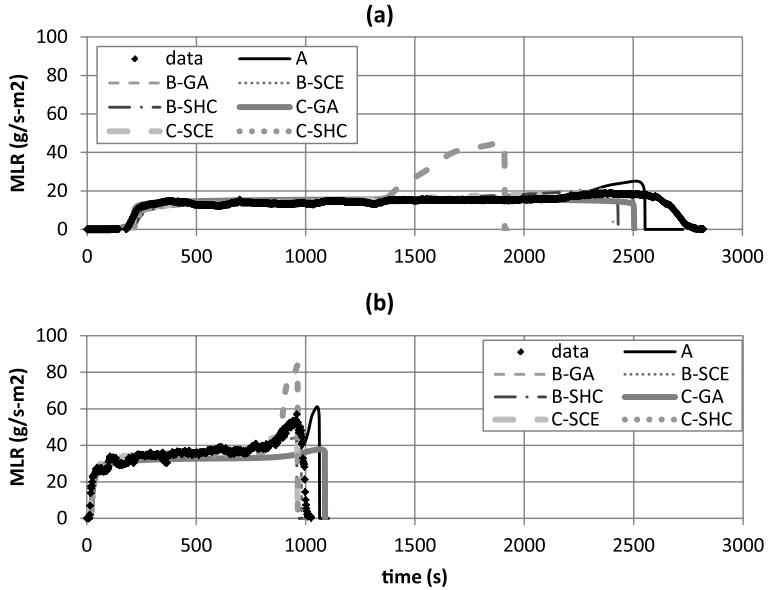

Figure 5-12. Mass-loss rate (MLR) comparisons for PMMA between actual MLR from experiment (data) and modeled MLR (A, B-GA, B-SCE, B-SHC, C-GA, C-SCE, C-SHC) at applied heat flux of (a) 23 and (b) 64 kW/m². Note that data shown were not included in the model-parameter-estimation process; hence, these two cases are considered as extrapolation cases.

5.1.2.12 MODELING OUTPUT: SURFACE TEMPERATURE (T_{surf})

- Case used in optimization process

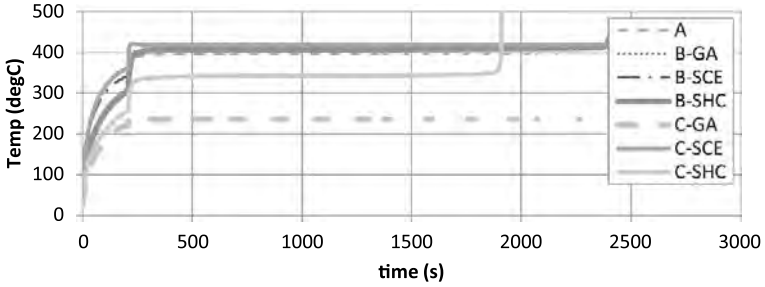

Figure 5-13. Surface-temperature (T_{surf}) comparisons for PMMA modeling using parameters estimated from different approaches – direct measurement, literature search, or approximation (A); measurement and numerical optimization (B-GA, B-SCE, B-SHC); mostly numerical optimization (C-GA, C-SCE, C-SHC) at applied heat flux of 46 kW/m². Note that data shown were used to estimate model-parameter values via numerical optimization using GA, SCE, or SHC routines.

- Extrapolation

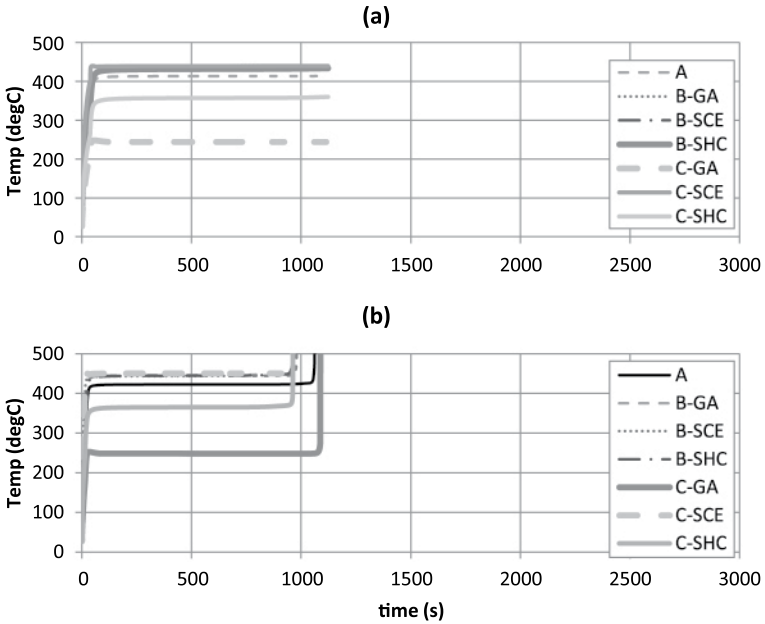

Figure 5-14. Surface-temperature (T_{surf}) comparisons for PMMA modeling using parameters estimated from different approaches – direct measurement, literature search, or approximation (A); measurement and numerical optimization (B-GA, B-SCE, B-SHC); mostly numerical optimization (C-GA, C-SCE, C-SHC) at applied heat flux of (a) 23 and (b) 64 kW/m². Note that data shown were not included in the model-parameter-estimation process; hence, these two cases are considered as extrapolation cases.

5.1.3 Commentary

GENERAL COMMENTS

- TG/DTG
  - Whether kinetic modeling is conducted independently using TGA data (A, B-GA, B-BSE, B-SHC) or as a part of numerical optimization (C-GA, C-SCE, C-SHC), decomposition of PMMA is considered to occur within the temperature range of 200°C to 400°C.
  - Among GA, SCE and SHC, estimation of SCE was closest, followed by SHC and GA to TGA data
  - Having surface temperature data as an additional optimization, target should have provided constraints to the optimization problem, because kinetic parameters directly determine the surface temperature. However, this approach was not utilized, for uncertainty in surface temperature measurement was too high – 350 ± 50°C
- Comparison Between Data and Computed-Modeling Outputs
  - Better agreement between data and modeling outputs for the peak MLR is found when kinetic parameters are estimated through a separate process using TGA data (A, B-GA, B-BSE, B-SHC) compared with numerical optimization along with estimating other unknowns together (C-GA, C-SCE, C-SHC)
  - Average MLR and time-to-peak-MLR from all modeling cases show good agreement with data
  - Simulated surface temperature at steady burning of PMMA is greater (less than 10 s) than that of measurement for cases B-GA, B-SCE, B-SHC and C-SCE, while simulated surface temperature is lower (greater than 50 s) than that of measurement for case C-GA. Results from cases A and C-SHC are in good agreement.
- MLR
  - Direct Measurement or Optimization at HF = 46 kW/m^2: Good agreement exists between experiment data and all modeling results, whether modeled with measured parameters or optimized in the time frame of exposure to heating source up to steady burning. However, in the later time, where the peak occurs, the result from C-SHC becomes unsatisfying, considering the data with its uncertainty, while others can be considered as satisfying.
  - Direct Measurement or Extrapolation at HF = 23 kW/m^2: Good agreement exists between experiment data and all modeling results, except for C-SHC case.
  - Direct Measurement or Extrapolation at HF = 64 kW/m^2: Good agreement exists between experiment data and all modeling results, except for C-GA and C-SHC case.
- Surface Temperature
  - See above

LIMITATION IN MODELING

- When considering limitation of the parameters in simulating PMMA, the modeler should take into account the applicability of the parameters and their associated uncertainties. For example, any assumptions used when determining a parameter value via experiment direct or indirect measurements can be utilized to understand when the parameter value becomes inappropriate. For this example of pyrolysis modeling of PMMA, most consideration can be given to the parameters related to decomposition kinetics.
- In this example, kinetic modeling was conducted with TGA data obtained from nitrogen environment. However, studies[49,51,52] have suggested that PMMA decomposes differently with respect to heating rates and availability of oxygen. The decomposition rate of PMMA increases with respect to oxygen concentration, because oxygen aids unzipping of the polymer by being involved in the depolymerization process of the polymer. Also, the oxygen dependency increases at lower heating rates than at higher heating rates. Possible explanation for this can be given by considering the diffusion of oxygen from nearby gas phase to the condense phase. At lower heating rates, decomposition rate is relatively slow; therefore, the time allowed for oxygen to diffuse to the polymer layer and be involved in the decomposition process is relatively longer. However, at higher heating rates, decomposition rate is relatively higher even without the involvement of oxygen in the decomposition process. This results in a shorter time scale for transportation of oxygen via diffusion to the condense phase. In other words, the positive effect of enhancing decomposition by having oxygen involved in the process, compared to decomposition in non-oxidative condition, is compensated by the time necessary for oxygen diffusion to occur from the gas phase to the condense phase. Hence, the increase in decomposition rate of PMMA due to the presence of oxygen in the gas phase is more profound in conditions with lower heating rates than in higher heating rates. Visual observations of the surface phenomena during PMMA decomposition also provide evidence that above explanation is reasonable. Based on experimental work conducted by Beaulieu[49] during decomposition of PMMA, "bubbling" occurs on the surface. The bubbles are relatively large, forming a thick layer of bubbles when irradiated at lower heat-flux levels and they are smaller, forming a thin bubbling layer, when irradiated at higher heat-flux levels. Considering the bubbling is an effective way of the polymer to enhance oxygen diffusion and larger bubbles entrains more oxygen, reduction in decomposition rate due to increasing time necessary for oxygen diffusion at higher heat-flux levels seems plausible, with bubbles becoming smaller as increasing from a lower heat flux to a higher heat flux.

- Figure 5-15 shows TGA thermograms of PMMA decomposition conducted under constant heating rates – 2, 5, 10 and 20 K/min – and two different environments – nitrogen and air (data obtained from work conducted by Matala[34]). As shown below and discussed earlier, there is significant difference between the curves produced from nitrogen and air tests. This indicates that decomposition kinetics is different in two cases, and the difference is due to oxygen diffusion from the gas phase surrounding the solid sample surface with respect to the "bubbling" phenomenon.

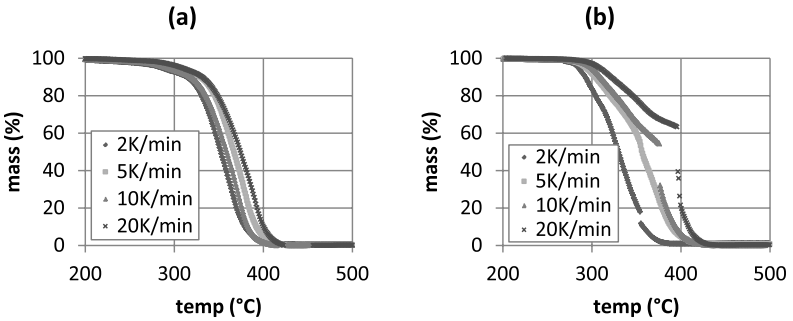

Figure 5-15. TGA thermograms of PMMA decomposition conducted under constant-heating rates – 2, 5, 10, and 20K/min – and two different environments – (a) nitrogen and (b) air

Case 2: Single-Step Decomposition Reaction With Residue Production

Virtual Microstructure of Virgin Material

- Homogeneous single layer

Decomposition Kinetics Type

- Type 0 or 1: fuel (solid) → residue (solid) + pyrolyzates (gas)
- Weight-loss rate (DTG) with respect to temperature described with a single peak independent of the testing environment (inert or oxidative)

General Model Parameter Table

- Although actual virgin material is porous, porous nature of material is implicitly accounted for in density only (no gas phase, only condense phases – virgin state fuel and residue – considered in modeling)
- Reduced Model Parameter Table (see Table 5-14)

Table 5-14. Model-parameter table for Case 2 examples

		No	Condense Phase (*i=1,2*)	
Material Property		**1**	ρ_i	Density
		2	k_i	Thermal conductivity
		3	c_i	Specific-heat capacity
		4	κ_i	Absorption coefficient
Parameters for Specifying Conditions		**5**	ε_i	Emissivity
			Heterogeneous RxN (*k=1*)	
Thermal Decomposition	Finite-Thickness Reaction Zone	**6**	n_k	Reaction order
			Z_k	Pre-exponential factor
			E_k	Activation energy
		7	ΔH_k	Heat
	Infinitely-Thin Reaction Zone	**6**	T_p	Pyrolysis temperature
		7	ΔH_p	heat

Example 5.2 Modeling Triple-layered Corrugated Cardboard

5.2.1 Model Parameter Table

ID				B-GA	B-SCE	B-SHC	C-GA	C-SCE	C-SHC
Parameter			Unit	Comparable Non-optimization and Optimization			Mostly Optimization		
Thermo-physical Property	i = 1 (fuel)	ρ_i	kg/m^3	110			110		
				Measurement			Measurement		
		k_i	W/m-K	0.08 ± 0.01			0.13	0.21	0.21
				Measurement			GA	SCE	SHC
		c_i	J/kg-K	2.8	2.3	0.6	2.0	2.4	1.7
				GA	SCE	SHC	GA	SCE	SHC
	i = 2 (residue)	ρ_i	kg/m^3	25	20	11	26	10	43
				GA	SCE	SHC	GA	SCE	SHC
		k_i	W/m-K	0.29	0.32	0.32	0.20	0.35	0.20
				GA	SCE	SHC	GA	SCE	SHC
		c_i	J/kg-K	1.5	1.1	0.2	1.0	0.8	2.2
				GA	SCE	SHC	GA	SCE	SHC
Optical Property	i = 1 (fuel)	κ_i	/m	10^6			10^6		
				Approximated as opaque			Approximated as opaque		
		ε_i	-	0.88 ± 0.01			0.72	0.50	0.65
				Measurement			GA	SCE	SHC
	i = 2 (residue)	κ_i	/m	10^6			10^6		
				Approximated as opaque			Approximated as opaque		
		ε_i	-	1			0.82	0.93	0.96
				Approximated			GA	SCE	SHC
Thermal Decomposition Kinetics and Heats		n_k	-	1			3.7	3.0	2.2
				Approximated			GA	SCE	SHC
		Z_k	/s	1.1 x 10^{21}			3.9 x 10^6	9.8 x 10^{19}	6.0 x 10^{14}
				Model Fitting with single heating rate TGA data			GA	SCE	SHC
		E_k	J/mol	2.49 x 10^5			7.0 x 10^4	2.47 x 10^5	3.02 x 10^5
				Model Fitting with single heating rate TGA data			GA	SCE	SHC
		ΔH_k	kJ/kg	123	512	809	88	54	0.7
				GA	SCE	SHC	GA	SCE	SHC
Model Dependent Parameter		h_{crz}	W/m^2-K	19	8	14	10	8	10
				GA	SCE	SHC	GA	SCE	SHC
		n_{kz}(i=1)	-	5.6	4.6	7.6	0		
				GA	SCE	SHC	Approximated		

*Note that GA, SCE and SHC refer to optimization routines – Genetic Algorithm, Shuffled Complex Evolution, and Stochastic Hill-climber.

5.2.2 Validation

5.2.2.1 MODELING GOAL

Estimate model parameters for conducting modeling of pyrolysis of triple-layered corrugated cardboard under various heating rates – heat-flux levels ranging up to ~ 100kW/m^2.

5.2.2.2 MODEL TYPE

GPYRO

5.2.2.3 MODELING APPROACH

- Instantaneous release of volatiles from solid to the gas phase
- Local thermal equilibrium between the solid and the volatiles
- No condensation of gaseous products
- No porosity effects

Further details can be found from Reference 43.

When conducting the 1D simulation for the FPA set-up, insulation at back surface is not modeled explicitly but included as some heat loss to the back surface. In this example case, only AN FPA experiment with nitrogen as purge gas will be considered; hence, there is no ignition phenomenon to be modeled.

5.2.2.4 EXPERIMENT DESCRIPTION

Fire Propagation Apparatus Test

5.2.2.5 DATA SET

- Fire Propagation Apparatus (FPA) test data of triple-wall corrugated cardboard, i.e., two layers of corrugated cardboard (thickness, δ is 30 mm) impinged with effective heat fluxes (EHF) of 20 to 110 kW/m^2 is found. Data were reproduced from Chaos' paper[43], which are shown below for 20, 60 and 110 kW/m^2 cases for mass loss rate (MLR) and surface temperature measurements using pyrometer (see Figure 5-16):

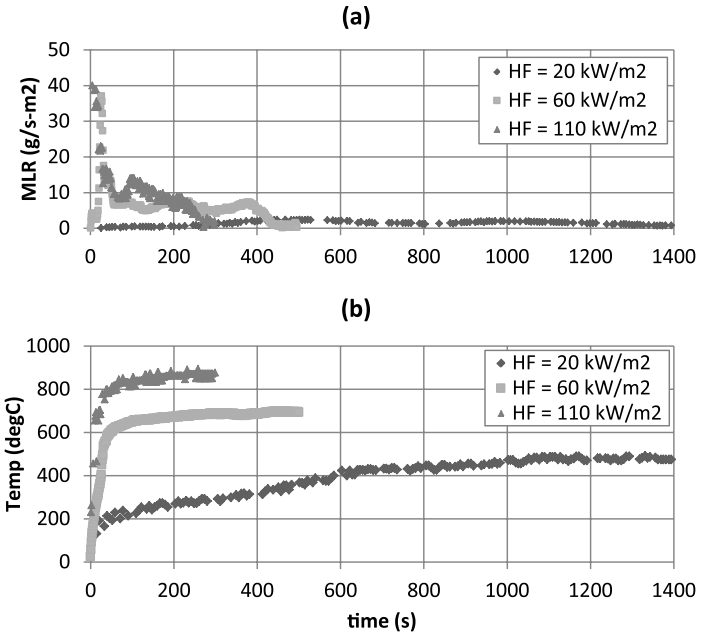

Figure 5-16. Fire propagation apparatus (FPA) Test Data – (a) mass-loss rate; and (b) surface-temperature profile – of triple-wall corrugated cardboard, i.e., two layers of corrugated cardboard (thickness, δ is 30 mm) impinged with effective heat fluxes (EHF) of 20 to 110 kW/m²

5.2.2.6 OPTIMIZATION TARGETS

MLR, cumulative mass loss (CML), and surface-temperature data with triple-layered corrugated cardboard sample from Fire Propagation Apparatus test at HF = 60 kW/m²

5.2.2.7 SENSITIVE PARAMETERS

ε_i, $\rho_{i=2}$, n_k, Z_k, E_k, ΔH_k

5.2.2.8 UNCERTAINTY

Uncertainty in Experiment Data

- Data is acquired from two repeating FPA tests of triple-wall corrugated cardboard under 60 kW/m² heat-flux level with nitrogen atmosphere.
- Uncertainty analysis is conducted based on these two data sets. The uncertainties are quantified with confidence intervals with α = 0.05 and assuming normal distribution of population (size 2).
- Assume:
  - Uncertainties are comparable to the same sample tested at various heat-flux levels

Uncertainty in Modeling Outputs

- Typically, uncertainty is considered for GA optimization cases (B-GA, C-GA) only by taking an average of a large population of near-optimals with their confidence intervals to quantify uncertainty when numerical optimization is used to estimate unknowns. However, in this case, GA found the best optimized parameter set that has relatively large fitness than other near-optimals. Therefore, estimation of uncertainty of GA's optimization was not possible; hence, was considered as certain.

5.2.2.9 TG / DTG PREDICTIONS AT 10 °C/MIN HEATING RATE USING ESTIMATED KINETIC PARAMETERS

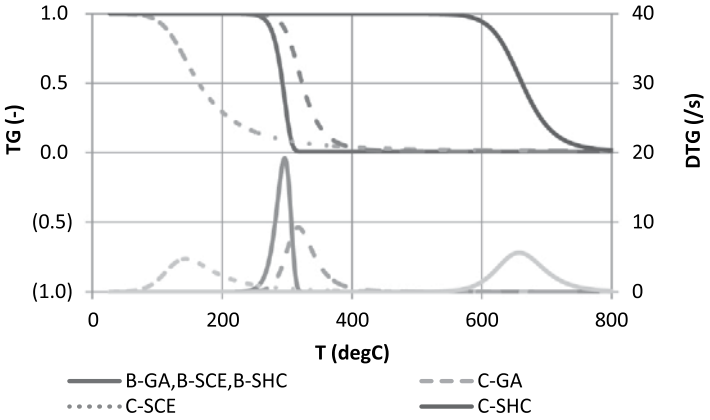

Figure 5-17. TG/DTG Curves at 10°C/min heating rate with different estimation results for kinetic parameters for thermal decomposition of corrugated cardboard: For better comparison, TG and DTG thermograms have been scaled to result in 100% conversion.

5.2.2.10 COMPARISON BETWEEN DATA AND COMPUTED-MODELING OUTPUTS

- Modeling is conducted for case with HF = 46 kW/m^2, thickness = 29 mm

Table 5-15. Comparison between experiment data from fire-propagation apparatus test and modeling outputs using estimated parameter values via either measurements and numerical optimization (B-GA, B-SCE, B-SHC) or mostly numerical optimization (C-GA, C-SCE, C-SHC)

	Data	B-GA	B-SCE	B-SHC	C-GA	C-SCE	C-SHC
Peak MLR (g/m^{2}s)	35 ± 4	28	24	53	23	29	N/A
Avg MLR (g/m^{2}s)	5.7 ± 0.6	4.6	5.4	5.9	4.8	6.0	N/A
t to pMLR (s)	27 ± 1	19	13	19	4	12	N/A
Ts at 300 s (°c)	696 ± 16	685	682	684	679	679	685

5.2.2.11 MODELING OUTPUT: MASS-LOSS RATE (MLR)

- Case used in optimization process

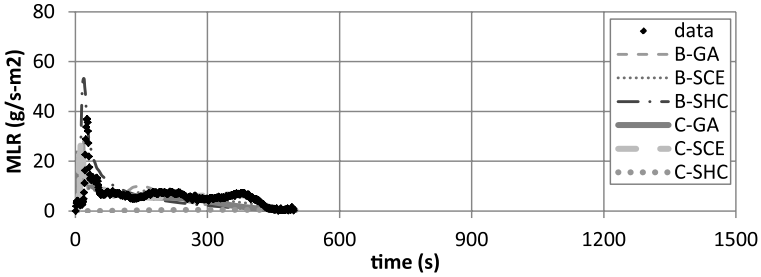

Figure 5-18. Mass-loss rate (MLR) comparisons for corrugated cardboard between actual MLR from experiment (data) and modeled MLR (B-GA, B-SCE, B-SHC, C-GA, C-SCE, C-SHC) at applied heat flux of 60 kW/m². Note that data shown were used to estimate model-parameter values via numerical optimization using GA, SCE, or SHC routines.

- Extrapolation

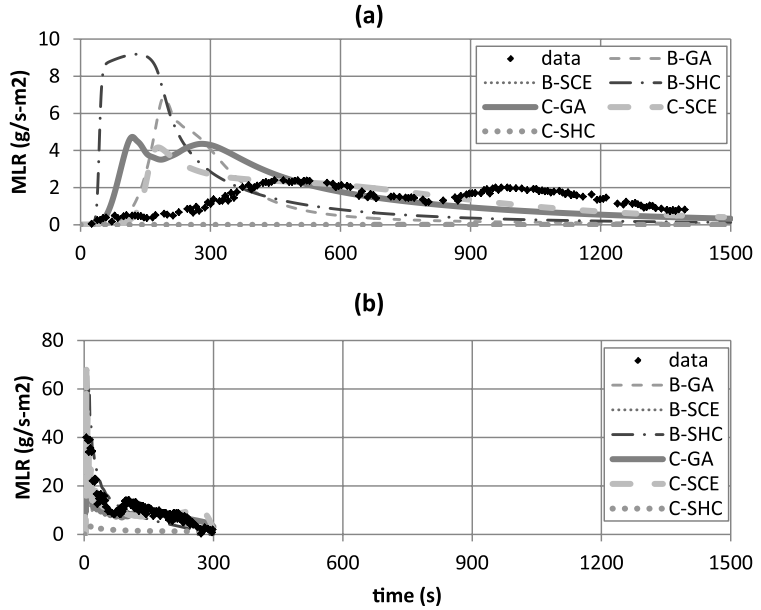

Figure 5-19. Mass-loss rate (MLR) comparisons for corrugated cardboard between actual MLR from experiment (data) and modeled MLR (B-GA, B-SCE, B-SHC, C-GA, C-SCE, C-SHC) at applied heat flux of (a) 20 and (b) 110 kW/m². Note that data shown were not included in the model parameter estimation process; hence, these two cases are considered as extrapolation cases.

5.2.2.12 MODELING OUTPUT: SURFACE TEMPERATURE (T_{surf})

- Case used in optimization process

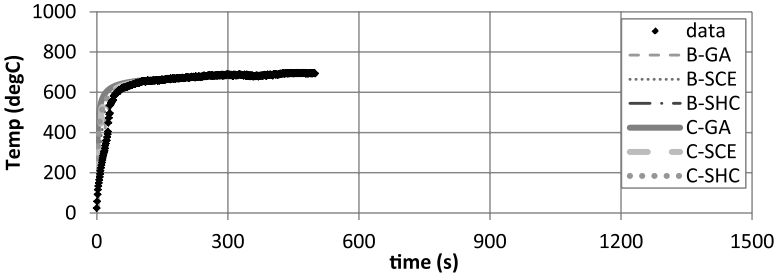

Figure 5-20. Surface-temperature (T_{surf}) comparisons for corrugated cardboard between actual T_{surf} from experiment (data) and modeled T_{surf} (B-GA, B-SCE, B-SHC, C-GA, C-SCE, C-SHC) at applied heat flux of 60 kW/m². Note that data shown were used to estimate model-parameter values via numerical optimization using GA, SCE or SHC routines.

- Extrapolation

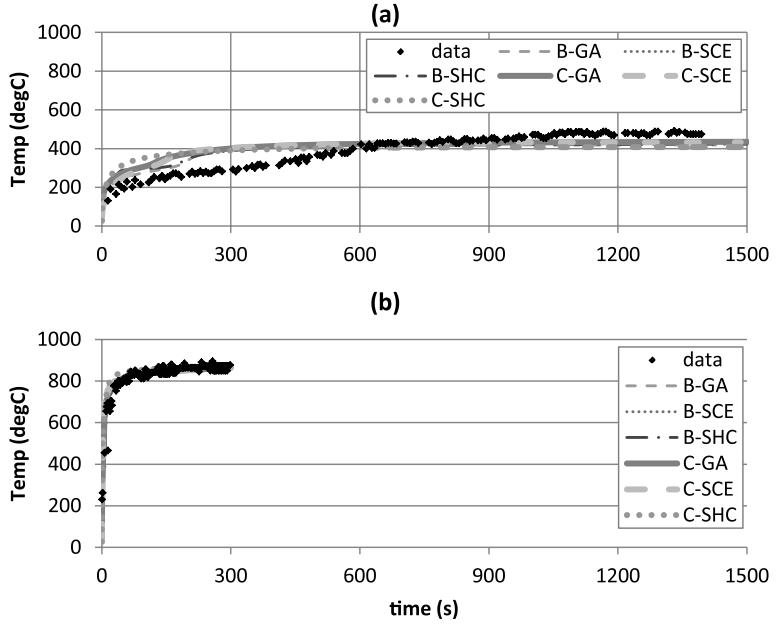

Figure 5-21. Surface-temperature (T_{surf}) comparisons for corrugated cardboard between actual T_{surf} from experiment (data) and modeled T_{surf} (B-GA, B-SCE, B-SHC, C-GA, C-SCE, C-SHC) at applied heat flux of (a) 20 and (b) 110 kW/m². Note that data shown were not included in the model-parameter-estimation process; hence, these two cases are considered as extrapolation cases.

5.2.3 Commentary

GENERAL COMMENTS

- TG/DTG
  - When kinetic modeling is conducted independently using TGA data (B-GA, B-BSE, B-SHC), the DTG peak exist near 300°C.
  - Among GA, SCE, and SHC, optimization of SCE of kinetic parameters as part of other unknown parameter estimation is closest to actual TGA data (B-GA, B-SCE, B-SHC), followed by GA and SHC.
  - Optimization of SHC of kinetic parameters along with other unknown parameter estimation is considered as unsuccessful, because decomposition temperature is excessively high (see mass-loss rate optimization and extrapolation results)
- Comparison between Data and Computed-Modeling Outputs
  - Generally, better agreement between data and modeling outputs is found when kinetic parameters are estimated through a separate process using TGA data (B-GA, B-BSE, B-SHC) than numerical optimization, along with estimating other unknowns together (C-GA, C-SCE, C-SHC)
  - None of the modeled peak MLRs is in quantitative agreement with data
  - Average MLR of B-SCE, B-SHC and C-SCE are in good agreement with data
  - None of the modeled time to peak MLRs is in quantitative agreement with data
  - Surface temperatures at 300 s of B-GA, B-SCE, B-SHC, and C-SHC are in good agreement with data
- MLR
  - Optimization at HF = 60 kW/m^2: Although the peak may be off for some cases, generally good agreement exists between experiment data and all modeling results considering the trend, except for that of C-SHC, indicating that optimization of C-SHC – optimizing for all unknowns using SHC – was unsuccessful. Oscillation in the MLR curve is due to the inhomogeneity of the sample – corrugated cardboard – which is not captured in modeling due to the homogeneous assumption made when solving the problem.
  - Extrapolation at HF = 20 kW/m^2: Poor agreement exists between experiment data and all modeling results. None of the modeling cases is able to capture the slow increase in mass-loss rate in the earlier times after exposure to heating source.
  - Extrapolation at HF = 110 kW/m^2: Good agreement exists between experiment data and all modeling results, except for C-SHC case.
- Surface Temperature
  - Optimization at HF = 60 kW/m^2: Generally good agreement exists between experiment data and all modeling results considering the trend, even for that of C-SHC. Also, when thermal conductivity of the sample at its virgin state was independently measured and that value was used, modeling was able to capture the slow increase in surface temperature up until 400°C followed by a jump up to ~550°C.

- Extrapolation at HF = 20 kW/m^2: Poor agreement exists between experiment data and all modeling results. None of the modeling cases is able to capture the slow increase in surface temperature in the earlier times after exposure to heating source.
- Extrapolation at HF = 110 kW/m^2: Good agreement exists between experiment data and all modeling results, including C-SHC case.

LIMITATION IN MODELING

- When considering limitation of the parameters in modeling corrugated cardboard, the modeler should take into account the applicability of the parameters and their associated uncertainties. For example, any assumptions used when determining a parameter value via experiment direct or indirect measurements can be utilized to understand when the parameter value becomes inappropriate. For this example of pyrolysis modeling of corrugated cardboard, most consideration can be given to the parameters related to decomposition kinetics.
- As shown in the figure below of corrugated cardboard decomposed in TGA at 20 K/min under nitrogen and air atmosphere, the simplified kinetic modeling using a one-step decomposition mechanism is only true for a "dry" sample tested in nitrogen. Clearly, decomposition of a "dry" sample in air results in two distinct DTG peaks. Therefore, the effect of the simplification (one-step) made to kinetic modeling should be addressed when discussing large-scale simulation quality of the parallel panel experiment using the optimized parameter set from this exercise.

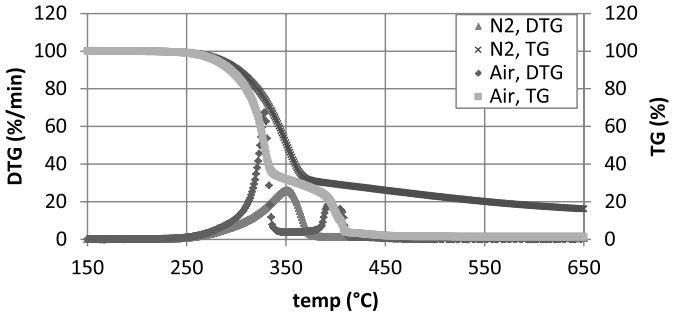

Figure 5-22. TGA thermograms of corrugated cardboard decomposition conducted under constant-heating rate of 20 °C/min and two different environments – nitrogen and air

Case 3: Two-Step Decomposition Reaction With Residue Production

Virtual Microstructure of Virgin Material

- Effective homogeneous single layer

Decomposition Kinetics Type

- Type 3 with two-step reaction
  - Reactant_1 (solid) → Product1 (solid) + pyrolyzates (gas)
  - Reactant_2 (solid) → Product2 (solid) + pyrolyzates (gas)
- Weight-loss rate (DTG) with respect to temperature described with two overlapping peaks independent of the testing environment (inert or oxidative)

General Model Parameter Table

- Although actual virgin material is porous, the porous nature of the material is implicitly accounted for in density only (no gas phase, only condense phases – Reactant 1 and 2, Product 1 and 2 – considered in modeling)
- Reduced Model Parameter Table (see Table 5-16)

Table 5-16. Model-parameter table for Case 3 examples

	No	**Condense Phase (*i=1,2,3,4*)**	
Material Property	**1**	ρ_i	Density
	2	k_i	Thermal conductivity
	3	c_i	Specific-heat capacity
	4	κ_i	Absorption coefficient
Parameters for Specifying Conditions	**5**	ε_i	Emissivity
		Heterogeneous RxN (*k=1,2*)	
Kinetic Parameters and Heats A n^{th} Order Model and Arrhenius-type Expression	**6**	n_k	Reaction order
		Z_k	Pre-exponential factor
		E_k	Activation energy
	7	ΔH_k	Heat

Example 5.3 Modeling FRP Composite with Modified Acrylic Resin with High-charring Inorganic Additive

An example case is shown for a fiberglass-reinforced polymer (FRP) composite with modified-acrylic resin with high-charring inorganic fire-retardant additive. Most of the approach and reference values of the input parameters for this simulation were obtained from Kim and Dembsey's work.[30]

Modified-acrylic resin (MA) is essentially unsaturated polyester (UPE) with Methacrylic Acid (MMA) replacing most of the styrene monomers. Flame-retarded resin with MA is manufactured by adding a filler-type inorganic additive (A) as an additive where its loading versus resin is **MA:A = 0.38:0.62** by weight. Typical inorganic additives are hydrates such as alumina trihydroxide (ATH) or magnesium hydroxide, antimony trioxide, borax, chalk, silica, etc.[53] Because this additive was known to give a high-charring effect, A was categorized with typical hydroxides used as flame-retardant fillers. These hydroxides works as a flame retardant by resulting in an endothermic dehydration reaction that produces oxides and water.[54,55] The water produced by this reaction vaporizes, which is an endothermic reaction, and the vapor dilutes the gaseous phase. The oxides remain in the char layer, which adds an insulative effect. This flame retardant is added with a relatively large amount (50 to 65%) compared with other types of additives. By adding a significant amount of an inorganic flame retardant, the polymer becomes more brittle. Because this is an inorganic additive, inserting this material into the polymer system by 50 to 65 wt% of its original polymer reduces the available fuel within the condensed phase. In addition to this effect, usually the additive has a higher heat capacity compared with the base polymer; hence, the flame retarded polymers with these types of hydroxides require more energy to increase the body temperature to its pyrolysis level. According to the product description, this resin with the flame-retardant additive is formulated to be Class I per ASTM E 84[56] (flame spread index < 20 and smoke developed < 225).

→ **Propose two parallel reactions for MA and A thermal decomposition**

Figure 5-23. Cross-section of FRP composite with modified-acrylic resin with high-charring inorganic additive

Composite panels were fabricated by vacuum bagging for a relatively high glass-content composite (31 ± 2 wt% of glass, thickness of 8.9 ± 0.2 mm) using two different types of fiberglass mats that were wetted with resin (see Figure 5-23 for cross-section of composite). The two types of fiberglass (E-glass) used in the composite are a chopped-strand mat and a glass-roving woven mat with an area density of 25 g/m^2 and 880 g/m^2, respectively. The chopped-strand mat is thinner and more porous than the woven mat. The laminate schedule (provided by the manufacturer) is chopped-strand mat and roving alternating three times with another chopped-strand mat layer at the end. Visual inspection of a polished cross-section of the composite slab is consistent with this laminate schedule, but with polymer-resin layers between each fiberglass layer. The chopped-strand mat layer is difficult to identify in the cross section, perhaps because more resin is soaked into this layer than the roving layer. The roving layer is observed as a prominent glass layer possibly because the resin is absorbed only at the fiberglass layer surfaces leaving the interior with primarily glass.
→ **Apply effective homogeneous single layer of resin, additive and fiberglass mixture**

5.3.1 Model Parameter Table

ID				GA(avg)	GA(best)	SCE	SHC
Parameter			Unit	Comparable Non-optimization and Optimization			
Thermo-physical Property	i = 1 (Resin)	ρ_i	kg/m^3	1200			
				Measurement			
		k_i	W/m-K	0.23 ± 0.02	0.21	0.54	0.04
				GA	GA	SCE	SHC
		c_i	J/kg-K	1400 ± 100	2200	300	1300
				GA	GA	SCE	SHC
	i = 2 (R_residue)	ρ_i	kg/m^3	253			
				Measurement, Kinetic Modeling			
		k_i	W/m-K	0.19 ± 0.02	0.12	0.08	0.31
				GA	GA	SCE	SHC
		c_i	J/kg-K	1900 ± 200	1600	1800	1800
				GA	GA	SCE	SHC
	i = 3 (Additive)	ρ_i	kg/m^3	2300			
				Measurement			
		k_i	W/m-K	1.22 ± 0.10	1.44	0.82	2.74
				GA	GA	SCE	SHC
		c_i	J/kg-K	1200 ± 100	930	2500	2400
				GA	GA	SCE	SHC
	i = 4 (A_residue)	ρ_i	kg/m^3	1558			
				Measurement, Kinetic Modeling			
		k_i	W/m-K	0.24 ± 0.04	0.22	0.59	0.36
				GA	GA	SCE	SHC
		c_i	J/kg-K	1200 ± 100	2200	300	780
				GA	GA	SCE	SHC
	i = 5 (Glass)	ρ_i	kg/m^3	2600			
				Reference (MSDS)			
		k_i	W/m-K	0.18 ± 0.02	0.15	0.30	0.09
				GA	GA	SCE	SHC
		c_i	J/kg-K	400 ± 100	170	300	110
				GA	GA	SCE	SHC
Optical Property	i = 1 (R)	κ_i	/m	10^6			
				Approximated as opaque			
		ε_i	-	0.84 ± 0.03	0.81	0.82	1.24
				GA	GA	SCE	SHC
	i = 2 (R_res)	κ_i	/m	10^6			
				Approximated as opaque			
		ε_i	-	0.90 ± 0.03	0.87	1.00	0.97
				GA	GA	SCE	SHC
	i = 3 (A)	κ_i	/m	10^6			
				Approximated as opaque			
		ε_i	-	0.81 ± 0.04	0.77	1.00	0.84
				GA	GA	SCE	SHC

	i = 4 (A_res)	κ_i	/m	10^6			
				Approximated as opaque			
		ε_i	-	0.89 ± 0.03	0.96	1.00	0.42
				GA	GA	SCE	SHC
	i = 5 (Glass)	κ_i	/m	10^6			
				Approximated as opaque			
		ε_i	-	0.88 ± 0.02	0.90	1.00	1.41
				GA	GA	SCE	SHC
Kinetics and Heats	k = 1 R → $R_{residue}$+vap↑	n_k	-	1.3		Model Fitting with Multiple-Heating-Rate TGA Data	
		Z_k	/s	3.2×10^{12}			
		E_k	J/mol	1.83×10^5			
		ΔH_k	kJ/kg	$(2.5 \pm 0.2) \times 10^3$	2.0×10^3	2.6×10^3	2.6×10^3
				GA	GA	SCE	SHC
	k = 2 A → $A_{residue}$ + vap↑	n_k	-	5.0		Model Fitting with Multiple-Heating-Rate TGA Data	
		Z_k	/s	1.6×10^{12}			
		E_k	J/mol	1.60×10^5			
		ΔH_k	kJ/kg	3760 ± 1130 (30%)			
				Measurement, DSC			
Model-Dependent Parameter		n_{kz} (i=5)	-	0.59 ± 0.06	0.58	0.01	0.18
				GA	GA	SCE	SHC
		n_c (i=5)	-	0.53 ± 0.06	0.37	0.88	-0.26
				GA	GA	SCE	SHC
		γ (i=2)	m	0.00348 ± 0.00134	0.00051	0.00002	0.02482
				GA	GA	SCE	SHC
		γ (i=4)	m	0.00475 ± 0.00184	0.00625	0.00001	0.05832
				GA	GA	SCE	SHC
		γ (i=5)	m	0.00769 ± 0.00225	0.00001	0.00003	-0.02453
				GA	GA	SCE	SHC

*Note that GA, SCE and SHC refer to optimization routines – Genetic Algorithm, Shuffled Complex Evolution, and Stochastic Hill-climber. For GA, there are two cases. GA(avg) is the average estimated values from ~50 near-optimal-parameter-sets population. GA(best) is the parameter set with best fitness among those near-optimal population.

5.3.2 Validation

5.3.2.1 MODELING GOAL

Estimate model parameters for conducting modeling of pyrolysis of modified-acrylic resin with high-charring additive FRP composite under various heating rates – heat-flux levels ranging from 25 kW/m^2 to 75kW/m^2.

5.3.2.2 MODEL TYPE

GPYRO

5.3.2.3 MODELING APPROACH

- Instantaneous release of volatiles from solid to the gas phase
- Local thermal equilibrium between the solid and the volatiles
- No condensation of gaseous products
- No porosity effects
- When conducting the GPYRO simulation for the cone calorimeter set-up, metal edge frame will be ignored, and backing is insulated. The ignition phenomenon is interpreted as the following in the simulations: at a known time-of-ignition (from experiment data), additional heat flux of 20 kW/m^2 is applied to the surface to simulate heat flux from the flame. This value is estimated from a measurement from this material pyrolyzing in the cone with a total heat-flux gauge measuring heat flux impinging on the sample surface (see Figure 5-24– test conducted at 50 kW/m^2 applied heat flux; from time-of-ignition an increase in measured heat flux is observed due to flame).

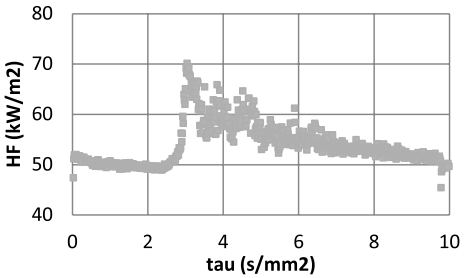

Figure 5-24. Total heat flux measured from sample surface during cone calorimeter test

- For the back surface, an additional layer of insulation with known properties is modeled to simulate some heat loss through the back. The contact resistance (hcrz) between the FRP composite and the insulation is estimated as roughly as 10 W/m^{2}K and that of insulation layer and ambient as 1 W/m^{2}K.
- In addition to the parameters introduced in the previous section (see parameter table), the model (GPYRO) has a coefficient (γ, GAMMA) that is used to model radiative heat transfer through the pores. This parameter with T^3 is a model-dependent parameter that is added as another term in the effective thermal conductivity. γ is used for porous fiberglass and decomposed solid species, which results in more a porous state due to the weight loss; therefore, more radiative-heat transfer through the gas phase pores, i.e., for condense-phase species *i = 2* (A_residue), *4* (MA_residue) and *5* (G).
- Another set of parameters included as unknowns is the temperature-dependent terms used to describe the variation of thermal conductivity and specific-heat capacity with respect to temperature increase: $k(T) = k_0(T/T_r)^{n_k}$ and, $c(T) = c_0(T/T_r)^{n_c}$, respectively, where T_r is a reference temperature. Only properties of fiberglass is temperature dependent knowing that for high glass-content FRP composite, glass may be a controlling factor for its fire behavior. This approach is utilized to give much flexibility during parameter estimation for fiberglass.

5.3.2.4 EXPERIMENT DESCRIPTION

Cone calorimeter Test

5.3.2.5 DATA SET

- Cone calorimeter (cone) test data of modified-acrylic resin with high-charring additive FRP composite (thickness, δ is 8.9 ± 0.2 mm, density, ρ is 1900 kg/m^3) impinged with effective heat fluxes (EHF) of 25 to 75 kW/m^2 is obtained and are shown below (see Figure 5-25) for mass-loss rate (MLR), surface and back-face temperature measurements:

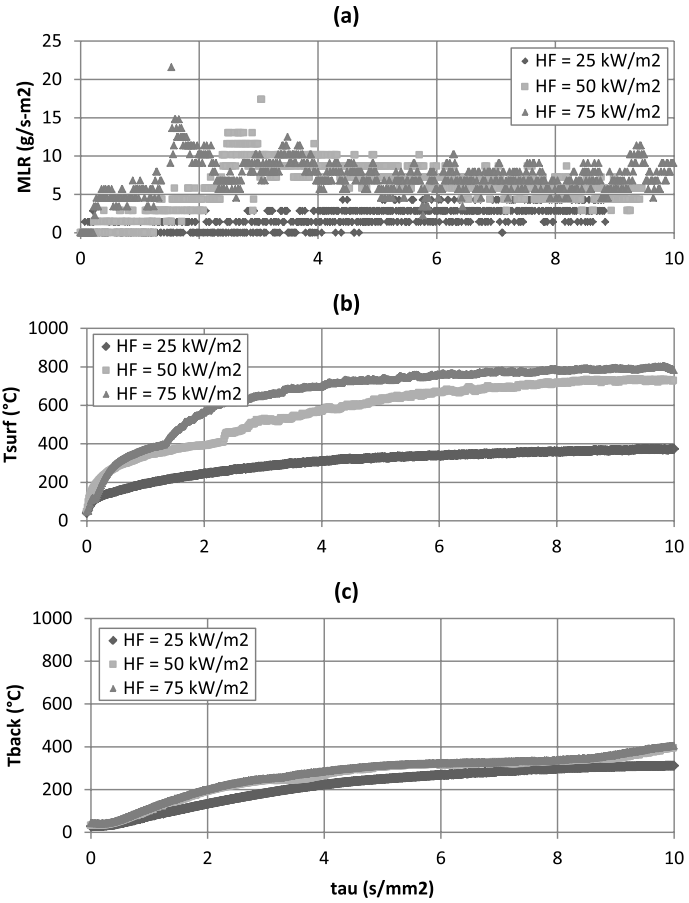

Figure 5-25. Cone calorimeter
Cone test data of modified-acrylic resin with high-charring additive FRP composite (thickness, δ is 8.9 ± 0.2 mm, density, ρ is 1900 kg/m^3) impinged with effective heat fluxes (EHF) of 25 to 75 kW/m^2

5.3.2.6 OPTIMIZATION TARGETS

Mass-loss rate (MLR), cumulative mass loss (CML), surface (T_s), and back (T_b) surface temperature data with FRP composite sample from cone calorimeter test at HF = 50 kW/m^2

5.3.2.7 SENSITIVE PARAMETERS

- Identified by conducting OAT method (see Appendix for detail)
- R residue's ε, A_residue's *k*, A_residue's γ, G's n_k, G's n_c

5.3.2.8 UNCERTAINTY

Uncertainty in Experiment Data

- Data is acquired from three repeating cone tests of modified-acrylic resin with inorganic high-charring additive FRP composite with relatively high glass content under 50 kW/m^2 heat flux level.
- The uncertainties in the MLR and thermocouple measurements at front surface were quantified by comparing data from these three identical FRP composite tests. Note that normalized time, time divided by sample thickness square, i.e., τ = time/δ^2, is used to remove the effect of different sample thicknesses when comparing. Because the data is transient, values at different times (τ = 1, 3, 5 and 7 s/mm^2) from each test have been used to calculate the standard deviation at each time. Then these are averaged and used to estimate uncertainty by applying student t distribution with a sample size of three and calculating the 95% confidence interval: uncertainty in MLR and T_s are **± 2.2g/sm^2** and **± 67 °C**, respectively.
- Assume:
  - Uncertainties are comparable to the same sample tested at various heat flux levels
  - Data set found above is close to the averaged curves from multiple identical tests under same conditions

Uncertainty in Modeling Outputs

- Baseline case: HF = 50 kW/m^2, thickness = 8.7 mm
- Sensitive parameters varied one at a time from baseline to its max and min by considering uncertainty
- Uncertainty is considered for GA optimization case only using ~50 near-optimal parameter sets
- Integration of uncertainty is calculated by the Law of Propagation of Uncertainty: uncertainty in model's MLR, Ts, and Tb are ± 1.2g/sm2, ± 6 °C and ± 43 °C, respectively.

5.3.2.9 TG / DTG PREDICTIONS AT 10 °C/MIN HEATING RATE USING ESTIMATED KINETIC PARAMETERS

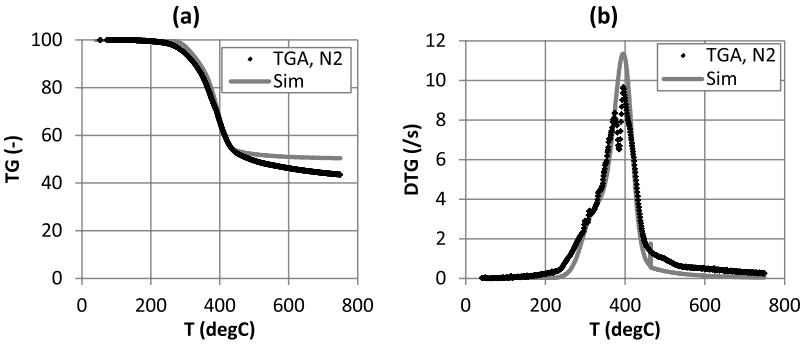

Figure 5-26. TG/DTG curves at 10°C/min heating rate with different estimation results for kinetic parameters for thermal decomposition of fire retarded-FRP composite: testing of resin with additive sample (~10mg) with nitrogen purge

5.3.2.10 COMPARISON BETWEEN DATA AND COMPUTED-MODELING OUTPUTS

- Modeling is conducted for case with HF = 46 kW/m^2, thickness = 29 mm

Table 5-17. Comparison between experiment data from cone calorimeter test and modeling outputs using estimated parameter values using numerical optimization (GA, SCE, SHC)

	Data	GA(avg)	GA(best)	SCE	SHC
Peak MLR (g/m^{2}s)	27 ± 31	10.7 ± 1.2	11.4	10.6	12.4
Avg MLR (g/m^{2}s)	5.8 ± 1.6	6.3 ± 1.2	6.1	6.2	8.1
t to pMLR (s)	200 ± 70	196	189	189	196
Ts at τ = 1 s/mm^2 (°c)	341 ± 54	336 ± 6	327	339	326
Ts at τ = 3 s/mm^2 (°c)	541 ± 100	496 ± 6	515	519	450
Ts at τ = 5 s/mm^2 (°c)	632 ± 9	583 ± 6	607	611	517
Tb at τ = 1 s/mm^2 (°c)	101 ± 14	111 ± 43	117	91	133
Tb at τ = 3 s/mm^2 (°c)	240 ± 23	274 ± 43	276	265	289
Tb at τ = 5 s/mm^2 (°c)	299 ± 25	302 ± 43	302	302	330

5.3.2.11 MODELING OUTPUT: MASS-LOSS RATE (MLR)

- Case used in optimization process

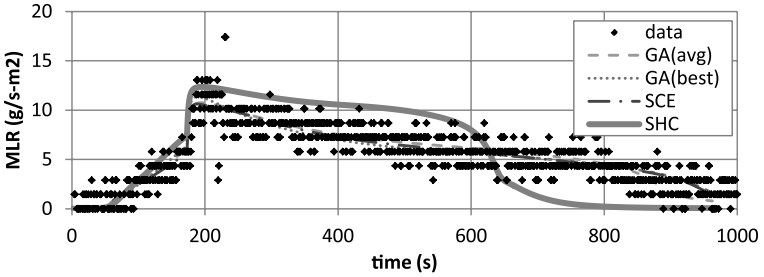

Figure 5-27. Mass-loss rate (MLR) comparisons for FRP composite with modified acrylic resin with high-charring inorganic additive between actual MLR from experiment (data) and modeled MLR (GA, SCE, SHC) at applied heat flux of 50 kW/m^2. Note that data shown were used to estimate model-parameter values via numerical optimization using GA, SCE, or SHC routines.

- Extrapolation

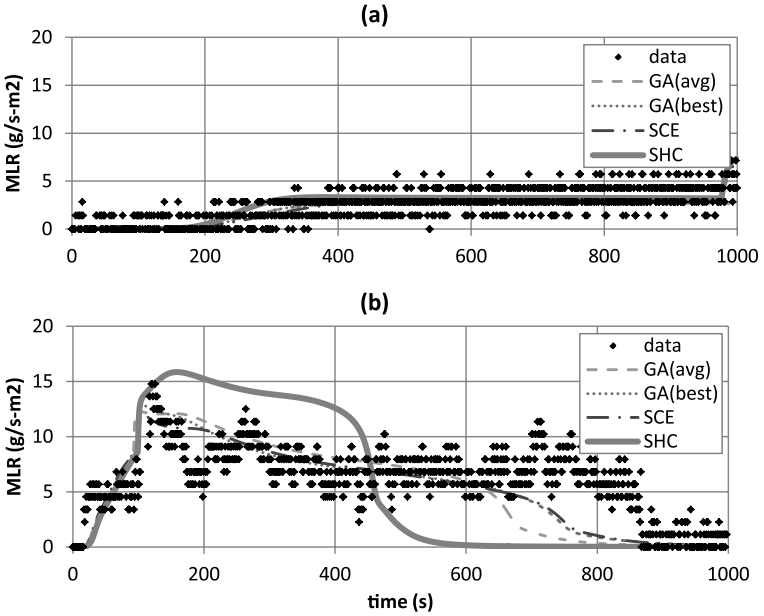

Figure 5-28. Mass-loss rate (MLR) comparisons for FRP composite with modified acrylic resin with high-charring inorganic additive between actual MLR from experiment (data) and modeled MLR (GA, SCE, SHC) at applied heat flux of (a) 25 and (b) 75 kW/m^2. Note that data shown were not included in the model-parameter-estimation process; hence, these two cases are considered as extrapolation cases.

5.3.2.12 MODELING OUTPUT: SURFACE TEMPERATURE (T_{SURF})

- Case used in optimization process

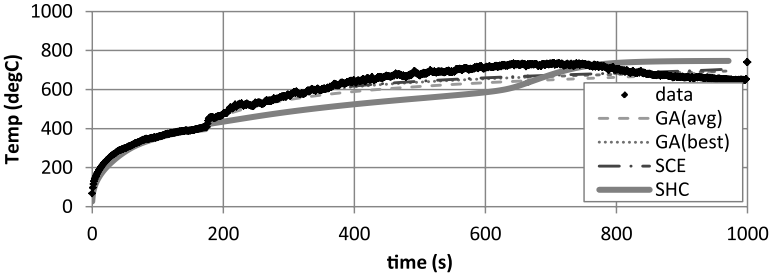

Figure 5-29. Surface-temperature (T_{surf}) comparisons for FRP composite with modified-acrylic resin with high-charring inorganic additive between actual T_{surf} from experiment (data) and modeled T_{surf} (GA, SCE, SHC) at applied heat flux of 50 kW/m². Note that data shown were used to estimate model-parameter values via numerical optimization using GA, SCE, or SHC routines.

- Extrapolation

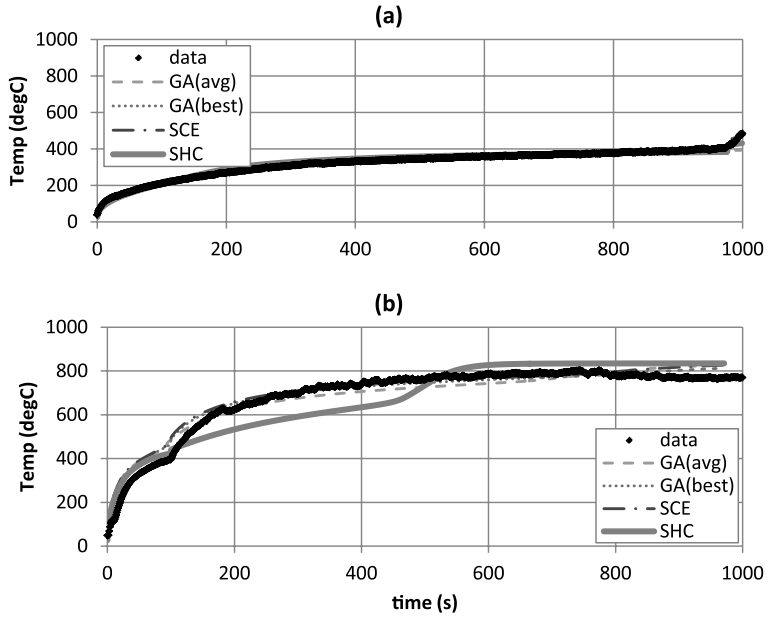

Figure 5-30. Surface-temperature (T_{surf}) comparisons for FRP Composite with modified acrylic resin with high-charring inorganic additive between actual T_{surf} from experiment (data) and modeled T_{surf} (GA, SCE, SHC) at applied heat flux of (a) 25 and (b) 75 kW/m². Note that data shown were not included in the model-parameter-estimation process; hence, these two cases are considered as extrapolation cases.

5.3.2.13 MODELING OUTPUT: BACK SURFACE TEMPERATURE (T_{back})

- Case used in optimization process

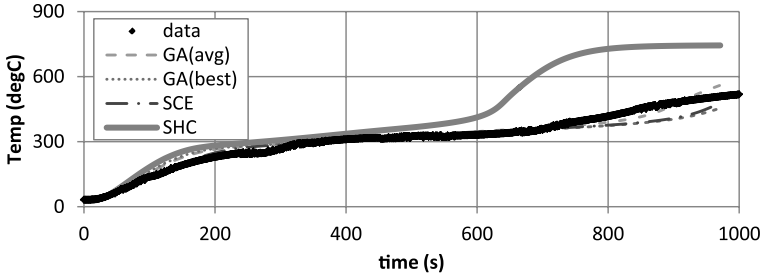

Figure 5-31. Back-surface-temperature (T_{back}) comparisons for FRP composite with modified-acrylic resin with high-charring inorganic additive between actual T_{back} from experiment (data) and modeled T_{back} (GA, SCE, SHC) at applied heat flux of 50 kW/m². Note that data shown were used to estimate model-parameter values via numerical optimization using GA, SCE, or SHC routines.

- Extrapolation

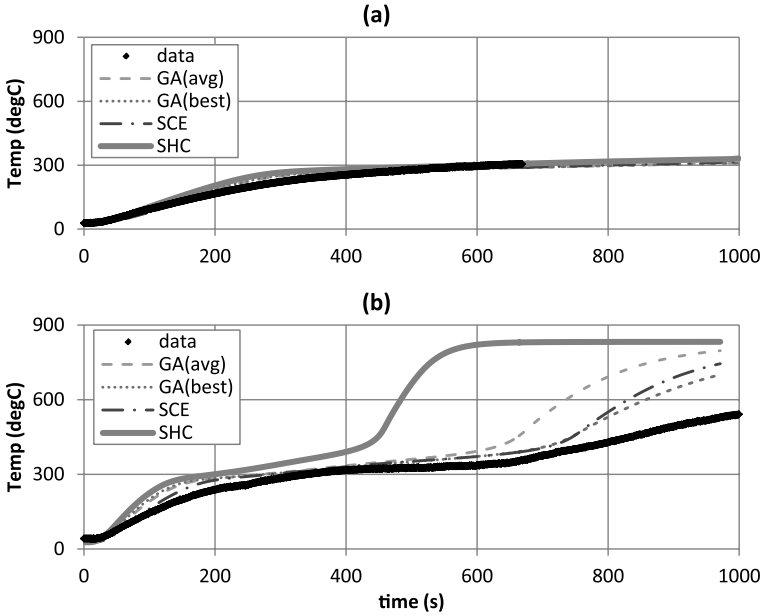

Figure 5-32. Back-surface-temperature (T_{back}) comparisons for FRP composite with modified acrylic resin with high-charring inorganic additive between actual T_{back} from experiment (data) and modeled T_{back} (GA, SCE, SHC) at applied heat flux of (a) 25 and (b) 75 kW/m². Note that data shown were not included in the model-parameter-estimation process; hence, these two cases are considered as extrapolation cases.

5.3.3 Commentary

GENERAL COMMENTS

- TG/DTG
  - Good agreement between simulated TG/DTG thermograms and those of actual from TGA experiment is shown when thermal decomposition kinetics is modeled using multiple heating rate data.
  - Proposed kinetic model does not account for minor mass loss at relatively lower and higher temperature range.
- Comparison between Data and Computed Modeling Outputs
  - Modeled peak MLRs are all in quantitative agreement with data considering its uncertainty.
  - Avg MLRs of modeling are in good agreement with data except for that of SHC
  - Modeled time to peak MLRs are all in quantitative agreement with data
  - Modeled surface temperatures at earlier time (τ = 1 s/mm^2) show good agreement with data while at later times (τ = 3 and 5 s/mm^2) modeling results deviates from experiment results; however, considering that there is flame interfering with data collection from surface thermocouple, uncertainty in data should probably be larger.
  - Modeled back-surface temperatures at different times from GA(avg) show good agreement with data considering the modeling uncertainty. Those from GA(best), SCE and SHC are off by ~ 10 °C from experiment results.
- MLR
  - Optimization at HF = 50 kW/m^2: Generally good agreement exists between experiment data and all modeling results considering the trend, except for that of SHC indicating that optimization of SHC was close to being unsuccessful.
  - Extrapolation at HF = 25 kW/m^2: Good agreement exists between experiment data and all modeling results. All of the modeling cases are able to capture the slow increase in mass-loss rate in the earlier times after exposure to heating source and a jump near 1000 s due to ignition.
  - Extrapolation at HF = 75 kW/m^2: Good agreement exists between experiment data and all modeling results, except for SHC case. SHC's prediction is slightly higher than data and predictions from other cases; however, considering the uncertainty in the data, this falls within the acceptable bounds.
- Surface Temperature
  - Optimization at HF = 50 kW/m^2: Generally good agreement exists between experiment data and all modeling results considering the trend, even for that of SHC. Note that after ignition (post-ignition stage) the flame interferes with data reading of thermocouple on surface.
  - Extrapolation at HF = 25 kW/m^2: Good agreement exists between experiment data and all modeling results.
  - Extrapolation at HF = 75 kW/m^2: Good agreement exists between experiment data and all modeling results, except for SHC case.

LIMITATION IN MODELING

- When considering limitation of the parameters in modeling this fire-retarded FRP composite, the modeler should take into account the applicability of the parameters and their associated uncertainties. For example, any assumptions used when determining a parameter value via experiment direct or indirect measurements can be utilized to understand when the parameter value becomes inappropriate. For this example, most consideration can be given to the parameters related to decomposition kinetics. One should be cautious that these findings can cause this FRP composite to behave differently under changing conditions, which were not included in the parameter-estimation process.
- First, the reaction-order-type kinetic model can be used to fit the DTG data with some degree of satisfaction for all reactions (see +A-R and R). However, the estimated reaction order is high as 5 for +A-R reaction. This indicates that the model is forced to fit the data, knowing that the reaction order in this magnitude is rare to find in the literatures. Also, the DSC data confirms that the reaction- order-type model was inappropriate for +A-R as well. Although the model is giving high correlation coefficients between the data and modeling for +A-R reaction, the DSC data show that +A-R should exist from 200°C and end before 400°C, where a strong endotherm is observed. When the data is fit with a reaction-order-type kinetic model, the additive decomposition temperature range extends beyond 400°C, ending near 600°C.
- Second, the decomposition of the additive reaction is best described by a kinetic model that describes a diffusion-controlled reaction (Jander's type model). The model type is reasonable considering that the model simulates the weight loss to be slow initially with respect to temperature increase and decays relatively fast after the weight-loss rate peak. This modeling becomes suitable for an additive decomposing within a resin-polymer system resulting in a time delay due to the time necessary to degrade the polymer near the additive. Consider the additive being mixed within the resin polymer. For the additive to undergo a decomposition reaction, the degradation of the resin polymer should occur simultaneously, because the additive is aggregated within the resin. Having the additive decomposition temperature lower than that of the resin, the decomposition of the additive is delayed until the temperature is higher to allow the resin to decompose. When this model is actually applied, it provides good estimate of the slow weight loss at the initial stage near 200°C and the temperature range for the entire reaction. Additionally, when this model is used, the modeling results for weight-loss rate after 300°C matches well with the actual DTG data together with R reaction described with a reaction-order-type kinetic model.

- Third, although kinetic modeling has been conducted to give best fitness between the modeling and the DTG data obtained over various heating rates (5 to 60°C/min), assuming that the kinetics are identical irrespective of heating rates, changes in the kinetic over four heating rates have been noticed. At lower heating rates, the portion of the sample weight consumed via R_residue oxidation increases where at higher heating rates it decreases. This can be explained by understanding that the R_residue oxidation reaction is controlled by oxygen diffusion from the ambient to the condense phase. At a low heating rate, more time is available for oxygen diffusion with respect to temperature change, allowing an increase in the weight loss due to oxidation. However, when the heating rate is higher, the conditions become the opposite and pyrolysis reaction (R) dominates. The fitness of the model to DTG data increases when this effect is accounted for in the modeling.

Example 5.4 Modeling Plywood

5.4.1 Model Parameter Table

Parameter			Unit	Comparable Non-optimization and Manual Optimization	
Thermo-physical Property	i = 1 (water)	ρ_i	kg/m^3	1000	
				Reference[57]	
		k_i	W/m-K	0.6	
				Reference[57]	
		c_i	J/kg-K	4200	
				Reference[57]	
	i = 2 (dry_wood)	ρ_i	kg/m^3	504 ± 10	
				Measurement	
		k_i	W/m-K	0.26	
				Manual Optimization with Initial Guess of 0.122 Measured at 20 °C (dry_wood, ASTM C518/E1225)	
		c_i	J/kg-K	2400	
				Manual Optimization with Initial Guess of 1200 Measured at 20 °C (dry_wood, ASTM E1269)	
	i = 3 (char)	ρ_i	kg/m^3	173	
				Measurement	
		k_i	W/m-K	0.12	
				Manual Optimization with Initial Guess of 0.122 Measured at 20 °C (dry_wood, ASTM C518/E1225)	
		c_i	J/kg-K	3700	
				Manual Optimization with Initial Guess of 1200 Measured at 20 °C (dry_wood, ASTM E1269)	
Optical Property	i = 1 (water)	ε_i	-	1.00	
				Approximated	
	i = 2 (dry_wood)	κ_i	/m	10^6	
				Approximated as opaque	
		ε_i	-	0.891 ± 0.018	
				Measurement, ASTM E903	
	i = 3 (char)	κ_i	/m	10^6	
				Approximated as opaque	
		ε_i	-	1.00	
				Approximated	
Kinetics and Heats	k = 1 water → vap↑	n_k	-	5.0	Model Fitting with Multiple Heating Rate TGA Data
		Z_k	/s	2.5 x 10^{12}	
		E_k	J/mol	83 x 10^4	
		ΔH_k	kJ/kg	2500 ± 800 (30%)	
				Measurement, DSC	
	k = 2 dry_wood → char + vap↑	n_k	-	1.7	Model Fitting with Multiple-Heating-Rate TGA Data
		Z_k	/s	5.0 x 10^{16}	
		E_k	J/mol	2.10 x 10^5	
		ΔH_k	kJ/kg	631	
				Manual Optimization	
Model-Dependent Parameter		γ (i=3)	m	0.0036	
				Manual Optimization	

5.4.2 Validation

5.4.2.1 MODELING GOAL

Estimate model parameters for conducting modeling of pyrolysis of plywood under various heating rates – heat-flux levels ranging from 25 kW/m^2 to 75kW/m^2.

5.4.2.2 MODEL TYPE

GPYRO

5.4.2.3 MODELING APPROACH

- Instantaneous release of volatiles from solid to the gas phase
- Local thermal equilibrium between the solid and the volatiles
- No condensation of gaseous products
- No porosity effects
- When conducting the GPYRO simulation for the cone calorimeter set-up, metal edge frame will be ignored and backing is insulated. The ignition phenomenon is interpreted as the following in the simulations: at a known time-of-ignition (from experiment data), additional heat flux of 20 kW/m^2 is applied to the surface to simulate heat flux from the flame. This value is estimated from a measurement from this material pyrolyzing in the cone with a total-heat-flux gauge measuring heat flux impinging on the sample surface. Figure 5-33 shows the total-heat-flux measurement from sample surface (test conducted at 50 kW/m^2 applied heat flux). From the time-of-ignition ($\tau \sim 0.1$ s/mm^2) an increase above the 50 kW/m^2 line in measured heat flux is observed due to flame. The oscillation in data in the time interval of ignition to $\tau = 1$ s/mm^2 is an artifact due to water evaporation, which had condensed near the water-cooled heat-flux gauge.

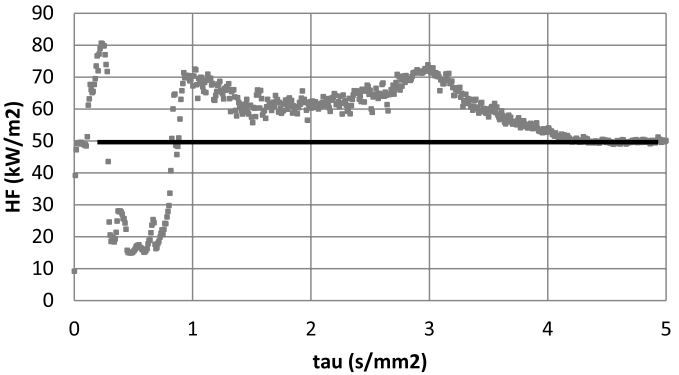

Figure 5-33. Total heat flux measured from sample surface during cone calorimeter test

- For the back surface, an additional layer of insulation with known properties is modeled to simulate some heat loss through the back. The contact resistance (hcrz) between the FRP composite and the insulation is estimated as roughly 10 W/m^{2}K and that of insulation layer and ambient as 1 W/m^{2}K.

- In addition to the parameters introduced in the previous section (see parameter table), the model (GPYRO) has a coefficient (γ, GAMMA) that is used to model radiative heat transfer through the pores. This parameter with T^3 is a model dependent parameter that is added as another term in the effective thermal conductivity. γ is used for porous fiberglass and decomposed solid species, which results in a more porous state due to the weight loss; therefore, more radiative heat transfer through the gas phase pores, i.e., for condense phase specie i = 2 (char).

5.4.2.4 EXPERIMENT DESCRIPTION

Cone Calorimeter Test

5.4.2.5 DATA SET

- Cone calorimeter (cone) test data of plywood (thickness, δ is 11.1 ± 0.1 mm, density, ρ is 540 ± 10 kg/m^3) impinged with effective heat fluxes (EHF) of 25 to 75 kW/m^2 is obtained and are shown below for mass-loss rate (MLR), surface and back face temperature measurements (see Figure 5-34):

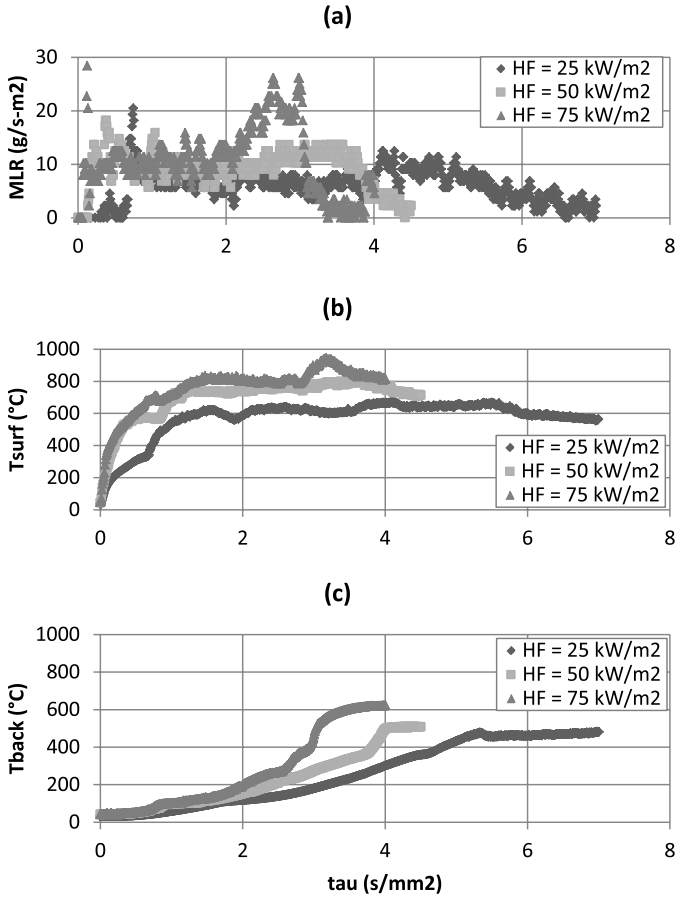

Figure 5-34. Cone calorimeter (cone) test data of plywood (thickness, δ is 11.1 ± 0.1 mm, density, ρ is 540 ± 10 kg/m^3) impinged with effective heat fluxes (EHF) of 25 to 75 kW/m^2

5.4.2.6 OPTIMIZATION TARGETS

Mass-loss rate (MLR), surface (T_s), and back (T_b) surface temperature data with plywood sample from cone calorimeter test at HF = 50 kW/m^2

5.4.2.7 SENSITIVE PARAMETERS

- ε_i, $\rho_{i=2}$, ΔH_k
- Kinetic parameters are considered to be certain in this example case.

5.4.2.8 UNCERTAINTY

Uncertainty in Experiment Data

- Data is acquired from two repeating cone tests of plywood under 50 kW/m^2 heat flux level.
- The uncertainties in the MLR and thermocouple measurements at front surface were quantified by comparing data from these two identical FRP composite tests. Note that the effect of different sample thicknesses was considered to be negligible for sample thicknesses in two tests were 11.1 and 11.2 mm. Because the data is transient, the standard deviation at each time step was calculated. Then these are averaged and multiplied by 2 to estimate uncertainty: uncertainty in MLR, T_s and T_b are ± 3.4g/sm^2, ± 54 °C and ± 27 °C, respectively.
- Assume:
  - Uncertainties are comparable to the same sample tested at various heat-flux levels
  - Data set found above is close to the averaged curves from multiple identical tests under same conditions

Uncertainty in Modeling Outputs

- Baseline case: HF = 50 kW/m^2, thickness = 8.7 mm
- Sensitive parameters – density of dry_wood and char, emissivity of water, dry_wood and char, heat-of-reaction for drying process, and thermal decomposition of dry_wood to char – varied one at a time from baseline to its max and min: ±10% of estimated value or uncertainty limits found from measurement experiment.
- Kinetic parameters are considered to be certain in this example
- Integration of uncertainty is calculated by the Law of Propagation of Uncertainty: uncertainty in model's MLR, T_s and T_b are **± 7.2g/sm^2**, **± 57 °C** and **± 157 °C** respectively.

5.4.2.9 TG / DTG PREDICTIONS AT 20 °C/MIN HEATING RATE USING ESTIMATED KINETIC PARAMETERS

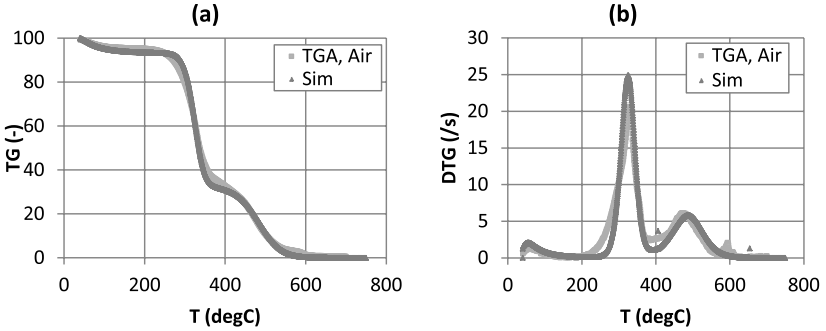

Figure 5-35. TG/DTG curves at 20°C/min heating rate with different estimation results for kinetic parameters for thermal decomposition of plywood: testing of plywood sample (~10mg) with air purge

* Note that only the first two peaks in the DTG curve in T < 400°C have been included in kinetic modeling for simplification of the parameter-estimation problem. This approach is considered to be reasonable, knowing that the third peak is due to char oxidation (confirmed by comparing thermograms from nitrogen and air-purge runs) and while flame exists on the surface, it is commonly accepted that char oxidation becomes minimal due to the oxygen-diffusion-limiting condition.

5.4.2.10 COMPARISON BETWEEN DATA AND COMPUTED MODELING OUTPUTS

- Modeling is conducted for case with HF = 50 kW/m^2, thickness = 11.2 mm

Table 5-18. Comparison between experiment data from cone calorimeter test and modeling outputs using estimated parameter values via measurements and manual optimization

	Data (Based on 2 tests, uncertainty as 2 times standard deviation)	Measurements and Manual Optimization
Peak MLR (g/m2s)	19.9 ± 4.8	18.1 ± 7.2
Avg MLR (g/m2s)	6.8 ± 0.5	6.6 ± 7.2
t to pMLR (s)	81 ± 113	23
Ts at 100 s (°c)	604 ± 112	628 ± 57
Ts at 200 s (°c)	734 ± 10	670 ± 57
Ts at 300 s (°c)	732 ± 45	689 ± 57
Tb at 100 s (°c)	68 ± 20	56 ± 157
Tb at 200 s (°c)	118 ± 1	185 ± 157
Tb at 300 s (°c)	196 ± 10	291 ± 157

5.4.2.11 MODELING OUTPUT: MASS-LOSS RATE (MLR)

- Case used in optimization process

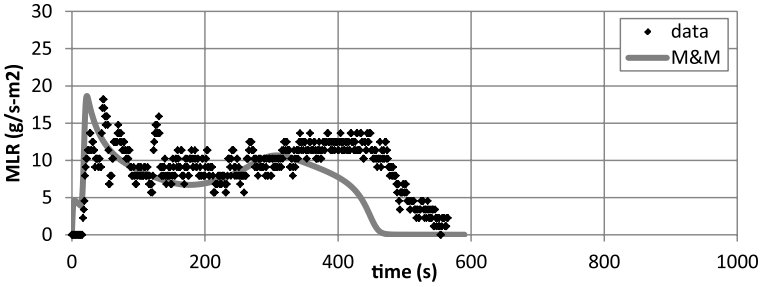

Figure 5-36. Mass-loss rate (MLR) comparisons for FRP composite with plywood between actual MLR from experiment (data) and modeled MLR (M&M) at applied heat flux of 50 kW/m². Note that data shown were used to estimate model-parameter values via manual optimization.

- Extrapolation

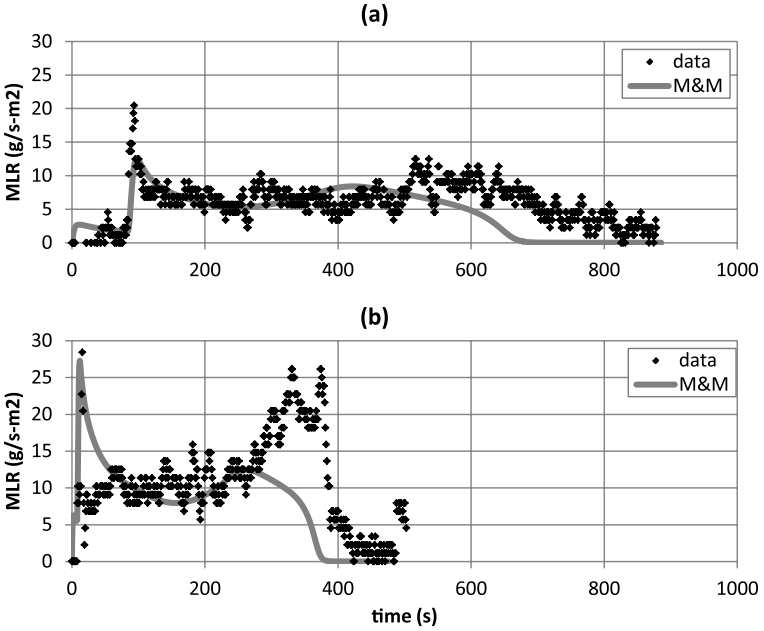

Figure 5-37. Mass-loss rate (MLR) comparisons for FRP composite with plywood between actual MLR from experiment (data) and modeled MLR (M&M) at applied heat flux of (a) 25 and (b) 75 kW/m². Note that data shown were not included in the model-parameter-estimation process; hence, these two cases are considered as extrapolation cases.

5.4.2.12 MODELING OUTPUT: SURFACE TEMPERATURE (T_{SURF})

- Case used in optimization process

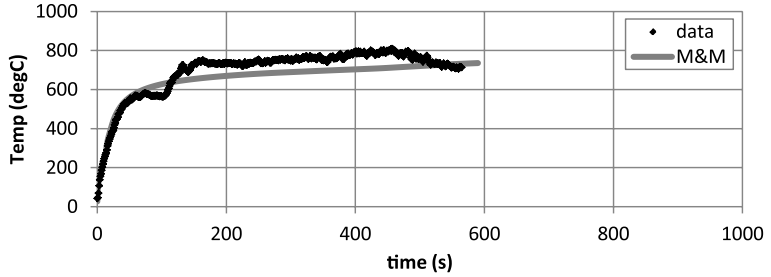

Figure 5-38. Surface-temperature (T_{surf}) comparisons for plywood between actual T_{surf} from experiment (data) and modeled T_{surf} (M&M) at applied heat flux of 50 kW/m². Note that data shown were used to estimate model-parameter values via manual optimization.

- Extrapolation

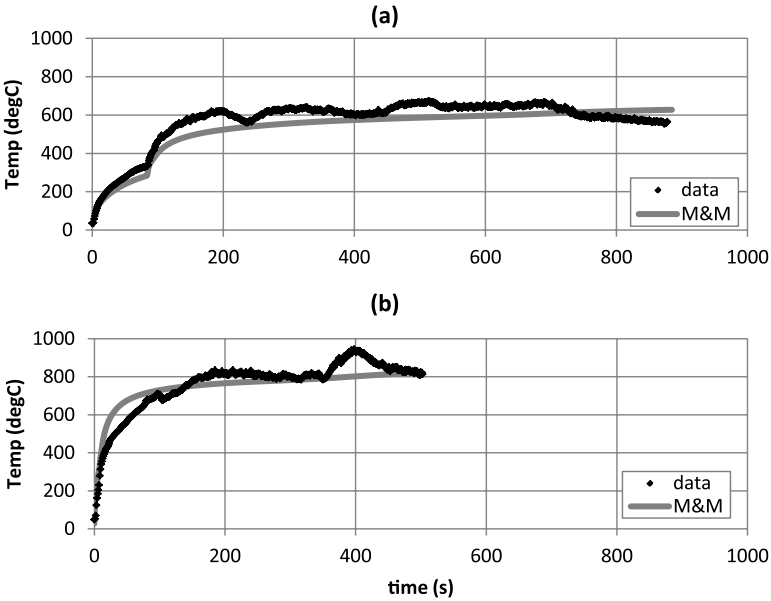

Figure 5-39. Surface-temperature (T_{surf}) comparisons for FRP composite with plywood between actual T_{surf} from experiment (data) and modeled T_{surf} (M&M) at applied heat flux of (a) 25 and (b) 75 kW/m². Note that data shown were not included in the model-parameter-estimation process; hence, these two cases are considered as extrapolation cases.

5.4.2.13 MODELING OUTPUT: BACK-SURFACE TEMPERATURE (T_{BACK})

- Case used in optimization process

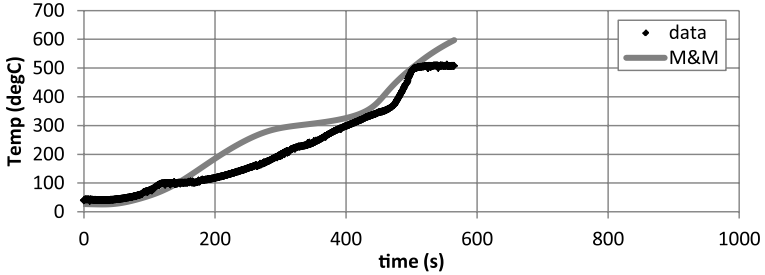

Figure 5-40. Back-surface-temperature (T_{back}) comparisons for plywood between actual T_{back} from experiment (data) and modeled T_{back} (M&M) at applied heat flux of 50 kW/m². Note that data shown were used to estimate model-parameter values via manual optimization.

- Extrapolation

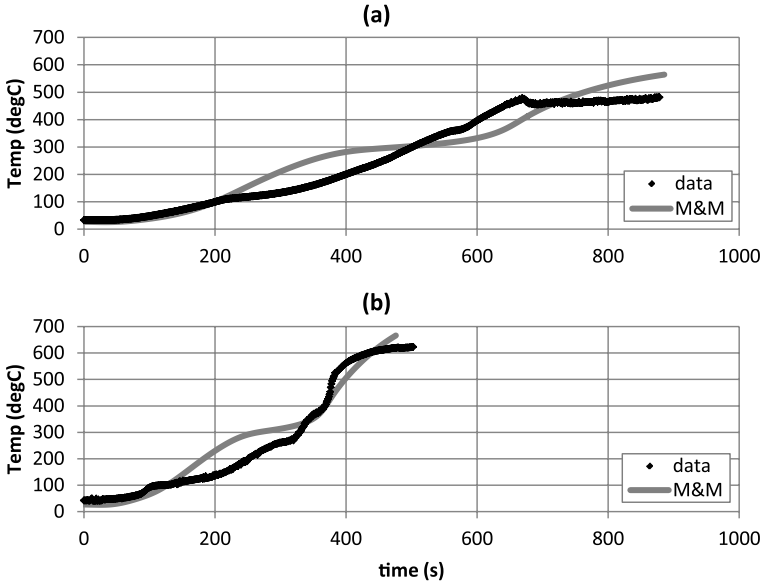

Figure 5-41. Back-surface-temperature (T_{back}) comparisons for plywood between actual T_{back} from experiment (data) and modeled T_{back} (M&M) at applied heat flux of (a) 25 and (b) 75 kW/m². Note that data shown were not included in the model-parameter-estimation process; hence, these two cases are considered as extrapolation cases.

5.4.3 Commentary

GENERAL COMMENTS

- TG/DTG
  - Good agreement between simulated TG/DTG thermograms and those of actual from TGA experiment is shown when thermal decomposition kinetics is modeled using multiple heating-rate data.
  - Proposed kinetic model does not account for mass loss due to char oxidation at relatively higher temperature range (T > 400°C).
- Comparison between Data and Computed Modeling Outputs
  - Modeled peak MLR, Avg MLR, time to peak MLR, and T_s and T_b at various times are all in quantitative agreement with data, considering its uncertainty.
- MLR
  - Optimization at HF = 50 kW/m^2: Generally good agreement exists between experiment data and all modeling results, considering the trend. Some deviation of modeling results from data is shown at later times, where the second peak is observed in the MLR curve. Near this region, bending of the sample toward the front surface occurs with respect to a rapid temperature increase throughout the back surface. This phenomenon is strictly a 3D behavior, which is not explicitly accounted for in current 1D model. Additionally, mass loss due to minor char oxidation at this region is speculated, for flame height becomes smaller and bending of sample may allow an ease to oxygen diffusion to solid phase.
  - Extrapolation at HF = 25 kW/m^2: Good agreement exists between experiment data and modeling results. Modeling is able to capture the initial mass-loss rate peak followed by a decrease qualitatively and quantitatively. A qualitative agreement between data and modeling results exists for the second mass-loss rate peak; however, actual sample in cone testing extends for a longer period of time (~100 s), while in modeling burn out time occurs earlier. This is probably due to excluding char oxidation in kinetic modeling.
  - Extrapolation at HF = 75 kW/m^2: Good agreement exists between experiment data and modeling results, except for the second peak in mass-loss rate curve. See above for discussion.
- Surface Temperature
  - Optimization at HF = 50 kW/m^2: Generally good agreement exists between experiment data and modeling results, considering the trend. Note that after ignition (post-ignition stage) the flame interferes with data reading of thermocouple on surface.
  - Extrapolation at HF = 25 kW/m^2: Good agreement exists between experiment data and modeling results.
  - Extrapolation at HF = 75 kW/m^2: Good agreement exists between experiment data and modeling results.

LIMITATION IN MODELING

- When considering limitation of the parameters in modeling this plywood, the modeler should take into account the applicability of the parameters and their associated uncertainties. For example, any assumptions used when determining a parameter value via experiment direct or indirect measurements can be utilized to understand when the parameter value becomes inappropriate. For this example, most consideration can be given to the parameters related to decomposition kinetics. One should be cautious that these findings can cause this FRP composite to behave differently under changing conditions, which were not included in the parameter-estimation process.
- In this example, drying is simplified as a heterogeneous reaction (i.e., an Arrhenius law temperature-dependent evaporation rate), which occurs near 100 °C based on TGA experiment results. However, water evaporation from a wet wood is governed by transport phenomena of liquid-phase water and vapor diffusion. Additionally, typically the water travels toward the back surface during heating and re-condensation may occur, allowing the back surface to be colder. This phenomenon will not be captured in this modeling.
- Any char oxidation has been considered to be minimal in this example, considering that with a flame sheet on material surface, oxygen diffusion becomes limited. However, when analyzing the cone calorimeter results, some oxidation is speculated, for the sample loses ~4 to 6% more of the initial sample weight comparing to TGA experiment.

References

1 McGrattan, K.; Hostikka, S.; McDermott, R.; Floyd, J.; Weinschenk, C.; and Overholt, K.; Fire Dynamics Simulator (Version 6) Technical Reference Guide, NIST Special Publication 1018-6, November (2013).

2 Stoliarov, S.I.; and Lyon, R.E., Federal Aviation Administration Technical Note,DOT/FAA/AR-TN08/17, (2008); available for download at http://www.fire.tc.faa.gov/reports/reports.asp.

3 Lautenberger, C., Gpyro – A Generalized Pyrolysis Model for Combustible Solids, Technical Reference, Version 0.700, 19 February (2009).

4 Siegel, R.; and Howell, J.R., Thermal Radiation Heat Transfer. Taylor & Francis, New York, 4th edition (2002).

5 Atkins, P.W., *Physical Chemistry*, W.H. Freeman and Company, San Francisco, CA (1978) 582-611.

6 Lautenberger, C., Gpyro – A Generalized Pyrolysis Model for Combustible Solids, Users' Guide, Version 0.700, 19 February (2009).

7 Adl-Zarrabin, B., *et al.*, "Using the TPS Method for Determining the Thermal Properties of Concrete and Wood at Elevated Temperature," *Fire and Materials*, 30 (2006) 359-369.

8 Gustafsson, S., "Transient Plane Source (TPS) Technique for Thermal Conductivity and Thermal Diffusivity Measurements of Solid Materials," *Review of Scientific Instruments*, 62 (1991) 797-804.

9 Gustafsson, S.; and Long, T., "Transient Plane Source (TPS) Technique for Measuring Thermal Properties of Building Materials," *Fire and Materials*, 19 (1995) 43-49.

10 Bentz, D., *et al.*, "A Slug Calorimeter for Evaluating the Thermal Performance of Fire Resistive Materials," *Fire and Materials*, 30 (2006) 257-270.

11 Bentz, D., *et al.*, "Towards a Methodology for the Characterization of Fire Resistive Materials with Respect to Thermal Performance Models," *Fire and Materials*, 30 (2006) 311-321.

12 Liu, W., *et al.*, "Understanding the Decomposition and Fire Performance Processes in Phosphorus and Nanomodified High Performance Epoxy Resins and Composites," *Polymer*, 48 (2007) 2345-2354.

13 Kashiwagi, T., *et al.*, "Flame Retardant Mechanism of Polyamide-6 Nanocomposites," *Polymer*, 45 (2004) 881-891.

14 Gilman, J., *et al.*, "A Study of the Flammability Reduction Mechanism of Polystyrene-Layered Silicate Nanocomposite: Layered Silicate Reinforced Carbonaceous Char," *Polym. Adv. Technol.*, 17 (2006) 263-271.

15 Zanetti, M., *et al.*, "Cone Calorimeter Combustion and Gasification Studies of Polymer Layered Silicate Nanocomposites," *Chem. Mater.*, 14 (2002) 881-887.

16 Lyon, R.E.; Safronava, N.; and Oztekin, E., A simple method for determining kinetic parameters for materials in fire models. Fire Saf Sci 2011; 10 (2011) 765-777.

17 Ozawa, T., "A new method of analyzing thermogravimetric data," *Bull. Chem. Soc. Jpn.*, 38 (1965) 1881-1886.

18 Flynn, J.H.; and Wall, L.A., "A quick, direct method for the determination of activation energy from thermogravimetric data," *J. Polym. Sci.Polym. Lett.*, 4 (1964) 323-328.

19 Friedman, H. L., "Kinetics of thermal degradation of char-forming plastics from Thermogravimetry. Application to a phenolic plastic," J. Polym. Sci., Pt. C 6 (1964) 183-195.

20 Flynn, J.H.; and Wall, L.A., "A quick, direct method for the determination of activation energy from thermogravimetric data," J. Polym. Sci. Polym. Lett. 4 (1966) 323-328.

21 Vyazovkin, S.V.; and Lesnikovich, A.I., Thermochim. Acta, 165 (1990) 273.

22 IUPAC Compendium of Chemical Terminology, 2nd ed. (1997) (http://old.iupac.org/goldbook)

23 Galwey, A. K.; and Brown, M. E., Arrhenius parameters and compensation behaviour in solid-state decompositions, Thermochimica Acta, 300:1-2 (1997) 107-115, ISSN 0040-6031, 10.1016/S0040-6031(96)03120-6.

24 Odian, G., Principles of Polymerization, John Wiley & Sons, 3rd ed., (1991).

25 Simms, D.L.; and Law, M., The ignition of wet and dry wood by radiation, Combustion and Flame, 11:5 (1967) 377-388, ISSN 0010-2180, 10.1016/0010-2180(67)90058-2.

26 Galgano, A.; and Di Blasi, C., Modeling the propagation of drying and decomposition fronts in wood, Combustion and Flame, 139:1-2 (2004) 16-27, ISSN 0010-2180, 10.1016/j.combustflame.2004.07.004.

27 Khan, M.; De Ris, J.L.; and Ogden, S.D., Effect of moisture on ignition time of cellulosic materials, in: Proceedings of the Ninth International Symposium on Fire Safety Science, (2008) 167-178.

28 Oztekin, E.S.; Crowley, S.B.; Lyon, R.E.; Stoliarov, S.I.; Patel, P.; and Hull T.R., Sources of variability in fire test data: A case study on poly(aryl ether ether ketone) (PEEK), Combustion and Flame, 159:4 (2012) 1720-1731, ISSN 0010-2180, 10.1016/j.combustflame.2011.11.009.

29 Takemori, M.T., Polymer Fatigue, Ann Rev. Mater Sci 14 (1984) 171-204.

30 Kim, E.; Dembsey, N.A.; and Dore, C.H., "Property Estimation for Pyrolysis Modeling Applied to Flame Retarded Modified Acrylic FRP Composites", in *Proceedings of Composites & Polycon 2010*, American Composites Manufacturers Association, Mandalay Bay, Las Vegas, NV, USA, 9-11 February, (2010).

31 Kim, E.; Dembsey, N.l and Lautenberger, C., Parameter Estimation for Pyrolysis Modeling Applied to Polyester FRP Composites with Different Glass Contents, *Fire and Materials 2009, 11th International Conference*, 26-28 January (2009), Hyatt Hotel at Fishermans Wharf, San Francisco, CA, USA.

32 Chaos, M.; Khan, M.; Krishnamoorthy, N.; Chatterjee, P.; Wang, Y.; Dorofeev, S.B., Experiments and Modeling of Single- and Triple-Wall Corrugated Cardboard: Effective Material Properties and Fire Behavior, in *Fire and Materials 2011*, 12th International Conference and Exhibition, 31 January–2 February (2011), Fisherman's Wharf, San Francisco, CA, USA.

33 Lautenberger, C.; Rein, G.; and Fernandez-Pello, C., "The Application of a Genetic Algorithm to Estimate Material Properties", Fire Safety Journal 41 (2006), 204–214.

34 Matala, A., "Estimation of Solid Phase Reaction Parameters for Fire Simulation," MS Thesis, University of Technology, Helsinki, (2008).

35 Webster, R., "Pyrolysis Model Parameter Optimization using a Customized Stochastic Hill-Climber Algorithm and Bench Scale Fire Test Data," MS Thesis, University of Maryland, (2009).

36 Aster, R.C.; Borchers, B.; and Thurber, C.H., Parameter Estimation and Inverse Problems, International Geophysics, Academic Press, 90 (2005) xi-xii. ISSN 0074-6142, ISBN 9780120656042, DOI: 10.1016/S0074-6142(05)80014-2.

37 Stoliarov, S. I.; Safronava, N.; and Lyon, R. E., The effect of variation in polymer properties on the rate of burning. Fire and Materials, 33 (2009) 257-271. doi: 10.1002/fam.1003.

38 Chaos, M.; Khan, M.M.; Krishnamoorthy, N.; de Ris, J.L.; and Dorofeev, S.B., Material Properties for CFD Fire Models, FM Global Open Source CFD Fire Modeling Workshop (2010).

39 Cacuci, D.G.; Ionescu-Bujor, M.; and Navon, I.M., *Sensitivity and Uncertainty Analysis; Theory; Volume 1*, Chapman & Hall / CRC Taylor & Francis Group, (2005).

40 Cacuci, D.G.; Ionescu-Bujor, M.; and Navon, I.M., *Sensitivity and Uncertainty Analysis; Applications to Large-Scale Systems; Volume 2*, Chapman & Hall / CRC Taylor & Francis Group, (2005).

41 Saltelli, A.; Chan, K.; and Scott, E.M., *Sensitivity Analysis*, Wiley, (2000).

42 Duan, Q.; Gupta, V.K.; and Sorooshian, S., Shuffled Complex Evolution Approach for Effective and Efficient Global Minimization, Journal of Optimization Theory and Applications 76 (1993) 501-521.

43 Chaos, M.; Khan, M.M.; Krishnamoorthy, N.; de Ris, J.L.; and Dorofeev, S.B., Bench-Scale Flammability Experiments: Determination of Material Properties Using Pyrolysis Models for Use in CFD Fire Simulations in *Interflam 2010*, Nottingham, U.K., 5-7 July (2010).

44 Chaos, M.; Khan, M.M.; Krishnamoorthy, N.; de Ris, J.L.; and Dorofeev, S.B, Evaluation of Optimization Schemes and Determination of Solid Fuel Properties for CFD Fire Models using Bench-scale Pyrolysis Tests, Proceedings of the Combustion Institute 33 (2010), doi:10.1016/j.proci.2010.07.018.

45 Brandrup, J,; Immergut, E.H.; Grulke, E.A.; Abe, A.; and Bloch, D.R., (Eds.) Polymer Handbook, fourth ed., John Wiley & Sons, New York, (1999).

46 Stoliarov, S.I.; and Walters, R.N., Polym. Degrad. Stab. 93 (2008), 422–427.

47 Brandrup, J.; Immergut, E.H.; Grulke, E.A.; Abe, A.; and Bloch, D.R., (Eds.) Polymer handbook. 4th edition, John Wiley & Sons, New York, (1999).

48 Stoliarov, S.I.; Crowley, S.; Lyon, R.E.; and Linteris, G.T., Prediction of the burning rates of non-charring polymers, Combustion and Flame, 156:5 (2009) 1068-1083. ISSN 0010-2180, DOI: 10.1016/j.combustflame.2008.11.010.

49 Beaulieu, P.A.; and Dembsey, N.A., "Effect of Oxygen on Flame Heat Flux in Horizontal and Vertical Orientations", *Fire Safety Journal*, 43:6 (2008) 410-428.

50 ASTM Standard D 7309-07, Test Method for Determining Flammability Characteristics of Plastics and Other Solid Materials Using Microscale Combustion Calorimetry, ASTM International, West Conshohocken, PA, (2007).

51 Kashiwagi, T.; and Ohlemiller, T.J., "A study of oxygen effects on nonflaming transient gasification of PMMA and PE during thermal irradiation," *Proceedings of the Combustion Institute*, 19 (1982) 815-823.

52 Kashiwagi T., Polymer combustion and flammability—role of the condensed phase. *Twenty-fifth Symposium (International) on Combustion*, Irvine, CA, (1994) 1423-1437.

53 Kulshreshtha, A.K.; and Vasile, C., Handbook of polymer blends and composites.

54 Lewin, M., Synergism and Catalysis in Flame Retardancy of Polymers, *Polym. Adv. Technol.* 12 (2001) 215-222.

55 LeVan, S.L., The Chemistry of Solid Wood; Chapter 14, Chemistry of Fire Retardancy, American Chemical Society, (1984).

56 ASTM Standard E 84-05, Test Method for Surface Burning Characteristics of Building Materials, , ASTM International, West Conshohocken, PA, (2005).

57 NIST Chemistry WebBook, http://webbook.nist.gov/.

Chapter 6
Conclusions

Conclusions 173

Conclusions

As an effort to create input data for fire models in a consistent manner and allow for compilation of accepted model input databases for various materials, a *Guide* for estimating material pyrolysis properties for fire modeling has been developed. The *Guide* provides standardized procedures for obtaining fire-model-input parameters related to the thermal decomposition of materials. Considering that these unknowns are dependent on the certain pyrolysis model of choice, this *Guide* describes a method to determine model type to be used for a material of interest (Chapter 2) followed by parameter-estimation procedures for three types of pyrolysis models: empirical (Chapter 3), simple analytical (Chapter 4), and comprehensive (Chapter 5) pyrolysis models.

Each chapter was designed to describe the pyrolysis-model type by presenting the modeling approach and assumptions used with its mathematical formulation identifying the model parameters to be obtained. This was followed by methods of estimating the unknown parameters via independent experiments for measurements or numerically using optimization routines. At the end of each chapter, example cases are included for better understanding of the procedure discussed previously. For each example in the three chapters – Chapter 3, 4, and 5 – detailed problem solutions are given in the appendices.

Appendix A
Uncertainty Analysis

Uncertainty Analysis 175
Type A Uncertainty 177
Type B Uncertainty 178
References 179

Uncertainty Analysis

The objective of a measurement is to determine the value of the measurand, i.e., the physical quantity that needs to be measured. The value of the measurand is generally not obtained from a direct measurement, but is determined as a function (f) from N input quantities X_1, X_2,…, X_N (see Eq.A(A)-1):

$$Y = f(X_1, X_2, \ldots, X_N) \qquad \text{Eq.A(A)-1}$$

where

Y = true value of the measurand;
f = functional relationship between measurand and input quantities; and
X_i = true values of the input quantities (i = 1 … N).

The input quantities may be categorized as:

- quantities whose values and uncertainties are directly determined from single or repeated observation; or
- quantities whose values and uncertainties are brought into the measurement from external sources, such as reference data obtained from handbooks.

An estimate of the value of the measurand, y, is obtained from Eq.A(A)-1 using input estimates x_1, x_2,…, x_N for the values of the N input quantities (see Eq.A(A)-2):

$$y = f(x_1, x_2, \ldots, x_N) \qquad \text{Eq.A(A)-2}$$

The standard uncertainty of y is obtained by appropriately combining the standard uncertainties of the input estimates x_1, x_2,…, x_N. If all input quantities are independent, the combined standard uncertainty of y is given by Eq.A(A)-3:

$$u_c(y) = \sqrt{\sum_{i=1}^{N} \left[\frac{\partial f}{\partial X_i}\right]_{x_i}^2 u^2(x_i)} \equiv \sqrt{\sum_{i=1}^{N} [c_i u(x_i)]^2} \qquad \text{Eq.A(A)-3}$$

where

u = standard uncertainty;
u_c = combined standard uncertainty; and
$c_{i,}$ = sensitivity coefficients.

Eq.A(A)-3 is referred to as the law of propagation of uncertainty[1,2] and based on a first-order Taylor series approximation of $Y = f(X_1, X_2, \ldots, X_N)$. When the nonlinearity of f is significant, higher-order terms must be included. When the input quantities are correlated, Eq.A(A)-3 must be revised to include the covariance terms. The combined standard uncertainty of y is then calculated from Eq.A(A)-4:

$$u_c(y) = \sqrt{\sum_{i=1}^{N} [c_i u(x_i)]^2 + 2 \sum_{i=1}^{N-1} \sum_{j=i+1}^{N} c_i c_j u(x_i) u(x_j) r(x_i, x_j)} \qquad \text{Eq.A(A)-4}$$

Where

$r(x_i,x_j)$ = estimated correlation coefficient between Xi and Xij.

Since the values of the input quantities are not known, the correlation coefficient is estimated on the basis of the measured values of the input quantities. The combined standard uncertainty in Eq.A(A)-3 and Eq.A(A)-4 is usually multiplied by a coverage factor to raise the confidence level, to obtain the "expanded" uncertainty. A multiplier of 2 is often used, which corresponds to a confidence level of approximately 95%.

The standard uncertainty of an input estimate x_i is obtained from the distribution of possible values of the input quantity X_i. There are two types of evaluations depending on how the distribution of possible values is obtained: Type A and Type B

Type A Uncertainty

Type A uncertainty is also known as aleatory, stochastic, variability or irreducible uncertainty. This uncertainty is characterized by inherent randomness, which cannot be reduced further. Typically, Type A uncertainty is modeled with a probability distribution projected with repeated data acquisition, i.e., evaluation of this standard uncertainty of x_i is based on the frequency distribution, which is estimated from a series of n repeated observations $x_{i,k}$ ($k = 1 \ldots n$). See Eq.A(A)-5:

$$u(x_i) \approx \sqrt{s^2(\bar{x}_i)} = \sqrt{\frac{s^2(\bar{x}_i)}{n}} = \sqrt{\frac{\sum_{k=1}^{n}\left(x_{i,k} - \bar{x}_i\right)^2}{n(n-1)}} \qquad \text{Eq.A(A)-5}$$

Type B Uncertainty

Type B uncertainty[3] is also known as the state-of-knowledge uncertainty, subjective uncertainty, or reducible uncertainty. This uncertainty is characterized by the degree of understanding of the given problem, which is not directly based on repeated measurements. In this case the uncertainty is determined from previous measurements, experience or general knowledge, manufacturer specifications, data provided in calibration certificates, uncertainties assigned to reference data taken from handbooks, etc. Type B uncertainty can be reduced by increasing the understanding of the problem by collecting relevant data.

An example of taking into account for Type B uncertainty is considering the effect of different ignition scenarios in pyrolysis modeling using Empirical Models (see Chapter 3). To consider this effect, the modeler may conduct a series of experiments using different ignition scenarios that are plausible. Then the modeler can decide to conduct modeling with the most challenging scenario that may have a small but non-negligible probability of occurrence.

References

1 Taylor, B.N.; and Kuyatt, C.E., Guidelines for evaluating and expressing the uncertainty of NIST measurement results. *NIST Technical Note 1297*. NIST, Gaithersburg, MD, USA, (1994).

2 ISO. *Guide to the Expression of Uncertainty in Measurement*, ISBN 92-67-10188-9. International Organization for Standardization, Geneva, Switzerland, (1993).

3 Swiler, L.P.; Paez, T.L.; and Mayes, R.L., Epistemic Uncertainty Quantification Tutorial, http://dakota.sandia.gov/papers/294_swi.pdf

Appendix B
Example Solutions for Chapter 3

Example 3.1 Modeling Sofa 181
Obtain Parameters via Experiment 181
Validation and Commentary 183
Example 3.2 Modeling PMMA 186
Obtain Parameters via Experiment 186
Validation and Commentary 188
Example 3.3 Modeling Corrugated Cardboard 189
Obtain Parameters via Experiment 189
Validation and Commentary 192
Example 3.4 Modeling Fire Retarded FRP Composite 193
Obtain Parameters via Experiment 193
Validation and Commentary 196
Example 3.5 Modeling Plywood 197
Obtain Parameters via Experiment 197
Validation and Commentary 199
References 200

Example 3.1 Modeling Sofa

Obtain Parameters via Experiment

Run model

SELECT MODEL: EMPIRICAL USING FULL-SCALE CALORIMETER DATA

UNDERSTAND EXPERIMENT

A furniture calorimeter typically consists of a weighing platform placed on the floor of the laboratory beneath a hood connected to an instrumented exhaust duct (see Figure A(B)-1). The specimen is placed on the platform and ignited with the specified ignition source. The products of combustion are collected in the hood and extracted through the exhaust duct. Measurements of the concentration of oxygen (and typically also carbon dioxide and carbon monoxide), flow rate (from bidirectional probe and thermocouple measurements) and light transmission in the exhaust duct are used to determine heat release and smoke-production rate as a function of time.

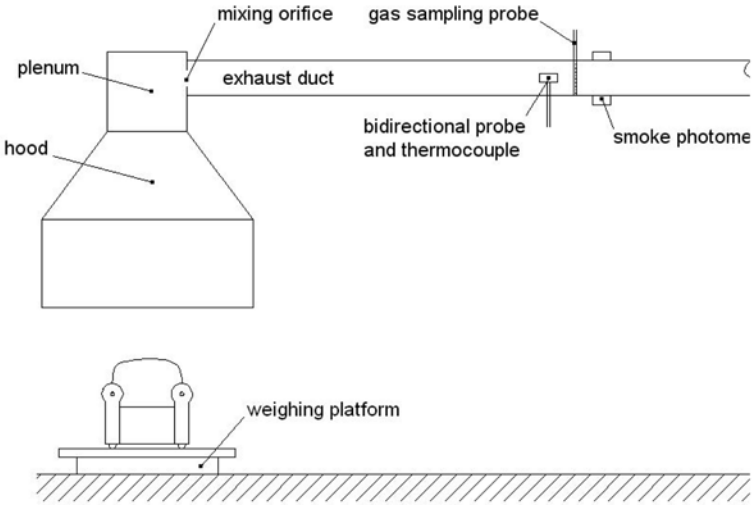

Figure A(B)-1. Schematic of a furniture calorimeter

Furniture calorimeters were initially developed in the 1980s. These calorimeters have since been used to obtain heat-release rate and related data for a wide range of other types of combustibles.

CONFIGURE MODEL CONDITIONS BASED ON UNDERSTANDING OF EXPERIMENT

In the model, the phenomena discussed above are simulated as below. Basic assumptions are as follows:

- Pre-ignition stage is
  - Inert: decomposition before ignition is neglected
  - Always the same as in furniture calorimeter test
- Ignition scenario is the same as in furniture calorimeter experiment: time-to-ignition is the same in modeling as determined in experiment
- Post-ignition stage is
  - Considered to have instantaneous release of volatiles from solid to gas phase: typically an area is specified that can be correlated to the actual burning object where energy is released to the gas phase
  - Considered to be the same as in furniture calorimeter test in terms of heat-release rate or mass-loss rate

ACQUIRE DATA SETS THAT CAN REPRESENT BURNING BEHAVIOR OF INTEREST

Experiment data of a single seat sofa mockup is found for pyrolysis modeling using Empirical Model. This sofa mockup was burnt under a hood of a furniture calorimeter. The mockup consisted of a steel frame with untreated polyurethane foam cushions (80% of the combustible mass) and a cotton fabric (20% of the combustible mass). Total combustible mass was 3.93 kg. The test was performed according to *ASTM E 1537* and *CAL TB 133*. The ignition source consisted of a 0.25 m square tubular propane burner producing a 19 kW flame for 80 seconds applied to the top of the seat cushion.

ESTIMATE UNKNOWNS

1. Time-to-Ignition

   Time-to-ignition of the furniture is found from the experiment procedure, where a propane burner producing a 19 kW flame is placed to the furniture for 80 sec. in the initial phase of the test.

2. HRR

   To check repeatability of the data, four identical tests of the same sofa mockup have been conducted (see Figure A(B)-2). Using these data, an average heat-release rate is calculated at each time step and will be used as an input for pyrolysis modeling with Empirical Model for burning objects.

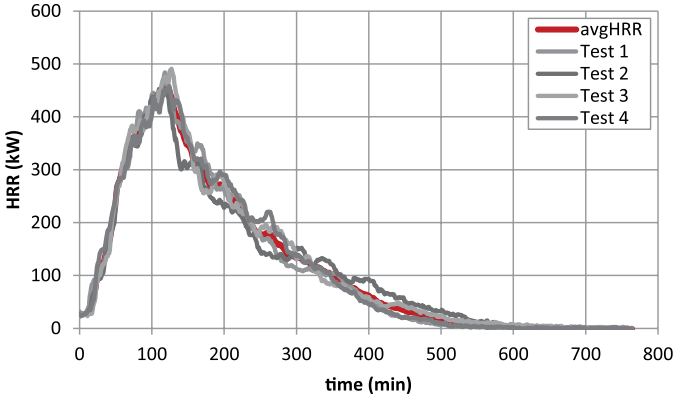

Figure A(B)-2. HRR curve from furniture calorimeter experiment of 4 identical tests of the same sofa mockup

Obtain Uncertainty for Estimated Parameters

Because time-to-ignition is directly given from the experiment procedure, this parameter can be considered as certain. For the uncertainty in HRR, uncertainty analysis is conducted based on above four data sets. The uncertainty of HRR is estimated by first calculating the confidence interval for 95% confidence level ($\alpha = 0.05$), assuming student t distribution with a sample size of three (four data sets) at each time step. Then an average confidence interval is calculated for the time interval of interest ($0 < t < 800$ min), which results in **± 20.4 kW**.

Validation and Commentary

When using Empirical Model to simulate pyrolysis of a sofa, furniture-calorimeter test data has been utilized to estimate the time-to-ignition from exposure to a propane burner and the energy released from burning. As noted in the Understanding Model section of the chapter, this approach is limited as follows in terms of the conditions being comparable to those found in the fire scenario on interest:

- Ignition scenario and exposure conditions

A basic assumption used in empirical models is that the ignition scenario and exposure conditions in the fire are comparable to those used in the laboratory. Therefore, any changes made in the ignition scenario and exposure conditions have to be accounted for by the model user when applying the data to empirical models. The furniture-calorimeter experiment in this example is conducted under certain conditions: ignition is achieved by applying propane flame on the horizontal surface (seating cushion) for 80 s and sufficient supply of air is provided throughout its burning phase. To illustrate the effect of altering the conditions in HRR curves, two other HRR curves are shown below:

- Effect of ignition source strength:
  Two identical single-seat sofas were obtained for testing (see Figure A(B)-3). In the first test the sofa was ignited with a 45 W butane gas flame applied to the center of the seat cushion for 20 s. In the second test 59 ml (2 oz) of gasoline was poured on the seat cushion to simulate an incendiary fire. The resulting heat-release-rate measurements are shown below. In this case the use of the weaker ignition source delays the propagation to full involvement by approximately 170 s. For this case the effect of ignition-source strength can relatively easily be accounted for, although in practice it may not be trivial to determine the exact time period over which to shift the HRR curve. The effect can be much more pronounced when the source strength is close to the level needed to obtain sustained burning.

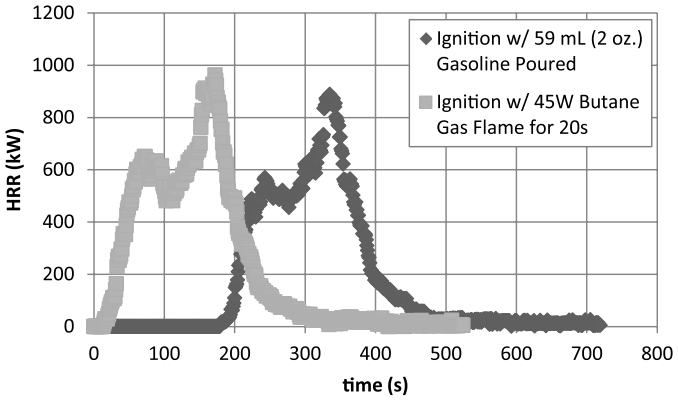

Figure A(B)-3. Effect of ignition source strength: single-seat sofas tested in furniture-calorimeter test with different ignition source – ignition with 59 mL gasoline poured (◆) or with 45 W butane gas flame (■)

- Effect of ignition location:
  Two tests were conducted on a steel-framed-seat sofa mockup according to the same procedure and using the same padding and fabric as in the tests described in this example case (see Figure A(B)-4). In the first test the burner flame was applied to the seat cushion on the right side. In the second test the burner was applied to the center seat cushion. The resulting HRR measurements are compared in Figure A(B)-4. In the first test the flames spread from the right side to the left side. When the flames reached the armrest on the left side, part of the material on the right side had already been consumed. This resulted in a relatively steady HRR that peaked slightly above 400 kW. In the second test the flames spread in two directions. As a result, the heat rate continuously increased until the two armrests ignited and a peak heat-release rate of close to 1 MW was reached. This case illustrates that a seemingly small difference in the ignition scenario can have a surprisingly dramatic effect on fire growth.

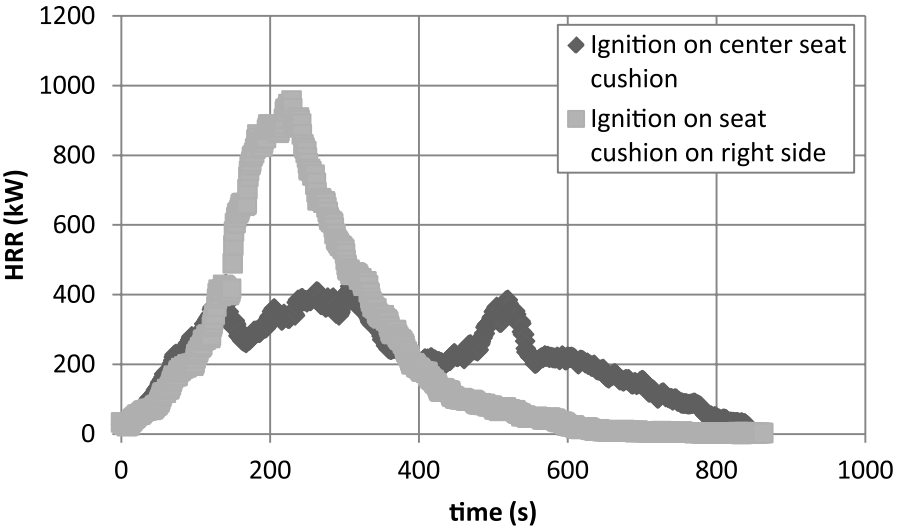

Figure A(B)-4. Effect of ignition location: steel-framed-seat sofa mockups tested in furniture-calorimeter test with different ignition location – ignition on center seat cushion (◆) or seat cushion on right side (■)

- Heat and mass transfer

This is a multi-dimensional problem, and the dimensional effect is implicitly addressed in modeling by a single parameter – HRR or MLR and effective heat of combustion.

Example 3.2 Modeling PMMA

Obtain Parameters via Experiment

Run model

SELECT MODEL: EMPIRICAL USING BENCH-SCALE CALORIMETER DATA

UNDERSTAND EXPERIMENT

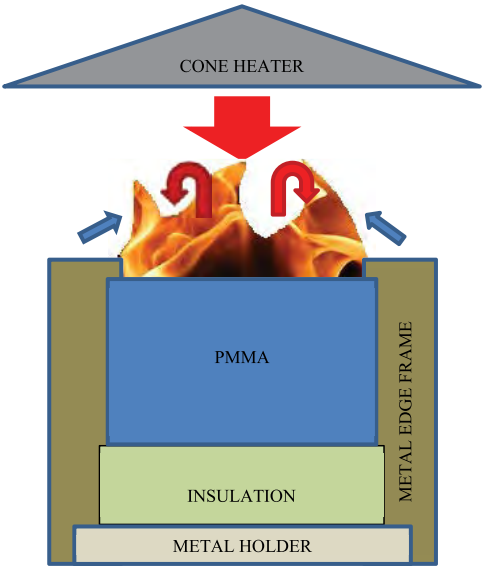

Figure A(B)-5. Simplified representation of a cone calorimeter test of PMMA

A simplified representation of a cone calorimeter test of PMMA is shown in Figure A(B)-5. The sample is placed on top of an insulation, which sits on a metal holder. Another metal frame is placed on top of the sample, insulation, and the holder. A metal edge frame is used as well.

Front Surface: As heating starts by opening the shutter to allow radiation from the cone heater to impinge on the sample surface (large red arrow), cooling also begins via natural convection (blue arrows) and re-radiation. The surface decomposes with bubbling with respect to temperature increase occurring through heat conduction and/or in-depth radiative transport. The pyrolyzates leave through the surface until complete burn-off because this material leaves no residue. When ignition occurs as the fuel vapor concentration above the surface exceeds its LFL (lower flammable limit), additional heat flux from the flame is introduced on the surface (red arrows). Regression of the sample surface with respect to consumption of PMMA in pyrolysis occurs.

Back surface: The sample is placed on top of insulation. In the experiment, air gap of few millimeters thickness exist between the sample and the insulation due to thermal contact. Due to the insulation, nothing leaves through the back face when 1D assumption holds for the experiment.

CONFIGURE MODEL CONDITIONS BASED ON UNDERSTANDING OF EXPERIMENT

In the model, the phenomena discussed above are simulated as below. Basic assumptions are as follows:

- Pre-ignition stage is
  - Inert: decomposition with bubbling before ignition is neglected
  - Always the same as in cone calorimeter test with a specified heat flux impinging on material's surface (typically ~50 kW/m^2 is used)
- Ignition phenomenon is the same as in cone calorimeter experiment: time- to-ignition is the same in modeling as determined in experiment
- Post-ignition stage is
  - Considered to have instantaneous release of volatiles from solid to gas phase: bubbling layer is neglected and is considered as a surface phenomena
  - Considered to be the same as in cone calorimeter test in terms of heat release rate or mass-loss rate per unit area

ACQUIRE DATA SETS THAT CAN REPRESENT BURNING BEHAVIOR OF INTEREST

Cone calorimeter test data of black PMMA with thickness of 18 mm, density of 1170 kg/m^3, and applied heat flux of 50 kW/m^2 is found.

ESTIMATE UNKNOWNS

1. Time-to-Ignition

   t_{ig} = 22 s after exposure to heating

2. MLR and Effective HoC

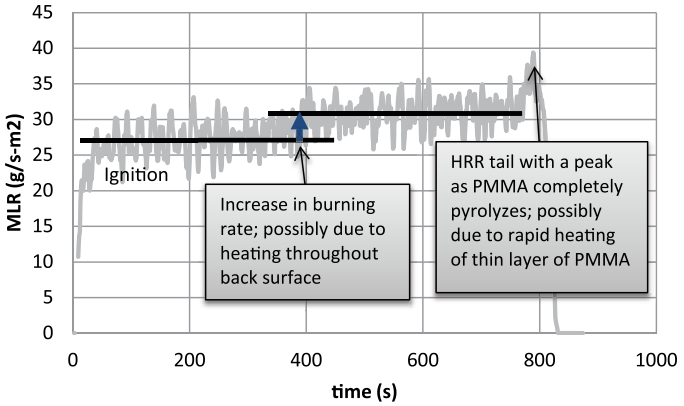

Figure A(B)-6. MLR curve from cone calorimeter experiment of PMMA

MLR curve with effective heat of combustion calculated from a cone experiment will be used directly (see Figure A(B)-6). This MLR data is from a PMMA test at 50kW/m^2 with sample thickness of 18 mm. The MLR profile changes with respect to the burning history of the sample. From time-of-ignition, initial steady-state-burning phase occurs. Then, near t = 400 s after exposure to heating, second steady-state-burning phase is reached, which has a slightly higher mass-loss rate

than the initial phase, possibly due to the thermal wave penetrating to the back surface and increasing heating. At the end of the test, a mass-loss rate peak is observed. This is probably due to the rapid heating of thin layer of residual PMMA. Understanding the MLR profile enables modelers to adjust the curve when using it as an input to a pyrolysis model if needed. For example, the modeler may decide to only use data from time-to-ignition up to the initial steady-state burning phase if PMMA involved in a fire scenario of interest has a thickness greater than what has been used in the experiment (18 mm).

Effective heat-of-combustion is calculated from the heat-release rate and mass-loss rate data at every measurement, as discussed in Model Parameter Measurement Methods. The average with its confidence interval with 95% confidence is: **24.8 ± 0.1 kJ/g**. Note that this average and confidence interval has been obtained for the steady-burning phases only due to significant changes in effective heat-of-combustion values near ignition and burn-off periods at the start and the end of testing, respectively.

Obtain Uncertainty for Estimated Parameters

For estimating the uncertainty in parameters, experimental uncertainty can be used, as the parameters are obtained from data directly. From the experiment work done by Beaulieu and Dembsey[1] on thermally-thick-behaving black PMMA using AFM apparatus, the experiment uncertainty in time-to-ignition and mass-loss rate at steady burning were determined as ± 2 s and ± 3 g/m^{2}s, respectively. The test results were compared with other literature values using different apparatuses, such as cone calorimeter as well, which were considered as consistent. This uncertainty information will be used when comparing modeling output to experiment data.

Validation and Commentary

When using Empirical Model to simulate pyrolysis of PMMA, PMMA test data from a bench-scale cone calorimeter experiment at a set heat-flux level has been utilized to estimate the time-to-ignition from exposure to heating and the energy released from burning of PMMA. As noted in the Uncertainty part of the chapter, this approach is limited as follows in terms of the conditions being comparable to those found in the fire scenario of interest:

- Ignition scenario: piloted ignition with an electric sparker
- Exposure conditions: electrically heated coil uniformly heating PMMA with a set heat flux impinging on the front surface where this applied heat-flux level during testing is assumed to be representative average (over space and time) for the fire scenario that is being modeled
- Heat and mass transfer: one-dimensional, i.e., perpendicular to the exposed surface
- Surface burning data: edge effects in material testing are not included; therefore, data per unit area can be applied to simulate larger areas by simply multiplying the material surface area involved in fire

Example 3.3 Modeling Corrugated Cardboard

Obtain Parameters via Experiment

Run model

SELECT MODEL: EMPIRICAL USING BENCH-SCALE CALORIMETER DATA

UNDERSTAND EXPERIMENT

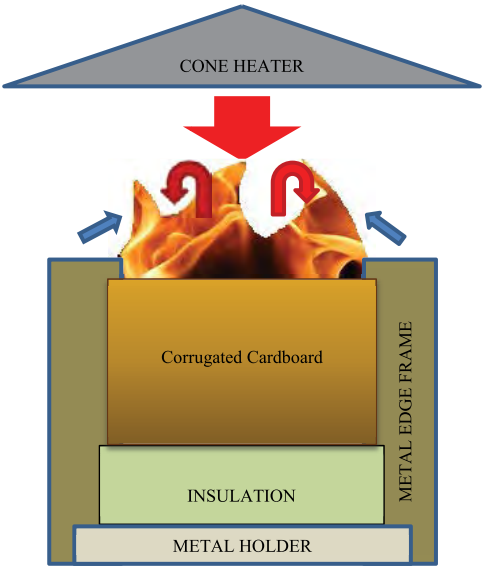

Figure A(B)-7. Simplified representation of a cone calorimeter test of corrugated cardboard

A simplified representation of a cone calorimeter test of triple-layered corrugated cardboard is shown above (see Figure A(B)-7). The sample is placed on top of an insulation, which sits on a metal holder. Another metal frame is placed on top of the sample, insulation, and the holder. A metal edge frame is used as well.

Front Surface: As heating starts by opening the shutter to allow radiation from the cone heater to impinge on sample surface (large red arrow), cooling also begins via natural convection (blue arrows) and re-radiation. The surface decomposes with charring, i.e., surface becoming black and white smoke, which typically indicates moisture loss with heating of the sample. Note that the surface becomes non-uniformly black due to corrugation showing linear shading. As the surface layer is burned away, it exfoliates toward the sides and opens up, allowing the first layer of the corrugation to appear on the surface. Then the middle flat layer of the cardboard, which separates

the two layers of corrugation, starts to burn, allowing the heat release to grow. As this layer is decomposed throughout, the second layer of the corrugation becomes involved in the burning process. Followed by the burning of the second corrugation layer, the last flat layer of the cardboard – back surface of the sample – burns. This results in another growing phase in the heat-release-rate curve. When ignition occurs as the fuel vapor concentration above the surface exceeds its LFL (lower flammable limit), additional heat flux from the flame is introduced on the surface (red arrows).

Back surface: The sample is placed on top of insulation. In the experiment, an air gap of few millimeters thickness exists between the sample and the insulation due to thermal contact. Nothing leaves through the back face with the insulation when 1D assumption holds for the experiment.

CONFIGURE MODEL CONDITIONS BASED ON UNDERSTANDING OF EXPERIMENT

In the model, the phenomena discussed above are simulated as below. Basic assumptions are as follows:

- Pre-ignition stage is
  - Inert: non-uniform charring is considered to be evenly distributed
  - Always the same as in cone calorimeter test with a specified heat flux impinging on material's surface
- Ignition phenomenon is the same as in cone calorimeter experiment: time-to-ignition is the same in modeling as determined in experiment
- Post-ignition stage is
  - Considered to have instantaneous release of volatiles from solid to gas phase
  - Considered to be the same as in cone calorimeter test in terms of heat-release rate or mass-loss rate per unit area

ACQUIRE DATA SETS THAT CAN REPRESENT BURNING BEHAVIOR OF INTEREST

Cone calorimeter test data of triple-layer cardboard with thickness of 15 mm, density of 116 kg/m^3, and applied heat flux of 25 kW/m^2 is found.

ESTIMATE UNKNOWNS

1. Time-to-Ignit ion

   t_{ig} = 32 ± 4 s after exposure to heating

2. MLR and Effective HoC

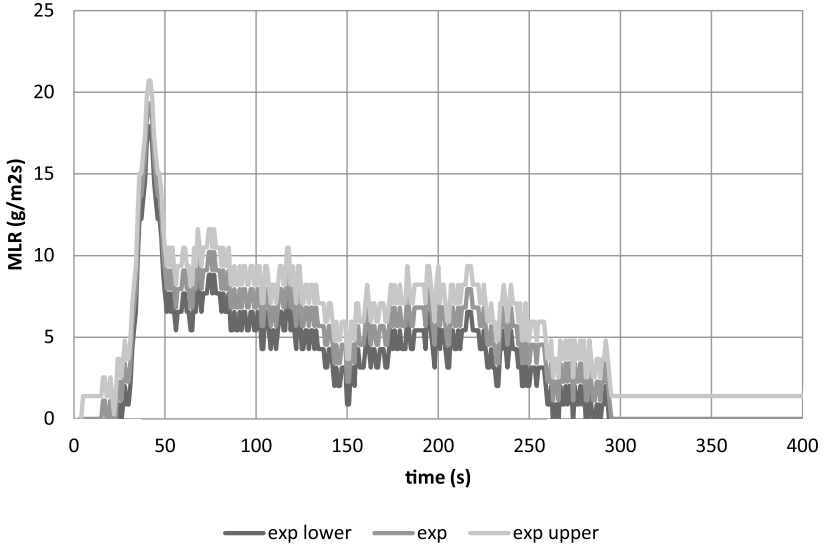

Figure A(B)-8. MLR curve from cone calorimeter test of corrugated cardboard

MLR curve with effective heat-of-combustion calculated from a cone experiment will be used directly (see Figure A(B)-8). This MLR data is from a triple-layer cardboard test at 25 kW/m^2 with sample thickness of 15 mm. The MLR profile changes with respect to the burning history of the sample.

Effective heat-of-combustion is calculated from the heat-release rate and mass-loss-rate data at every measurement, as discussed in Model Parameter Measurement Methods. The average of two tests with its confidence interval calculated by 2 times the standard deviation is: **13.5 ± 0.5 kJ/g**.

Obtain Uncertainty for Estimated Parameters

The uncertainty in the mass-loss-rate data is estimated via statistical approach, taking the standard deviation (0.58 g/sm^2) from the mean of a steady burning of five identical PMMA tests conducted in a cone calorimeter.[2] The estimated uncertainty is 1.4 g/sm^2, which is found by calculating the 95% confidence interval applying student t distribution with a sample size of five.

The uncertainty in time-to-ignition data is estimated via statistical approach, taking four identical cone calorimeter test data at heat flux 25 kW/m^2 of this cardboard. 95% confidence interval is calculated for each heat-flux level assuming student t distribution.

The uncertainty in effective heat-of-combustion is estimated by average heat-release rate divided by average mass-loss rate of two identical tests. Two times the standard deviation is used as its uncertainty band.

Validation and Commentary

When using Empirical Model to simulate pyrolysis of this triple-layer cardboard, test data from a bench-scale cone calorimeter experiment at a set heat-flux level has been utilized to estimate the time-to-ignition from exposure to heating and the energy released from burning of this cardboard. As noted in the Understanding Model part of the chapter, this approach is limited as follows in terms of the conditions being comparable to those found in the fire scenario on interest:

- Ignition scenario: piloted ignition with an electric sparker
- Exposure conditions: electrically heated coil uniformly heating sample with a set heat flux impinging on the front surface, where this applied heat-flux level during testing is assumed to be representative average (over space and time) for the fire scenario that is being modeled
- Heat and mass transfer: one-dimensional, i.e., perpendicular to the exposed surface
- Surface-burning data: edge effects in material testing are not included; therefore, data per unit area can be applied to simulate larger areas by simply multiplying the material surface area involved in fire

Example 3.4 Modeling Fire Retarded FRP Composite

Obtain Parameters via Experiment

Run model

SELECT MODEL: EMPIRICAL USING BENCH-SCALE CALORIMETER DATA

UNDERSTAND EXPERIMENT

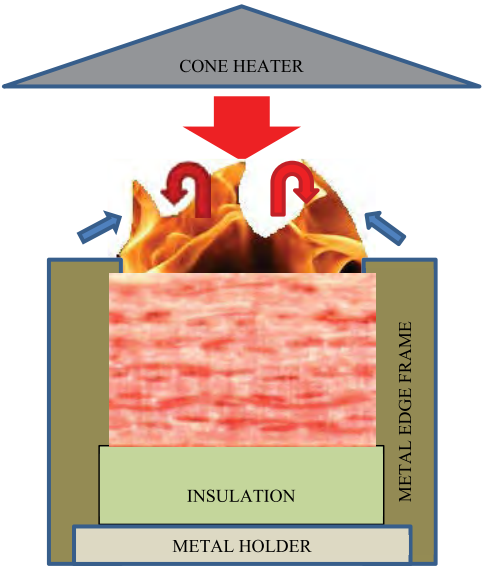

Figure A(B)-9. Simplified representation of a cone calorimeter test of fire-retarded fiberglass- reinforced polymer (FRP) Composite

A simplified representation of a cone calorimeter test of fire-retarded fiberglass-reinforced polymer (FRP) composite is shown in Figure A(B)-9. The sample is placed on top of an insulation, which sits on a metal holder. Another metal frame is placed on top of the sample, insulation, and the holder. A metal edge frame is used as well.

Front Surface: As heating starts by opening the shutter to allow radiation from the cone heater to impinge on sample surface (large red arrow), cooling also begins via natural convection (blue arrows) and re-radiation. The surface decomposes with charring, i.e., surface becoming black and white smoke, which typically indicates moisture loss with heating of the sample. Note that the surface becomes non-uniformly black. As thermal decomposition of the resin with additive progresses, blackened surface becomes white, as the resin leaves a white powder-type residue

(possible due to decomposition of fire-retardant additive). Shrinkage or regression during pyrolysis can be considered to be minimal for this material. When ignition occurs as the fuel vapor concentration above the surface exceeds its LFL (lower flammable limit), additional heat flux from the flame is introduced on the surface (red arrows).

Back surface: The sample is placed on top of insulation. In the experiment, an air gap of few millimeters thickness exist between the sample and the insulation due to thermal contact. Nothing leaves through the back face with the insulation when 1D assumption holds for the experiment.

CONFIGURE MODEL CONDITIONS BASED ON UNDERSTANDING OF EXPERIMENT

In the model, the phenomena discussed above are simulated as below. Basic assumptions are as follows:

- Pre-ignition stage is
  - Inert: non-uniform charring is considered to be evenly distributed
  - Always the same as in cone calorimeter test with a specified heat flux impinging on material's surface
- Ignition phenomenon is the same as in cone calorimeter experiment: time-to-ignition is the same in modeling as determined in experiment
- Post-ignition stage is
  - Considered to have instantaneous release of volatiles from solid to gas phase
  - Considered to be the same as in cone calorimeter test in terms of heat-release rate or mass-loss rate per unit area

ACQUIRE DATA SETS THAT CAN REPRESENT BURNING BEHAVIOR OF INTEREST

Cone calorimeter test data of this FRP composite with thickness of 9.2 mm, density of 1900 kg/m^3, and applied heat flux of 50 kW/m^2 is found.

ESTIMATE UNKNOWNS

1. Time-to-Ignition

   t_{ig} = 175 ± 36 s after exposure to heating

2. MLR and Effective HoC

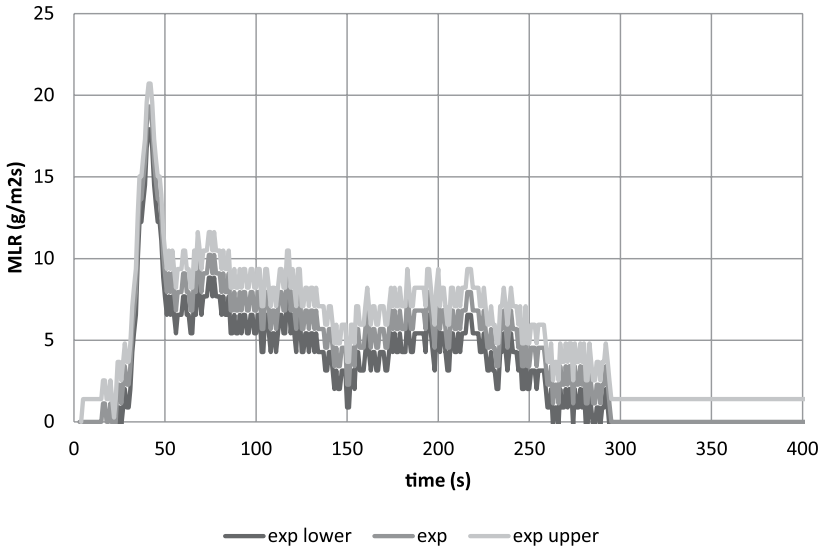

Figure A(B)-10. MLR curve from cone calorimeter test of fire-retarded FRP composite

MLR curve with effective heat-of-combustion calculated from a cone experiment will be used directly (see Figure A(B)-10). This MLR data is from FRP composite test at 50 kW/m^2 with sample average thickness of 9.2 mm. The MLR profile changes with respect to the burning history of the sample.

Effective heat-of-combustion is calculated from the heat-release rate and mass-loss-rate data at every measurement as discussed in Model Parameter Measurement Methods. The average of four tests with its confidence interval calculated by 95% confidence using student t distribution is: **14.7 ± 3.8 kJ/g**.

Obtain Uncertainty for Estimated Parameters

The uncertainty in the mass-loss-rate data is estimated via statistical approach, taking the standard deviation (0.58 g/sm^2) from the mean of a steady burning of five identical PMMA tests conducted in a cone calorimeter[2] The estimated uncertainty is 1.4 g/sm^2, which is found by calculating the 95% confidence interval applying student t distribution with a sample size of five.

The uncertainty in time-to-ignition data is estimated via statistical approach, taking four identical cone calorimeter test data at heat flux 50 kW/m^2 of this cardboard. 95% confidence interval is calculated for each heat-flux level assuming student t distribution.

The uncertainty in effective heat-of-combustion is estimated by average heat-release rate divided by average mass-loss rate of four identical tests. 95% confidence interval is calculated for each heat-flux level assuming student t distribution.

Validation and Commentary

When using Empirical Model to simulate pyrolysis of this fire-retarded FRP composite, test data from a bench-scale cone calorimeter experiment at a set heat-flux level has been utilized to estimate the time-to-ignition from exposure to heating and the energy released from burning of this material. As noted in the Understanding Model part of the chapter, this approach is limited as follows in terms of the conditions being comparable to those found in the fire scenario of interest:

- Ignition scenario: piloted ignition with an electric sparker
- Exposure conditions: electrically heated coil uniformly heating sample with a set heat flux impinging on the front surface, where this applied heat-flux level during testing is assumed to be representative average (over space and time) for the fire scenario that is being modeled
- Heat and mass transfer: one-dimensional, i.e., perpendicular to the exposed surface
- Surface-burning data: edge effects in material testing are not included and therefore data per unit area can be applied to simulate larger areas by simply multiplying the material surface area involved in fire

Example 3.5 Modeling Plywood

Obtain Parameters via Experiment

Run model

SELECT MODEL: EMPIRICAL USING BENCH-SCALE CALORIMETER DATA

UNDERSTAND EXPERIMENT

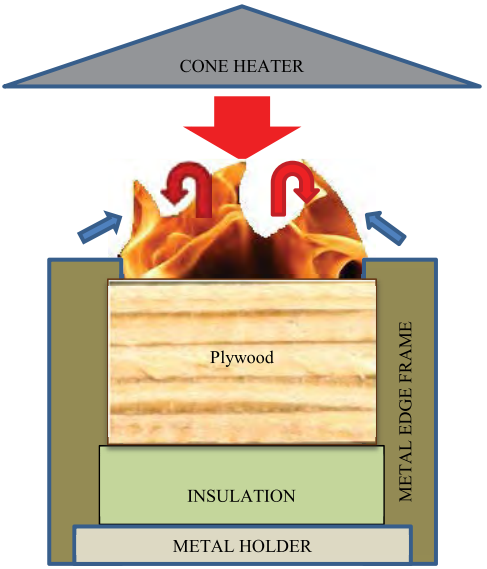

Figure A(B)-11. Simplified representation of a cone calorimeter test of plywood

A simplified representation of a cone calorimeter test of plywood is shown in Figure A(B)-11. The sample is placed on top of an insulation, which sits on a metal holder. Another metal frame is placed on top of the sample, insulation and the holder. A metal edge frame is used as well.

Front Surface: As heating starts by opening the shutter to allow radiation from the cone heater to impinge on sample surface (large red arrow), cooling also begins via natural convection (blue arrows) and re-radiation. The surface decomposes with moisture loss at first appearing as white smoke followed by thermal decomposition of the wood component. When ignition occurs as the fuel vapor concentration above the surface exceeds its LFL (lower flammable limit), additional heat flux from the flame is introduced on the surface (red arrows). As decomposition occurs under flaming condition, relatively uniform cracks appear on the surface with some shrinkage, allowing easy evacuation of the pyrolyzates to the gas phase even as the pyrolysis front propagates toward in-depth. Near the burn-out leaving grey residue, the center of the sample bends upward then quickly falls apart resulting in flame out.

Back surface: The sample is placed on top of insulation. In the experiment, an air gap of few millimeters thickness exists between the sample and the insulation resulting in some thermal resistance. Due to the insulation, nothing leaves through the back face when 1D assumption holds for the experiment.

CONFIGURE MODEL CONDITIONS BASED ON UNDERSTANDING OF EXPERIMENT

In the model, the phenomena discussed above are simulated as below. Basic assumptions are as follows:

- Pre-ignition stage is
  - Inert: non-uniform charring is considered to be evenly distributed
  - Always the same as in cone calorimeter test with a specified heat flux impinging on material's surface
- Ignition phenomenon is the same as in cone calorimeter experiment: time to ignition is the same in modeling as determined in experiment
- Post-ignition stage is
  - Considered to have instantaneous release of volatiles from solid to gas phase
  - Considered to be the same as in cone calorimeter test in terms of heat release rate or mass loss rate per unit area

ACQUIRE DATA SETS THAT CAN REPRESENT BURNING BEHAVIOR OF INTEREST

Cone calorimeter test data of triple-layer cardboard with thickness of 11.1 mm, density of 542 kg/m^3, and applied heat flux of 50 kW/m^2 is found.

ESTIMATE UNKNOWNS

1. Time-to-Ignition

   $t_{ig} = 27 \pm 9$ s after exposure to heating

2. MLR and Effective HoC

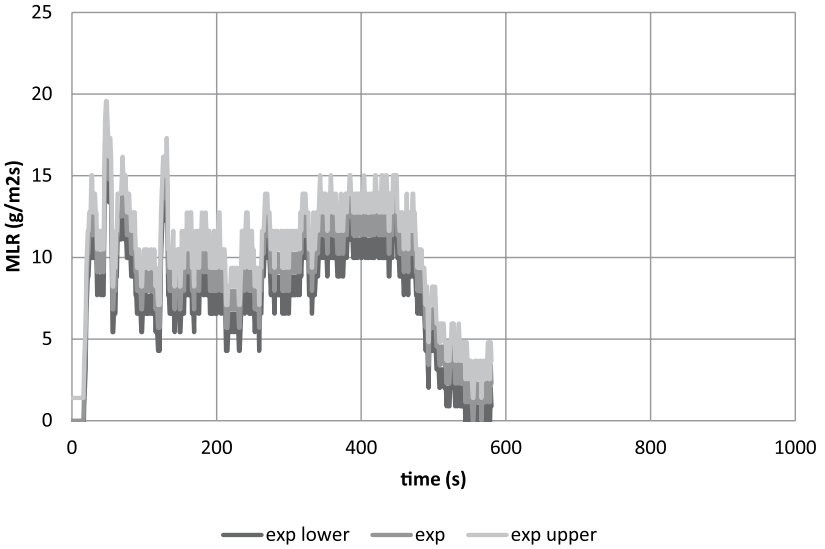

Figure A(B)-12. MLR curve from cone calorimeter test of plywood

MLR curve with effective heat-of-combustion calculated from a cone experiment will be used directly (see Figure A(B)-12). This MLR data is from a triple-layer cardboard test at 50 kW/m^2 with sample thickness of 11.1 mm. The MLR profile changes with respect to the burning history of the sample.

Effective heat-of-combustion is calculated from the heat-release rate and mass-loss-rate data at every measurement as discussed in Model Parameter Measurement Methods. The average of two tests with its confidence interval calculated by 2 times the standard deviation is: **11.0 ± 0.3 kJ/g**.

Obtain Uncertainty for Estimated Parameters

The uncertainty in the mass-loss-rate data is estimated via statistical approach, taking the standard deviation (0.58 g/sm^2) from the mean of a steady burning of five identical PMMA tests conducted in a cone calorimeter.[2] The estimated uncertainty is 1.4 g/sm^2, which is found by calculating the 95% confidence interval applying student t distribution with a sample size of 5.

The uncertainty in time-to-ignition data is estimated via statistical approach, taking four identical cone calorimeter test data at heat flux 25 kW/m^2 of this cardboard. 95% confidence interval is calculated for each heat flux level assuming student t distribution.

The uncertainty in effective heat-of-combustion is estimated by average heat-release rate divided by average mass-loss rate of two identical tests. Two times the standard deviation is used as its uncertainty band.

Validation and Commentary

When using Empirical Model to simulate pyrolysis of this plywood, test data from a bench-scale cone calorimeter experiment at a set heat-flux level has been utilized to estimate the time-to-ignition from exposure to heating and the energy released from burning of this material. As noted in the Understanding Model part of the chapter, this approach is limited as follows in terms of the conditions being comparable to those found in the fire scenario of interest:

- Ignition scenario: piloted ignition with an electric sparker
- Exposure conditions: electrically heated coil uniformly heating sample with a set heat flux impinging on the front surface where this heat-flux level during testing is assumed to be representative average (over space and time) for the fire scenario that is being modeled
- Heat and mass transfer: one-dimensional, i.e., perpendicular to the exposed surface
- Surface-burning data: edge effects in material testing are not included; therefore, data per unit area can be applied to simulate larger areas by simply multiplying the material surface area involved in fire

References

1 Beaulieu, P.A.; and Dembsey, N.A., "Effect of Oxygen on Flame Heat Flux in Horizontal and Vertical Orientations", *Fire Safety Journal*, 43:6 (2008) 410-428.

2 Zhao, Lei, Bench Scale Apparatus Measurement Uncertainty and Uncertainty Effects on Measurement of Fire Characteristics of Material Systems, MS Thesis, Fire Protection Engineering, WPI, 2005-04-27, ETD-050105-182456

Appendix C - Example Solutions for Chapter 4

Example 4.1 Modeling PMMA 202
Measure Parameters 202
Obtain Parameters via Data Analysis 204
Validation 213
Commentary 218
Example 4.2 Modeling Corrugated Cardboard 219
Measure Parameters 219
Obtain Parameters via Data Analysis 220
Validation 229
Commentary 232
Example 4.3 Modeling Fire-Retarded FRP Composite 233
Measure Parameters 233
Obtain Parameters via Data Analysis 234
Validation 243
Commentary 247
Example 4.4 Modeling Plywood 248
Measure Parameters 248
Obtain Parameters via Data Analysis 249
Validation 259
Commentary 262
Example 4.5 Modeling GRP with Balsa Wood Core Sandwich Composite 263
Measure Parameters 263
Obtain Parameters via Data Analysis 265
Validation 274
Commentary 277
Example 4.6 Modeling Thin FRP Composite Sheet 278
Measure Parameters 278
Obtain Parameters via Data Analysis 280
Validation 289
Commentary 292
References 293

Example 4.1 Modeling PMMA

Measure Parameters

1. Ambient Temperature

Direct measurement of ambient temperature is made as 20°C.

2. Surface Temperature at Ignition

This parameter will be obtained via Ignition Data Analysis, i.e., no direct measurements will be performed.

3. Critical Heat Flux for Ignition

By bracketing to within +/- 0.5 kW/m^2 in cone calorimeter tests, $\dot{q}''_{cr}$ has been determined to be 10.5 kW/m^2. Ignition data is provided below for PMMAs with thickness of 18.0 mm, density of 1170 kg/m^3 (see Table A(C)-1):

Table A(C)-1. Ignition data from cone calorimeter tests for PMMA

Heat Flux (kW/m²)	t_{ig} (s)
10	NI
11	1138
12	961
15	471
25	87
25	84
25	97
25	90
50	24
50	22
75	14
75	11

4. Thermal Inertia

This parameter will be obtained via Ignition Data Analysis, i.e., no direct measurements will be performed.

5. Effective Heat-of-Combustion

This parameter will be obtained via Burning-Rate Data Analysis, i.e., no direct measurements will be performed.

6. Heat-of-Gasification

This parameter will be obtained via Burning-Rate Data Analysis, i.e., no direct measurements will be performed.

7. Convection Coefficient

Because this is a material laid in horizontal position in a cone calorimeter, h_c = 12 W/m^{2}K is used based on literature reference.

8. Surface Emissivity/Absorptivity

Emissivity is approximated as 0.9.

Summary

Table A(C)-2. Summary of model parameter table with estimated values via direct measurements, literature search, or approximation

Ignition Parameters	T_∞	20 °C
	T_{ig}	Ignition Data Analysis
	$\dot{q}''_{cr}$	10.5 kW/m^2
	$k\rho c$	Ignition Data Analysis
Burning-Rate Parameters	$\Delta h_{c,eff}$	Burning-Rate Data Analysis
	Δh_g	Burning-Rate Data Analysis
	h_c	12 W/m^{2}K
	ε	0.9

Obtain Parameters via Data Analysis

Run model

SELECT MODEL: THERMALLY THICK MODEL FOR IGNITION ANALYSIS (QUINTIERE AND HARKLEROAD, ASTM E 1321) AND STEADY-BURNING MODEL

UNDERSTAND EXPERIMENT AND FIRE CHARACTERISTICS OF MATERIAL

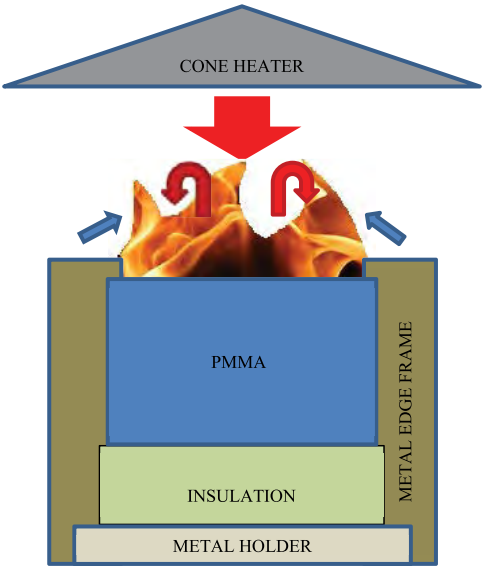

Figure A(C)-1. Simplified representation of a cone calorimeter test of PMMA

A simplified representation of a cone calorimeter test of PMMA is shown in Figure A(C)-1. The sample is placed on top of an insulation, which sits on a metal holder. Another metal frame is placed on top of the sample, insulation and the holder. A metal edge frame is used as well.

Front Surface: As heating starts by opening the shutter to allow radiation from the cone heater to impinge on sample surface (large red arrow), cooling also begins via natural convection (blue arrows) and re-radiation. The surface decomposes with bubbling with respect to temperature increase occurring through heat conduction and/or in-depth radiative transport. The pyrolyzates leave through the surface until complete burn-off, because this material leaves no residue. When ignition occurs as the fuel-vapor concentration above the surface exceeds its LFL (lower flammable limit), additional heat flux from the flame is introduced on the surface (red arrows). Regression of the sample surface occurs with respect to consumption of PMMA in pyrolysis.

Back surface: The sample is placed on top of insulation. In the experiment, an air gap of a few millimeters thickness exists between the sample and the insulation due to thermal contact. Due to the insulation, nothing leaves through the back face when 1D assumption holds for the experiment.

CONFIGURE MODEL CONDITIONS BASED ON UNDERSTANDING OF EXPERIMENT AND MATERIAL CHARACTERISTICS

In the model, the phenomena discussed above are simulated as below. Basic assumptions are as follows:

- Pre-ignition stage is:
  - Inert: decomposition with bubbling before ignition is neglected
  - Thermally thick: heat transfer does not reach back surface
- Post-ignition stage is:
  - Considered to have instantaneous release of volatiles from solid to gas phase: bubbling layer is neglected and is considered as a surface phenomenon
  - Considered to have a constant thickness: regression of PMMA is neglected
  - Steady burning: heat loss equals heat gain at front surface

ACQUIRE DATA SETS

Cone calorimeter test data of black PMMA with thickness of 18 mm, density of 1170 kg/m^3, and applied heat-flux levels ranging from 10 to 75 kW/m^2 is found. For Ignition Data analysis, only time-to-ignition with respect to applied heat-flux data will be used. For burning-rate-data analysis, data for the entire testing time duration, mass loss and heat release during testing period with respect to applied heat flux will be used.

CONDUCT IGNITION DATA ANALYSIS

1. Estimate T_{ig}

   Heat balance at front surface during steady burning is as follow:

$$\varepsilon \dot{q}''_{cr} = h_c(T_{ig} - T_\infty) + \varepsilon\sigma(T_{ig}^4 - T_\infty^4)$$

   Knowing that emissivity is approximated as 0.9, critical heat flux is estimated as 10.5 kW/m^2, and heat-transfer coefficient in cone calorimeter experiment is estimated as 12.0 W/m^{2}K, ignition temperature, T_{ig} is calculated as:

$$\mathbf{T_{ig} = 318\ °C}$$

2. Estimate h_{ig}

   h_{ig} is the total heat-transfer coefficient at ignition; therefore, at steady-state burning stage, the following can be defined:

$$\varepsilon \dot{q}''_{cr} \equiv h_{ig}(T_{ig} - T_\infty)$$

   Knowing the ignition temperature, h_{ig} can be calculated:

$$\mathbf{h_{ig} = 31.7\ W/m^2K}$$

3. Calculate $\dot{q}''_{cr} / \dot{q}''_{e}$ versus $\sqrt{t_{ig}}$ from ignition data (see Table A(C)-3)

Table A(C)-3. $\dot{q}''_{cr} / \dot{q}''_{e}$ versus $\sqrt{t_{ig}}$

Heat Flux	t_{ig}	CHF/HF	$t_{ig}^{0.5}$
(kW/m²)	(s)		($s^{0.5}$)
10	NI		
11	1138	0.9546	33.73
12	961	0.8750	31.00
15	471	0.7000	21.70
25	87	0.4200	9.33
25	84	0.4200	9.17
25	97	0.4200	9.85
50	22	0.2100	4.69
75	11	0.1400	3.32

4. Plot $\dot{q}''_{cr} / \dot{q}''_{e}$ versus $\sqrt{t_{ig}}$ to estimate the time needed to reach "steady-state" burning, t* and thermal inertia, kρc

Recall $\frac{\dot{q}''_{cr}}{\dot{q}''_{e}} = \mathrm{F}(t_{ig}) = \begin{cases} \frac{2\ h_{ig}\sqrt{t_{ig}}}{\sqrt{\pi k\rho c}} & t_{ig} \le t^* \\ 1 & t_{ig} > t^* \end{cases}$ for piloted-ignition data where t* is the time

when $\dot{q}''_{cr} / \dot{q}''_{e}$ =1. Thermal inertia can be estimated from the best-fit line through t = 0. Its slope at $0 < t < t^*$ is $\frac{2\ h_{ig}}{\sqrt{\pi k\rho c}}$; therefore, $k\rho c = \frac{4\ h_{ig}^2}{\pi \cdot (slope)^2}$. Note that in the analysis, few data points at lower heat-flux levels with large time-to-ignition data were excluded (see Figure A(C)-2, open circles) to increase fitness of the best-fit line. This approach is reasonable, considering that at this region analysis assumptions of having inert and thermally thick conditions are less likely to be satisfied.

$$\boldsymbol{k\rho c = 0.649\ kJ^2/m^4K^2s}$$

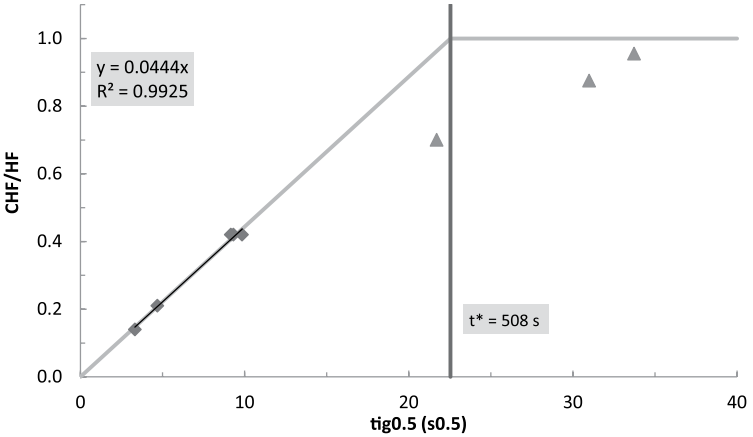

Figure A(C)-2. Plot of $\dot{q}''_{cr} / \dot{q}''_{e}$ versus $\sqrt{t_{ig}}$

CONDUCT BURNING-RATE DATA ANALYSIS

1. Estimate $\Delta h_{c,eff}$

There are two approaches in estimating the effective heat of combustion via calorimeter tests: by using the peak in HRR or the average heat released over the entire test. In this example, $\Delta h_{c,eff}$ will be estimated by considering the total heat released divided by the total amount of mass loss during a test. Cone test results at 25, 50 and 75 kW/m^2 are summarized below (see Table A(C)-4):

Table A(C)-4. Estimation of effective heat-of-combustion using cone calorimeter test results at applied heat flux of 25, 50 and 75 kW/m^2

Heat Flux	t_{start}	$Mass_{start}$	t_{end}	$Mass_{end}$	Total HR	Total ML	$\Delta h_{c,eff}$
(kW/m^2)	(s)	(g)	(s)	(g)	(kW/m^2)	(g/m^2)	(kJ/g)
25	0	222.7	1330	0.0	539.9	222.7	24.2
50	0	236.9	838	0.0	586.8	236.9	24.8
75	0	221.1	645	0.0	550.9	221.1	24.9
Average							24.6

$$\Delta h_{c,eff} = 24.6 \text{ kJ/g}$$

2. Estimate Δh_g

Recall $\Delta h_g \equiv \frac{\dot{q}''_{net}}{\dot{m}''} = \frac{\dot{q}_e'' + \dot{q}_f'' - \dot{q}_l''}{\dot{m}''}$; therefore, when plotting mass-loss rates at different radiant-heat-flux levels during steady-burning condition, the reciprocal of the slope of the best-fit line should be the heat-of-gasification (see Table A(C)-5 and Figure A(C)-3).

$$\Delta h_g = 2.9 \text{ kJ/g}$$

Table A(C)-5. Estimation of effective heat-of-gasification using cone calorimeter test results at applied heat flux of 25, 50 and 75 kW/m²

Heat Flux (kW/m^2)	t_{start} (s)	t_{end} (s)	Total ML (g)	MLR (g/m^2s)
25	0	1330	222.7	16.7
50	0	838	236.9	28.3
75	0	645	221.1	34.3

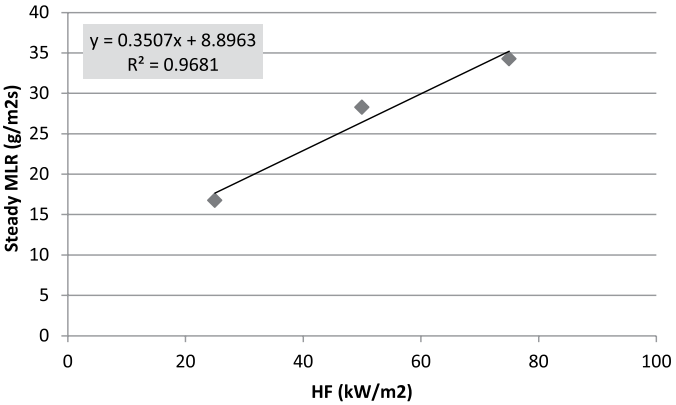

Figure A(C)-3. Plot of steady MLR versus different applied heat-flux levels – 25, 50 and 75 kW/m²

Obtain Uncertainty for Estimated Parameters

UNCERTAINTY FOR MEASURED PARAMETERS

1. δT_∞

Fluctuation in ambient temperature during testing is estimated to be less than ±10% of reported measurement data.

2. $\delta \dot{q}''_{cr}$

The resolution of bracketing experiment was 1 kW/m^2; hence, uncertainty can be estimated as ± 0.5 kW/m^2.

3. δh_c

Considering that the reference values sited in the *Guide* for different apparatuses and set-up have two significant figures, uncertainty for this convection coefficient can be estimated as ± 0.5 W/m^2K.

4. $\delta \varepsilon$

Based on literature review, black PMMA's emissivity should be within ± 10% of what has been approximated in this example.

1. δT_{ig}

See Chapter 4 for detail.

$$\frac{\partial \dot{q}''_{cr}}{\partial T_{ig}} = \frac{h_c + 4\varepsilon\sigma T_{ig}^3}{\varepsilon}$$

$$= \frac{\left(0.012\frac{kW}{m^2K}\right) + 4(0.9)\left(5.67\times10^{-11}\frac{kW}{K^4m^2}\right)\left((318+273)K\right)^3}{(0.9)}$$

$$\approx 0.06015\frac{kW}{m^2K}$$

$$\frac{\partial \dot{q}''_{cr}}{\partial \varepsilon} = \frac{-\dot{q}''_{cr} + \sigma(T_{ig}^4 - T_\infty^4)}{\varepsilon}$$

$$= \frac{-\left(10.5\frac{kW}{m^2}\right) + \left(5.67\times10^{-11}\frac{kW}{K^4m^2}\right)\left(\left((318+273)K\right)^4 - \left((20+273)K\right)^4\right)}{(0.9)}$$

$$\approx -4.445\frac{kW}{m^2}$$

$$\frac{\partial \dot{q}''_{cr}}{\partial h_c} = \frac{T_{ig} - T_\infty}{\varepsilon}$$

$$= \frac{\left((318+273)K\right) - \left((20+273)K\right)}{(0.9)}$$

$$\approx 331.1K$$

$$\frac{\partial \dot{q}''_{cr}}{\partial T_\infty} = \frac{-h_c - 4\varepsilon\sigma T_\infty^3}{\varepsilon}$$

$$= \frac{-\left(0.012\frac{kW}{m^2K}\right) - 4(0.9)\left(5.67\times10^{-11}\frac{kW}{K^4m^2}\right)\left((20+273)K\right)^3}{(0.9)}$$

$$\approx -0.01904\frac{kW}{m^2K}$$

Therefore,

$$\delta T_{ig} = \left(\frac{\partial \dot{q}''_{cr}}{\partial T_{ig}}\right)^{-1}\sqrt{\left(\delta\dot{q}''_{cr}\right)^2 - \left(\left(\frac{\partial \dot{q}''_{cr}}{\partial \varepsilon}\delta\varepsilon\right)^2 + \left(\frac{\partial \dot{q}''_{cr}}{\partial h_c}\delta h_c\right)^2 + \left(\frac{\partial \dot{q}''_{cr}}{\partial T_\infty}\delta T_\infty\right)^2\right)}$$

$$= \left(0.06015\frac{kW}{m^2K}\right)^{-1}\sqrt{\left(0.5\frac{kW}{m^2}\right)^2 - \left(\begin{array}{l}\left(\left(-4.445\frac{kW}{m^2}\right)(0.09)\right)^2 \\ \quad + \left((331.1K)\left(0.5\times10^{-3}\frac{kW}{m^2K}\right)\right)^2 \\ \quad + \left(\left(-0.01904\frac{kW}{m^2K}\right)(2K)\right)^2\end{array}\right)}$$

$$\approx 4.11K$$

2. δ(kρc)

See Chapter 4 for detail.

The uncertainty of the slope of the best-fit line, 0.0444 $s^{-0.5}$, can be estimated through calculating 2 times the standard error of the slope, which is +/- 0.00136 $s^{-0.5}$.

$$\frac{\partial(k\rho c)}{\partial(slope)} = \frac{-8}{\pi\cdot(slope)^3}\left(\frac{\varepsilon\dot{q}''_{cr}}{T_{ig}-T_\infty}\right)^2$$

$$= \frac{-8}{\pi\cdot\left(0.0444s^{-0.5}\right)^3}\left(\frac{(0.9)\left(10.5\frac{\frac{kJ}{s}}{m^2}\right)}{((318+273)K)-((20+273)K)}\right)^2$$

$$\approx -29.33\frac{kJ^2}{m^4K^2s^{0.5}}$$

$$\frac{\partial(k\rho c)}{\partial\varepsilon} = \frac{8}{\pi\cdot(slope)^2}\left(\frac{\dot{q}''_{cr}}{T_{ig}-T_\infty}\right)^2\varepsilon$$

$$= \frac{8}{\pi\cdot\left(0.0444s^{-0.5}\right)^2}\left(\frac{\left(10.5\frac{\frac{kJ}{s}}{m^2}\right)}{((318+273)K)-((20+273)K)}\right)^2(0.9)$$

$$\approx 1.446\frac{kJ^2}{m^4K^2s}$$

$$\frac{\partial(k\rho c)}{\partial\dot{q}''_{cr}} = \frac{8}{\pi\cdot(slope)^2}\left(\frac{\varepsilon}{T_{ig}-T_\infty}\right)^2\dot{q}''_{cr}$$

$$= \frac{8}{\pi\cdot\left(0.0440s^{-0.5}\right)^2}\left(\frac{(0.9)}{((318+273)K)-((20+273)K)}\right)^2\left(10.5\frac{\frac{kJ}{s}}{m^2}\right)$$

$$\approx 0.1239\frac{kJ}{m^2K^2}$$

$$\frac{\partial(k\rho c)}{\partial T_{ig}} = \frac{-8}{\pi\cdot(slope)^2}\left(\frac{\varepsilon\dot{q}''_{cr}}{T_{ig}-T_\infty}\right)^2\frac{1}{T_{ig}-T_\infty}$$

$$= \frac{-8}{\pi\cdot\left(0.0444s^{-0.5}\right)^2}\left(\frac{(0.9)\left(10.5\frac{\frac{kJ}{s}}{m^2}\right)}{((318+273)K)-((20+273)K)}\right)^2\frac{1}{((318+273)K)-((20+273)K)}$$

$$\approx -0.00437\frac{kJ^2}{m^4K^3s}$$

$$\frac{\partial(k\rho c)}{\partial T_\infty} = \frac{8}{\pi\cdot(slope)^2}\left(\frac{\varepsilon\dot{q}''_{cr}}{T_{ig}-T_\infty}\right)^2\frac{1}{T_{ig}-T_\infty}$$

$$= \frac{8}{\pi\cdot\left(0.0444s^{-0.5}\right)^2}\left(\frac{(0.9)\left(10.5\frac{\frac{kJ}{s}}{m^2}\right)}{((318+273)K)-((20+273)K)}\right)^2\frac{1}{((318+273)K)-((20+273)K)}$$

$$\approx 0.00437\frac{kJ^2}{m^4K^3s}$$

Therefore,

$$\delta(k\rho c) = \sqrt{\begin{array}{l}\left(\frac{\partial(k\rho c)}{\partial(slope)}\delta(slope)\right)^2+\left(\frac{\partial(k\rho c)}{\partial\varepsilon}\delta\varepsilon\right)^2+\left(\frac{\partial(k\rho c)}{\partial\dot{q}''_{cr}}\delta\dot{q}''_{cr}\right)^2\\ +\left(\frac{\partial(k\rho c)}{\partial T_{ig}}\delta T_{ig}\right)^2+\left(\frac{\partial(k\rho c)}{\partial T_\infty}\delta T_\infty\right)^2\end{array}}$$

$$= \sqrt{\begin{array}{l}\left(\left(-29.33\frac{kJ^2}{m^4K^2s^{0.5}}\right)\left(0.00136s^{-0.5}\right)\right)^2+\left(\left(1.446\frac{kJ^2}{m^4K^2s}\right)(0.09)\right)^2\\ +\left(\left(-0.1239\frac{kJ}{m^2K^2}\right)\left(0.5\frac{kW}{m^2}\right)\right)^2+\left(\left(-0.00436\frac{kJ^2}{m^4K^3s}\right)(4.1K)\right)^2\\ +\left(\left(0.00436\frac{kJ^2}{m^4K^3s}\right)(2K)\right)^2\end{array}}$$

$$\approx 0.151\frac{kJ^2}{m^4K^2s}$$

UNCERTAINTY FOR ESTIMATED PARAMETERS USING BURNING-RATE DATA ANALYSIS

1. $\delta\Delta h_{c,eff}$

This parameter is estimated by considering the average of the total heat released divided by the total amount of mass loss during three cone tests at 25, 50 and 75 kW/m^2 heat-flux levels. Assuming the estimated $\Delta h_{c,eff}$ at each test results in normal distribution, confidence interval with $\alpha = 0.05$ (95%) can be predicted using student t distribution with a sample size of three, which is ± 0.9 kJ/g.

2. $\delta\Delta h_g$

See Chapter 4 for detail.

The uncertainty of the slope (=$1/\Delta h_g$=0.351g/kJ) can be estimated through calculating 2 times the standard error of the slope of the best-fit line, which is +/- 0.127. Therefore, the uncertainty in Δh_g is

$$\frac{d(\Delta h_g)}{d(slope)} = -\frac{1}{(slope)^2}$$
$$= -\frac{1}{\left(0.351\frac{g}{kJ}\right)^2}$$
$$\approx -8.13\frac{kJ^2}{g^2}$$

Therefore,

$$\delta(\Delta h_g) = \sqrt{\left(\frac{d(\Delta h_g)}{d(slope)}\delta(slope)\right)^2}$$
$$= \sqrt{\left(\left(-8.13\frac{kJ^2}{g^2}\right)(0.1274 g/kJ)\right)^2}$$
$$\approx 1.036\frac{kJ}{g}$$

UNCERTAINTY SUMMARY

Table A(C)-6. Summary of model-parameter table with estimated values with uncertainty

Ignition Parameters	T_∞	20 ± 2 °C
	T_{ig}	318 ± 4 °C
	$\dot{q}''_{cr}$	10.5 ± 0.5 kW/m^2
	kρc	0.649 ± 0.151 kJ^2/m^{4}K^{2}s
Burning-Rate Parameters	$\Delta h_{c,eff}$	24.6 ± 0.9 kJ/g
	Δh_g	2.9 ± 1.0 kJ/g
	h_c	12 ± 0.5 W/m^{2}K
	ε	0.9 ± 0.09

Validation

Analyze Simulation Quality

DETERMINE DATA AND MODEL OUTPUT UNCERTAINTY TO MAKE COMPARISON

1. Conduct uncertainty analysis of data

From the experiment work done by Beaulieu and Dembsey[1] on thermally-thick behaving black PMMA using AFM apparatus, the experiment uncertainty in time-to-ignition and mass-loss rate at steady burning were determined as ± 2 s and ± 3 g/m^{2}s, respectively. The test results were compared with other literature values using different apparatuses such as cone calorimeter in this work, which were considered as consistent. This uncertainty information will be used when comparing modeling output to experiment data.

2. Conduct uncertainty analysis for MLR profile modeling

Because uncertainty information of the data is found in terms of time-to-ignition and mass-loss rate, mass-loss-rate profile is considered as the modeling output of interest for comparison purposes. For Simple Analytical Models, time-to-ignition (t_{ig}) and steady-burning rate ($\dot{m}''$) are needed when simulating the mass-release-rate profile. The uncertainty in MLR profile in modeling can be determined via considering the uncertainties in the calculation results below:

$$t_{ig} \pm \delta t_{ig}$$
$$\dot{m}'' \pm \delta \dot{m}''$$

To determine the uncertainty in time-to-ignition, recall:

$$\frac{\dot{q}''_{cr}}{\dot{q}''_e} = \mathrm{F}(t_{ig}) = \begin{cases} \dfrac{2\ h_{ig}\sqrt{t_{ig}}}{\sqrt{\pi k \rho c}} & t_{ig} \le t^* \\ 1 & t_{ig} > t^* \end{cases}$$

Knowing that all heat-flux levels of interest, 25, 50 and 75 kW/m^2, are above the critical heat flux, time-to-ignition should be smaller than t*. Hence, uncertainty in t_{ig} can be estimated from linear-regression process as:

$$\frac{\dot{q}''_{cr}}{\dot{q}''_e} = \frac{2\ h_{ig}}{\sqrt{\pi k \rho c}}\sqrt{t_{ig}}$$

The above equation can be re-written as below after conducting linear regression:

$$y\ estimate = (slope)\sqrt{t_{ig}}$$

Therefore,

$$t_{ig} = \left(\frac{y\ estimate}{slope}\right)^2$$

Assuming that the y estimate and slope are independent and propagating the uncertainties in these two variables in estimating the time to ignition, the following calculation can be made:

$$\delta t_{ig} = \sqrt{\left(\frac{\partial t_{ig}}{\partial(y\ estimate)}\delta(y\ estimate)\right)^2 + \left(\frac{\partial t_{ig}}{\partial(slope)}\delta(slope)\right)^2}$$

where

$$\frac{\partial t_{ig}}{\partial(y\ estimate)} = \frac{2\cdot(y\ estimate)}{(slope)^2}$$

$$\frac{\partial t_{ig}}{\partial(slope)} = -\frac{2\cdot(y\ estimate)^2}{(slope)^3}$$

with δ(*y estimate)* and δ(*slope)* estimated through calculating 2 times the standard error of the y estimate and slope of the best-fit line, which are 0.002365 and 0.001363 $s^{-0.5}$, respectively.

To determine the uncertainty in steady-heat-release rate at post-ignition stage, recall:

$$\Delta h_g \equiv \frac{\dot{q}''_{net}}{\dot{m}''} = \frac{\dot{q}_e'' + \dot{q}_f'' - \dot{q}_l''}{\dot{m}''}$$

Above equation can be rearranged to

$$\dot{m}'' = \frac{1}{\Delta h_g}\dot{q}_e'' + \frac{\dot{q}_f'' - \dot{q}_l''}{\Delta h_g}$$

The steady-burning rate at post-ignition stage is determined by the best-fit line obtained when data are plotted as steady-burning rate versus applied heat flux. The uncertainty in steady-burning rate can be determined by considering 2 times the standard error of the y estimates, i.e., $\dot{m}''$, which is obtained through linear-regression process: **± 4.5 g/m²s**.

COMPARE DATA WITH SIMULATION RESULTS WITH CONSIDERATION OF UNCERTAINTIES

Parameters in this simple analytical pyrolysis model have been estimated with cone calorimeter test data from 25, 50 and 75 kW/m². To check the quality of the modeling using the estimated parameters, three cases have been simulated and compared with experiment data, with the consideration of their uncertainty bands as shown in table and figures below (see Table A(C)-7).

Table A(C)-7. Comparison of time-to-ignition at different heat-flux levels from actual experiment and pyrolysis modeling

Heat-Flux Level	Actual t_{ig} (s) $t_{ig} \pm \delta t_i$	Model t_{ig} (s) $t_{ig} \pm \delta t_i$
25 kW/m²	87 ± 2	90 ± 12
50 kW/m²	22 ± 2	22 ± 5
75 kW/m²	11 ± 2	10 ± 3

All three cases show good overlap between the data and simulation of time-to-ignition and the mass-loss rate during steady burning, considering the uncertainties, i.e., the parameter estimation was conducted successfully (see Figure A(C)-4, Figure A(C)-5 and Figure A(C)-6).

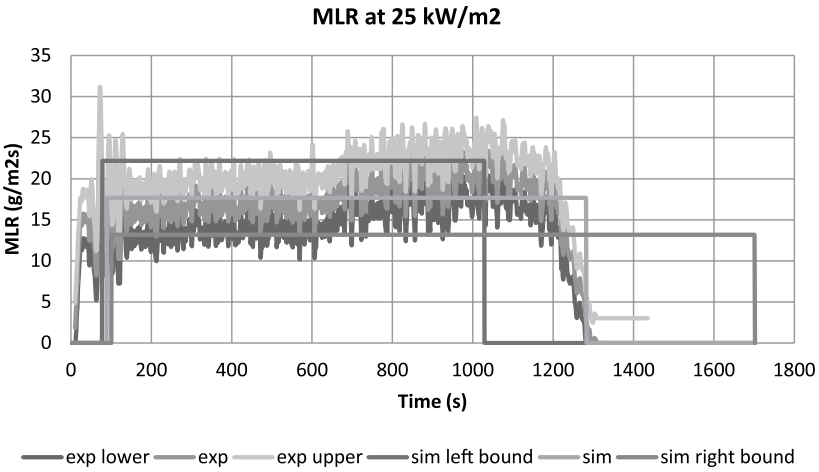

Figure A(C)-4. Mass-loss rate (MLR) comparisons for PMMA between actual MLR from experiment (exp) and modeled MLR (sim) at 25 kW/m². Note that data shown were used to estimate model-parameter values.

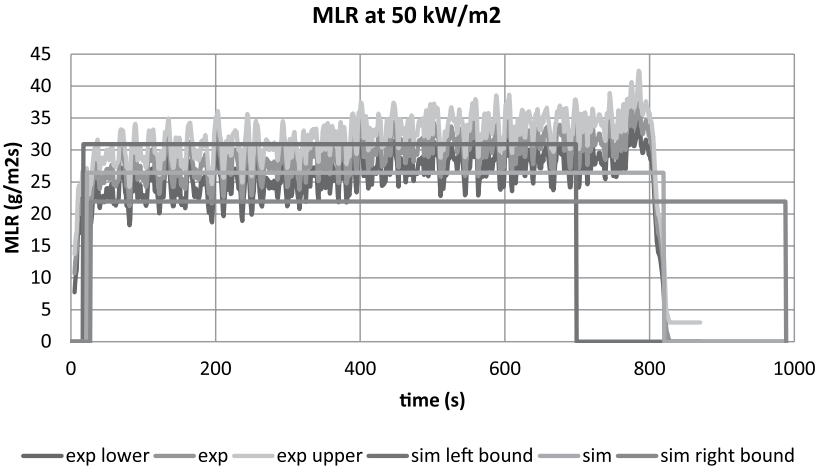

Figure A(C)-5. Mass-loss rate (MLR) comparisons for PMMA between actual MLR from experiment (exp) and modeled MLR (sim) at 50 kW/m². Note that data shown were used to estimate model-parameter values.

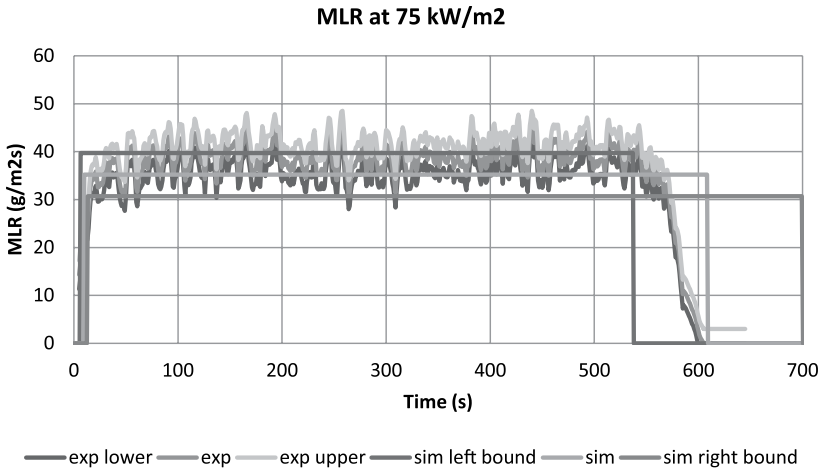

Figure A(C)-6. Mass-loss rate (MLR) comparisons for PMMA between actual MLR from experiment (exp) and modeled MLR (sim) at 75 kW/m². Note that data shown were used to estimate model-parameter values.

Validate Simulation Quality upon Extrapolation

In this example, cone calorimeter data at applied heat flux of 25, 50, and 75 kW/m² were used to estimate the unknown model parameters. In order to check the performance of modeling with the estimated parameters, PMMA AFM tests[1] conducted under 28.4 and 60 kW/m² are used to compare with modeling outputs – time-of-ignition and MLR at steady-burning stage (see Table A(C)-8).

Table A(C)-8. Comparison of time-to-ignition at different heat-flux levels from actual experiment and pyrolysis modeling

Heat-Flux Level	Actual t_{ig} (s) $t_{ig} \pm \delta t_i$	Model t_{ig} (s) $t_{ig} \pm \delta t_i$
28.4 kW/m²	102 ± 2	70 ± 12
60 kW/m²	31 ± 2	16 ± 5

In modeling time-to-ignition, the model's outputs are shorter than those from AFM tests for both heat-flux levels. This discrepancy can be explained by considering the in-depth absorption of radiation during heating of PMMA. The data from AFM tests, where IR lamps are used to heat the samples, possibly were subject to in-depth radiative absorption delaying ignition, knowing that the PMMA samples are somewhat transparent. However, this phenomenon is not accounted for in modeling assumptions and in parameter estimation process where cone calorimeter test data is used – in the cone, radiation is absorbed mostly on the surface.

In modeling the MLR at steady-burning stage, both cases show good overlap between the data and simulation, considering the uncertainties (see Figure A(C)-7 and Figure A(C)-8).

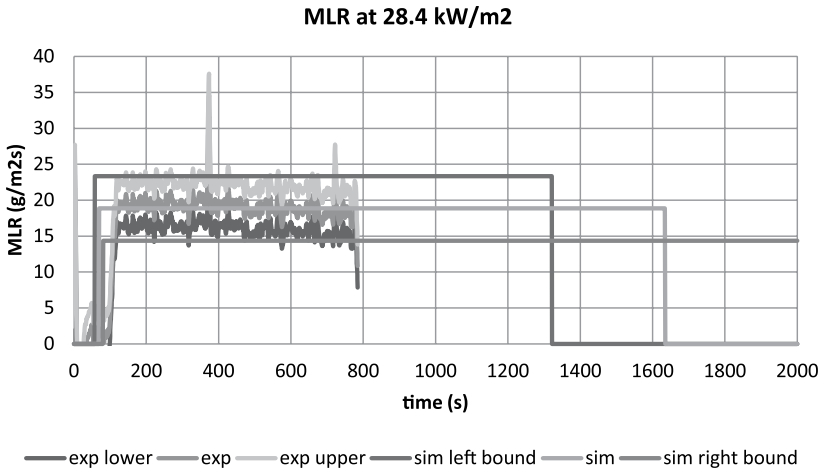

Figure A(C)-7. Mass-loss rate (MLR) comparisons for PMMA between actual MLR from experiment (exp) and modeled MLR (sim) at 28.4 kW/m². Note that data shown were not included in the model-parameter-estimation process; hence, this case is considered as extrapolation case.

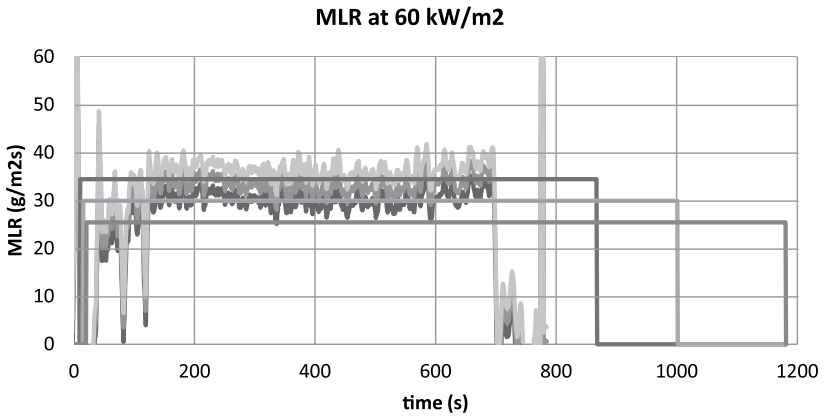

Figure A(C)-8. Mass-loss rate (MLR) comparisons for PMMA between actual MLR from experiment (exp) and modeled MLR (sim) at 60 kW/m². Note that data shown were not included in the model-parameter-estimation process; hence, this case is considered as extrapolation case.

Commentary

When using Simple Analytical Model to simulate pyrolysis of black PMMA (density 1170 kg/m^3, thickness 18 mm), test data from a bench-scale cone calorimeter experiment at several heat-flux levels have been utilized to estimate the time-to-ignition from exposure to heating and the mass-loss rate at steady-burning stage after ignition. The comparison between the model outputs (time-to-ignition and steady-burning rate) and the data from bench-scale experiment showed good agreement for both checking purposes, where the same heat-flux levels (25, 50, and 75 kW/m^2) used in parameter estimation have been considered, and extrapolation purposes where heat-flux levels (28.4 and 60 kW/m^2) not included in the parameter estimation process have been considered.

Although the modeling predictions of time-to-ignition and steady-burning rate in this example seem to be reasonable, limitations of Simple Analytical Modeling has been acknowledged in literature for modeling black PMMA at relatively high applied heat-flux levels.[1] At high heat-flux levels, the assumption of having an inert condition during pre-ignition stage and neglecting thermal decomposition behavior, such as bubbling, cannot be made where these effects become more profound on the temperature profile and ignition process of PMMA. Therefore, caution should be given when conducting modeling for cases with higher heat-flux levels.

Example 4.2 Modeling Corrugated Cardboard

Measure Parameters

1. Ambient Temperature

Direct measurement of ambient temperature is made as 23°C.

2. Surface Temperature at Ignition

This parameter will be obtained via Ignition Data Analysis, i.e., no direct measurements will be performed.

3. Critical Heat Flux for Ignition

Corrugated cardboard's CHF is measured to between 8 and 10 kW/m^2 from cone calorimeter testing by bracketing. Hence, CHF is 9 ± 1 kW/m^2.

4. Thermal Inertia

This parameter will be obtained via Ignition Data Analysis, i.e., no direct measurements will be performed.

5. Effective Heat-of-Combustion

This parameter will be obtained via Burning-Rate Data Analysis, i.e., no direct measurements will be performed.

6. Heat-of-Gasification

This parameter will be obtained via Burning-Rate Data Analysis, i.e., no direct measurements will be performed.

7. Convection Coefficient

Because this is a material laid in horizontal position in a cone calorimeter, $h_c = 12$ W/m^2K is used based on literature reference.

8. Surface Emissivity/Absorptivity

Emissivity is approximated as 0.9.

Summary

Table A(C)-9. Summary of model-parameter table with estimated values via direct measurements, literature search, or approximation

Ignition Parameters	T_∞	23 °C
	T_{ig}	Ignition Data Analysis
	$\dot{q}''_{cr}$	9 kW/m^2
	$k\rho c$	Ignition Data Analysis
Burning-Rate Parameters	$\Delta h_{c,eff}$	Burning-Rate Data Analysis
	Δh_g	Burning-Rate Data Analysis
	h_c	12 W/m^{2}K
	ε	0.9

Obtain Parameters via Data Analysis

Run Model

SELECT MODEL: THERMALLY THICK MODEL FOR IGNITION ANALYSIS (QUINTIERE AND HARKLEROAD, ASTM E 1321) AND STEADY-BURNING MODEL

UNDERSTAND EXPERIMENT AND FIRE CHARACTERISTICS OF MATERIAL

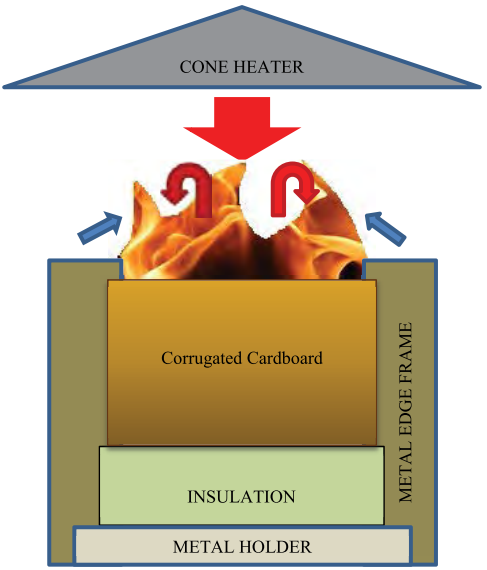

Figure A(C)-9. Simplified representation of a cone calorimeter test of corrugated cardboard

A simplified representation of a cone calorimeter test of triple-layered corrugated cardboard is shown in Figure A(C)-9. The sample is placed on top of an insulation, which sits on a metal holder. Another metal frame is placed on top of the sample, insulation and the holder. A metal edge frame is used as well.

Front Surface: As heating starts by opening the shutter to allow radiation from the cone heater to impinge on sample surface (large red arrow), cooling also begins via natural convection (blue arrows) and re-radiation. The surface decomposes with charring, i.e., surface becoming black and white smoke, which typically indicates moisture loss with heating of the sample. Note that the surface becomes non-uniformly black due to corrugation showing linear shading. As the surface layer is burned away, it exfoliates toward the sides and opens up, allowing the first layer of the corrugation to appear on the surface. Then the middle flat layer of the cardboard, which separates the two layers of corrugation, starts to burn, allowing the heat release to grow. As this layer is decomposed throughout, the second layer of the corrugation becomes involved in burning process. Followed by the burning of the second corrugation layer, the last flat layer of the cardboard – the back surface of the sample – burns. This results in another growing phase in the heat-release-rate curve. When ignition occurs as the fuel vapor concentration above the surface exceeds its LFL (lower flammable limit), additional heat flux from the flame is introduced on the surface (red arrows).

Back surface: The sample is placed on top of insulation. In the experiment, an air gap of a few millimeters thickness exists between the sample and the insulation due to thermal contact. Nothing leaves through the back face with the insulation when 1D assumption holds for the experiment.

CONFIGURE MODEL CONDITIONS BASED ON UNDERSTANDING OF EXPERIMENT AND MATERIAL CHARACTERISTICS

In the model, the phenomena discussed above are simulated as below. Basic assumptions are as follows:

- Pre-ignition stage is:
  - Inert: non-uniform charring is considered to be evenly distributed
  - Thermally thick: heat transfer does not reach back surface
- Post-ignition stage is:
  - Considered to have instantaneous release of volatiles from solid to gas phase
  - Considered to have a constant thickness: exfoliation of surface layers is neglected
  - Steady burning: heat loss equals heat gain at front surface

ACQUIRE DATA SETS

Cone calorimeter test data of triple layered corrugated cardboard with thickness of 15 mm, density of 116 kg/m^3 and applied heat flux levels ranging from 8 to 75 kW/m^2 are found. For Ignition Data analysis, only time-to-ignition with respect to applied heat-flux data will be used. For burning-rate data analysis, data for the entire testing time duration, mass loss, and heat release during testing period with respect to applied heat flux will be used.

CONDUCT IGNITION DATA ANALYSIS

1. Estimate T_{ig}

Heat balance at front surface during steady burning is as follow:

$$\varepsilon \dot{q}''_{cr} = h_c(T_{ig} - T_\infty) + \varepsilon\sigma(T_{ig}^4 - T_\infty^4)$$

Knowing that emissivity is approximated as 0.9, critical heat flux is estimated as 9 kW/m^2, and heat-transfer in cone calorimeter experiment is estimated as 12.0 W/m^{2}K, ignition temperature, T_{ig} is calculated as:

$$\mathbf{T_{ig} = 293\ °C}$$

2. Estimate h_{ig}

h_{ig} is the total-heat-transfer coefficient at ignition; therefore, at steady-state burning stage, the following can be defined:

$$\varepsilon \dot{q}''_{cr} \equiv h_{ig}(T_{ig} - T_\infty)$$

Knowing the ignition temperature, hig can be calculated:

$$\mathbf{h_{ig} = 30.0\ W/m^2K}$$

3. Calculate $\dot{q}''_{cr} / \dot{q}''_{e}$ versus $\sqrt{t_{ig}}$ from ignition data

Table A(C)-10. $\dot{q}''_{cr} / \dot{q}''_{e}$ versus $\sqrt{t_{ig}}$

Heat Flux (kW/m²)	t_{ig} (s)	CHF/HF	$t_{ig}^{0.5}$ ($s^{0.5}$)
8	NI		
10	387	0.9000	19.67
15	103	0.6000	10.15
20	52	0.4500	7.21
25	32	0.3600	5.66
25	34	0.3600	5.83
25	33	0.3600	5.74
25	28	0.3600	5.29
40	9	0.2250	3.00
40	11	0.2250	3.32
50	11	0.1800	3.32
60	8	0.1500	2.83
60	8	0.1500	2.83
75	2	0.1200	1.41

4. Plot $\dot{q}''_{cr} / \dot{q}''_{e}$ versus $\sqrt{t_{ig}}$ to estimate the time needed to reach "steady-state" burning, t* and thermal inertia, kρc

Recall $\frac{\dot{q}''_{cr}}{\dot{q}''_{e}} = F(t_{ig}) = \begin{cases} \frac{2\ h_{ig}\sqrt{t_{ig}}}{\sqrt{\pi k\rho c}} & t_{ig} \le t^* \\ 1 & t_{ig} > t^* \end{cases}$ for piloted-ignition data, where t* is the time when $\dot{q}''_{cr} / \dot{q}''_{e} = 1$. Thermal inertia can be estimated from the best-fit line through t = 0. Its slope at $0 < t < t^*$ is $\frac{2\ h_{ig}}{\sqrt{\pi k\rho c}}$; therefore, $k\rho c = \frac{4\ h_{ig}^2}{\pi \cdot (slope)^2}$. Note that in the analysis, few data points at lower heat-flux levels with large time-to-ignition data were excluded (see Figure A(C)-10, open circles) to increase fitness of the best-fit line. This approach is reasonable, considering that at this region analysis assumptions of having inert and thermally thick conditions are less likely to be satisfied.

$k\rho c$ = 0.297 kJ²/m⁴K²s

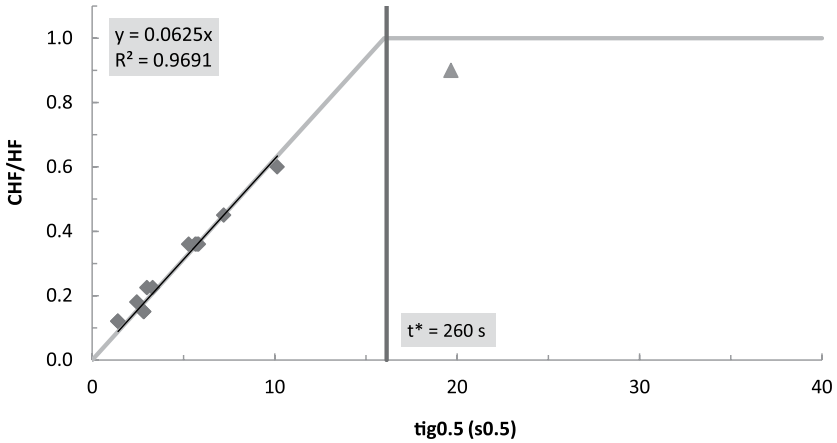

Figure A(C)-10. Plot of $\dot{q}''_{cr} / \dot{q}''_{e}$ versus $\sqrt{t_{ig}}$

CONDUCT BURNING-RATE DATA ANALYSIS

1. Estimate $\Delta h_{c,eff}$

There are two approaches in estimating the effective heat-of-combustion via calorimeter tests: by using the peak in HRR or the average heat released over the entire test. In this example, $\Delta h_{c,eff}$ will be estimated by considering the average heat-release rate divided by the average mass-loss rate during a test. Cone test results ranging from 15 to 75 kW/m² are used:

$\Delta h_{c,eff}$ = 13.9 kJ/g

2. Estimate Δh_g

Recall $\Delta h_g \equiv \frac{\dot{q}''_{net}}{\dot{m}''} = \frac{\dot{q}_e'' + \dot{q}_f'' - \dot{q}_l''}{\dot{m}''}$; therefore, when plotting mass-loss rates at different radiant-heat-flux levels during steady-burning condition, the reciprocal of the slope of the best-fit line should be the heat-of-gasification (see Table A(C)-11 and Figure A(C)-11).

$$\Delta h_g = 21.6 \text{ kJ/g}$$

Table A(C)-11. Estimation of effective heat-of-gasification using cone calorimeter test results at applied heat flux ranging between 25 and 75 kW/m²

Heat Flux (kW/m^2)	avgMLR (g/m^2s)
25	6.70
25	6.59
40	6.93
50	7.95
60	8.64
60	9.09
75	8.30

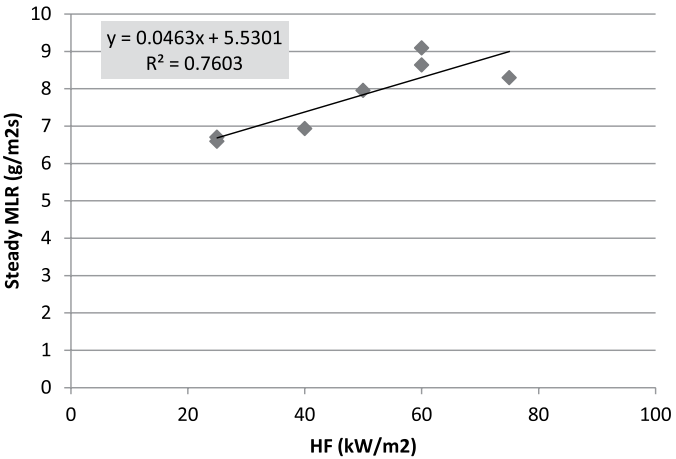

Figure A(C)-11. Plot of steady MLR versus different applied heat-flux levels – 25 to 75 kW/m²

Obtain Uncertainty for Estimated Parameters

UNCERTAINTY FOR MEASURED PARAMETERS

1. δT_∞

Fluctuation in ambient temperature during testing is estimated to be less than ±15% of reported measurement data.

2. $\delta \dot{q}''_{cr}$

The resolution of bracketing experiment was 2 kW/m²; hence, uncertainty can be estimated as ± 1 kW/m².

3. δh_c

Considering that the reference values sited in the *Guide* for different apparatuses and set-up have two significant figures, uncertainty for this convection coefficient can be estimated as ± 0.5 W/m²K.

4. $\delta \varepsilon$

Based on literature review, cardboard's emissivity should be within ± 10% of what has been approximated in this example.

UNCERTAINTY FOR ESTIMATED PARAMETERS USING IGNITION DATA ANALYSIS

1. δT_{ig}

See Chapter 4 for detail.

$$\frac{\partial \dot{q}''_{cr}}{\partial T_{ig}} = \frac{h_c + 4\varepsilon\sigma T_{ig}^3}{\varepsilon}$$

$$= \frac{\left(0.012\frac{kW}{m^2K}\right) + 4(0.9)\left(5.67\times10^{-11}\frac{kW}{K^4m^2}\right)\left((293+273)K\right)^3}{(0.9)}$$

$$\approx 0.05446\frac{kW}{m^2K}$$

$$\frac{\partial \dot{q}''_{cr}}{\partial \varepsilon} = \frac{-\dot{q}''_{cr} + \sigma(T_{ig}^4 - T_\infty^4)}{\varepsilon}$$

$$= \frac{-\left(9\frac{kW}{m^2}\right) + \left(5.67\times10^{-11}\frac{kW}{K^4m^2}\right)\left(\left((293+273)K\right)^4 - \left((23+273)K\right)^4\right)}{(0.9)}$$

$$\approx -4.018\frac{kW}{m^2}$$

$$\frac{\partial \dot{q}''_{cr}}{\partial h_c} = \frac{T_{ig} - T_\infty}{\varepsilon}$$

$$= \frac{\left((293+273)K\right) - \left((23+273)K\right)}{(0.9)}$$

$$\approx 300.0K$$

$$\frac{\partial \dot{q}''_{cr}}{\partial T_\infty} = \frac{-h_c - 4\varepsilon\sigma T_\infty^3}{\varepsilon}$$

$$= \frac{-\left(0.012\frac{kW}{m^2K}\right) - 4(0.9)\left(5.67\times10^{-11}\frac{kW}{K^4m^2}\right)((23+273)K)^3}{(0.9)}$$

$$\approx -0.01922\frac{kW}{m^2K}$$

Therefore,

$$\delta T_{ig} = \left(\frac{\partial \dot{q}''_{cr}}{\partial T_{ig}}\right)^{-1}\sqrt{\left(\delta\dot{q}''_{cr}\right)^2 - \left(\left(\frac{\partial \dot{q}''_{cr}}{\partial \varepsilon}\delta\varepsilon\right)^2 + \left(\frac{\partial \dot{q}''_{cr}}{\partial h_c}\delta h_c\right)^2 + \left(\frac{\partial \dot{q}''_{cr}}{\partial T_\infty}\delta T_\infty\right)^2\right)}$$

$$= \left(0.05446\frac{kW}{m^2K}\right)^{-1}\sqrt{\left(1\frac{kW}{m^2}\right)^2 - \left(\begin{array}{l}\left(\left(-4.018\frac{kW}{m^2}\right)(0.09)\right)^2 \\ \quad + \left(\left(300.0K\right)\left(0.5\times10^{-3}\frac{kW}{m^2K}\right)\right)^2 \\ \quad + \left(\left(-0.01922\frac{kW}{m^2K}\right)(3.45K)\right)^2\end{array}\right)}$$

$$\approx 16.9K$$

2. δ(kρc)

See Chapter 4 for detail.

The uncertainty of the slope of the best-fit line, 0.0620 $s^{-0.5}$, can be estimated through calculating 2 times the standard error of the slope, which is +/- 0.00282 $s^{-0.5}$.

$$\frac{\partial(k\rho c)}{\partial(slope)} = \frac{-8}{\pi\cdot(slope)^3}\left(\frac{\varepsilon\dot{q}''_{cr}}{T_{ig}-T_\infty}\right)^2$$

$$= \frac{-8}{\pi\cdot\left(0.0620s^{-0.5}\right)^3}\left(\frac{(0.9)\left(9\frac{\frac{kJ}{s}}{m^2}\right)}{((293+273)K)-((23+273)K)}\right)^2$$

$$\approx -9.612\frac{kJ^2}{m^4K^2s^{0.5}}$$

$$\frac{\partial(k\rho c)}{\partial \varepsilon} = \frac{8}{\pi \cdot (slope)^2}\left(\frac{\dot{q}''_{cr}}{T_{ig} - T_\infty}\right)^2 \varepsilon$$

$$= \frac{8}{\pi \cdot \left(0.0620 s^{-0.5}\right)^2}\left(\frac{\left(9\frac{\frac{kJ}{s}}{m^2}\right)}{((293+273)K) - ((23+273)K)}\right)^2 (0.9)$$

$$\approx 0.662 \frac{kJ^2}{m^4 K^2 s}$$

$$\frac{\partial(k\rho c)}{\partial \dot{q}''_{cr}} = \frac{8}{\pi \cdot (slope)^2}\left(\frac{\varepsilon}{T_{ig} - T_\infty}\right)^2 \dot{q}''_{cr}$$

$$= \frac{8}{\pi \cdot \left(0.060 s^{-0.5}\right)^2}\left(\frac{(0.9)}{((293+273)K) - ((23+273)K)}\right)^2 \left(9\frac{\frac{kJ}{s}}{m^2}\right)$$

$$\approx 0.0662 \frac{kJ}{m^2 K^2}$$

$$\frac{\partial(k\rho c)}{\partial T_{ig}} = \frac{-8}{\pi \cdot (slope)^2}\left(\frac{\varepsilon \dot{q}''_{cr}}{T_{ig} - T_\infty}\right)^2 \frac{1}{T_{ig} - T_\infty}$$

$$= \frac{-8}{\pi \cdot \left(0.0620 s^{-0.5}\right)^2}\left(\frac{(0.9)\left(9\frac{\frac{kJ}{s}}{m^2}\right)}{((293+273)K) - ((23+273)K)}\right)^2 \frac{1}{((293+273)K) - ((23+273)K)}$$

$$\approx -0.00221 \frac{kJ^2}{m^4 K^3 s}$$

$$\frac{\partial(k\rho c)}{\partial T_\infty} = \frac{8}{\pi \cdot (slope)^2}\left(\frac{\varepsilon \dot{q}''_{cr}}{T_{ig} - T_\infty}\right)^2 \frac{1}{T_{ig} - T_\infty}$$

$$= \frac{8}{\pi \cdot \left(0.0620 s^{-0.5}\right)^2}\left(\frac{(0.9)\left(9\frac{\frac{kJ}{s}}{m^2}\right)}{((293+273)K) - ((23+273)K)}\right)^2 \frac{1}{((293+273)K) - ((23+273)K)}$$

$$\approx 0.00221 \frac{kJ^2}{m^4 K^3 s}$$

Therefore,

$$\delta(k\rho c) = \sqrt{\left(\frac{\partial(k\rho c)}{\partial(slope)}\delta(slope)\right)^2 + \left(\frac{\partial(k\rho c)}{\partial\varepsilon}\delta\varepsilon\right)^2 + \left(\frac{\partial(k\rho c)}{\partial\dot{q}''_{cr}}\delta\ddot{q}''_{cr}\right)^2 + \left(\frac{\partial(k\rho c)}{\partial T_{ig}}\delta T_{ig}\right)^2 + \left(\frac{\partial(k\rho c)}{\partial T_{\infty}}\delta T_{\infty}\right)^2}$$

$$= \sqrt{\left(\left(-9.612\frac{kJ^2}{m^4K^2s^{0.5}}\right)\left(0.00282s^{-0.5}\right)\right)^2 + \left(\left(0.662\frac{kJ^2}{m^4K^2s}\right)(0.09)\right)^2 + \left(\left(-0.0662\frac{kJ}{m^2K^2}\right)\left(1\frac{kW}{m^2}\right)\right)^2 + \left(\left(-0.00221\frac{kJ^2}{m^4K^3s}\right)(16.9K)\right)^2 + \left(\left(0.00221\frac{kJ^2}{m^4K^3s}\right)(3.45K)\right)^2}$$

$$\approx 0.101\frac{kJ^2}{m^4K^2s}$$

UNCERTAINTY FOR ESTIMATED PARAMETERS USING BURNING-RATE DATA ANALYSIS

1. $\delta\Delta h_{c,eff}$

This parameter is estimated by considering the average of the heat-release rate divided by the average mass-loss rate during cone tests at 15 to 75 kW/m^2 heat-flux levels. Assuming the estimated $\Delta h_{c,eff}$ at each test results in normal distribution, confidence interval with $\alpha = 0.05$ (95%) can be predicted using student t distribution with a sample size of nine, which is ± 1.3 kJ/g.

2. $\delta\Delta h_g$

See Chapter 4 for detail.

The uncertainty of the slope (=1/Δh_g=0.04625g/kJ) can be estimated through calculating 2 times the standard error of the slope of the best-fit line, which is +/- 0.02323. Therefore, the uncertainty in Δh_g is

$$\frac{d(\Delta h_g)}{d(slope)} = -\frac{1}{(slope)^2}$$

$$= -\frac{1}{\left(0.04625\frac{g}{kJ}\right)^2}$$

$$\approx -467\frac{kJ^2}{g^2}$$

Therefore,

$$\delta(\Delta h_g) = \sqrt{\left(\frac{d(\Delta h_g)}{d(slope)}\delta(slope)\right)^2}$$

$$= \sqrt{\left(\left(-467\frac{kJ^2}{g^2}\right)(0.02323g/kJ)\right)^2}$$

$$\approx 10.9\frac{kJ}{g}$$

Table A(C)-12. Summary of model-parameter table with estimated values with uncertainty

Ignition Parameters	T_∞	23 ± 3.45 °C
	T_{ig}	293 ± 17 °C
	$\dot{q}''_{cr}$	9 ± 1 kW/m^2
	kρc	0.297 ± 0.101 kJ^2/m^{4}K^{2}s
Burning-Rate Parameters	$\Delta h_{c,eff}$	13.9 ± 1.3 kJ/g
	Δh_g	21.6 ± 10.9 kJ/g
	h_c	12 ± 0.5 W/m^{2}K
	ε	0.9 ± 0.09

Validation

Analyze Simulation Quality

DETERMINE DATA AND MODEL OUTPUT UNCERTAINTY TO MAKE COMPARISON

1. Conduct uncertainty analysis of data

The uncertainty in the mass-loss-rate data used for comparison between data and model outputs is estimated via statistical approach, taking the standard deviation (0.58 g/sm^2) from the mean of a steady burning of five identical PMMA tests conducted in a cone calorimeter.[2] The estimated uncertainty is 1.4 g/sm^2, which is found by calculating the 95% confidence interval applying student t distribution with a sample size of five.

The uncertainty in time-to-ignition data used for comparison is estimated via statistical approach, taking two to four identical cone calorimeter test data at heat fluxes ranging from 25 to 75 kW/m^2 of this cardboard. 95% confidence interval is calculated for each heat-flux level assuming student t distribution.

2. Conduct uncertainty analysis for MLR profile modeling

Because uncertainty information of the data is found in terms of time-to-ignition and mass-loss rate, mass-loss-rate profile is considered as the modeling output of interest for comparison purposes. For Simple Analytical Models, time-to-ignition (t_{ig}) and steady-burning rate ($\dot{m}''$) are needed when simulating the mass-release-rate profile. The uncertainty in MLR profile in modeling can be determined via considering the uncertainties in these calculation results as below:

$$t_{ig} \pm \delta t_{ig}$$
$$\dot{m}'' \pm \delta \dot{m}''$$

To determine the uncertainty in time-to-ignition, recall:

$$\frac{\dot{q}''_{cr}}{\dot{q}''_e} = F(t_{ig}) = \begin{cases} \dfrac{2\ h_{ig}\sqrt{t_{ig}}}{\sqrt{\pi k\rho c}} & t_{ig} \le t^* \\ 1 & t_{ig} > t^* \end{cases}$$

Knowing that all of heat-flux levels of interest, 25, 50, and 75 kW/m^2, are above the critical heat flux, time-to-ignition should be smaller than t*. Hence, uncertainty in t_{ig} can be estimated from linear-regression process as below:

$$\frac{\dot{q}_{cr}^{"}}{\dot{q}_{e}^{"}} = \frac{2}{\sqrt{\pi k \rho c}} \frac{h_{ig}}{\sqrt{t_{ig}}}$$

The above equation can be re-written as below after conducting linear regression:

$$y\ estimate = (slope)\sqrt{t_{ig}}$$

Therefore,

$$t_{ig} = \left(\frac{y\ estimate}{slope}\right)^2$$

Assuming that the y estimate and slope are independent and propagating the uncertainties in these two variables in estimating the time to ignition, the following calculation can be made:

$$\delta t_{ig} = \sqrt{\left(\frac{\partial t_{ig}}{\partial (y\ estimate)} \delta (y\ estimate)\right)^2 + \left(\frac{\partial t_{ig}}{\partial (slope)} \delta (slope)\right)^2}$$

where

$$\frac{\partial t_{ig}}{\partial (y\ estimate)} = \frac{2 \cdot (y\ estimate)}{(slope)^2}$$

$$\frac{\partial t_{ig}}{\partial (slope)} = -\frac{2 \cdot (y\ estimate)^2}{(slope)^3}$$

with δ(*y estimate)* and δ(*slope)* estimated through calculating 2 times the standard error of the y estimate and slope of the best-fit line.

To determine the uncertainty in steady-heat-release rate at post-ignition stage, recall:

$$\Delta h_g \equiv \frac{\dot{q}_{net}^{"}}{\dot{m}"} = \frac{\dot{q}_e" + \dot{q}_f" - \dot{q}_l"}{\dot{m}"}$$

Above equation can be rearranged to

$$\dot{m}^{"} = \frac{1}{\Delta h_g} \dot{q}_e^{"} + \frac{\dot{q}_f^{"} - \dot{q}_l^{"}}{\Delta h_g}$$

The steady-burning rate at post-ignition stage is determined by the best-fit line obtained when data is plotted as steady-burning rate versus applied heat flux. The uncertainty in steady-burning rate can be determined by considering 2 times the standard error of the y estimates, i.e., $\dot{m}"$, which is obtained through linear-regression process: **± 1.1 g/m^{2}s**.

COMPARE DATA WITH SIMULATION RESULTS WITH CONSIDERATION OF UNCERTAINTIES

Parameters in this simple analytical pyrolysis model have been estimated with cone calorimeter test data from 25, 50, and 75 kW/m^2. To check the quality of the modeling using the estimated parameters, three cases have been simulated and compared with experiment data with the consideration of their uncertainty bands as shown in Table A(C)-13 and figures – Figure A(C)-12, Figure A(C)-13 and Figure A(C)-14 – below.

Table A(C)-13. Comparison of time-to-ignition at different heat-flux levels from actual experiment and pyrolysis modeling

Heat Flux Level	Actual t_{ig} (s) $t_{ig} \pm \delta t_i$	Model t_{ig} (s) $t_{ig} \pm \delta t_i$
25 kW/m^2	32 ± 4	34 ± 10
50 kW/m^2	18 ± 89	8 ± 5
75 kW/m^2	2 ± 5	4 ± 3

All three cases show good overlap between the data and simulation of time-to-ignition and the mass-loss rate during steady burning, considering the uncertainties, i.e., the parameter estimation was conducted successfully.

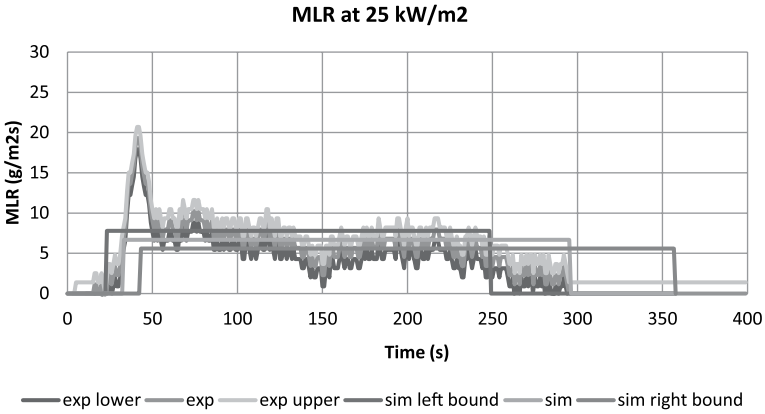

Figure A(C)-12. Mass-loss rate (MLR) comparisons for corrugated cardboard between actual MLR from experiment (exp) and modeled MLR (sim) at 25 kW/m². Note that data shown were used to estimate model-parameter values.

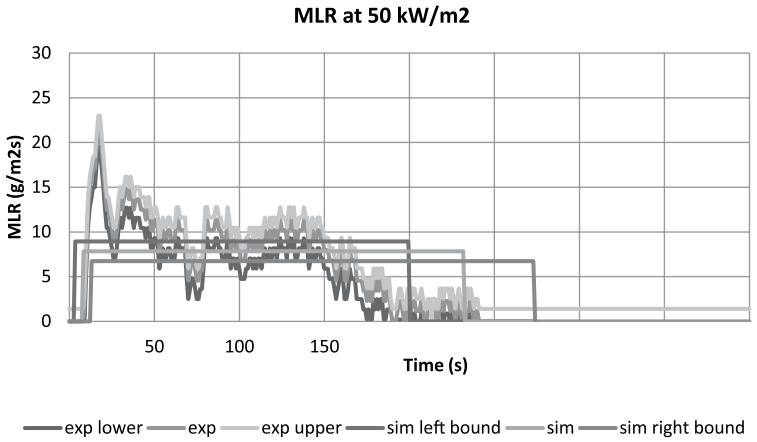

Figure A(C)-13. Mass-loss rate (MLR) comparisons for corrugated cardboard between actual MLR from experiment (exp) and modeled MLR (sim) at 50 kW/m². Note that data shown were used to estimate model-parameter values.

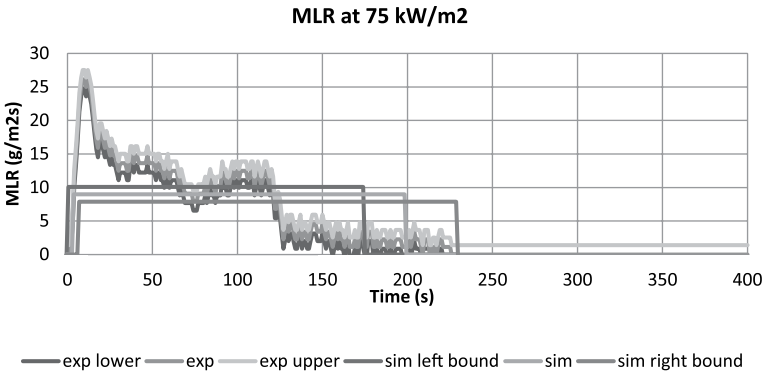

Figure A(C)-14. Mass-loss rate (MLR) comparisons for corrugated cardboard between actual MLR from experiment (exp) and modeled MLR (sim) at 75 kW/m^2. Note that data shown were used to estimate model-parameter values.

Validate Simulation Quality upon Extrapolation

In this example, cone calorimeter data at applied heat flux ranging from 8 to 75 kW/m^2 were used to estimate the unknown model parameters. Assuming that the estimated parameters for this corrugated cardboard will be used in pyrolysis modeling at applied heat-flux levels that are within above range, no additional check becomes necessary.

Commentary

When using Simple Analytical Model to simulate pyrolysis of triple-layered corrugated cardboard (density 116 kg/m^3, thickness 15 mm), test data from a bench-scale cone calorimeter experiment at several heat-flux levels have been utilized to estimate the time-to-ignition from exposure to heating and the mass-loss rate at steady-burning stage after ignition. The comparison between the model outputs (time-to-ignition and steady-burning rate) and the data from bench-scale experiment showed good agreement for both checking purposes, where the same heat-flux levels (25, 50, and 75 kW/m^2) used in parameter estimation have been considered.

Although the modeling predictions of time-to-ignition and steady-burning rate in this example seems to be reasonable, limitation of this Simple Analytical Modeling should be noted, which is that the model is for thermally-thick-behaving materials and steady burning after ignition.

Example 4.3 Modeling Fire-Retarded FRP Composite

Measure Parameters

1. Ambient Temperature

Direct measurement of ambient temperature is made as 23°C.

2. Surface Temperature at Ignition

This parameter will be obtained via Ignition Data Analysis, i.e.- no direct measurements will be performed.

3. Critical Heat Flux for Ignition

Corrugated cardboard's CHF is measured to between 28 and 30 kW/m^2 from cone calorimeter testing by bracketing. Hence, CHF is 29 ± 1 kW/m^2.

4. Thermal Inertia

This parameter will be obtained via Ignition Data Analysis, i.e., no direct measurements will be performed.

5. Effective Heat-of-Combustion

This parameter will be obtained via Burning-Rate Data Analysis, i.e., no direct measurements will be performed.

6. Heat-of-Gasification

This parameter will be obtained via Burning-Rate Data Analysis, i.e., no direct measurements will be performed.

7. Convection Coefficient

Because this is a material laid in horizontal position in a cone calorimeter, h_c = 12 W/m^2K is used based on literature reference.

8. Surface Emissivity/Absorptivity

Emissivity is approximated as 0.9.

Summary

Table A(C)-14. Summary of model-parameter table with estimated values via direct measurements, literature search, or approximation

Ignition Parameters	T_∞	23 °C
	T_{ig}	Ignition Data Analysis
	$\dot{q}''_{cr}$	29 kW/m^2
	$k\rho c$	Ignition Data Analysis
Burning-Rate Parameters	$\Delta h_{c,eff}$	Burning-Rate Data Analysis
	Δh_g	Burning-Rate Data Analysis
	h_c	12 W/m^{2}K
	ε	0.9

Obtain Parameters via Data Analysis

Run model

SELECT MODEL: THERMALLY THICK MODEL FOR IGNITION ANALYSIS (QUINTIERE AND HARKLEROAD, ASTM E 1321) AND STEADY-BURNING MODEL

UNDERSTAND EXPERIMENT AND FIRE CHARACTERISTICS OF MATERIAL

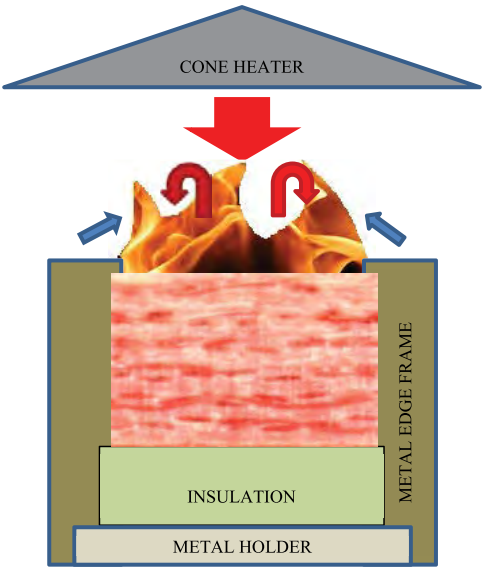

Figure A(C)-15. Simplified representation of a cone calorimeter test of fire-retarded fiberglass-reinforced polymer (FRP) composite

A simplified representation of a cone calorimeter test of fire-retarded fiberglass-reinforced polymer (FRP) composite is shown in Figure A(C)-15. The sample is placed on top of an insulation, which sits on a metal holder. Another metal frame is placed on top of the sample, insulation, and the holder. A metal edge frame is used as well.

Front Surface: As heating starts by opening the shutter to allow radiation from the cone heater to impinge on the sample surface (large red arrow), cooling also begins via natural convection (blue arrows) and re-radiation. The surface decomposes with charring, i.e., surface becoming black and white smoke, which typically indicates moisture loss with heating of the sample. Note that the surface becomes non-uniformly black. As thermal decomposition of the resin with additive progresses, the blackened surface becomes white, as the resin leaves a white powder-type residue (possible due to decomposition of the fire-retardant additive). Shrinkage or regression during pyrolysis can be considered to be minimal for this material. When ignition occurs as the fuel-vapor concentration above the surface exceeds its LFL (lower flammable limit), additional heat flux from the flame is introduced on the surface (red arrows).

Back surface: The sample is placed on top of insulation. In the experiment, an air gap of a few millimeters thickness exists between the sample and the insulation due to thermal contact. Nothing leaves through the back face with the insulation when 1D assumption holds for the experiment.

CONFIGURE MODEL CONDITIONS BASED ON UNDERSTANDING OF EXPERIMENT AND MATERIAL CHARACTERISTICS

In the model, the phenomena discussed above are simulated as below. Basic assumptions are as follows:

- Pre-ignition stage is:
  - Inert: non-uniform charring is considered to be evenly distributed
  - Thermally thick: heat transfer does not reach back surface
- Post-ignition stage is:
  - Considered to have instantaneous release of volatiles from solid to gas phase
  - Considered to have a constant thickness
  - Steady burning: heat loss equals heat gain at front surface after ignition

ACQUIRE DATA SETS

Cone calorimeter test data of fire-retarded fiberglass-reinforced polymer (FRP) composite with thickness of 9.2 mm, density of 1900 kg/m^3, and applied heat-flux levels ranging from 20 to 75 kW/m^2 is found. For Ignition Data analysis, only time-to-ignition with respect to applied heat-flux data will be used. For burning-rate data analysis, data for the entire testing-time duration, mass loss and heat release during testing period with respect to applied heat flux will be used.

CONDUCT IGNITION DATA ANALYSIS

1. Estimate T_{ig}

Heat balance at front surface during steady burning is as follow:

$$\varepsilon \dot{q}''_{cr} = h_c(T_{ig} - T_\infty) + \varepsilon\sigma(T_{ig}^4 - T_\infty^4)$$

Knowing that emissivity is approximated as 0.9, critical heat flux is estimated as 9 kW/m^2, and heat transfer coefficient in cone calorimeter experiment is estimated as 12.0 W/m^{2}K, ignition temperature, T_{ig} is calculated as:

$$\mathbf{T_{ig} = 523\ °C}$$

2. Estimate h_{ig}

h_{ig} is the total heat-transfer coefficient at ignition; therefore, at steady-state burning stage, the following can be defined:

$$\varepsilon \dot{q}''_{cr} \equiv h_{ig}(T_{ig} - T_\infty)$$

Knowing the ignition temperature, hig can be calculated:

$$\mathbf{h_{ig} = 52.2\ W/m^2K}$$

3. Calculate $\dot{q}''_{cr} / \dot{q}''_{e}$ versus $\sqrt{t_{ig}}$ from ignition data

Table A(C)-15. $\dot{q}''_{cr} / \dot{q}''_{e}$ versus $\sqrt{t_{ig}}$

Heat Flux (kW/m²)	t_{ig} (s)	CHF/HF	$t_{ig}^{0.5}$ ($s^{0.5}$)
28	NI		
30	484	0.9667	22.00
40	269	0.7250	16.40
40	242	0.7250	15.56
50	143	0.5800	11.96
50	195	0.5800	13.96
50	178	0.5800	13.34
50	183	0.5800	13.53
60	132	0.4833	11.49
75	72	0.3867	8.49
75	83	0.3867	9.11
75	96	0.3867	9.80
75	98	0.3867	9.90

4. Plot $\dot{q}''_{cr} / \dot{q}''_{e}$ versus $\sqrt{t_{ig}}$ to estimate the time needed to reach "steady-state" burning, t* and thermal inertia, kρc

Recall $\frac{\dot{q}''_{cr}}{\dot{q}''_{e}} = F(t_{ig}) = \begin{cases} \frac{2\ h_{ig}\sqrt{t_{ig}}}{\sqrt{\pi k\rho c}} & t_{ig} \le t^* \\ 1 & t_{ig} > t^* \end{cases}$ for piloted-ignition data where t* is the time when $\dot{q}''_{cr} / \dot{q}''_{e} = 1$. Thermal inertia can be estimated from the best-fit line through t = 0. Its slope at $0 < t < t^*$ is $\frac{2\ h_{ig}}{\sqrt{\pi k\rho c}}$; therefore, $k\rho c = \frac{4\ h_{ig}^2}{\pi \cdot (slope)^2}$. Note that in the analysis, all data points at lower heat-flux levels with large time-to-ignition data were included, for this gave a better fitness of the best-fit line (see Figure A(C)-16).

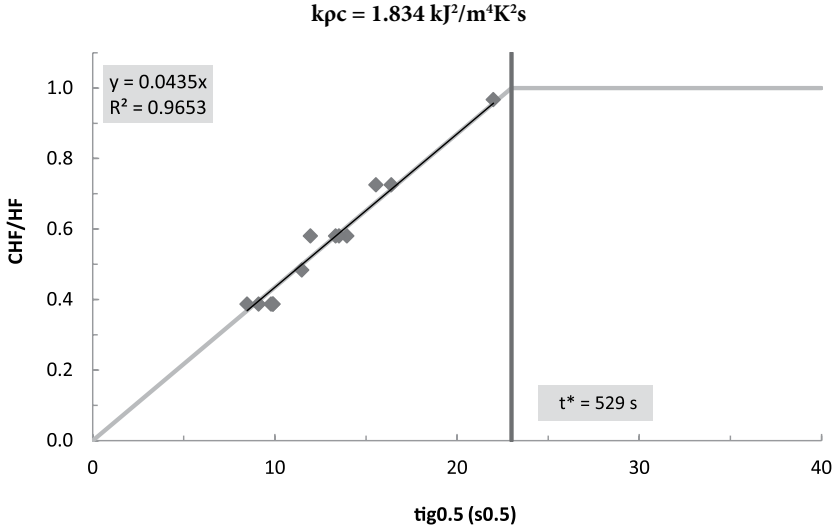

Figure A(C)-16. Plot of $\dot{q}''_{cr} / \dot{q}''_{e}$ versus $\sqrt{t_{ig}}$

CONDUCT BURNING-RATE DATA ANALYSIS

1. Estimate $\Delta h_{c,eff}$

There are two approaches in estimating the effective heat-of-combustion via calorimeter tests: by using the peak in HRR or the average heat released over the entire test. In this example, $\Delta h_{c,eff}$ will be estimated by considering the average heat-release rate divided by the average mass-loss rate during a test. Cone test results ranging from 30 to 75 kW/m² are used:

$$\Delta h_{c,eff} = 18.3 \text{ kJ/g}$$

2. Estimate Δh_g

Recall $\Delta h_g \equiv \frac{\dot{q}''_{net}}{\dot{m}''} = \frac{\dot{q}_e'' + \dot{q}_f'' - \dot{q}_l''}{\dot{m}''}$; therefore, when plotting mass-loss rates at different radiant heat-flux levels during steady-burning condition, the reciprocal of the slope of the best-fit line should be the heat-of-gasification (see Table A(C)-16 and Figure A(C)-17).

$$\Delta h_g = 13.7 \text{ kJ/g}$$

Table A(C)-16. Estimation of effective heat-of-gasification using cone calorimeter test results at applied heat flux ranging between 25 and 75 kW/m²

Heat Flux (kW/m^2)	avgMLR (g/m^2s)
25	6.70
25	6.59
40	6.93
50	7.95
60	8.64
60	9.09
75	8.30

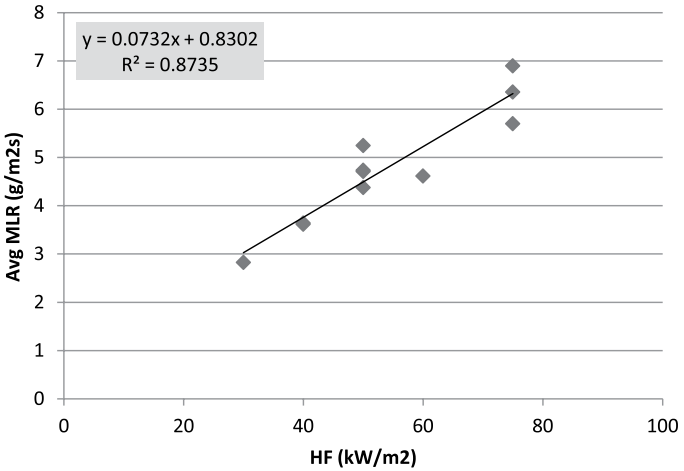

Figure A(C)-17. Plot of steady MLR versus different applied heat-flux levels – 25 to 75 kW/m²

Obtain Uncertainty for Estimated Parameters

UNCERTAINTY FOR MEASURED PARAMETERS

1. δT_∞

Fluctuation in ambient temperature during testing is estimated to be less than ±15% of reported measurement data.

2. $\delta \dot{q}''_{cr}$

The resolution of bracketing experiment was 2 kW/m^2; hence, uncertainty can be estimated as ± 1 kW/m^2.

3. δh_c

Considering that the reference values sited in the *Guide* for different apparatuses and set-up have two significant figures, uncertainty for this convection coefficient can be estimated as ± 0.5 W/m^{2}K.

4. $\delta \varepsilon$

Emissivity measurement of fire-retarded FRP composite sample (preconditioned in an oven to remove moisture) was conducted using a pyrometer at an optical-property-measuring laboratory (ASTM E408). The average value of three measurements were 0.912 with a confidence interval of ± 0.007 (student t distribution, $\alpha = 0.05$, sample size of 3). This is close to what has been assumed in the analysis. Additionally, considering that the surface becomes black as soon as it is exposed to heating from the cone, emissivity of thermally degrading plywood should be within ± 10% of what has been approximated in this example.

Uncertainty for estimated parameters using ignition data analysis

1. δT_{ig}

See Chapter 4 for detail.

$$\frac{\partial \dot{q}''_{cr}}{\partial T_{ig}} = \frac{h_c + 4\varepsilon\sigma T_{ig}^3}{\varepsilon}$$

$$= \frac{\left(0.012\frac{kW}{m^2K}\right) + 4(0.9)\left(5.67\times10^{-11}\frac{kW}{K^4m^2}\right)\left((523+273)K\right)^3}{(0.9)}$$

$$\approx 0.1277\frac{kW}{m^2K}$$

$$\frac{\partial \dot{q}''_{cr}}{\partial \varepsilon} = \frac{-\dot{q}''_{cr} + \sigma(T_{ig}^4 - T_\infty^4)}{\varepsilon}$$

$$= \frac{-\left(9\frac{kW}{m^2}\right) + \left(5.67\times10^{-11}\frac{kW}{K^4m^2}\right)\left(\left((523+273)K\right)^4 - \left((23+273)K\right)^4\right)}{(0.9)}$$

$$\approx -7.413\frac{kW}{m^2}$$

$$\frac{\partial \dot{q}''_{cr}}{\partial h_c} = \frac{T_{ig} - T_\infty}{\varepsilon}$$
$$= \frac{((523+273)K) - ((23+273)K)}{(0.9)}$$
$$\approx 555.6K$$

$$\frac{\partial \dot{q}''_{cr}}{\partial T_\infty} = \frac{-h_c - 4\varepsilon\sigma T_\infty^3}{\varepsilon}$$
$$= \frac{-\left(0.012\frac{kW}{m^2K}\right) - 4(0.9)\left(5.67\times10^{-11}\frac{kW}{K^4m^2}\right)((23+273)K)^3}{(0.9)}$$
$$\approx -0.01922\frac{kW}{m^2K}$$

Therefore,

$$\delta T_{ig} = \left(\frac{\partial \dot{q}''_{cr}}{\partial T_{ig}}\right)^{-1}\sqrt{\left(\delta\dot{q}''_{cr}\right)^2 - \left(\left(\frac{\partial \dot{q}''_{cr}}{\partial \varepsilon}\delta\varepsilon\right)^2 + \left(\frac{\partial \dot{q}''_{cr}}{\partial h_c}\delta h_c\right)^2 + \left(\frac{\partial \dot{q}''_{cr}}{\partial T_\infty}\delta T_\infty\right)^2\right)}$$
$$= \left(0.1277\frac{kW}{m^2K}\right)^{-1}\sqrt{\left(1\frac{kW}{m^2}\right)^2 - \left(\begin{array}{l}\left(\left(-7.413\frac{kW}{m^2}\right)(0.09)\right)^2 \\ \quad + \left((555.6K)\left(0.5\times10^{-3}\frac{kW}{m^2K}\right)\right)^2 \\ \quad + \left(\left(-0.01922\frac{kW}{m^2K}\right)(3.45K)\right)^2\end{array}\right)}$$
$$\approx 5\ 4K$$

2. δ(kρc)

See Chapter 4 for detail.

The uncertainty of the slope of the best-fit line, 0.04349 $s^{-0.5}$, can be estimated through calculating 2 times the standard error of the slope, which is +/- 0.001384 $s^{-0.5}$.

$$\frac{\partial(k\rho c)}{\partial(slope)} = \frac{-8}{\pi\cdot(slope)^3}\left(\frac{\varepsilon\dot{q}''_{cr}}{T_{ig} - T_\infty}\right)^2$$
$$= \frac{-8}{\pi\cdot\left(0.04349s^{-0.5}\right)^3}\left(\frac{(0.9)\left(29\frac{\frac{kJ}{s}}{m^2}\right)}{((523+273)K) - ((23+273)K)}\right)^2$$
$$\approx -84.35\frac{kJ^2}{m^4K^2s^{0.5}}$$

$$\frac{\partial(k\rho c)}{\partial \varepsilon} = \frac{8}{\pi \cdot (slope)^2}\left(\frac{\dot{q}''_{cr}}{T_{ig} - T_\infty}\right)^2 \varepsilon$$

$$= \frac{8}{\pi \cdot \left(0.04349 s^{-0.5}\right)^2}\left(\frac{\left(29\frac{\frac{kJ}{s}}{m^2}\right)}{((523+273)K) - ((23+273)K)}\right)^2 (0.9)$$

$$\approx 4.076 \frac{kJ^2}{m^4 K^2 s}$$

$$\frac{\partial(k\rho c)}{\partial \dot{q}''_{cr}} = \frac{8}{\pi \cdot (slope)^2}\left(\frac{\varepsilon}{T_{ig} - T_\infty}\right)^2 \dot{q}''_{cr}$$

$$= \frac{8}{\pi \cdot \left(0.04349 s^{-0.5}\right)^2}\left(\frac{(0.9)}{((523+273)K) - ((23+273)K)}\right)^2 \left(29\frac{\frac{kJ}{s}}{m^2}\right)$$

$$\approx 0.1265 \frac{kJ}{m^2 K^2}$$

$$\frac{\partial(k\rho c)}{\partial T_{ig}} = \frac{-8}{\pi \cdot (slope)^2}\left(\frac{\varepsilon \dot{q}''_{cr}}{T_{ig} - T_\infty}\right)^2 \frac{1}{T_{ig} - T_\infty}$$

$$= \frac{-8}{\pi \cdot \left(0.04349 s^{-0.5}\right)^2}\left(\frac{(0.9)\left(29\frac{\frac{kJ}{s}}{m^2}\right)}{((523+273)K) - ((23+273)K)}\right)^2 \frac{1}{((523+273)K) - ((23+273)K)}$$

$$\approx -0.007337 \frac{kJ^2}{m^4 K^3 s}$$

$$\frac{\partial(k\rho c)}{\partial T_\infty} = \frac{8}{\pi\cdot(slope)^2}\left(\frac{\varepsilon\dot{q}''_{cr}}{T_{ig}-T_\infty}\right)^2\frac{1}{T_{ig}-T_\infty}$$

$$= \frac{8}{\pi\cdot\left(0.04349s^{-0.5}\right)^2}\left(\frac{(0.9)\left(29\frac{\frac{kJ}{s}}{m^2}\right)}{((523+273)K)-((23+273)K)}\right)^2\frac{1}{((523+273)K)-((23+273)K)}$$

$$\approx 0.007337\frac{kJ^2}{m^4K^3s}$$

Therefore,

$$\delta(k\rho c) = \sqrt{\begin{array}{l}\left(\frac{\partial(k\rho c)}{\partial(slope)}\delta(slope)\right)^2+\left(\frac{\partial(k\rho c)}{\partial\varepsilon}\delta\varepsilon\right)^2+\left(\frac{\partial(k\rho c)}{\partial\dot{q}''_{cr}}\delta\dot{q}''_{cr}\right)^2\\ +\left(\frac{\partial(k\rho c)}{\partial T_{ig}}\delta T_{ig}\right)^2+\left(\frac{\partial(k\rho c)}{\partial T_\infty}\delta T_\infty\right)^2\end{array}}$$

$$= \sqrt{\begin{array}{l}\left(\left(-84.35\frac{kJ^2}{m^4K^2s^{0.5}}\right)\left(0.001384s^{-0.5}\right)\right)^2+\left(\left(4.076\frac{kJ^2}{m^4K^2s}\right)(0.09)\right)^2\\ +\left(\left(-1265\frac{kJ}{m^2K^2}\right)\left(1\frac{kW}{m^2}\right)\right)^2+\left(\left(-0.007337\frac{kJ^2}{m^4K^3s}\right)(5.4K)\right)^2\\ +\left(\left(0.007337\frac{kJ^2}{m^4K^3s}\right)(3.45K)\right)^2\end{array}}$$

$$\approx 0.408\frac{kJ^2}{m^4K^2s}$$

UNCERTAINTY FOR ESTIMATED PARAMETERS USING BURNING-RATE DATA ANALYSIS

1. $\delta\Delta h_{c,eff}$

This parameter is estimated by considering the average of the heat-release rate divided by the average mass-loss rate during cone tests at 30 to 75 kW/m^2 heat-flux levels. Assuming the estimated $\Delta h_{c,eff}$ at each test results in normal distribution, confidence interval with $\alpha = 0.05$ (95%) can be predicted using student t distribution with a sample size of 10, which is ± 6.7 kJ/g.

2. $\delta\Delta h_g$

See Chapter 4 for detail.

The uncertainty of the slope (=1/Δh_g=0.07324g/kJ) can be estimated through calculating 2 times the standard error of the slope of the best-fit line, which is +/- 0.01858. Therefore, the uncertainty in Δh_g is

$$\frac{d(\Delta h_g)}{d(slope)} = -\frac{1}{(slope)^2}$$
$$= -\frac{1}{\left(0.07324\frac{g}{kJ}\right)^2}$$
$$\approx -186.4\frac{kJ^2}{g^2}$$

Therefore,

$$\delta(\Delta h_g) = \sqrt{\left(\frac{d(\Delta h_g)}{d(slope)}\delta(slope)\right)^2}$$
$$= \sqrt{\left(\left(-186.4\frac{kJ^2}{g^2}\right)(0.01858 g/kJ)\right)^2}$$
$$\approx 3.5\frac{kJ}{g}$$

UNCERTAINTY SUMMARY

Table A(C)-17. Summary of model-parameter table with estimated values with uncertainty

Ignition Parameters	T_∞	23 ± 3.45 °C
	T_{ig}	523 ± 5 °C
	$\dot{q}''_{cr}$	29 ± 1 kW/m^2
	kρc	1.834 ± 0.408 kJ^2/m^{4}K^{2}s
Burning-Rate Parameters	$\Delta h_{c,eff}$	18.3 ± 6.7 kJ/g
	Δh_g	13.7 ± 3.5 kJ/g
	h_c	12 ± 0.5 W/m^{2}K
	ε	0.9 ± 0.09

Validation

Analyze Simulation Quality

DETERMINE DATA AND MODEL OUTPUT UNCERTAINTY TO MAKE COMPARISON

1. Conduct uncertainty analysis of data

The uncertainty in the mass-loss rate data used for comparison between data and model outputs is estimated via statistical approach, taking the standard deviation (0.58 g/sm^2) from the mean of a steady burning of five identical PMMA tests conducted in a Cone calorimeter.[2] The estimated uncertainty is 1.4 g/sm^2, which is found by calculating the 95% confidence interval applying student t distribution with a sample size of five.

The uncertainty in time-to-ignition data used for comparison is estimated via statistical approach, taking four to five identical cone calorimeter test data at heat fluxes at 50 and 75 kW/m^2 of this FRP composite. 95% confidence interval is calculated for each heat-flux level assuming student t distribution.

2. Conduct uncertainty analysis for MLR profile modeling

Because uncertainty information of the data is found in terms of time-to-ignition and mass-loss rate, mass-loss-rate profile is considered as the modeling output of interest for comparison purposes. For Simple Analytical Models, time-to-ignition (t_{ig}) and steady-burning rate ($\dot{m}''$) are needed when simulating the mass-release-rate profile. The uncertainty in MLR profile in modeling can be determined via considering the uncertainties in these calculation results as below:

$$t_{ig} \pm \delta t_{ig}$$
$$\dot{m}'' \pm \delta \dot{m}''$$

To determine the uncertainty in time-to-ignition, recall:

$$\frac{\dot{q}''_{cr}}{\dot{q}''_e} = \mathrm{F}(t_{ig}) = \begin{cases} \dfrac{2}{\sqrt{\pi k\rho c}} h_{ig}\sqrt{t_{ig}} & t_{ig} \le t^* \\ 1 & t_{ig} > t^* \end{cases}$$

Knowing that all of heat-flux levels of interest, 50 and 75 kW/m^2, are above the critical heat flux, time-to-ignition should be smaller than t*. Hence, uncertainty in t_{ig} can be estimated from linear-regression process as below:

$$\frac{\dot{q}''_{cr}}{\dot{q}''_e} = \frac{2}{\sqrt{\pi k\rho c}} h_{ig}\sqrt{t_{ig}}$$

Above equation can be re-written as below after conducting linear regression:

$$y\ estimate = (slope)\sqrt{t_{ig}}$$

Therefore,

$$t_{ig} = \left(\frac{y\ estimate}{slope}\right)^2$$

Assuming that the y estimate and slope are independent and propagating the uncertainties in these two variables in estimating the time to ignition, the following calculation can be made:

$$\delta t_{ig} = \sqrt{\left(\frac{\partial t_{ig}}{\partial(y\ estimate)}\delta(y\ estimate)\right)^2 + \left(\frac{\partial t_{ig}}{\partial(slope)}\delta(slope)\right)^2}$$

where

$$\frac{\partial t_{ig}}{\partial(y\ estimate)} = \frac{2\cdot(y\ estimate)}{(slope)^2}$$
$$\frac{\partial t_{ig}}{\partial(slope)} = -\frac{2\cdot(y\ estimate)^2}{(slope)^3}$$

with δ(*y estimate)* and δ(*slope)* estimated through calculating 2 times the standard error of the y estimate and slope of the best-fit line.

To determine the uncertainty in the steady-heat-release rate at post-ignition stage, recall:

$$\Delta h_g \equiv \frac{\dot{q}''_{net}}{\dot{m}''} = \frac{\dot{q}_e'' + \dot{q}_f'' - \dot{q}_l''}{\dot{m}''}$$

The above equation can be rearranged to

$$\dot{m}'' = \frac{1}{\Delta h_g}\dot{q}_e'' + \frac{\dot{q}_f'' - \dot{q}_l''}{\Delta h_g}$$

The steady-burning rate at post-ignition stage is determined by the best-fit line obtained when data is plotted as steady-burning rate versus applied heat flux. The uncertainty in steady-burning rate can be determined by considering 2 times the standard error of the y estimates, i.e. $\dot{m}''$, which is obtained through linear-regression process: **± 0.9 g/m²s**.

COMPARE DATA WITH SIMULATION RESULTS WITH CONSIDERATION OF UNCERTAINTIES

Parameters in this simple analytical pyrolysis model have been estimated with cone calorimeter test data from 50 and 75 kW/m². To check the quality of the modeling using the estimated parameters, three cases have been simulated and compared with experiment data with the consideration of their uncertainty bands as shown in Table A(C)-18 and figures – Figure A(C)-18 and Figure A(C)-19 – below.

Table A(C)-18. Comparison of time-to-ignition at different heat-flux levels from actual experiment and pyrolysis modeling

Heat-Flux Level	Actual t_{ig} (s) $t_{ig} \pm \delta t_i$	Model t_{ig} (s) $t_{ig} \pm \delta t_i$
50 kW/m²	175 ± 36	178 ± 42
75 kW/m²	89 ± 14	79 ± 27

Both cases show good overlap between the data and simulation of time-to-ignition and the mass-loss rate during steady burning considering the uncertainties, i.e., the parameter estimation was conducted successfully. Note that when calculating the burnout time in pyrolysis modeling, it was assumed that only 29% of the initial weight is lost and 71% of polymer (resin and additive) residue with inert fiberglass mats remain.

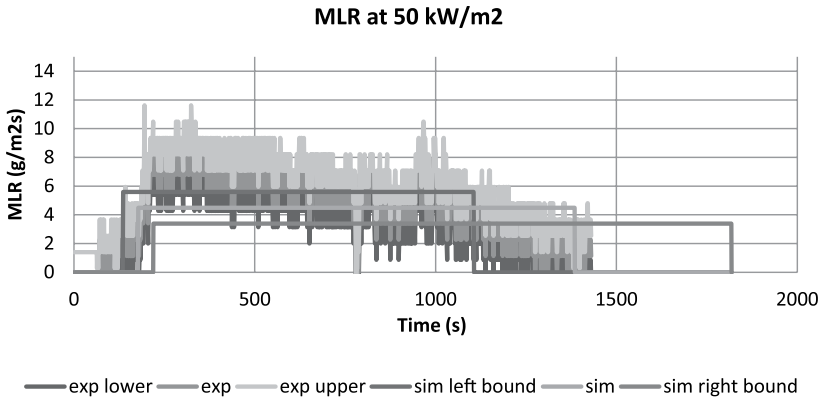

Figure A(C)-18. Mass-loss rate (MLR) comparisons for fire-retarded FRP composite between actual MLR from experiment (exp) and modeled MLR (sim) at 50 kW/m². Note that data shown were used to estimate model-parameter values.

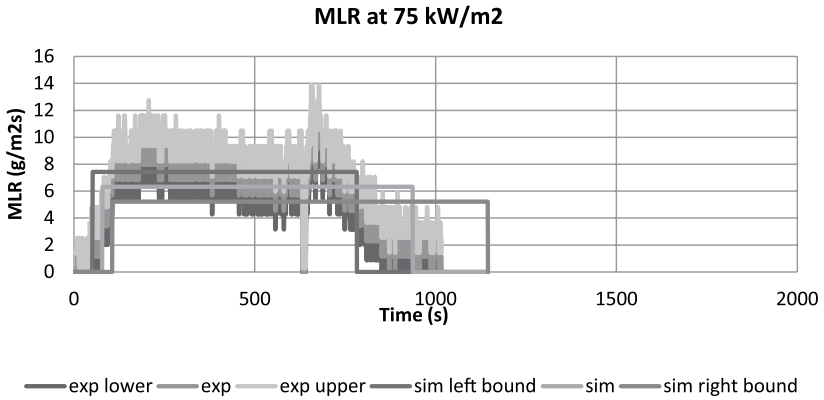

Figure A(C)-19. Mass-loss rate (MLR) comparisons for fire-retarded FRP composite between actual MLR from experiment (exp) and modeled MLR (sim) at 75 kW/m². Note that data shown were used to estimate model-parameter values.

Validate Simulation Quality upon Extrapolation

In this example, cone calorimeter data at applied heat flux ranging from 25 to 75 kW/m² were used to estimate the unknown model parameters. Assuming that the estimated parameters for this corrugated cardboard will be used in pyrolysis modeling at applied heat-flux levels that are within the above range, no additional check becomes necessary.

Commentary

When using Simple Analytical Model to simulate pyrolysis of a fire-retarded fiberglass-reinforced polymer (FRP) composite (density 2100 kg/m^3, thickness 8.9 mm, 71 wt% of composite remains as residue), test data from a bench-scale cone calorimeter experiment at several heat-flux levels have been utilized to estimate the time-to-ignition from exposure to heating and the mass-loss rate at steady-burning stage after ignition. The comparison between the model outputs (time-to-ignition and steady-burning rate) and the data from bench-scale experiment showed good agreement for both checking purposes where the same heat-flux levels (50 and 75 kW/m^2) used in parameter estimation have been considered.

Although the modeling predictions of time-to-ignition and steady-burning rate in this example seems to be reasonable, limitation of this Simple Analytical Modeling should be noted, which is that the model is for thermally-thick-behaving materials and steady burning after ignition.

Example 4.4 Modeling Plywood

Measure Parameters

1. Ambient Temperature

Direct measurement of ambient temperature is made as 20°C.

2. Surface Temperature at Ignition

This parameter will be obtained via Ignition Data Analysis, i.e., no direct measurements will be performed.

3. Critical Heat Flux for Ignition

By bracketing to within +/- 0.5 kW/m^2 in cone calorimeter tests, $\dot{q}''_{cr}$ has been determined to be 14.5 kW/m^2 (see Table A(C)-26). Ignition data is provided below for this plywood with thickness of 11.1 ± 0.1 mm, density of 542 ± 11 kg/m^3 (t-distribution, α = 0.05, sample size of 10):

Table A(C)-19. Ignition data from cone calorimeter tests of plywood

Heat Flux	t_{ig}
(kW/m^2)	(s)
14	NI
15	572

4. Thermal Inertia

This parameter will be obtained via Ignition Data Analysis, i.e., no direct measurements will be performed.

5. Effective Heat of Combustion

This parameter will be obtained via Burning-Rate Data Analysis, i.e., no direct measurements will be performed.

6. Heat-of-Gasification

This parameter will be obtained via Burning-Rate Data Analysis, i.e., no direct measurements will be performed.

7. Convection Coefficient

Because this is a material laid in horizontal position in a cone calorimeter, h_c = 12 W/m^{2}K is used based on literature reference.

8. Surface Emissivity/Absorptivity

Emissivity is approximated as 0.9.

Summary

Table A(C)-20. Summary of model-parameter table with estimated values via direct measurements, literature search, or approximation

Ignition Parameters	T_{∞}	20 °C
	T_{ig}	Ignition Data Analysis
	$\dot{q}''_{cr}$	14.5 kW/m^2
	$k\rho c$	Ignition Data Analysis
Burning-Rate Parameters	$\Delta h_{c,eff}$	Burning-Rate Data Analysis
	Δh_g	Burning-Rate Data Analysis
	h_c	12 W/m^{2}K
	ε	0.9

Obtain Parameters via Data Analysis

Run model

SELECT MODEL: THERMALLY THICK MODEL FOR IGNITION ANALYSIS (QUINTIERE AND HARKLEROAD, ASTM E 1321) AND STEADY-BURNING MODEL

UNDERSTAND EXPERIMENT AND FIRE CHARACTERISTICS OF MATERIAL

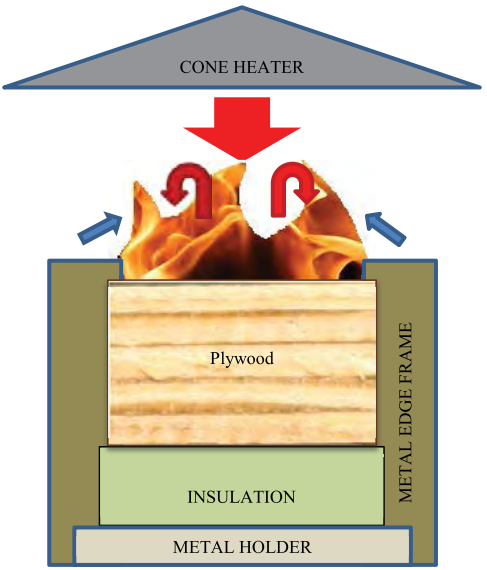

Figure A(C)-20. Simplified representation of a cone calorimeter test of plywood

A simplified representation of a cone calorimeter test of plywood is shown in Figure A(C)-20. The sample is placed on top of an insulation, which sits on a metal holder. Another metal frame is placed on top of the sample, insulation, and the holder. A metal edge frame is used as well.

Front Surface: As heating starts by opening the shutter to allow radiation from the cone heater to impinge on sample surface (large red arrow), cooling also begins via natural convection (blue arrows) and re-radiation. The surface decomposes with moisture loss at first appearing as white smoke followed by thermal decomposition of the wood component. When ignition occurs as the fuel-vapor concentration above the surface exceeds its LFL (lower flammable limit), additional heat flux from the flame is introduced on the surface (red arrows). As decomposition occurs under flaming condition, relatively uniform cracks appear on the surface with some shrinkage, allowing easy evacuation of the pyrolyzates to the gas phase even as the pyrolysis front propagates toward in-depth. Near the burn-out leaving grey residue, the center of the sample bends upward then quickly falls apart resulting in flameout.

Back surface: The sample is placed on top of insulation. In the experiment, an air gap of a few millimeters thickness exist between the sample and the insulation resulting in some thermal resistance. Due to the insulation, nothing leaves through the back face when 1D assumption holds for the experiment.

CONFIGURE MODEL CONDITIONS BASED ON UNDERSTANDING OF EXPERIMENT AND MATERIAL CHARACTERISTICS

In the model, the phenomena discussed above are simulated as below. Basic assumptions are as follows:

- Pre-ignition stage is:
  - Inert: decomposition before ignition is neglected
  - Thermally thick: heat transfer does not reach back surface
- Post-ignition stage is:
  - Considered to have instantaneous release of volatiles from solid to gas phase: any mass-transportation effect on pyrolysis is neglected, and pyrolysis is considered as surface phenomena only
  - Considered to have a constant thickness: shrinkage, regression and bending at end of plywood is neglected
  - Steady burning: heat loss equals heat gain at front surface

ACQUIRE DATA SETS

Cone calorimeter test data of Douglas Fir plywood with thickness of 11.1 ± 0.1 mm (student t distribution, $\alpha = 0.05$, sample size of 10), density of 542 ± 11 kg/m^3 (student t distribution, $\alpha = 0.05$, sample size of 10) and applied heat-flux levels ranging from 14 to 100 kW/m^2 is found. For ignition data analysis, only time-to-ignition with respect to applied heat-flux data will be used. For burning-rate data analysis, data for the entire testing time duration, mass loss and heat release during testing period with respect to applied heat flux will be used.

CONDUCT IGNITION DATA ANALYSIS

1. Estimate T_{ig}

Heat balance at front surface during steady burning is as follow:

$$\varepsilon \dot{q}''_{cr} = h_c(T_{ig} - T_\infty) + \varepsilon\sigma(T_{ig}^4 - T_\infty^4)$$

Knowing that emissivity is approximated as 0.9, critical heat flux is estimated as 14.5 kW/m^2, and heat transfer coefficient in cone calorimeter experiment is estimated as 12.0 W/m^{2}K, ignition temperature, T_{ig} is calculated as:

$$\mathbf{T_{ig} = 377\ °C}$$

2. Estimate h_{ig}

h_{ig} is the total heat-transfer coefficient at ignition; therefore, at steady-state-burning stage, the following can be defined:

$$\varepsilon \dot{q}''_{cr} \equiv h_{ig}(T_{ig} - T_\infty)$$

Knowing the ignition temperature, h_{ig} can be calculated:

$$\mathbf{h_{ig} = 36.5\ W/m^2K}$$

3. Calculate $\dot{q}''_{cr} / \dot{q}''_e$ versus $\sqrt{t_{ig}}$ from ignition data

Table A(C)-21. $\dot{q}''_{cr} / \dot{q}''_e$ versus $\sqrt{t_{ig}}$

Heat Flux (kW/m²)	t_{ig} (s)	CHF/HF	$t_{ig}^{0.5}$ ($s^{0.5}$)
14	NI		
15	572	0.9667	23.92
25	102	0.5800	10.08
50	27	0.2900	5.16
75	9	0.1933	3.06
100	3	0.1450	1.63

4. Plot $\dot{q}''_{cr} / \dot{q}''_{e}$ versus $\sqrt{t_{ig}}$ to estimate the time needed to reach "steady-state" burning, t* and thermal inertia, kρc

Recall $\frac{\dot{q}''_{cr}}{\dot{q}''_{e}} = F(t_{ig}) = \begin{cases} \frac{2\ h_{ig}\sqrt{t_{ig}}}{\sqrt{\pi k\rho c}} & t_{ig} \le t^* \\ 1 & t_{ig} > t^* \end{cases}$ for piloted-ignition data, where t* is the time when $\dot{q}''_{cr} / \dot{q}''_{e} = 1$. Thermal inertia can be estimated from the best-fit line through t = 0. Its slope at $0 < t < t^*$ is $\frac{2\ h_{ig}}{\sqrt{\pi k\rho c}}$; therefore, $k\rho c = \frac{4\ h_{ig}^2}{\pi \cdot (slope)^2}$. Note that in the analysis, few data points at lower heat-flux levels with large time-to-ignition data were excluded (see Figure A(C)-21, open circles) to increase fitness of the best-fit line. This approach is reasonable, considering that at this region analysis assumptions of having inert and thermally thick conditions are less likely to be satisfied.

$$k\rho c = 0.501\ \text{kJ}^2/\text{m}^4\text{K}^2\text{s}$$

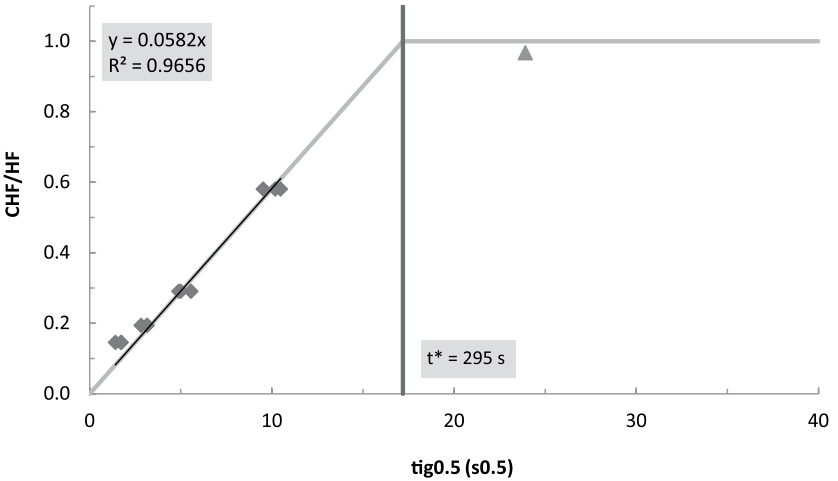

Figure A(C)-21. Plot of $\dot{q}''_{cr} / \dot{q}''_{e}$ versus $\sqrt{t_{ig}}$

CONDUCT BURNING-RATE DATA ANALYSIS

1. Estimate $\Delta h_{c,eff}$

There are two approaches in estimating the effective heat of combustion via calorimeter tests: by using the peak in HRR or the average heat released over the entire test. In this example, $\Delta h_{c,eff}$ will be estimated by considering the total heat released divided by the total amount of mass loss during a test. Nine cone test results at 25, 50, and 75 kW/m^2 are used to calculate the effective heat-of-combustion with its confidence interval using student t distribution and α = 0.05:

$$\Delta h_{c,eff} = 14.4 \pm 1.2\ \text{kJ/g}$$

2. Estimate Δh_g

Recall $\Delta h_g \equiv \frac{\dot{q}''_{net}}{\dot{m}''} = \frac{\dot{q}_e'' + \dot{q}_f'' - \dot{q}_l''}{\dot{m}''}$; therefore, when plotting mass-loss rates at different radiant heat-flux levels during steady-burning condition, the reciprocal of the slope of the best-fit line should be the heat-of-gasification. Note that for this material – Douglas Fir plywood – a strict steady-burning phase does not exist where a constant MLR appears. Therefore, an average MLR value will be used to estimate heat-of-gasification (see Table A(C)-22 and Figure A(C)-22).

$$\Delta h_g = 8.0 \text{ kJ/g}$$

Table A(C)-22. Estimation of effective heat-of-gasification using cone calorimeter test results at applied heat flux ranging between 25 and 75 kW/m²

Heat Flux (kW/m^2)	Avg MLR (g/m^2s)
25	7.1
25	6.5
25	8.0
75	13.6
50	11.0
50	10.2
75	13.6
75	13.7
75	12.9

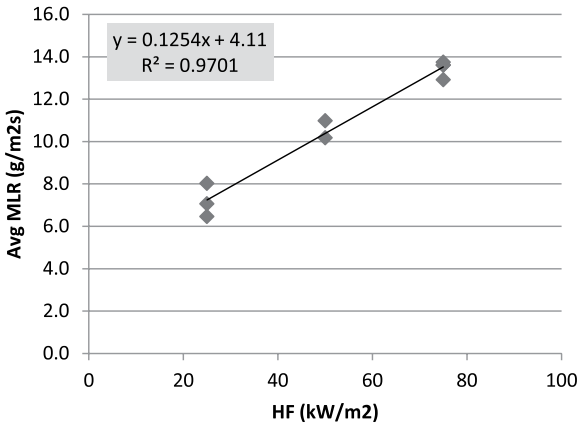

Figure A(C)-22. Plot of steady MLR versus different applied heat-flux levels – 25 to 75 kW/m²

UNCERTAINTY FOR MEASURED PARAMETERS

1. δT_∞

Fluctuation in ambient temperature during testing is estimated to be less than ±10% of reported measurement data.

2. $\delta \dot{q}''_{cr}$

The resolution of bracketing experiment was 1 kW/m^2; hence, uncertainty can be estimated as ± 0.5 kW/m^2. To be conservative, ± 1 kW/m^2 will be used in the analysis.

3. δh_c

Considering that the reference values sited in the *Guide* for different apparatuses and set-up have two significant figures, uncertainty for this convection coefficient can be estimated as ± 0.5 W/m^{2}K.

4. $\delta \varepsilon$

Emissivity measurement of dry-plywood sample (preconditioned in an oven to remove moisture) was conducted using a pyrometer at an optical-property-measuring laboratory (ASTM E408). The average value of three measurements were 0.891 with a confidence interval of ± 0.018 (student t distribution, $\alpha = 0.05$, sample size of three). This is close to what has been assumed in the analysis. Additionally, considering that the surface becomes black as soon as it is exposed to heating from the cone, emissivity of thermally degrading plywood should be within ± 10% of what has been approximated in this example.

UNCERTAINTY FOR ESTIMATED PARAMETERS USING IGNITION DATA ANALYSIS

1. δT_{ig}

See Chapter 4 for detail.

$$\frac{\partial \dot{q}''_{cr}}{\partial T_{ig}} = \frac{h_c + 4\varepsilon\sigma T_{ig}^3}{\varepsilon}$$

$$= \frac{\left(0.012\frac{kW}{m^2K}\right) + 4(0.9)\left(5.67\times10^{-11}\frac{kW}{K^4m^2}\right)((377+273)K)^3}{(0.9)}$$

$$\approx 0.0756\frac{kW}{m^2K}$$

$$\frac{\partial \dot{q}''_{cr}}{\partial \varepsilon} = \frac{-\dot{q}''_{cr} + \sigma(T_{ig}^4 - T_\infty^4)}{\varepsilon}$$

$$= \frac{-\left(14.5\frac{kW}{m^2}\right) + \left(5.67\times10^{-11}\frac{kW}{K^4m^2}\right)\left(((377+273)K)^4 - ((20+273)K)^4\right)}{(0.9)}$$

$$\approx -5.330\frac{kW}{m^2}$$

$$\frac{\partial \dot{q}''_{cr}}{\partial h_c} = \frac{T_{ig} - T_\infty}{\varepsilon}$$
$$= \frac{((377+273)K) - ((20+273)K)}{(0.9)}$$
$$\approx 397K$$
$$\frac{\partial \dot{q}''_{cr}}{\partial T_\infty} = \frac{-h_c - 4\varepsilon\sigma T_\infty^3}{\varepsilon}$$
$$= \frac{-\left(0.012\frac{kW}{m^2K}\right) - 4(0.9)\left(5.67\times10^{-11}\frac{kW}{K^4m^2}\right)((20+273)K)^3}{(0.9)}$$
$$\approx -0.01904\frac{kW}{m^2K}$$

Therefore,

$$\delta T_{ig} = \left(\frac{\partial \dot{q}''_{cr}}{\partial T_{ig}}\right)^{-1}\sqrt{(\delta \dot{q}''_{cr})^2 - \left(\left(\frac{\partial \dot{q}''_{cr}}{\partial \varepsilon}\delta\varepsilon\right)^2 + \left(\frac{\partial \dot{q}''_{cr}}{\partial h_c}\delta h_c\right)^2 + \left(\frac{\partial \dot{q}''_{cr}}{\partial T_\infty}\delta T_\infty\right)^2\right)}$$
$$= \left(0.0756\frac{kW}{m^2K}\right)^{-1}\sqrt{\left(1\frac{kW}{m^2}\right)^2 - \left(\begin{array}{l}\left(\left(-5.33\frac{kW}{m^2}\right)(0.09)\right)^2 \\ \quad + \left((397K)\left(0.5\times10^{-3}\frac{kW}{m^2K}\right)\right)^2 \\ \quad + \left(\left(-0.01904\frac{kW}{m^2K}\right)(2K)\right)^2\end{array}\right)}$$
$$\approx 11.3K$$

2. δ(kρc)

See Chapter 4 for detail.

The uncertainty of the slope of the best-fit line, 0.0444 $s^{-0.5}$, can be estimated through calculating 2 times the standard error of the slope, which is +/- 0.00136 $s^{-0.5}$.

$$\frac{\partial(k\rho c)}{\partial(slope)} = \frac{-8}{\pi\cdot(slope)^3}\left(\frac{\varepsilon \dot{q}''_{cr}}{T_{ig} - T_\infty}\right)^2$$
$$= \frac{-8}{\pi\cdot\left(0.0582s^{-0.5}\right)^3}\left(\frac{(0.9)\left(14.5\frac{kJ}{\frac{s}{m^2}}\right)}{((377+273)K) - ((20+273)K)}\right)^2$$
$$\approx -17.3\frac{kJ^2}{m^4K^2s^{0.5}}$$

$$\frac{\partial(k\rho c)}{\partial \varepsilon} = \frac{8}{\pi \cdot (slope)^2}\left(\frac{\dot{q}''_{cr}}{T_{ig} - T_\infty}\right)^2 \varepsilon$$

$$= \frac{8}{\pi \cdot \left(0.0582 s^{-0.5}\right)^2}\left(\frac{\left(14.5 \frac{\frac{kJ}{s}}{m^2}\right)}{((377+273)K) - ((20+273)K)}\right)^2 (0.9)$$

$$\approx 1.12 \frac{kJ^2}{m^4 K^2 s}$$

$$\frac{\partial(k\rho c)}{\partial \dot{q}''_{cr}} = \frac{8}{\pi \cdot (slope)^2}\left(\frac{\varepsilon}{T_{ig} - T_\infty}\right)^2 \dot{q}''_{cr}$$

$$= \frac{8}{\pi \cdot \left(0.0582 s^{-0.5}\right)^2}\left(\frac{(0.9)}{((377+273)K) - ((20+273)K)}\right)^2 \left(14.5 \frac{\frac{kJ}{s}}{m^2}\right)$$

$$\approx 0.0693 \frac{kJ}{m^2 K^2}$$

$$\frac{\partial(k\rho c)}{\partial T_{ig}} = \frac{-8}{\pi \cdot (slope)^2}\left(\frac{\varepsilon \dot{q}''_{cr}}{T_{ig} - T_\infty}\right)^2 \frac{1}{T_{ig} - T_\infty}$$

$$= \frac{-8}{\pi \cdot \left(0.0582 s^{-0.5}\right)^2}\left(\frac{(0.9)\left(14.5 \frac{\frac{kJ}{s}}{m^2}\right)}{((377+273)K) - ((20+273)K)}\right)^2 \frac{1}{((377+273)K) - ((20+273)K)}$$

$$\approx -0.00282 \frac{kJ^2}{m^4 K^3 s}$$

$$\frac{\partial(k\rho c)}{\partial T_\infty} = \frac{8}{\pi \cdot (slope)^2}\left(\frac{\varepsilon \dot{q}''_{cr}}{T_{ig} - T_\infty}\right)^2 \frac{1}{T_{ig} - T_\infty}$$

$$= \frac{8}{\pi \cdot \left(0.0582 s^{-0.5}\right)^2}\left(\frac{(0.9)\left(14.5 \frac{kJ}{\frac{s}{m^2}}\right)}{((377+273)K) - ((20+273)K)}\right)^2 \frac{1}{((377+273)K) - ((20+273)K)}$$

$$\approx 0.00282 \frac{kJ^2}{m^4 K^3 s}$$

Therefore,

$$\delta(k\rho c) = \sqrt{\begin{aligned}&\left(\frac{\partial(k\rho c)}{\partial(slope)}\delta(slope)\right)^2 + \left(\frac{\partial(k\rho c)}{\partial \varepsilon}\delta\varepsilon\right)^2 + \left(\frac{\partial(k\rho c)}{\partial \dot{q}''_{cr}}\delta\dot{q}''_{cr}\right)^2 \\ &+ \left(\frac{\partial(k\rho c)}{\partial T_{ig}}\delta T_{ig}\right)^2 + \left(\frac{\partial(k\rho c)}{\partial T_\infty}\delta T_\infty\right)^2\end{aligned}}$$

$$= \sqrt{\begin{aligned}&\left(\left(-17.3 \frac{kJ^2}{m^4 K^2 s^{0.5}}\right)\left(0.00318 s^{-0.5}\right)\right)^2 + \left(\left(1.12 \frac{kJ^2}{m^4 K^2 s}\right)(0.09)\right)^2 \\ &+ \left(\left(0.0693 \frac{kJ}{m^2 K^2}\right)\left(1 \frac{kW}{m^2}\right)\right)^2 + \left(\left(-0.00282 \frac{kJ^2}{m^4 K^3 s}\right)(11.3K)\right)^2 \\ &+ \left(\left(0.00282 \frac{kJ^2}{m^4 K^3 s}\right)(2K)\right)^2\end{aligned}}$$

$$\approx 0.138 \frac{kJ^2}{m^4 K^2 s}$$

UNCERTAINTY FOR ESTIMATED PARAMETERS USING BURNING-RATE DATA ANALYSIS

1. $\delta\Delta h_{c,eff}$

Cone test results at 25, 50, and 75 kW/m^2 are used to calculate the effective heat-of-combustion. Uncertainty of this value is estimated with its confidence interval using student t distribution and $\alpha = 0.05$: **± 1.2 kJ/g**

2. $\delta\Delta h_g$

See Chapter 4 for detail.

The uncertainty of the slope (=$1/\Delta h_g$=0.125g/kJ) can be estimated through calculating 2 times the standard error of the slope of the best-fit line, which is +/- 0.167. Therefore, the uncertainty in Δh_g is

$$\frac{d(\Delta h_g)}{d(slope)} = -\frac{1}{(slope)^2}$$
$$= -\frac{1}{\left(0.125\frac{g}{kJ}\right)^2}$$
$$\approx -63.6\frac{kJ^2}{g^2}$$

Therefore,

$$\delta(\Delta h_g) = \sqrt{\left(\frac{d(\Delta h_g)}{d(slope)}\delta(slope)\right)^2}$$
$$= \sqrt{\left(\left(-63.6\frac{kJ^2}{g^2}\right)(0.0167 g/kJ)\right)^2}$$
$$\approx 1.06\frac{kJ}{g}$$

UNCERTAINTY SUMMARY

Table A(C)-23. Summary of model-parameter table with estimated values with uncertainty

Ignition Parameters	T_∞	20 ± 2 °C
	T_{ig}	377 ± 11 °C
	$\dot{q}''_{cr}$	14.5 ± 1 kW/m^2
	$k\rho c$	0.501 ± 0.138 kJ^2/m^{4}K^{2}s
Burning-Rate Parameters	$\Delta h_{c,eff}$	14.4 ± 1.2 kJ/g
	Δh_g	8.0 ± 1.1 kJ/g
	h_c	12 ± 0.5 W/m^{2}K
	ε	0.9 ± 0.09

Validation

Analyze Simulation Quality

DETERMINE DATA AND MODEL OUTPUT UNCERTAINTY TO MAKE COMPARISON

1. Conduct uncertainty analysis of data

The uncertainty in the mass-loss rate data used for comparison between data and model outputs is estimated via statistical approach, taking the standard deviation (0.58 g/sm^2) from the mean of a steady burning of five identical PMMA tests conducted in a cone calorimeter.[2] The estimated uncertainty is 1.4 g/sm^2, which is found by calculating the 95% confidence interval applying student t distribution with a sample size of five.

The uncertainty in time-to-ignition data used for comparison is estimated via statistical approach, taking three to four identical cone calorimeter test data at heat fluxes ranging from 25 to 75 kW/m^2 of this plywood. 95% confidence interval is calculated for each heat-flux level assuming student t distribution.

2. Conduct uncertainty analysis for MLR profile modeling

Because uncertainty information of the data is found in terms of time-to-ignition and mass-loss rate, the mass-loss-rate profile is considered as the modeling output of interest for comparison purposes. For Simple Analytical Models, time-to-ignition (t_{ig}) and steady-burning rate ($\dot{m}''$) are needed when simulating the mass-release-rate profile. The uncertainty in MLR profile in modeling can be determined via considering the uncertainties in the calculation results below:

$$t_{ig} \pm \delta t_{ig}$$

$$\dot{m}'' \pm \delta \dot{m}''$$

To determine the uncertainty in time to ignition, recall:

$$\frac{\dot{q}''_{cr}}{\dot{q}''_{e}} = \mathrm{F}(t_{ig}) = \begin{cases} \dfrac{2}{\sqrt{\pi k \rho c}} h_{ig} \sqrt{t_{ig}} & t_{ig} \leq t^* \\ 1 & t_{ig} > t^* \end{cases}$$

Knowing that all of heat-flux levels of interest, 25, 50, and 75 kW/m^2, are above the critical heat flux, time-to-ignition should be smaller than t*. Hence, uncertainty in t_{ig} can be estimated from linear-regression process as below:

$$\frac{\dot{q}''_{cr}}{\dot{q}''_{e}} = \frac{2}{\sqrt{\pi k \rho c}} h_{ig} \sqrt{t_{ig}}$$

Above equation can be re-written as below after conducting linear regression:

$$y\ estimate = (slope)\sqrt{t_{ig}}$$

Therefore,

$$t_{ig} = \left(\frac{y\ estimate}{slope}\right)^2$$

Assuming that the y estimate and slope are independent and propagating the uncertainties in these two variables in estimating the time to ignition, the following calculation can be made:

$$\delta t_{ig}= \sqrt{\left(\frac{\partial t_{ig}}{\partial(y\ estimate)}\delta(y\ estimate)\right)^2+\left(\frac{\partial t_{ig}}{\partial(slope)}\delta(slope)\right)^2}$$

where

$$\frac{\partial t_{ig}}{\partial(y\ estimate)}=\frac{2\cdot(y\ estimate)}{(slope)^2}$$

$$\frac{\partial t_{ig}}{\partial(slope)}=-\frac{2\cdot(y\ estimate)^2}{(slope)^3}$$

with $\delta(y\ estimate) = \delta(slope)$ estimated through calculating 2 times the standard error of the y estimate and slope of the best-fit line, which are 0.0653 and 0.00318 $s^{-0.5}$, respectively.

To determine the uncertainty in the steady-heat-release rate at post-ignition stage, recall:

$$\Delta h_g \equiv \frac{\dot{q}^{"}_{net}}{\dot{m}''}=\frac{\dot{q}_e''+\dot{q}_f''-\dot{q}_l''}{\dot{m}''}$$

The above equation can be rearranged to

$$\dot{m}^{"}=\frac{1}{\Delta h_g}\dot{q}^{"}_e+\frac{\dot{q}^{"}_f-\dot{q}^{"}_l}{\Delta h_g}$$

The steady-burning rate at post-ignition stage is determined by the best-fit line obtained when data is plotted as steady-burning rate versus applied heat flux. The uncertainty in steady-burning rate can be determined by considering 2 times the standard error of the y estimates, i.e., $\dot{m}''$, which is obtained through linear-regression process: **± 1.1 g/m²s**.

COMPARE DATA WITH SIMULATION RESULTS WITH CONSIDERATION OF UNCERTAINTIES

Parameters in this simple analytical pyrolysis model have been estimated with cone calorimeter test data from 25, 50, and 75 kW/m². To check the quality of the modeling using the estimated parameters, three cases have been simulated and compared with experiment data with the consideration of their uncertainty bands as shown in Table A(C)-24 and figures below.

Table A(C)-24. Comparison of time-to-ignition at different heat-flux levels from actual experiment and pyrolysis modeling

Heat-Flux Level	Actual t_{ig} (s) $t_{ig} \pm \delta t_i$	Model t_{ig} (s) $t_{ig} \pm \delta t_i$
25 kW/m²	93 ± 43	99 ± 25
50 kW/m²	15 ± 3	25 ± 12
75 kW/m²	9 ± 4	11 ± 8

All three cases show good overlap between the data and simulation of time-to-ignition and the mass-loss rate during steady burning considering the uncertainties, i.e., the parameter estimation was conducted successfully (see Figure A(C)-23, Figure A(C)-24 and Figure A(C)-25).

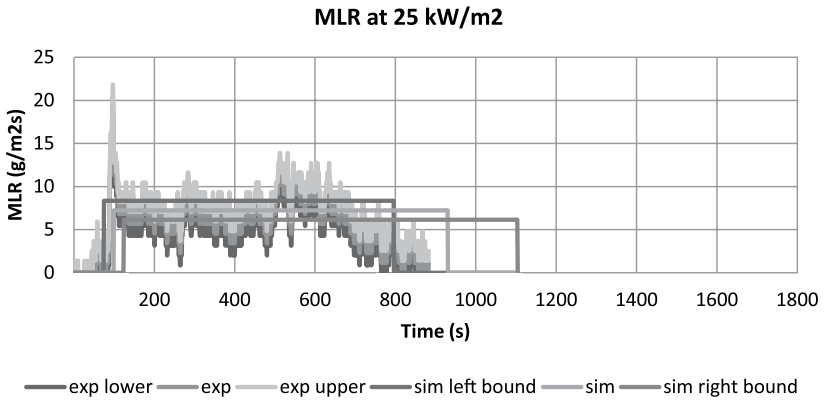

Figure A(C)-23. Mass-loss rate (MLR) comparisons for plywood between actual MLR from experiment (exp) and modeled MLR (sim) at 25 kW/m². Note that data shown were used to estimate model-parameter values.

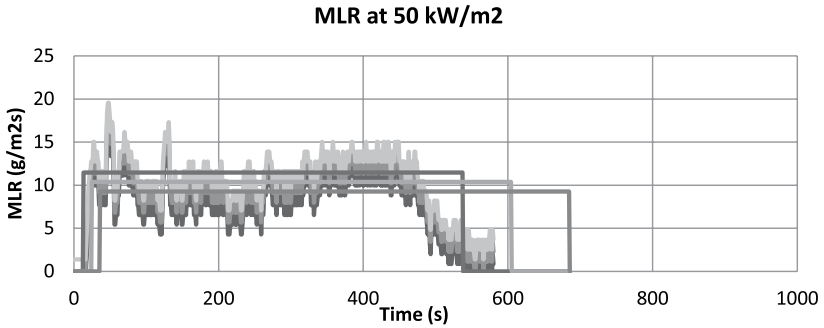

Figure A(C)-24. Mass-loss rate (MLR) comparisons for plywood between actual MLR from experiment (exp) and modeled MLR (sim) at 50 kW/m². Note that data shown were used to estimate model-parameter values.

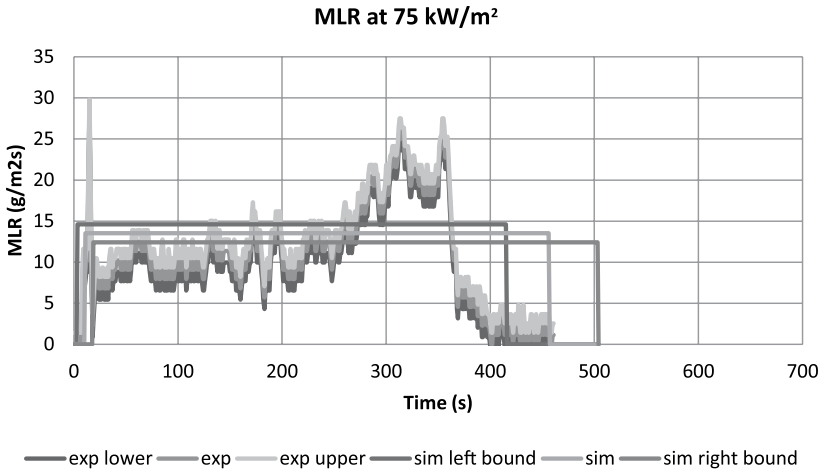

Figure A(C)-25. Mass Loss rate (MLR) comparisons for plywood between actual MLR from experiment (exp) and modeled MLR (sim) at 75 kW/m2. Note that data shown were used to estimate model-parameter values.

Commentary

When using Simple Analytical Model to simulate pyrolysis of Douglas Fir plywood, test data from a bench-scale cone calorimeter experiment at several heat-flux levels have been utilized to estimate the time-to-ignition from exposure to heating and the mass-loss rate at steady-burning stage after ignition. The comparison between the model outputs (time-to-ignition and steady-burning rate) and the data from bench-scale experiment showed good agreement for both checking purposes, where the same heat flux levels (25, 50 and 75 kW/m^2) used in parameter estimation have been considered.

Although the modeling predictions of time-to-ignition and steady-burning rate in this example seems to be reasonable, limitation of this Simple Analytical Modeling should be noted, which is that the model is for thermally-thick-behaving materials and steady burning after ignition.

Example 4.5 Modeling GRP with Balsa Wood Core Sandwich Composite

This material is composed of approximately 1 mm thickness of laminated glass-reinforced polymer (GRP) over approximately 25 mm thickness of resin-soaked balsa wood core as a skin layer (sandwich construction). The resin used in the GRP and with balsa wood is vinyl ester (VEX). The light-weight balsa wood core acts as an insulating layer for the thin GRP skin and allows the ignition data to behave thermally-thin. This thermal behavior is examined by plotting $1/t_{ig}^{n}$ vs. applied heat flux where its best fitness of a linear regression occurs near n = 0.9.

Measure Parameters

1. Ambient Temperature

Direct measurement of ambient temperature is made as 20°C.

2. Surface Temperature at Ignition

This parameter will be obtained via Ignition Data Analysis, i.e., no direct measurements will be performed.

3. Critical Heat Flux for Ignition

By bracketing to within +/- 2.5 kW/m^2 in cone calorimeter tests, $\dot{q}''_{cr}$ has been determined to be 12.5 kW/m^2. Ignition data is provided below for this sandwich composite with thickness of ~1 mm of GRP skin layer on surfaces out of 28 mm of the entire composite, density of 500 kg/m^3 (see Table A(C)-25):

Table A(C)-25. Ignition data from cone calorimeter tests for GRP with balsa wood core sandwich composite

Heat Flux	t_{ig}
(kW/m^2)	(s)
10	NI
15	792

4. Thermal Inertia

This parameter will be obtained via Ignition Data Analysis, i.e., no direct measurements will be performed.

5. Effective Heat-of-Combustion

This parameter will be obtained via BurningRate Data Analysis, i.e., no direct measurements will be performed.

6. Heat-of-Gasification

This parameter will be obtained via Burning-Rate Data Analysis, i.e., no direct measurements will be performed.

7. Convection Coefficient

Because this is a material laid in horizontal position in a cone calorimeter, h_c = 12 W/m^{2}K is used based on literature reference.

8. Surface Emissivity/Absorptivity

Emissivity is approximated as 0.9.

Summary

Table A(C)-26. Summary of model-parameter table with estimated values via direct measurements, literature search, or approximation

Ignition Parameters	T_∞	20 °C
	T_{ig}	Ignition Data Analysis
	$\dot{q}''_{cr}$	12.5 kW/m^2
	$k\rho c$	Ignition Data Analysis
Burning-Rate Parameters	$\Delta h_{c,eff}$	Burning-Rate Data Analysis
	Δh_g	Burning-Rate Data Analysis
	h_c	12 W/m^{2}K
	ε	0.9

Obtain Parameters via Data Analysis

Run model

SELECT MODEL: THERMALLY THIN MODEL FOR IGNITION ANALYSIS AND STEADY-BURNING MODEL

UNDERSTAND EXPERIMENT AND FIRE CHARACTERISTICS OF MATERIAL

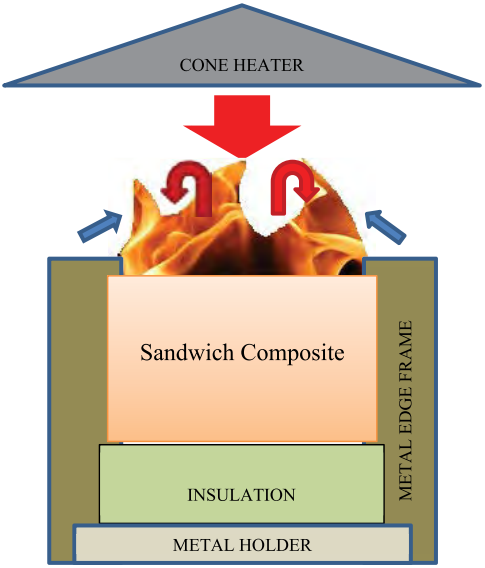

Figure A(C)-26. Simplified representation of a cone calorimeter test of sandwich composite

A simplified representation of a cone calorimeter test of this sandwich composite is shown in Figure A(C)-26. The sample is placed on top of an insulation, which sits on a metal holder. Another metal frame is placed on top of the sample, insulation and the holder. A metal edge frame is used as well.

Front Surface: As heating starts by opening the shutter to allow radiation from the cone heater to impinge on sample surface (large red arrow), cooling also begins via natural convection (blue arrows) and re-radiation. The surface decomposes with small bubbles appearing on the surface and blackening. When ignition occurs as the fuel-vapor concentration above the surface exceeds its LFL (lower flammable limit), additional heat flux from the flame is introduced on the surface (red arrows). The flame height and its intensity are the greatest when the resin in the skin layer (GRP composite) is pyrolyzing. After the skin layer is consumed, the flame become shorter and scatters on the surface as the fuel vapor produced in the balsa wood core layer is diffusing through the inert glass layers left in the skin layer on the surface. This short and scattering flame continues throughout flameout.

Back surface: The sample is placed on top of insulation. In the experiment, an air gap of a few millimeters thickness exist between the sample and the insulation resulting in some thermal resistance. Due to the insulation, nothing leaves through the back face when 1D assumption holds for the experiment.

CONFIGURE MODEL CONDITIONS BASED ON UNDERSTANDING OF EXPERIMENT AND MATERIAL CHARACTERISTICS

In the model, the phenomena discussed above are simulated as below. Basic assumptions are as follows:

- Pre-ignition stage is:
  - Inert: decomposition with bubbling and changing color on THE surface before ignition is neglected
  - Thermally thin GRP skin: heat transfer reaches back surface quickly, and the surface layer (vinylester resin GRP) is considered to have uniform temperature throughout
  - Control volume for ignition analysis is the thermally-thin GRP skin layer on the front surface facing the heating source
- Post-ignition stage is:
  - Considered to have instantaneous release of volatiles from solid to gas phase: any mass-transportation effect on pyrolysis is neglected, and pyrolysis is considered as surface phenomenon only
  - Considered to have a constant thickness
  - Steady burning: heat loss equals heat gain at front surface
  - 30% of the GRP skin layer (density of 2000 kg/m^3) is consumed via burning, and this information is used to calculate the model's burnout-time prediction

ACQUIRE DATA SETS

Cone calorimeter test data of this sandwich composite panel with thickness of 28 mm, density of 500 and applied heat flux levels ranging from 15 to 90 kW/m^2 is found. For ignition data analysis, only time to ignition with respect to applied heat flux data will be used. For burning rate data analysis, data for the entire testing time duration, mass loss and heat release during testing period with respect to applied heat flux will be used.

CONDUCT IGNITION DATA ANALYSIS

1. Estimate T_{ig}

   Heat balance at front surface during steady burning is as follow:

$$\varepsilon \dot{q}''_{cr} = h_c(T_{ig} - T_\infty) + \varepsilon\sigma(T_{ig}^4 - T_\infty^4)$$

   Knowing that emissivity is approximated as 0.9, critical heat flux is estimated as 12.5 kW/m^2, and heat transfer coefficient in Cone calorimeter experiment is estimated as 12.0 W/m^{2}K, ignition temperature, T_{ig} is calculated as:

$$\mathbf{T_{ig} = 350\ °C}$$

2. Estimate h_{ig}

   h_{ig} is the total heat transfer coefficient at ignition; therefore, at steady state burning stage, following can be defined:

$$\varepsilon \dot{q}''_{cr} \equiv h_{ig}(T_{ig} - T_\infty)$$

   Knowing the ignition temperature, hig can be calculated:

$$\mathbf{h_{ig} = 34.1\ W/m^2K}$$

3. Calculate $\dot{q}''_{cr} / \dot{q}''_{e}$ versus t_{ig} from ignition data

Table A(C)-27. $\dot{q}''_{cr} / \dot{q}''_{e}$ versus $\sqrt{t_{ig}}$

Heat Flux (kW/m²)	t_{ig} (s)	CHF/HF	Heat Flux (kW/m²)	t_{ig} (s)	CHF/HF
10	NI		50	42	0.2500
15	792	0.8333	50	50	0.2500
15	1017	0.8333	50	43	0.2500
15	703	0.8333	50	47	0.2500
20	243	0.6250	50	46	0.2500
20	297	0.6250	50	35	0.2500
20	702	0.6250	50	45	0.2500
20	1044	0.6250	50	44	0.2500
20	256	0.6250	50	60	0.2500
20	266	0.6250	50	55	0.2500
25	139	0.5000	60	34	0.2083
25	191	0.5000	60	38	0.2083
30	89	0.4167	75	24	0.1667
30	123	0.4167	75	22	0.1667
35	93	0.3571	80	26	0.1563
35	82	0.3571	80	21	0.1563
35	93.0	0.3571	85	24.00	0.1471
35	98	0.3571	85	19	0.1471
40	55	0.3125	90	21	0.1389
40	66	0.3125	90	21.00	0.1389

4. Plot $\dot{q}''_{cr} / \dot{q}''_{e}$ versus t_{ig} to estimate the time needed to reach "steady-state" burning, t* and thermal capacity, ρcδ

Recall $\frac{\dot{q}''_{cr}}{\dot{q}''_{e}} = \mathrm{F}(t_{ig}) = \begin{cases} \frac{h_{ig}\, t_{ig}}{\rho c \delta} & t_{ig} \le t^* \\ 1 & t_{ig} > t^* \end{cases}$ for piloted ignition data where t* is the time

when $\dot{q}''_{cr} / \dot{q}''_{e} = 1$. Thermal inertia can be estimated from the best fit line through t = 0. Its slope at $0 < t < t^*$ is $\frac{h_{ig}}{\rho c \delta}$; therefore, $\rho c \delta = \frac{h_{ig}}{(slope)}$. Note that in the analysis, few data points at lower heat flux levels with large time to ignition data were excluded (see Figure A(C)-27, open circles) to increase fitness of the best-fit line. This approach is reasonable considering that at this region analysis assumptions of having inert, thermally-thin and negligible heat loss conditions are less likely to be satisfied.

$$\boldsymbol{\rho c \delta = 7.625\ kJ/m^2K}$$

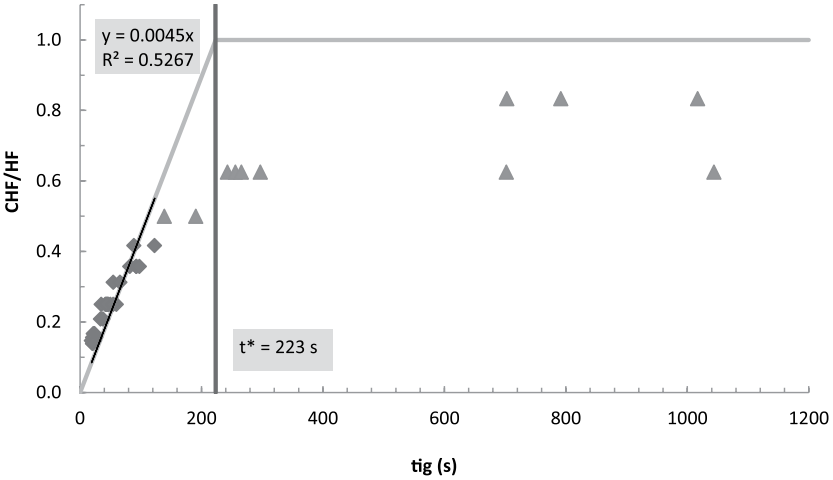

Figure A(C)-27. Plot of $\dot{q}''_{cr} / \dot{q}''_{e}$ versus $\sqrt{t_{ig}}$

CONDUCT BURNING RATE DATA ANALYSIS

1. Estimate $\Delta h_{c,eff}$

There are two approaches in estimating the effective heat of combustion via calorimeter tests: by using the peak in HRR or the average heat released over the entire test. In this example, $\Delta h_{c,eff}$ will be estimated by considering the average peak heat released divided by the average peak mass loss during a test. Cone test results ranging from 30 to 90 kW/m^2 are used to calculate the effective heat of combustion with its confidence interval using student t distribution and $\alpha = 0.05$:

$$\mathbf{\Delta h_{c,eff} = 23.5 \pm 2.1\ kJ/g}$$

2. Estimate Δh_g

Recall $\Delta h_g \equiv \frac{\dot{q}''_{net}}{\dot{m}''} = \frac{\dot{q}_e'' + \dot{q}_f'' - \dot{q}_l''}{\dot{m}''}$; therefore, when plotting mass loss rates at different radiant heat flux levels during steady burning condition, the reciprocal of the slope of the best-fit line should be the heat-of-gasification. Note that for this material – sandwich composite – a strict steady-burning phase does not exist where a constant MLR appears. The burning of the resin in the front surface-skin layer (vinyl-ester resin GRP composite) occurs with ignition and lasts about 1 min. or so with increasing mass-loss rate and heat-release rate showing up as the initial peak in the MLR and HRR curve. Considering that the model control volume is the first GRP skin layer and HoG is estimated to calculate the energy necessary for gasification of the GRP skin layer, HoG is calculated in the time interval where the initial peaks of the MLR and HRR curve are found; hence, both MLR and HRR are found from the peak averaged values at different heat-flux levels (see Table A(C)-28 and Figure A(C)-28).

$$\mathbf{\Delta h_g = 8.0\ kJ/g}$$

Table A(C)-28. Estimation of effective heat-of-gasification using cone calorimeter test results at applied heat flux ranging between 30 and 90 kW/m²

Heat Flux (kW/m^2)	peakAvgMLR (g/m2s)
30	10.53
30	12.09
35	12.53
35	12.75
35	12.01
35	12.68
40	12.69
40	13.26
50	12.87
50	12.12
50	12.27
60	14.39
60	16.14
75	17.31
75	17.85
80	16.08
85	17.51
90	20.20
90	20.18

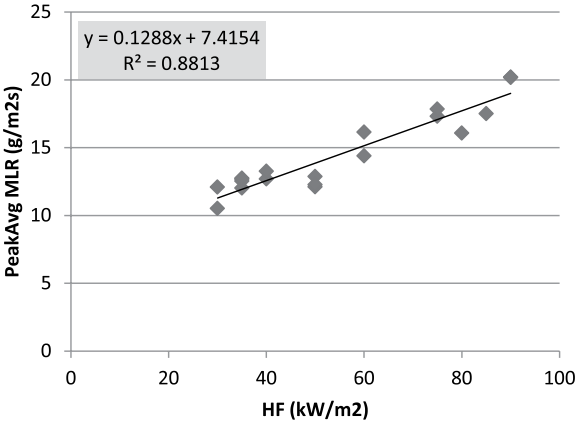

Figure A(C)-28. Plot of steady MLR versus different applied heat-flux levels – 25 to 75 kW/m²

Obtain Uncertainty for Estimated Parameters

UNCERTAINTY FOR MEASURED PARAMETERS

1. δT_∞

Fluctuation in ambient temperature during testing is estimated to be less than ±25% of reported measurement data.

2. $\delta \dot{q}''_{cr}$

The resolution of bracketing experiment was 5 kW/m^2; hence, uncertainty can be estimated as ± 2.5 kW/m^2.

3. δhc

Considering that the reference values sited in the *Guide* for different apparatuses and set-up have two significant figures, uncertainty for this convection coefficient can be estimated as ± 0.5 W/m^{2}K.

4. $\delta \varepsilon$

Emissivity measurement of this sample was conducted using an IR camera with its surface blackened – 0.92 ± 0.02. This is close to what has been assumed in the analysis. The emissivity uncertainty is considered to be ± 10% of what has been approximated in this example.

UNCERTAINTY FOR ESTIMATED PARAMETERS USING IGNITION DATA ANALYSIS

1. δT_{ig}

See Chapter 4 for detail.

$$\frac{\partial \dot{q}''_{cr}}{\partial T_{ig}} = \frac{h_c + 4\varepsilon\sigma T_{ig}^3}{\varepsilon}$$

$$= \frac{\left(0.012\frac{kW}{m^2K}\right) + 4(0.9)\left(5.67\times10^{-11}\frac{kW}{K^4m^2}\right)\left((350+273)K\right)^3}{(0.9)}$$

$$\approx 0.06818\frac{kW}{m^2K}$$

$$\frac{\partial \dot{q}''_{cr}}{\partial \varepsilon} = \frac{-\dot{q}''_{cr} + \sigma(T_{ig}^4 - T_\infty^4)}{\varepsilon}$$

$$= \frac{-\left(12.5\frac{kW}{m^2}\right) + \left(5.67\times10^{-11}\frac{kW}{K^4m^2}\right)\left(\left((350+273)K\right)^4 - \left((20+273)K\right)^4\right)}{(0.9)}$$

$$\approx -4.863\frac{kW}{m^2}$$

$$\frac{\partial \dot{q}''_{cr}}{\partial h_c} = \frac{T_{ig} - T_\infty}{\varepsilon}$$
$$= \frac{((350+273)K) - ((20+273)K)}{(0.9)}$$
$$\approx 367K$$
$$\frac{\partial \dot{q}''_{cr}}{\partial T_\infty} = \frac{-h_c - 4\varepsilon\sigma T_\infty^3}{\varepsilon}$$
$$= \frac{-\left(0.012\frac{kW}{m^2K}\right) - 4(0.9)\left(5.67\times10^{-11}\frac{kW}{K^4m^2}\right)((20+273)K)^3}{(0.9)}$$
$$\approx -0.01904\frac{kW}{m^2K}$$

Therefore,

$$\delta T_{ig} = \left(\frac{\partial \dot{q}''_{cr}}{\partial T_{ig}}\right)^{-1}\sqrt{(\delta \dot{q}''_{cr})^2 - \left(\left(\frac{\partial \dot{q}''_{cr}}{\partial \varepsilon}\delta\varepsilon\right)^2 + \left(\frac{\partial \dot{q}''_{cr}}{\partial h_c}\delta h_c\right)^2 + \left(\frac{\partial \dot{q}''_{cr}}{\partial T_\infty}\delta T_\infty\right)^2\right)}$$
$$= \left(0.0682\frac{kW}{m^2K}\right)^{-1}\sqrt{\left(2.5\frac{kW}{m^2}\right)^2 - \left(\begin{array}{l}\left(\left(-4.86\frac{kW}{m^2}\right)(0.09)\right)^2 \\ \quad + \left((367K)\left(0.5\times10^{-3}\frac{kW}{m^2K}\right)\right)^2 \\ \quad + \left(\left(-0.01904\frac{kW}{m^2K}\right)(5K)\right)^2\end{array}\right)}$$
$$\approx 36.0K$$

2. δ(**ρc**δ)

See Chapter 4 for detail.

The uncertainty of the slope of the best-fit line, 0.004475 /s, can be estimated through calculating 2 times the standard error of the slope, which is +/- 0.000379 /s.

$$\frac{\partial(\rho c\delta)}{\partial(slope)} = \frac{-1}{(slope)^2}\left(\frac{\varepsilon \dot{q}''_{cr}}{T_{ig} - T_\infty}\right)$$
$$= \frac{-1}{(0.004475/s)^2}\left(\frac{(0.9)\left(12.5\frac{kJ}{s\,m^2}\right)}{((350+273)K) - ((20+273)K)}\right)$$
$$\approx -1702\frac{kJ\cdot s}{m^2K}$$

$$\frac{\partial(\rho c\delta)}{\partial\varepsilon} = \frac{1}{(slope)}\left(\frac{\dot{q}''_{cr}}{T_{ig}-T_{\infty}}\right)\varepsilon$$

$$= \frac{1}{(0.004475/s)}\left(\frac{\left(12.5\frac{\frac{kJ}{s}}{m^2}\right)}{((350+273)K)-((20+273)K)}\right)(0.9)$$

$$\approx 8.464\frac{kJ}{m^2K}$$

$$\frac{\partial(\rho c\delta)}{\partial\dot{q}''_{cr}} = \frac{1}{(slope)}\left(\frac{\varepsilon}{T_{ig}-T_{\infty}}\right)$$

$$= \frac{1}{(0.004475/s)^2}\left(\frac{(0.9)}{((350+273)K)-((20+273)K)}\right)$$

$$\approx 7.617\frac{s}{K}$$

$$\frac{\partial(\rho c\delta)}{\partial T_{ig}} = \frac{-1}{(slope)}\left(\frac{\varepsilon\dot{q}''_{cr}}{T_{ig}-T_{\infty}}\right)\frac{1}{T_{ig}-T_{\infty}}$$

$$= \frac{-1}{(0.004475/s)}\left(\frac{(0.9)\left(12.5\frac{\frac{kJ}{s}}{m^2}\right)}{((350+273)K)-((20+273)K)}\right)\frac{1}{((350+273)K)-((20+273)K)}$$

$$\approx -0.0231\frac{kJ\cdot s}{m^2K^2}$$

$$\frac{\partial(\rho c\delta)}{\partial T_{\infty}} = \frac{1}{(slope)}\left(\frac{\varepsilon\dot{q}''_{cr}}{T_{ig}-T_{\infty}}\right)\frac{1}{T_{ig}-T_{\infty}}$$

$$= \frac{1}{(0.004475/s)}\left(\frac{(0.9)\left(12.5\frac{\frac{kJ}{s}}{m^2}\right)}{((350+273)K)-((20+273)K)}\right)\frac{1}{((350+273)K)-((20+273)K)}$$

$$\approx 0.0231\frac{kJ}{m^2K^2}$$

Therefore,

$$\delta(\rho c\delta) = \sqrt{\left(\frac{\partial(\rho c\delta)}{\partial(slope)}\delta(slope)\right)^2 + \left(\frac{\partial(\rho c\delta)}{\partial\varepsilon}\delta\varepsilon\right)^2 + \left(\frac{\partial(\rho c\delta)}{\partial\dot{q}''_{cr}}\delta\dot{q}''_{cr}\right)^2 + \left(\frac{\partial(\rho c\delta)}{\partial T_{ig}}\delta T_{ig}\right)^2 + \left(\frac{\partial(\rho c\delta)}{\partial T_\infty}\delta T_\infty\right)^2}$$

$$= \sqrt{\left(\left(-1702\frac{kJ\cdot s}{m^2K}\right)(0.000379/s)\right)^2 + \left(\left(8.464\frac{kJ}{m^2K}\right)(0.09)\right)^2 + \left(\left(7.617\frac{s}{K}\right)\left(2.5\frac{kW}{m^2}\right)\right)^2 + \left(\left(-0.0231\frac{kJ}{m^2K^2}\right)(11.3K)\right)^2 + \left(\left(0.0231\frac{kJ}{m^2K^2}\right)(2.5K)\right)^2}$$

$$\approx 19.1\frac{kJ}{m^2K}$$

UNCERTAINTY FOR ESTIMATED PARAMETERS USING BURNING-RATE DATA ANALYSIS

1. $\delta\Delta h_{c,eff}$

Cone test results ranging from 30 to 90 kW/m^2 are used to calculate the effective heat-of-combustion. Uncertainty of this value is estimated with its confidence interval using student t distribution and α = 0.05: **± 2.1 kJ/g**

2. $\delta\Delta h_g$

See Chapter 4 for detail.

The uncertainty of the slope (=1/Δh_g=0.129g/kJ) can be estimated through calculating 2 times the standard error of the slope of the best-fit line, which is +/- 0.229. Therefore, the uncertainty in Δh_g is

$$\frac{d(\Delta h_g)}{d(slope)} = -\frac{1}{(slope)^2} = -\frac{1}{\left(0.129\frac{g}{kJ}\right)^2} \approx -60.3\frac{kJ^2}{g^2}$$

Therefore,

$$\delta(\Delta h_g) = \sqrt{\left(\frac{d(\Delta h_g)}{d(slope)}\delta(slope)\right)^2} = \sqrt{\left(\left(-60.3\frac{kJ^2}{g^2}\right)(0.0229g/kJ)\right)^2} \approx 1.38\frac{kJ}{g}$$

Table A(C)-29. Summary of model-parameter table with estimated values with uncertainty

Ignition Parameters	T_∞	20 ± 5 °C
	T_{ig}	350 ± 36 °C
	$\dot{q}''_{cr}$	12.5 ± 2.5 kW/m^2
	$\rho c \delta$	7.625 ± 19.1 kJ^2/m^{4}K^{2}s
Burning-Rate Parameters	$\Delta h_{c,eff}$	23.5 ± 2.1 kJ/g
	Δh_g	8.7 ± 1.4 kJ/g
	h_c	12 ± 0.5 W/m^{2}K
	ε	0.9 ± 0.09

Validation

Analyze Simulation Quality

DETERMINE DATA AND MODEL OUTPUT UNCERTAINTY TO MAKE COMPARISON

1. Conduct uncertainty analysis of data

The uncertainty in the mass-loss-rate data used for comparison between data and model outputs is estimated via statistical approach, taking the standard deviation (0.58 g/sm^2) from the mean of a steady burning of five identical PMMA tests conducted in a cone calorimeter.[2] The estimated uncertainty is 1.4 g/sm^2, which is found by calculating the 95% confidence interval applying student t distribution with a sample size of five.

The uncertainty in time-to-ignition data used for comparison is estimated via statistical approach, taking three to four identical cone clorimeter test data at heat fluxes ranging from 35 to 75 kW/m^2 of this plywood. 95% confidence interval is calculated for each heat-flux level assuming student t distribution.

2. Conduct uncertainty analysis for MLR profile modeling

Because uncertainty information of the data is found in terms of time-to-ignition and mass-loss rate, the mass-loss-rate profile is considered as the modeling output of interest for comparison purposes. For Simple Analytical Models, time-to-ignition (t_{ig}) and stead- burning rate ($\dot{m}''$) are needed when simulating the mass-release-rate profile. The uncertainty in the MLR profile in modeling can be determined via considering the uncertainties in these calculation results as below:

$$t_{ig} \pm \delta t_{ig}$$
$$\dot{m}'' \pm \delta \dot{m}''$$

To determine the uncertainty in time to ignition, recall:

$$\frac{\dot{q}''_{cr}}{\dot{q}''_e} = F(t_{ig}) = \begin{cases} \dfrac{h_{ig}\, t_{ig}}{\rho c \delta} & t_{ig} \le t^* \\ 1 & t_{ig} > t^* \end{cases}$$

Knowing that all heat-flux levels of interest, 35, 50, and 75 kW/m^2, are above the critical heat flux, time-to-ignition should be smaller than t*. Hence, uncertainty in t_{ig} can be estimated from linear-regression process as below:

$$\frac{\dot{q}_{cr}^{"}}{\dot{q}_{e}^{"}} = \frac{h_{ig}}{\rho c \delta} t_{ig}$$

The above equation can be re-written as below after conducting linear regression:

$$y\ estimate = (slope) t_{ig}$$

Therefore,

$$t_{ig} = \left(\frac{y\ estimate}{slope} \right)$$

Assuming that the y estimate and slope are independent and propagating the uncertainties in these two variables in estimating the time-to-ignition, the following calculation can be made:

$$\delta t_{ig} = \sqrt{\left(\frac{\partial t_{ig}}{\partial (y\ estimate)} \delta (y\ estimate) \right)^2 + \left(\frac{\partial t_{ig}}{\partial (slope)} \delta (slope) \right)^2}$$

where

$$\frac{\partial t_{ig}}{\partial (y\ estimate)} = \frac{1}{(slope)}$$

$$\frac{\partial t_{ig}}{\partial (slope)} = -\frac{(y\ estimate)}{(slope)^2}$$

with δ(*y estimate)* and δ(*slope)* estimated through calculating 2 times the standard error of the y estimate and slope of the best-fit line.

To determine the uncertainty in the steady-heat-release rate at post-ignition stage, recall:

$$\Delta h_g \equiv \frac{\dot{q}_{net}^{"}}{\dot{m}''} = \frac{\dot{q}_e'' + \dot{q}_f'' - \dot{q}_l''}{\dot{m}''}$$

The above equation can be rearranged to

$$\dot{m}^{"} = \frac{1}{\Delta h_g} \dot{q}_e^{"} + \frac{\dot{q}_f^{"} - \dot{q}_l^{"}}{\Delta h_g}$$

The steady-burning rate at post-ignition stage is determined by the best-fit line obtained when data is plotted as steady-burning rate versus applied heat flux. The uncertainty in steady-burning rate can be determined by considering 2 times the standard error of the y estimates, i.e. $\dot{m}''$, which is obtained through linear regression process: **± 2.1 g/m²s**.

COMPARE DATA WITH SIMULATION RESULTS WITH CONSIDERATION OF UNCERTAINTIES

Parameters in this simple analytical pyrolysis model have been estimated with cone calorimeter test data from 35, 50 and 75 kW/m^2. To check the quality of the modeling using the estimated parameters, three cases have been simulated and compared with experiment data with the consideration of their uncertainty bands as shown in Table A(C)-30 and figures below. Note that although the experiment data shows pyrolysis of the entire sandwich composite, from the front surface GRP skin layer to balsa wood core and through the back surface GRP skin layer (blue lines), the modeling results only account for pyrolysis of the front surface GRP skin layer (red lines). The GRP skin layer has a thickness, density, and inert residue fraction, including glass layers, of approximately 1.3 mm, 2000 kg/m^3 and 70%, respectively.

Table A(C)-30. Comparison of time-to-ignition at different heat-flux levels from actual experiment and pyrolysis modeling

Heat-Flux Level	Actual t_{ig} (s) $t_{ig} \pm \delta t_i$	Model t_{ig} (s) $t_{ig} \pm \delta t_i$
35 kW/m^2	92 ± 11	80 ± 27
50 kW/m^2	47 ± 5	56 ± 26
75 kW/m^2	23 ± 13	37 ± 26

All three cases show good overlap between the data and simulation of time-to-ignition and the mass-loss rate during steady burning, considering the uncertainties, i.e., the parameter estimation was conducted successfully (see Figure A(C)-29, Figure A(C)-30 and Figure A(C)-31).

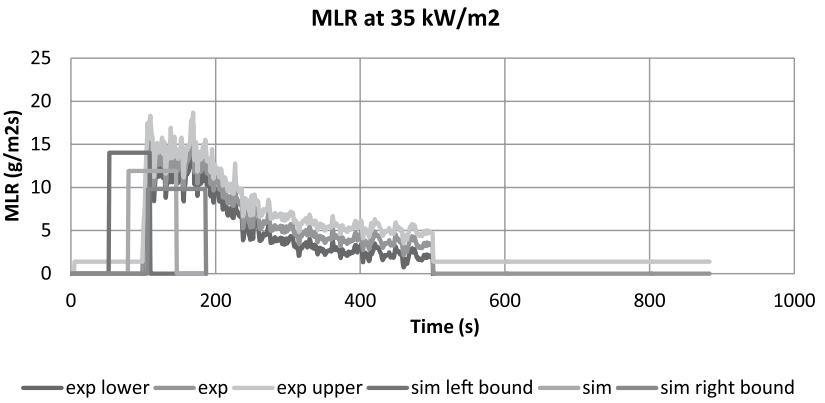

Figure A(C)-29. Mass-loss rate (MLR) comparisons for GRP with balsa wood core sandwich composite between actual MLR from experiment (exp) and modeled MLR (sim) at 25 kW/m^2. Note that data shown were used to estimate model-parameter values.

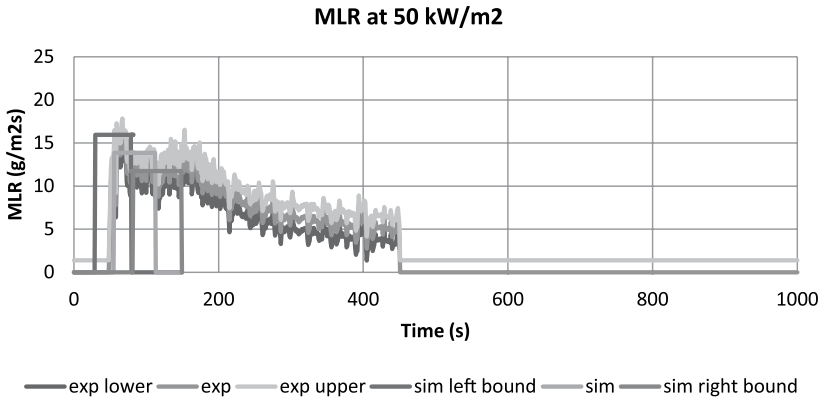

Figure A(C)-30. Mass-loss rate (MLR) comparisons for GRP with balsa wood core sandwich composite between actual MLR from experiment (exp) and modeled MLR (sim) at 50 kW/m². Note that data shown were used to estimate model-parameter values.

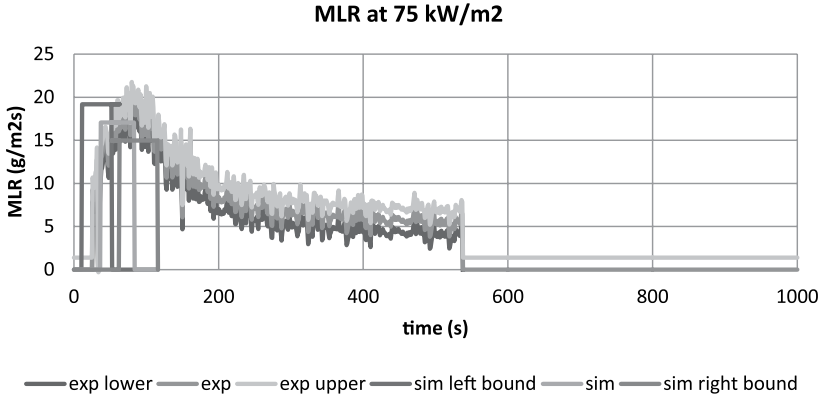

Figure A(C)-31. Mass-loss rate (MLR) comparisons for GRP with balsa wood core sandwich composite between actual MLR from experiment (exp) and modeled MLR (sim) at 75 kW/m². Note that data shown were used to estimate model-parameter values.

Commentary

In this example, Simple Analytical Model is used to simulate pyrolysis of the thermally-thin-behaving GRP skin layer of this sandwich composite (vinyl-ester GRP skin layers with resin-soaked balsa wood core). Test data from a bench-scale cone calorimeter experiment at several heat-flux levels have been utilized to estimate the time-to-ignition from exposure to heating and the mass-loss rate at steady-burning stage after ignition. The comparison between the model outputs (time-to-ignition and steady-burning rate) and the data from bench-scale experiment showed good agreement for both checking purposes where the same heat-flux levels (35, 50 and 75 kW/m²) used in parameter estimation have been considered.

Although the modeling predictions of time-to-ignition and steady-burning rate in this example seems to be reasonable, limitation of this Simple Analytical Modeling should be noted, which is that the model is for thermally-thin-behaving materials and steady burning after ignition.

Example 4.6 Modeling Thin FRP Composite Sheet

The rigid FRP panel chosen for use in full-scale testing is commercially available and advertised for use as ceiling and wall linings in environments designed to be moisture- and mold-free. The panel has a Class C (ASTM E84) flame-spread rating. It is consisted of modified-polyester copolymer and inorganic fillers as the resin base and reinforced with a weave of random-chopped fiberglass. The panel's thickness is 0.09" (2.3 mm) nominal, with a smooth backface and a pebbled, embossed white front surface. When this material is tested for ignition in a cone calorimeter test, thermally thin behavior is observed. This thermal characteristic is examined by plotting $1/t_{ig}^{n}$ vs. applied heat flux, where its best fitness of a linear regression occurs near n = 1.0.

Measure Parameters

1. Ambient Temperature

Direct measurement of ambient temperature is made as 23°C.

2. Surface Temperature at Ignition

This parameter will be obtained via Ignition Data Analysis, i.e., no direct measurements will be performed.

3. Critical Heat Flux for Ignition

By bracketing to within +/- 1 kW/m^2 in cone calorimeter tests, $\dot{q}''_{cr}$ has been determined to be 16 kW/m^2. Ignition data is provided below for this FRP composite with thickness of 2 mm and density of 1500 kg/m^3 (see Table A(C)-31):

Table A(C)-31. Ignition data from cone calorimeter tests for thin FRP composite sheet

Heat Flux	t_{ig}
(kW/m^2)	(s)
15	NI
17	269

4. Thermal Inertia

This parameter will be obtained via Ignition Data Analysis, i.e., no direct measurements will be performed.

5. Effective Heat-of-Combustion

This parameter will be obtained via Burning-Rate Data Analysis, i.e., no direct measurements will be performed.

6. Heat-of-Gasification

This parameter will be obtained via Burning-Rate Data Analysis, i.e., no direct measurements will be performed.

7. Convection Coefficient

Because this is a material laid in horizontal position in a cone calorimeter, h_c = 12 W/m^{2}K is used based on literature reference.

8. Surface Emissivity/Absorptivity

Emissivity is approximated as 0.9.

Summary

Table A(C)-32. Summary of model-parameter table with estimated values via direct measurements, literature search, or approximation

Ignition Parameters	T_∞	23 °C
	T_{ig}	Ignition Data Analysis
	$\dot{q}''_{cr}$	16 kW/m^2
	$k\rho c$	Ignition Data Analysis
Burning-Rate Parameters	$\Delta h_{c,eff}$	Burning-Rate Data Analysis
	Δh_g	Burning-Rate Data Analysis
	h_c	12 W/m^{2}K
	ε	0.9

Obtain Parameters via Data Analysis

Run model

SELECT MODEL: THERMALLY-THIN MODEL FOR IGNITION ANALYSIS AND STEADY-BURNING MODEL

UNDERSTAND EXPERIMENT AND FIRE CHARACTERISTICS OF MATERIAL

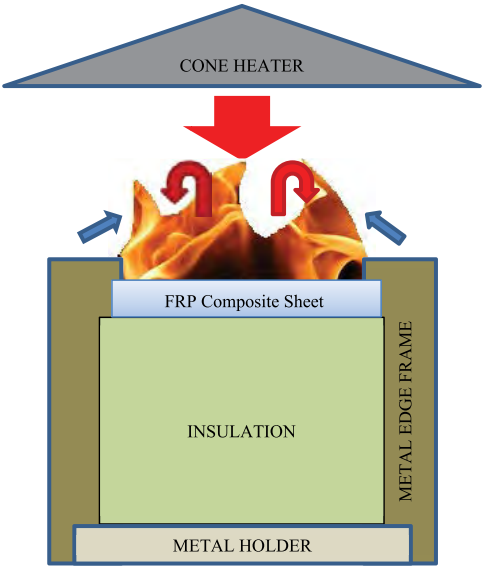

Figure A(C)-32. Simplified representation of a cone calorimeter test of FRP composite sheet

A simplified representation of a cone calorimeter test of this FRP composite sheet is shown in Figure A(C)-32. The sample is placed on top of an insulation, which sits on a metal holder. Another metal frame is placed on top of the sample, insulation and the holder. A metal edge frame is used as well.

Front Surface: As heating starts by opening the shutter to allow radiation from the cone heater to impinge on sample surface (large red arrow), cooling also begins via natural convection (blue arrows) and re-radiation. The surface decomposes with a small crackling sound and the surface becomes black. When ignition occurs as the fuel-vapor concentration above the surface exceeds its LFL (lower flammable limit), additional heat flux from the flame is introduced on the surface (red arrows).

Back surface: The sample is placed on top of insulation. In the experiment, an air gap of a few millimeters thickness exists between the sample and the insulation, resulting in some thermal resistance. Due to the insulation, nothing leaves through the back face when 1D assumption holds for the experiment.

CONFIGURE MODEL CONDITIONS BASED ON UNDERSTANDING OF EXPERIMENT AND MATERIAL CHARACTERISTICS

In the model, the phenomena discussed above are simulated as below. Basic assumptions are as follows:

- Pre-ignition stage is:
  - Inert: decomposition with crackling sound and changing color on the surface before ignition are neglected
  - Thermally thin: heat transfer reaches back surface quickly, and the entire layer is considered to have uniform temperature throughout
- Post-ignition stage is:
  - Considered to have instantaneous release of volatiles from solid to gas phase: any mass-transportation effect on pyrolysis is neglected, and pyrolysis is considered as surface phenomenaon only
  - Considered to have a constant thickness
  - Steady burning: heat loss equals heat gain at front surface
  - 40% of the FRP composite sheet (density of 1500 kg/m^3) is consumed via burning, and this information is used to calculate the model's burnout time prediction

ACQUIRE DATA SETS

A cone calorimeter test data of this FRP composite sheet with thickness of 2 mm, density of 1500 and applied heat-flux levels ranging from 15 to 75 kW/m^2 is found. For ignition data analysis, only time-to-ignition with respect to applied heat-flux data will be used. For burning-rate data analysis, data for the entire testing time duration, mass loss and heat release during testing period with respect to applied heat flux will be used.

CONDUCT IGNITION DATA ANALYSIS

1. Estimate T_{ig}

   Heat balance at front surface during steady burning is as follow:

$$\varepsilon \dot{q}''_{cr} = h_c(T_{ig} - T_\infty) + \varepsilon\sigma(T_{ig}^4 - T_\infty^4)$$

   Knowing that emissivity is approximated as 0.9, critical heat flux is estimated as 16 kW/m^2, and heat transfer coefficient in cone calorimeter experiment is estimated as 12.0 W/m^{2}K, ignition temperature, T_{ig} is calculated as:

$$\mathbf{T_{ig} = 397\ °C}$$

2. Estimate h_{ig}

   h_{ig} is the total heat-transfer coefficient at ignition; therefore, at steady-state-burning stage, the following can be defined:

$$\varepsilon \dot{q}''_{cr} \equiv h_{ig}(T_{ig} - T_\infty)$$

   Knowing the ignition temperature, h_{ig} can be calculated:

$$\mathbf{h_{ig} = 38.5\ W/m^2K}$$

3. Calculate $\dot{q}''_{cr} / \dot{q}''_{e}$ versus t_{ig} from ignition data

Table A(C)-33. $\dot{q}''_{cr} / \dot{q}''_{e}$ versus $\sqrt{t_{ig}}$

Heat Flux	t_{ig}	CHF/HF
(kW/m²)	(s)	
15	NI	
17	269	0.9412
20	207	0.8000
25	106	0.6400
25	117	0.6400
40	42	0.4000
40	52	0.4000
50	37	0.3200
50	39	0.3200
50	37	0.3200
60	26	0.2667
60	26	0.2667
75	24	0.2133
75	25	0.2133

4. Plot $\dot{q}''_{cr} / \dot{q}''_{e}$ versus t_{ig} to estimate the time needed to reach "steady-state" burning, t* and thermal capacity, ρcδ

Recall $\frac{\dot{q}''_{cr}}{\dot{q}''_{e}} = \mathrm{F}(t_{ig}) = \begin{cases} \frac{h_{ig}\, t_{ig}}{\rho c \delta} & t_{ig} \le t^* \\ 1 & t_{ig} > t^* \end{cases}$ for piloted-ignition data, where t* is the time when $\dot{q}''_{cr} / \dot{q}''_{e} = 1$. Thermal inertia can be estimated from the best-fit line through t = 0. Its slope at $0 < t < t^*$ is $\frac{h_{ig}}{\rho c \delta}$; therefore, $\rho c \delta = \frac{h_{ig}}{(slope)}$. Note that in the analysis, few data points at lower heat-flux levels with large time-to-ignition data were excluded (see Figure A(C)-33, open circles) to increase fitness of the best-fit line. This approach is reasonable, considering that at this region analysis assumptions of having inert, thermally-thin and negligible heat-loss conditions are less likely to be satisfied.

$$\boldsymbol{\rho c \delta = 4.333\ kJ/m^2K}$$

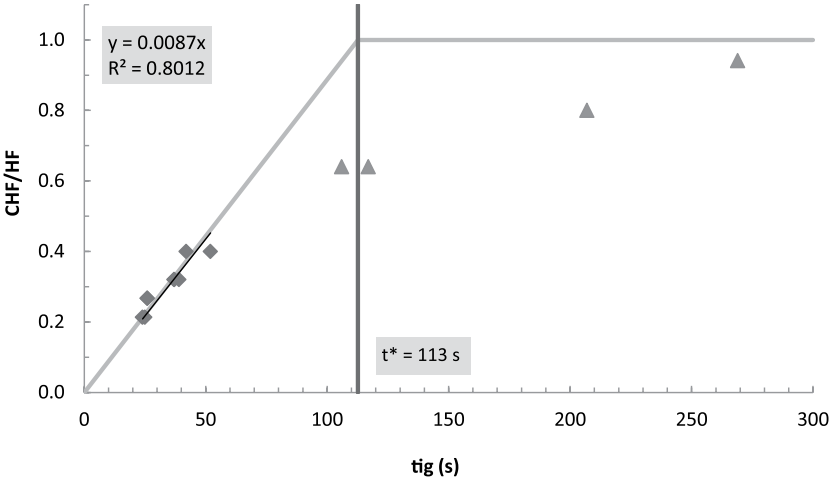

Figure A(C)-33. Plot of $\dot{q}''_{cr} / \dot{q}''_{e}$ versus $\sqrt{t_{ig}}$

CONDUCT BURNING-RATE DATA ANALYSIS

1. Estimate $\Delta h_{c,eff}$

There are two approaches in estimating the effective heat-of-combustion via calorimeter tests: by using the peak in HRR or the average heat released over the entire test. In this example, $\Delta h_{c,eff}$ will be estimated by considering the average peak heat released divided by the average peak mass loss during a test. Cone test results ranging from 30 to 90 kW/m^2 are used to calculate the effective heat-of-combustion with its confidence interval using student t distribution and $\alpha = 0.05$:

$$\mathbf{\Delta h_{c,eff} = 25.5 \pm 1.8\ kJ/g}$$

2. Estimate Δh_g

Recall $\Delta h_g \equiv \frac{\dot{q}''_{net}}{\dot{m}''} = \frac{\dot{q}_e'' + \dot{q}_f'' - \dot{q}_l''}{\dot{m}''}$; therefore, when plotting mass-loss rates at different radiant heat flux-levels during steady-burning condition, the reciprocal of the slope of the best-fit line should be the heat-of-gasification. In this example, average MLR and HRR will be used to estimate heat of gasification (see Table A(C)-34 and Figure A(C)-34).

$$\mathbf{\Delta h_g = 16.3\ kJ/g}$$

Table A(C)-34. Estimation of effective heat-of-gasification using cone calorimeter test results at applied heat flux ranging between 17 and 75 kW/m²

Heat Flux (kW/m^2)	AvgMLR (g/m2s)
17	2.23
20	2.64
25	2.61
25	2.85
40	3.80
50	3.84
50	4.72
50	4.58
60	4.69
60	3.34
75	6.44
75	6.16

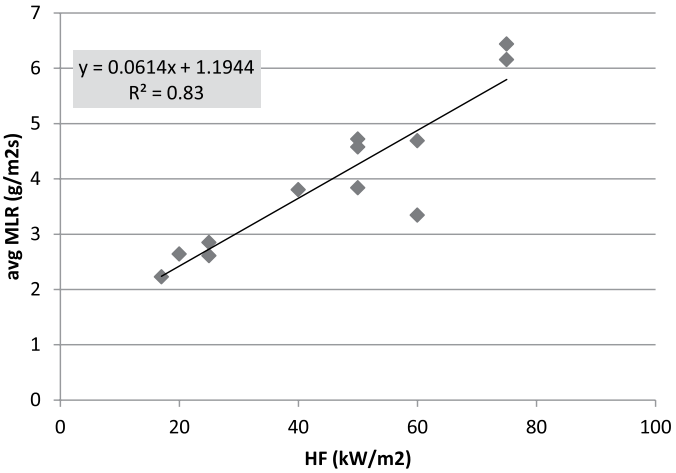

Figure A(C)-34. Plot of steady MLR versus different applied heat-flux levels – 25 to 75 kW/m²

Obtain Uncertainty for Estimated Parameters

UNCERTAINTY FOR MEASURED PARAMETERS

1. δT_∞

Fluctuation in ambient temperature during testing is estimated to be less than ±15% of reported measurement data.

2. $\delta \dot{q}''_{cr}$

The resolution of the bracketing experiment was 2 kW/m^2; hence, uncertainty can be estimated as ± 1 kW/m^2.

3. δhc

Considering that the reference values sited in the *Guide* for different apparatuses and set-up have two significant figures, uncertainty for this convection coefficient can be estimated as ± 0.5 W/m^{2}K.

4. $\delta \varepsilon$

The emissivity uncertainty is considered to be ± 10% of what has been approximated in this example.

UNCERTAINTY FOR ESTIMATED PARAMETERS USING IGNITION DATA ANALYSIS

1. δT_{ig}

See Chapter 4 for detail.

$$\frac{\partial \dot{q}''_{cr}}{\partial T_{ig}} = \frac{h_c + 4\varepsilon\sigma T_{ig}^3}{\varepsilon}$$

$$= \frac{\left(0.012\frac{kW}{m^2K}\right) + 4(0.9)\left(5.67\times10^{-11}\frac{kW}{K^4m^2}\right)((397+273)K)^3}{(0.9)}$$

$$\approx 0.0815\frac{kW}{m^2K}$$

$$\frac{\partial \dot{q}''_{cr}}{\partial \varepsilon} = \frac{-\dot{q}''_{cr} + \sigma(T_{ig}^4 - T_\infty^4)}{\varepsilon}$$

$$= \frac{-\left(16\frac{kW}{m^2}\right) + \left(5.67\times10^{-11}\frac{kW}{K^4m^2}\right)\left(((397+273)K)^4 - ((23+273)K)^4\right)}{(0.9)}$$

$$\approx -5.566\frac{kW}{m^2}$$

$$\frac{\partial \dot{q}''_{cr}}{\partial h_c} = \frac{T_{ig} - T_\infty}{\varepsilon}$$

$$= \frac{((397+273)K) - ((23+273)K)}{(0.9)}$$

$$\approx 416K$$

$$\frac{\partial \dot{q}''_{cr}}{\partial T_\infty} = \frac{-h_c - 4\varepsilon\sigma T_\infty^3}{\varepsilon}$$

$$= \frac{-\left(0.012\frac{kW}{m^2K}\right) - 4(0.9)\left(5.67\times10^{-11}\frac{kW}{K^4m^2}\right)\left((23+273)K\right)^3}{(0.9)}$$

$$\approx -0.01922\frac{kW}{m^2K}$$

Therefore,

$$\delta T_{ig} = \left(\frac{\partial \dot{q}''_{cr}}{\partial T_{ig}}\right)^{-1}\sqrt{\left(\delta\dot{q}''_{cr}\right)^2 - \left(\left(\frac{\partial \dot{q}''_{cr}}{\partial \varepsilon}\delta\varepsilon\right)^2 + \left(\frac{\partial \dot{q}''_{cr}}{\partial h_c}\delta h_c\right)^2 + \left(\frac{\partial \dot{q}''_{cr}}{\partial T_\infty}\delta T_\infty\right)^2\right)}$$

$$= \left(0.08155\frac{kW}{m^2K}\right)^{-1}\sqrt{\left(1\frac{kW}{m^2}\right)^2 - \left(\begin{array}{l}\left(\left(-5.566\frac{kW}{m^2}\right)(0.09)\right)^2 \\ \quad + \left((416K)\left(0.5\times10^{-3}\frac{kW}{m^2K}\right)\right)^2 \\ \quad + \left(\left(-0.01922\frac{kW}{m^2K}\right)(3.45K)\right)^2\end{array}\right)}$$

$$\approx 10.3K$$

2. δ(ρcδ)

See Chapter 4 for detail.

The uncertainty of the slope of the best-fit line, 0.008878 /s, can be estimated through calculating 2 times the standard error of the slope, which is +/- 0.000583 /s.

$$\frac{\partial(\rho c\delta)}{\partial(slope)} = \frac{-1}{(slope)^2}\left(\frac{\varepsilon\dot{q}''_{cr}}{T_{ig} - T_\infty}\right)$$

$$= \frac{-1}{(0.008878/s)^2}\left(\frac{(0.9)\left(16\frac{\frac{kJ}{s}}{m^2}\right)}{((397+273)K) - ((23+273)K)}\right)$$

$$\approx -488.4\frac{kJ\cdot s}{m^2K}$$

$$\frac{\partial(\rho c\delta)}{\partial\varepsilon} = \frac{1}{(slope)}\left(\frac{\dot{q}''_{cr}}{T_{ig}-T_{\infty}}\right)\varepsilon$$

$$= \frac{1}{(0.008878/s)}\left(\frac{\left(16\frac{\frac{kJ}{s}}{m^2}\right)}{((397+273)K)-((23+273)K)}\right)(0.9)$$

$$\approx 4.818\frac{kJ}{m^2K}$$

$$\frac{\partial(\rho c\delta)}{\partial\dot{q}''_{cr}} = \frac{1}{(slope)}\left(\frac{\varepsilon}{T_{ig}-T_{\infty}}\right)$$

$$= \frac{1}{(0.008878/s)^2}\left(\frac{(0.9)}{((397+273)K)-((23+273)K)}\right)$$

$$\approx 4.337\frac{s}{K}$$

$$\frac{\partial(\rho c\delta)}{\partial T_{ig}} = \frac{-1}{(slope)}\left(\frac{\varepsilon\dot{q}''_{cr}}{T_{ig}-T_{\infty}}\right)\frac{1}{T_{ig}-T_{\infty}}$$

$$= \frac{-1}{(0.008878/s)}\left(\frac{(0.9)\left(16\frac{\frac{kJ}{s}}{m^2}\right)}{((397+273)K)-((23+273)K)}\right)\frac{1}{((397+273)K)-((23+273)K)}$$

$$\approx -0.01160\frac{kJ\cdot s}{m^2K^2}$$

$$\frac{\partial(\rho c\delta)}{\partial T_{\infty}} = \frac{1}{(slope)}\left(\frac{\varepsilon\dot{q}''_{cr}}{T_{ig}-T_{\infty}}\right)\frac{1}{T_{ig}-T_{\infty}}$$

$$= \frac{1}{(0.008878/s)}\left(\frac{(0.9)\left(16\frac{\frac{kJ}{s}}{m^2}\right)}{((397+273)K)-((23+273)K)}\right)\frac{1}{((397+273)K)-((23+273)K)}$$

$$\approx 0.01160\frac{kJ}{m^2K^2}$$

Therefore,

$$\delta(\rho c\delta)=\sqrt{\left(\frac{\partial(\rho c\delta)}{\partial(slope)}\delta(slope)\right)^2+\left(\frac{\partial(\rho c\delta)}{\partial\varepsilon}\delta\varepsilon\right)^2+\left(\frac{\partial(\rho c\delta)}{\partial\dot{q}''_{cr}}\delta\dot{q}''_{cr}\right)^2+\left(\frac{\partial(\rho c\delta)}{\partial T_{ig}}\delta T_{ig}\right)^2+\left(\frac{\partial(\rho c\delta)}{\partial T_{\infty}}\delta T_{\infty}\right)^2}$$

$$=\sqrt{\left(\left(-488.4\frac{kJ\cdot s}{m^2K}\right)(0.000583/s)\right)^2+\left(\left(4.818\frac{kJ}{m^2K}\right)(0.09)\right)^2+\left(\left(4.337\frac{s}{K}\right)\left(1\frac{kW}{m^2}\right)\right)^2+\left(\left(-0.01160\frac{kJ}{m^2K^2}\right)(10.3K)\right)^2+\left(\left(0.01160\frac{kJ}{m^2K^2}\right)(3.45K)\right)^2}$$

$$\approx 4.369\frac{kJ}{m^2K}$$

UNCERTAINTY FOR ESTIMATED PARAMETERS USING BURNING-RATE DATA ANALYSIS

1. $\delta\Delta h_{c,eff}$

Cone test results ranging from 30 to 75 kW/m^2 are used to calculate the effective heat-of-combustion. Uncertainty of this value is estimated with its confidence interval using student t distribution and $\alpha = 0.05$: ± 1.8 kJ/g

2. $\delta\Delta h_g$

See Chapter 4 for detail.

The uncertainty of the slope (=1/Δh_g=0.06136 g/kJ) can be estimated through calculating 2 times the standard error of the slope of the best-fit line, which is +/- 0.01756. Therefore, the uncertainty in Δh_g is

$$\frac{d(\Delta h_g)}{d(slope)}=-\frac{1}{(slope)^2}$$

$$=-\frac{1}{\left(0.06136\frac{g}{kJ}\right)^2}$$

$$\approx -265.6\frac{kJ^2}{g^2}$$

Therefore,

$$\delta(\Delta h_g)=\sqrt{\left(\frac{d(\Delta h_g)}{d(slope)}\delta(slope)\right)^2}$$

$$=\sqrt{\left(\left(-265.6\frac{kJ^2}{g^2}\right)(0.01756g/kJ)\right)^2}$$

$$\approx 4.7\frac{kJ}{g}$$

Table A(C)-35. Summary of model-parameter table with estimated values with uncertainty

Ignition Parameters	T_∞	23 ± 3.45 °C
	T_{ig}	397 ± 10 °C
	$\dot{q}''_{cr}$	16 ± 1 kW/m^2
	$\rho c \delta$	4.333 ± 4.369 kJ^2/m^{4}K^{2}s
Burning-Rate Parameters	$\Delta h_{c,eff}$	25.5 ± 1.8 kJ/g
	Δh_g	16.3 ± 4.7 kJ/g
	h_c	12 ± 0.5 W/m^{2}K
	ε	0.9 ± 0.09

Validation

Analyze Simulation Quality

DETERMINE DATA AND MODEL OUTPUT UNCERTAINTY TO MAKE COMPARISON

1. Conduct uncertainty analysis of data

The uncertainty in the mass-loss-rate data used for comparison between data and model outputs is estimated via statistical approach, taking the standard deviation (0.58 g/sm^2) from the mean of a steady burning of five identical PMMA tests conducted in a cone calorimeter.[2] The estimated uncertainty is 1.4 g/sm^2, which is found by calculating the 95% confidence interval applying student t distribution with a sample size of five

The uncertainty in time-to-ignition data used for comparison is estimated via statistical approach, taking two to three identical cone calorimeter test data at heat fluxes ranging from 25 to 75 kW/m^2 of this FRP composite sheet. 95% confidence interval is calculated for each heat-flux level assuming student t distribution.

2. Conduct uncertainty analysis for MLR profile modeling

Because uncertainty information of the data is found in terms of time-to-ignition and mass-loss rate, the mass-loss-rate profile is considered as the modeling output of interest for comparison purposes. For Simple Analytical Models, time-to-ignition (t_{ig}) and steady-burning rate ($\dot{m}''$) are needed when simulating the mass-release-rate profile. The uncertainty in MLR profile in modeling can be determined via considering the uncertainties in these calculation results as below:

$$t_{ig} \pm \delta t_{ig}$$

$$\dot{m}'' \pm \delta \dot{m}''$$

To determine the uncertainty in time to ignition, recall:

$$\frac{\dot{q}''_{cr}}{\dot{q}''_e} = F(t_{ig}) = \begin{cases} \dfrac{h_{ig}\, t_{ig}}{\rho c \delta} & t_{ig} \le t^* \\ 1 & t_{ig} > t^* \end{cases}$$

Knowing that all of heat flux levels of interest, 25, 50, and 75 kW/m^2, are above the critical heat flux, time-to-ignition should be smaller than t*. Hence, uncertainty in t_{ig} can be estimated from linear-regression process as below:

$$\frac{\dot{q}_{cr}^{"}}{\dot{q}_{e}^{"}} = \frac{h_{ig}}{\rho c \delta} t_{ig}$$

The above equation can be re-written as below after conducting linear regression:

$$y\ estimate = (slope) t_{ig}$$

Therefore,

$$t_{ig} = \left(\frac{y\ estimate}{slope} \right)$$

Assuming that the y estimate and slope are independent and propagating the uncertainties in these two variables in estimating the time-to-ignition, the following calculation can be made:

$$\delta t_{ig} = \sqrt{\left(\frac{\partial t_{ig}}{\partial (y\ estimate)} \delta (y\ estimate) \right)^2 + \left(\frac{\partial t_{ig}}{\partial (slope)} \delta (slope) \right)^2}$$

where

$$\frac{\partial t_{ig}}{\partial (y\ estimate)} = \frac{1}{(slope)}$$

$$\frac{\partial t_{ig}}{\partial (slope)} = -\frac{(y\ estimate)}{(slope)^2}$$

with δ(*y estimate)* and δ(*slope)* estimated through calculating 2 times the standard error of the y estimate and slope of the best-fit line.

To determine the uncertainty in steady heat release rate at post ignition stage, recall:

$$\Delta h_g \equiv \frac{\dot{q}_{net}^{"}}{\dot{m}''} = \frac{\dot{q}_e'' + \dot{q}_f'' - \dot{q}_l''}{\dot{m}''}$$

The above equation can be rearranged to

$$\dot{m}^{"} = \frac{1}{\Delta h_g} \dot{q}_e^{"} + \frac{\dot{q}_f^{"} - \dot{q}_l^{"}}{\Delta h_g}$$

The steady burning rate at post-ignition stage is determined by the best-fit line obtained when data is plotted as steady-burning rate versus applied heat flux. The uncertainty in steady-burning rate can be determined by considering 2 times the standard error of the y estimates, i.e., $\dot{m}''$, which is obtained through linear-regression process: **± 1.2 g/m²s**.

COMPARE DATA WITH SIMULATION RESULTS WITH CONSIDERATION OF UNCERTAINTIES

Parameters in this simple analytical pyrolysis model have been estimated with cone calorimeter test data from 25, 50, and 75 kW/m^2. To check the quality of the modeling using the estimated parameters, three cases have been simulated and compared with experiment data, with the consideration of their uncertainty bands as shown in Table A(C)-36 and figures below. Note the inert residue fraction, including glass layers, of approximately 60% by weight.

Table A(C)-36. Comparison of time-to-ignition at different heat-flux levels from actual experiment and pyrolysis modeling

Heat-Flux Level	Actual t_{ig} (s) $t_{ig} \pm \delta t_i$	Model t_{ig} (s) $t_{ig} \pm \delta t_i$
25 kW/m^2	112 ± 70	72 ± 7
50 kW/m^2	38 ± 3	36 ± 6
75 kW/m^2	25 ± 6	24 ± 6

All three cases show good overlap between the data and simulation of time-to-ignition and the mass-loss rate during steady burning considering the uncertainties, i.e., the parameter estimation was conducted successfully (see Figure A(C)-35, Figure A(C)-36 and Figure A(C)-37).

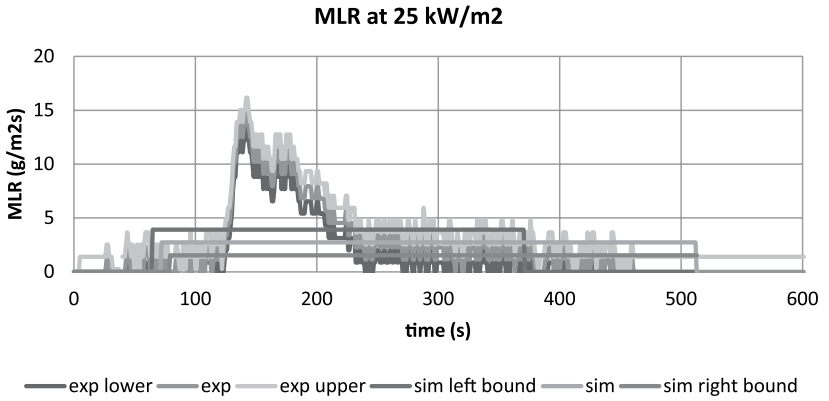

Figure A(C)-35. Mass-loss rate (MLR) comparisons for thin FRP composite sheet between actual MLR from experiment (exp) and modeled MLR (sim) at 25 kW/m². Note that data shown were used to estimate model-parameter values.

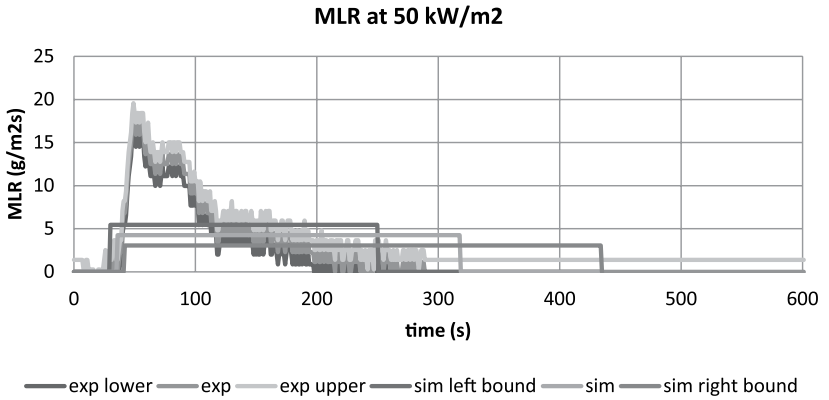

Figure A(C)-36. Mass-loss rate (MLR) comparisons for thin FRP composite sheet between actual MLR from experiment (exp) and modeled MLR (sim) at 50 kW/m². Note that data shown were used to estimate model-parameter values.

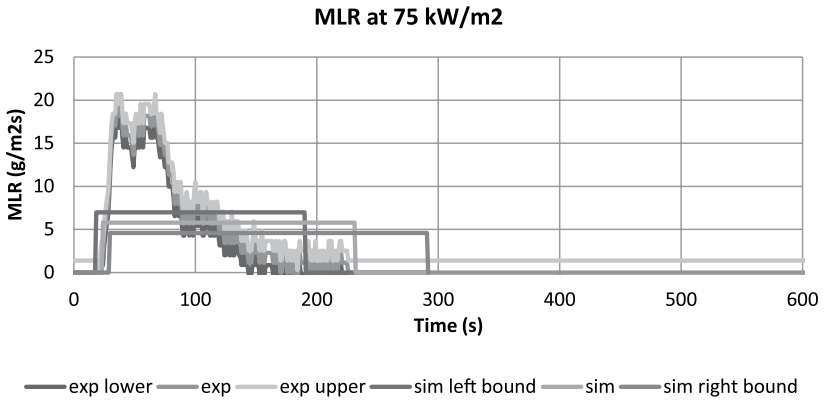

Figure A(C)-37. Mass-loss rate (MLR) comparisons for thin FRP composite sheet between actual MLR from experiment (exp) and modeled MLR (sim) at 75 kW/m^2. Note that data shown were used to estimate model-parameter values.

Commentary

In this example, Simple Analytical Model is used to simulate pyrolysis of thermally-thin-behaving FRP composite sheet. Test data from a bench-scale cone calorimeter experiment at several heat-flux levels have been utilized to estimate the time-to-ignition from exposure to heating and the mass-loss rate at steady burning stage after ignition. The comparison between the model outputs (time-to-ignition and steady-burning rate) and the data from bench-scale experiment showed good agreement for both checking purposes, where the same heat-flux levels (25, 50, and 75 kW/m^2) used in parameter estimation have been considered. To improve modeling results, one may consider taking the peak average of the mass-loss rate and the heat-release rates to estimate heat-of-gasification, for most of the burning occurs near the peak. The tail following the peak (MLR or HRR curve) extends for a longer period of time until flameout, where a smaller percentage of the combustible resin between fiberglass layers is burning off at in-depth.

Although the modeling predictions of time-to-ignition and steady-burning rate in this example seem to be reasonable, limitation of this Simple Analytical Modeling should be noted, which is that the model is for thermally-thin-behaving materials and steady burning after ignition.

References

1 Beaulieu, P.A.; and Dembsey, N.A., "Flammability Characteristics at Applied Heat Flux Levels up to 200 kW/m²", *Fire and Materials*, 32:2 (2008) 61-86. [DOI10.1002/fam.948]

2 Zhao, Lei, Bench Scale Apparatus Measurement Uncertainty and Uncertainty Effects on Measurement of Fire Characteristics of Material Systems, MS Thesis, Fire Protection Engineering, WPI, 2005-04-27, ETD-050105-182456

Appendix D
Example Solutions for Chapter 5

Example Solutions for Chapter 5. 295
Example 5.1 Modeling PMMA 295
Measure Parameters 295
Obtain Parameters via Numerical Optimization 299
Validation 303
Example 5.2 - Modeling Corrugated Cardboard 310
Measure Parameters 310
Obtain Parameters via Numerical Optimization 312
Validation 318
Commentary 322
Example 5.3 Modeling Modified Acrylic FRP Composite 325
Measure Parameters 326
Obtain Parameters via Numerical Optimization 332
Validation 338
Commentary 345
Example 5.4 Modeling Plywood 348
Measure Parameters 348
Obtain Parameters via Numerical Optimization 351
Validation 355
Commentary 360
References. 362

Example Solutions for Chapter 5

Example 5.1 Modeling PMMA

An example case is shown for a poly(methylmethacrylate), PMMA. Most of the approach and reference values of the input parameters for this simulation were obtained from Stoliarov's work.[1] Note that for this example, three approaches will be used to estimate model parameters: (1) direct measurement, literature search or approximation denoted as Approach A; (2) combination of non-optimization and optimization method denoted as Approach B-GA, B-SCE or B-SHC; and (3) mostly optimization method denoted as Approach C-GA, C-SCE or C-SHC. For optimization routines, Genetic Algorithm (GA), Shuffled Complex Evolution (SCE), or Stochastic Hill-climber (SHC) is applied.

Measure Parameters

When conducting parameter estimation via independent experiments, consider the following:

- Check consistency between model used in experiment analysis and pyrolysis model
- Use statistical approach for determining uncertainty, otherwise, meet equivalency to this requirement

1. Density

Bulk density is measured by the cone calorimeter experiment conducted at room temperature (≈298K), weighing sample's mass, and dividing mass with sample volume, which was 1200 kg/m^3.

$$\rho = 1200 \text{ kg/m}^3$$

2. Thermal Conductivity

This was measured using a Thermoflixer apparatus (SWO Polymertechnik GmbH), which is based on the transient line source method.[2] The author had mentioned in this work[1] that the values determined from this experiment were significantly lower than the values from the literature, which were ranging from 0.19 to 0.25 W/m-K[3]. The difference in the measurements from different laboratories was explained by the sensitivity of the thermal conductivity to subtle variations in the polymer structure. See Figure A(D)-1 for comparison.

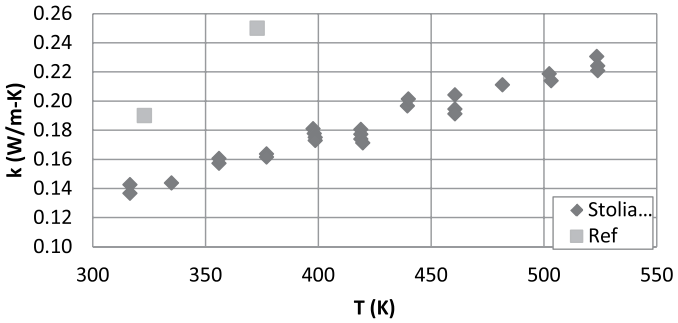

Figure A(D)-1. Thermal conductivity of PMMA

3. Specific-heat Capacity

This was measured using Differential Scanning Calorimetry (DSC). Details of this work are reported in ref[4]. From ref[4] a figure that compares Stoliarov's measurements to other reference[5] is reproduced (see Figure A(D)-2). In the simulation in this example, for consistency, Stoliarov's measurements will be used.

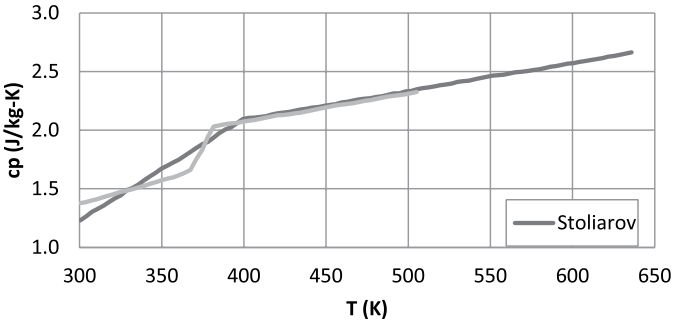

Figure A(D)-2. Heat capacity of PMMA

4. Absorption Coefficient

An expression (based on the assumption of exponential attenuation) that relates the transmissivity (τ) and absorption coefficient (α), where l is the polymer film thickness can be given as below:

$$K_s = \frac{2\ln(1-r) - \ln\tau}{l}$$

$$\mathbf{K_s = 2700/m}$$

5. Emissivity

To estimate emissivity of PMMA, average reflectivity was found by averaging the wavelength-dependent reflectivities measured over emissive-power distributions of a blackbody at 1000K, knowing that this temperature is the closest match to radiant-heater temperatures used in the burning-rate measurements. Emissivity of PMMA was estimated to be 1 – reflectivity.

$$\varepsilon = \mathbf{0.85}$$

6. Reaction Order, Pre-exponential Factor and Activation Energy

For this example case, where decomposition kinetics type is 2 (single peak in DTG over entire mass loss temperature range), the following approach is applicable:

CONDUCT DYNAMIC THERMOGRAVIMETRIC ANALYSIS (TGA) EXPERIMENTS IN NITROGEN

Thermogravimetic Analysis (TGA) experiments are conducted at various heating rates – 0.05, 0.17 and 0.5 K/s – with samples sizes ranging from 2 to 5 mg. Temperature range used in the tests is from 373 to 1003 K with nitrogen as purging gas. Considering that the decomposition-reaction rate can be written as weight-loss rate measured from TGA tests, reaction rates were calculated by numerical differentiation of mass loss data as:

$$r = \frac{\Delta m/m_0}{\Delta t}$$

1. Applying Arrhenius expression and assuming one-step decomposition-reaction mechanism, where virgin material decomposes to fuel vapor leaving no residue with first-order reaction-kinetic model, the reaction rate can be expressed in terms of weight loss and temperature. Note that n value is pre-determined as 1. This expression is consistent with FDS pyrolysis model.

$$r = Aexp\left(-\frac{E}{RT_s}\right)\left(\frac{1-m}{m_0}\right)^1$$

2. Plot $ln\left(\frac{r}{\left(\frac{1-m}{m_0}\right)^1}\right)$ vs. $\frac{1}{T}$ for all data obtained from different heating-rate experiments.

   Applying log to each side of the equation and rearranging it gives the following:

$$ln\left(\frac{r}{\left(\frac{1-m}{m_0}\right)^1}\right) = ln(A) - \frac{E}{RT}$$

   Therefore, plotting LHS term versus 1/Ts allows determination of activation energy (slope) and the pre-exponential coefficient (intercept) as shown in Figure A(D)-3 (reproduced from reference[1]).

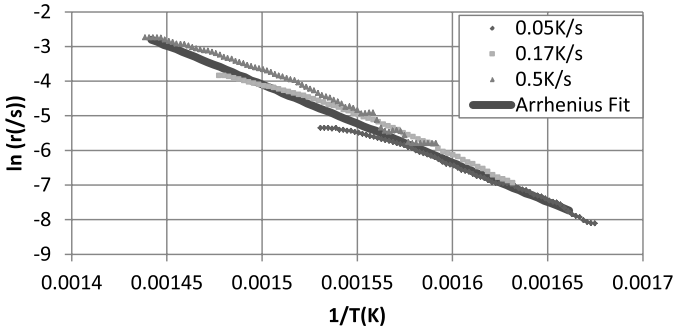

Figure A(D)-3. Kinetic modeling for decomposition of PMMA under nitrogen atmosphere: Arrhenius equation with n = 1 reaction model is used.

3. According to the good fitness of the linear trendline to the overall data with different heating rates, first-order approximation utilized in this kinetic modeling seems to be appropriate. The final estimated kinetic parameter values are:

$$\mathbf{A = 8.5 \times 10^{12}\ (/s);\ E = 1.88 \times 10^{5}\ (J/mol)}$$

7. Heat of Reaction

Heat-of-decomposition reaction was measured by Stoliarov in his previous work using Differential Scanning Calorimetry (DSC) with nitrogen as purging gas.[4] Heat is normalized by its initial sample weight.

$$\mathbf{\Delta H_r = 870\ kJ/kg}$$

Summary

The uncertainties in the estimated properties are as follows (see Table A(D)-1) for measured values. Note that these are determined from the data scatter and expressed as ±2 normalized standard errors. The standard errors are normalized by their mean. Exceptions are the uncertainties in emissivity and absorption coefficient, where crude estimates are given by the author due to lack of information. Note that although modeling PMMA can be done by direct mode, i.e., model parameters are estimated via direct measurements, literature search, and/or approximations, for comparison purposes two other approaches are considered in this example – using some or mostly optimization to estimate unknowns.

Table A(D)-1. Summary of estimated uncertainty for each model parameter

	No	Condense Phase (*i=1*)		Uncertainty (%)
Material Property	**1**	ρ_i	Density	± 5
	2	k_i	Thermal conductivity	± 15
	3	c_i	Specific-heat capacity	± 15
	4	κ_i	Absorption coefficient	± 50
Parameters for Specifying Conditions	**5**	ε_i	Emissivity	± 20
		Heterogeneous RxN (*k=1*)		
Heats assuming n^{th} order model and Arrhenius-type expression	**6**	n_k	Reaction order	N/A
		Z_k	Pre-exponential factor	± 50
		E_k	Activation energy	± 3
	7	ΔH_k	heat	± 15

Obtain Parameters via Numerical Optimization

Run model or Run Model in Pair with Numerical Optimization

SELECT MODEL: GPYRO

UNDERSTAND BENCH-SCALE EXPERIMENT SET-UP FOR MODELING SIMPLE CASES

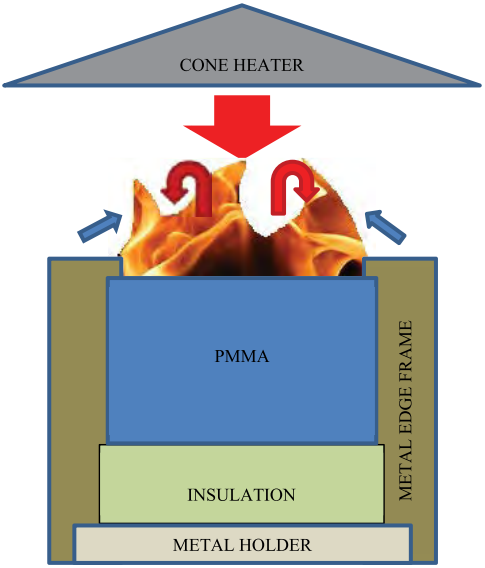

Figure A(D)-4. Simplified representation of a cone calorimeter test of PMMA

A simplified representation of a cone calorimeter test of PMMA is shown in Figure A(D)-4. The sample is placed on top of an insulation, which sits on a metal holder. Another metal frame is placed on top of the sample, insulation and the holder. A metal edge frame is used as well to allow the sample to be stationary with good contact between underlying insulation during decomposition with surface regression.

Front Surface: As heating starts by opening the shutter to allow radiation from the cone heater to heat the sample surface (large red arrow), cooling also begins via natural convection (blue arrows) and re-radiation. The surface decomposes with bubbling with respect to temperature increase occurring through heat conduction and/or in-depth radiative transport. The pyrolyzates leave through the surface until complete burn-off, because this material leaves no residue. When ignition occurs as the fuel-vapor concentration above the surface exceeds its LFL (lower flammable limit), additional heat flux from the flame is introduced on the surface (red arrows). Regression of the sample surface with respect to consumption of PMMA in pyrolysis occurs.

Back surface: The sample is placed on top of insulation. In the experiment, an air gap of a few millimeters thickness exist between the sample and the insulation due to thermal contact. Due to the insulation, nothing leaves through the back face when 1D assumption holds for the experiment.

CONFIGURE MODEL CONDITIONS BASED ON UNDERSTANDING OF EXPERIMENT SET-UP

In the model, the phenomena discussed above are simulated as below. Basic assumptions are as follows:

- Instantaneous release of volatiles from solid to the gas phase
- Local thermal equilibrium between the solid and the volatiles
- No condensation of gaseous products
- No porosity effects

Further details can be found from the *Technical Reference*[6] and *User's Guide*[7] of FDS (http://www.fire.nist.gov/fds/documentation.html).

When conducting the FDS simulation for the cone calorimeter set-up, the metal edge frame will be ignored and backing is insulated. Gas-phase combustion will be turned off by assuming that the ambient oxygen concentration is less than 10% (Yo2 = 0). Heat flux from the cone is set by using EXTERNAL_FLUX at the sample surface. The ignition phenomenon is interpreted as the following in the simulations: when mass-burning rate is above 10 $kW/m^2/\Delta H_c$,(criteria based on experiment observations[1]), additional heat flux of 20 kW/m^2 is added to EXTERNAL_FLUX to include the heating from the flame, assuming that the flame is transparent. This is the reference value found from the work of Beaulieu[8], where actual measurement of the flame heat flux of a black PMMA was conducted. The heat-of-combustion was determined using a microscale combustion calorimeter[9] operating in the following condition: pyrolysis in nitrogen atmosphere by heating samples (2 to 4 mg) at a fixed rate of 1 K/s from 373 to 1173 K. The value is normalized by initial sample weight: ΔH_c = 24100 kJ/kg

ACQUIRE DATA SETS THAT CAN REPRESENT BURNING BEHAVIOR OF INTEREST[i] OR THAT CAN BE USED IN NUMERICAL OPTIMIZATION PROCESS IN PAIR WITH PYROLYSIS MODELING FOR OBTAINING UNKNOWN MODEL PARAMETER VALUES[ii]

1. Maximum heat-flux level of interest for this parameter estimation is approximately 100kW/m^2.
2. Cone alorimeter test data of thick PMMA (thickness, δ ranging from 24 ~ 29 mm) impinged with effective heat fluxes (EHF) of 23, 46, and 69 kW/m^2 is found to show the burning behavior under various heat flux levels that are less than 100 kW/m^2. Data were reproduced from Stoliarov's paper,[1] which are shown in Figure A(D)-5:

[i] The simulations are conducted in a direct mode (i.e., all input values are obtained through other sources, such as references or independent measurements); hence, no data will be used to optimize the final results. However, cone calorimeter test data will be used to make the comparison between the simulation results and experiment data.

[ii] To conduct simulations, unknown parameters need to be obtained via numerical optimization for independent measurements of those parameters are cumbersome and impossible in most cases.

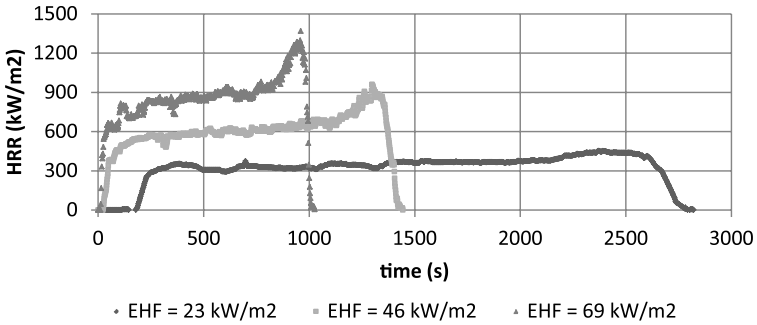

Figure A(D)-5. Cone experiment results of PMMA with effective heat flux and thickness ranging from 23 to 69 kW/m² and 24 to 29 mm, respectively

SELECT NUMERICAL OPTIMIZATION ROUTINE

- Genetic Algorithm (GA)
- Shuffled Complex Evolution (SCE)
- Stochastic Hill-climber (SHC)
- See Chapter 5 for more description of each optimization routine.

CONDUCT SIMULATIONS FOR THESE CASES TO COMPARE SIMULATION OUTPUT TO EXPERIMENT DATA, OR CONDUCT NUMERICAL OPTIMIZATION IN PAIR WITH SIMULATIONS USING EXPERIMENT DATA AS TARGETS

Simulations with GPYRO for the above three cases with EHF = 23 kW/m², EHF = 46 kW/m², and EHF = 69 kW/m² with sample thickness, δ = 26 mm are conducted.

*Obtain Confidence Intervals for Optimized Parameters**

- Baseline case: HF = 46 kW/m², thickness = 29 mm
- Sensitive parameters varied one at a time from baseline to its max and min by considering uncertainty; however, due to the compensation effect, pre-exponential factor and activation energy will be considered in pair to have max and min decomposition temperature
- Uncertainty is considered for GA optimization cases (B-GA, C-GA) only using 50 near-optimal parameter sets
- Integration of uncertainty is calculated by the Law of Propagation of Uncertainty

Parameter Estimation Results

ID			A	B-GA	B-SCE	B-SHC	C-GA	C-SCE	C-SHC
Parameter		Unit	Measurement, Literature, or Approximation	Comparable Non-optimization and Optimization			Mostly Optimization		
Thermo-physical Property	ρ_i	kg/m^3	1200 ± 60	1200 ± 60			1200 ± 60		
			Measurement	Measurement			Measurement		
	k_i	W/m-K	0.18 ± 0.01	0.30 ± 0.01	0.21	0.33	0.29 ± 0.01	0.29	0.19
			Literature[10]	GA	SCE	SHC	GA	SCE	SHC
	c_i	J/kg-K	2.2 ± 0.1	1.8 ± 0.1	0.7	1.7	2.0 ± 0.1	1.1	1.7
			Literature[4,10]	GA	SCE	SHC	GA	SCE	SHC
Optical Property	κ_i	/m	2700 ± 1400	± 86000	1000000	3600000	2200 ± 500	790000	350000
			Literature[10]	GA	SCE	SHC	GA	SCE	SHC
	ε_i	-	0.85 ± 0.16	0.91 ± 0.01	0.66	0.89	0.66 ± 0.01	0.99	0.54
			Literature[1]	GA	SCE	SHC	GA	SCE	SHC
Thermal Decomposition Kinetics and Heats	n_k	-	1	1			0.5 ± 0.1	0.5	1.5
			Approximated	Approximated			GA	SCE	SHC
	Z_k	/s	(8.5 ± 4.3) x 10^{12}	(8.5 ± 4.3) x 10^{12}			(1.3 ± 0.6) x 10^{16}	3.3 x 10^{15}	5.3 x 10^{19}
			Model Fitting with multiple heating rate TGA data	Model Fitting with multiple heating-rate TGA data			GA	SCE	SHC
	E_k	J/mol	(1.88 ± 0.06) x 10^5	(1.88 ± 0.06) x 10^5			(1.77 ± 0.01) x 10^5	2.27 x 10^5	2.43 x 10^5
			Model Fitting with multiple heating rate TGA data	Model Fitting with multiple heating-rate TGA data			GA	SCE	SHC
	ΔH_k	kJ/kg	870 ± 130	870 ± 130			1100 ± 21	1300	520
			Literature[4]	Literature[4]			GA	SCE	SHC
Model Dependent Parameter	h_{crz}	W/m^2-K	0	12 ± 3	2	14	38 ± 4	3	-32
			Approximated adiabatic condition at back surface	GA	SCE	SHC	GA	SCE	SHC

Validation

Analyze Simulation Quality

IDENTIFY SENSITIVE PARAMETERS FOR MODEL INPUTS

- ε_i, n_k, Z_k, E_k, ΔH_k
- See Chapter 5 for detail

DETERMINE DATA AND MODEL OUTPUT UNCERTAINTY

1. Check data reproducibility by repeating identical experiments[iii]

Data is acquired from five repeated PMMA tests under 49 kW/m^2 heat-flux level with medium-thickness samples (thickness, δ ranging from 7.7 ~ 9.4 mm).

2. Conduct uncertainty analysis of data

Uncertainty in PMMA cone calorimeter experiment is estimated based on five repeated PMMA tests under 49 kW/m^2 heat-flux level with medium-thickness samples (thickness, δ ranging from 7.7 ~ 9.4 mm). The surface temperatures measured from these tests showed that the values ranged from 260 to 370°C. The uncertainty of peak HRR, average HRR, time-to-ignition, and-time-to peak HRR are estimated by the five repeating PMMA tests via, taking two standard deviation of the difference and normalizing them by the mean of this parameter. Table A(D)-2 shows the analysis results from the tests, which were reproduced from Stoliarov's paper.[1] Assume that the uncertainty values estimated for five repeating PMMA tests conducted at 49 kW/m^2 heat flux level with medium-thickness samples are comparable to those of tests conducted under various heating rates, ranging from 23 to 69 kW/m^2 using thick PMMA samples.

Table A(D)-2. Summary of estimated uncertainty in PMMA cone calorimeter experiments based on 5 repeating tests under 49 kW/m^2 heat-flux level with medium-thickness sample (7.7 ~ 9.4 mm)

	peakHRR (kW/m^2)	avgHRR (kW/m^2)	t_{ig} (s)	t-peakHRR (s)
Average case	990	560	44	430
Uncertainty (%)	17	7	12	17

3. Conduct uncertainty analysis of model outputs of interest

The baseline case was selected at simulation with EHF = 46 kW/m^2, thickness = 26 mm. Sensitive parameters – ε_i, n_k, Z_k, E_k, ΔH_k – are varied in the simulations one at a time from baseline case.

- The effect of variation is calculated by considering the peak HRR (peakHRR), average HRR (avgHRR), time to peak HRR (t-peakHRR), and surface temperature (T_s). Results are shown in Table A(D)-3.

[iii] In general, data uncertainty is used to analyze the sensitivity of the input parameters; in numerical optimization to estimate unknown parameters; or to evaluate simulation quality later in the process. In this example, data uncertainty will be accounted for here, where simulation results with its uncertainty band are compared with data with its uncertainty band.

- Uncertainty for those modeling outputs is calculated using the Law of Propagation of Uncertainty. Note that when inputs are varied to its uncertainty boundary values – minimum or maximum – the maximum effect was selected in the analysis to estimate the maximum uncertainty.

Table A(D)-3. Comparison between experiment data from cone calorimeter test and modeling outputs using estimated parameter values via either direct measurement, literature search, or approximation (a); measurements and numerical optimization (B-GA, B-SCE, B-SHC); or mostly numerical optimization (C-GA, C-SCE, C-SHC)

	Data	A	B-GA	B-SCE	B-SHC	C-GA	C-SCE	C-SHC
Peak MLR (g/m^2s)	36.9 ±6.3	45.1 ±10.6	40.9 ±5.3	32.6	39.3	27.5 ±0.7	34.4	67.0
Avg MLR (g/m^2s)	24.9 ±1.7	24.2 ±5.2	26.7 ±2.7	25.9	26.6	24.0 ±0.5	26.4	28.0
t to pMLR (s)	1310 ±223	1408 ±252	1285 ±123	1317	1284	1391 ±32	1297	1233
Ts (°c)	350 ±50	413 ±21	433 ±20	407	409	244 ±3	419	343

COMPARE DATA WITH SIMULATION RESULTS

1. TG / DTG Predictions at 10 °C/min Heating Rate Using Estimated Kinetic Parameters

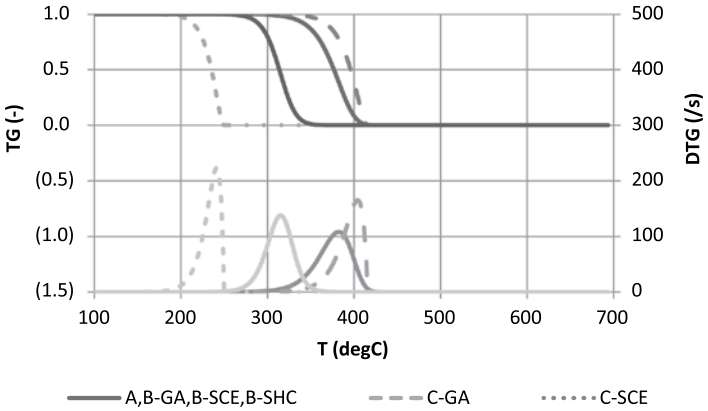

Figure A(D)-6. TG/DTG curves at 10°C/min heating rate with different estimation results for kinetic parameters for thermal decomposition of PMMA

2. Modeling Output: Mass-Loss Rate (MLR)

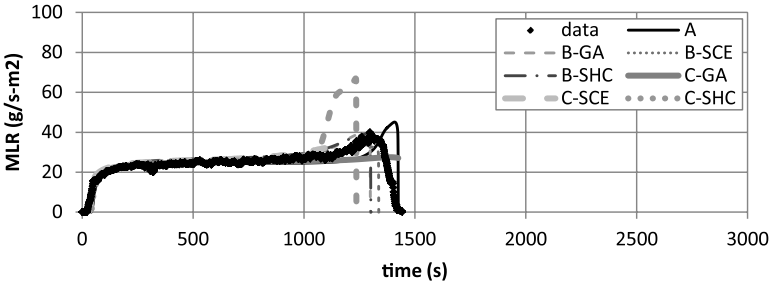

Figure A(D)-7. Mass-loss rate (MLR) comparisons for PMMA between actual MLR from experiment (data) and modeled MLR (A, B-GA, B-SCE, B-SHC, C-GA, C-SCE, C-SHC) at applied heat flux of 46 kW/m². Note that data shown were used to estimate model parameter values via numerical optimization using GA, SCE, or SHC routines.

3. Modeling Output: Surface Temperature (T_{surf})

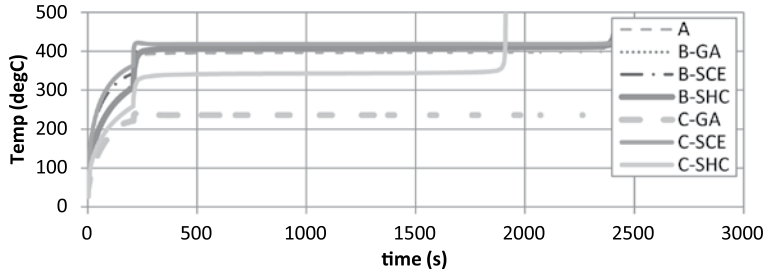

Figure A(D)-8. Surface temperature (T_{surf}) comparisons for PMMA modeling using parameters estimated from different approaches – direct measurement, literature search, or approximation (A); measurement and numerical optimization (B-GA, B-SCE, B-SHC); mostly numerical optimization (C-GA, C-SCE, C-SHC) at applied heat flux of 46 kW/m². Note that data shown were used to estimate model-parameter values via numerical optimization using GA, SCE, or SHC routines.

Validate simulation quality upon extrapolation

1. Modeling Output: Mass Loss Rate (MLR)

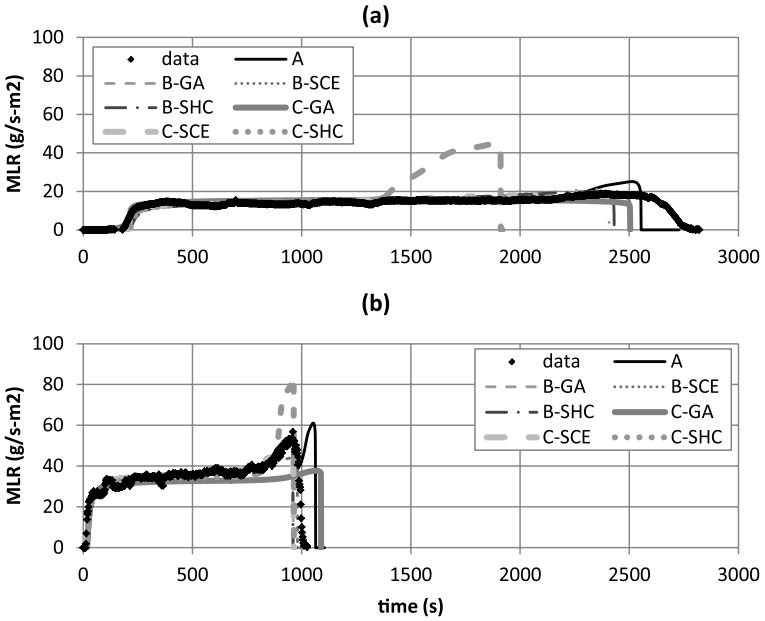

Figure A(D)-9. Mass-loss rate (MLR) comparisons for PMMA between actual MLR from experiment (data) and modeled MLR (A, B-GA, B-SCE, B-SHC, C-GA, C-SCE, C-SHC) at applied heat flux of (a) 23 and (b) 64 kW/m². Note that data shown were not included in the model- parameter-estimation process; hence, these two cases are considered as extrapolation cases.

2. Modeling Output: Surface Temperature (T_{surf})

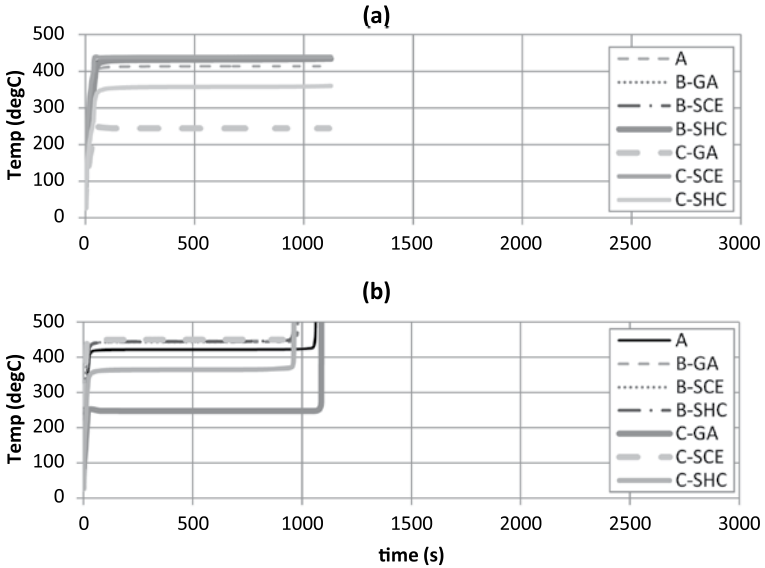

Figure A(D)-10. Surface temperature (T_{surf}) comparisons for PMMA modeling using parameters estimated from different approaches – direct measurement, literature search, or approximation (A); measurement and numerical optimization (B-GA, B-SCE, B-SHC); mostly numerical optimization (C-GA, C-SCE, C-SHC) at applied heat flux of (a) 23 and (b) 64 kW/m². Note that data shown were not included in the model-parameter-estimation process; hence, these two cases are considered as extrapolation cases.

Commentary

General Comments

- TG/DTG
  - Whether kinetic modeling is conducted independently using TGA data (A, B-GA, B-BSE, B-SHC) or as a part of numerical optimization (C-GA, C-SCE, C-SHC), decomposition of PMMA is considered to occur within the temperature range of 200°C to 400°C.
  - Among GA, SCE, and SHC, estimation of SCE was closest, followed by SHC and GA to TGA data.
  - Having surface-temperature data as additional optimization target should have provided constraints to the optimization problem, for kinetic parameters directly determine the surface temperature. However, this approach was not utilized, for uncertainty in surface-temperature measurements was too high – 350 ± 50°C

- Comparison between Data and Computed Modeling Outputs
  - Better agreement between data and modeling outputs for the peak MLR is found when kinetic parameters are estimated through a separate process using TGA data (A, B-GA, B-BSE, B-SHC) than numerical optimization along with estimating other unknowns together (C-GA, C-SCE, C-SHC).
  - Avg MLR and time to peak MLR from all modeling cases show good agreement with data.
  - Simulated surface temperature at steady burning of PMMA is greater (less than 10 s) than that of measurement for cases B-GA, B-SCE, B-SHC, and C-SCE, while simulated surface temperature is lower (greater than 50 s) than that of measurement for case C-GA. Results from cases A and C-SHC are in good agreement.
- MLR
  - Direct Measurement or Optimization at HF = 46 kW/m^2: Good agreement exists between experiment data and all modeling results, whether modeled with measured parameters or optimized in the time frame of exposure to heating source up to steady burning. However, in the later time, where the peak occurs, result from C-SHC becomes unsatisfying, considering the data with its uncertainty, while others can be considered as satisfying.
  - Direct Measurement or Extrapolation at HF = 23 kW/m^2: Good agreement exists between experiment data and all modeling results, except for the C-SHC case.
  - Direct Measurement or Extrapolation at HF = 64 kW/m^2: Good agreement exists between experiment data and all modeling results, except for C-GA and C-SHC cases.
- Surface Temperature
  - See above.

Limitation in Modeling

- When considering limitation of the parameters in simulating PMMA, the modeler should take into account the applicability of the parameters and their associated uncertainties. For example, any assumptions used when determining a parameter value via experiment direct or indirect measurements can be utilized to understand when the parameter value becomes inappropriate. For this example of pyrolysis modeling of PMMA, most consideration can be given to the parameters related to decomposition kinetics.
- In this example, kinetic modeling for this example was conducted with TGA data obtained from a nitrogen environment. However, studies[8,10,11] have suggested that PMMA decomposes differently with respect to heating rates and availability of oxygen. The decomposition rate of PMMA increases with respect to oxygen concentration, because oxygen aids unzipping of the polymer by being involved in the depolymerization process of the polymer. Also, the oxygen dependency increases at lower heating rates than at higher heating rates. A possible explanation for this can be given by considering the diffusion of oxygen from the nearby gas phase to the condense phase. At lower heating rates, the decomposition rate is relatively slow; therefore, the time allowed for oxygen to diffuse to the polymer layer and be involved in the decomposition process is relatively longer. However, at

higher heating rates, the decomposition rate is relatively higher even without the involvement of oxygen in the decomposition process. This results in shorter time scale for transportation of oxygen via diffusion to the condense phase. In other words, the positive effect of enhancing decomposition by having oxygen involved in the process, compared to decomposition in non-oxidative condition, is compensated by the time necessary for oxygen diffusion to occur from the gas phase to the condense phase. Hence, the increase in decomposition rate of PMMA due to the presence of oxygen in the gas phase is more profound in conditions with lower heating rates than in higher heating rates. Visual observations of the surface phenomena during PMMA decomposition also provide evidence that the above explanation is reasonable. Based on experimental work conducted by Beaulieu,[8] during decomposition of PMMA, "bubbling" occurs on the surface. The bubbles are relatively large, forming a thick layer of bubbles when irradiated at lower heat-flux levels; and they are smaller, forming a thin bubbling layer, when irradiated at higher heat-flux levels. Considering that bubbling is an effective way for the polymer to enhance oxygen diffusion and larger bubbles entrains more oxygen, reduction in the decomposition rate due to the increasing time necessary for oxygen diffusion at higher heat-flux levels seems plausible with bubbles becoming smaller as increasing from a lower heat flux to a higher heat flux.

- Figure A(D)-11 is TGA a thermogram of PMMA decomposition conducted under constant heating rates – 2, 5, 10, and 20 K/min – and two different environments – nitrogen and air (data obtained from work conducted by Matala[13]). As shown below and discussed earlier, there is significant difference between the curves produced from nitrogen and air tests. This indicates that decomposition kinetics are different in the two cases, and the difference is due to oxygen diffusion from the gas phase surrounding the solid sample surface with respect to the "bubbling" phenomenon.

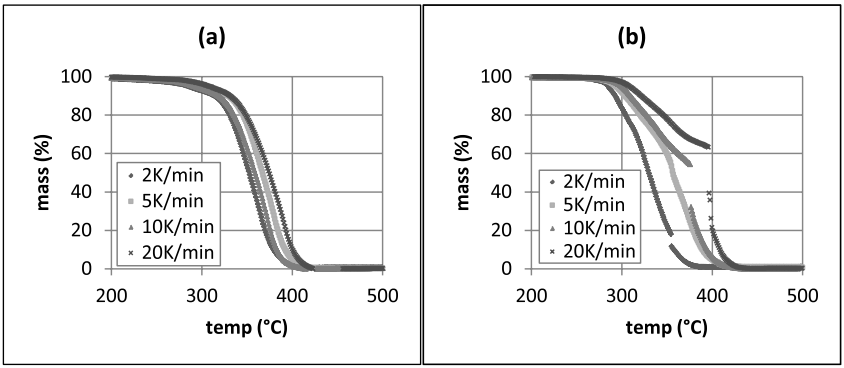

Figure A(D)-11. TGA thermograms of PMMA decomposition conducted under constant heating rates – 2, 5, 10 and 20K/min – and two different environments – (a) nitrogen and (b) air

Example 5.2
Modeling Corrugated Cardboard

An example case is shown for triple-layered corrugated cardboard. Most of the approach and reference values of the input parameters for this simulation were obtained from Chaos' work.[14,15] Note that for this example, two approaches will be used to estimate model parameters – (1) combination of non-optimization and optimization method denoted as Approach B-GA, B-SCE or B-SHC; and (2) mostly optimization method denoted as Approach C-GA, C-SCE or C-SHC. For optimization routines, Genetic Algorithm (GA), Shuffled Complex Evolution (SCE), or Stochastic Hill-climber (SHC) is applied.

Measure Parameters

When conducting parameter estimation via independent experiments, consider the followings:

- Check consistency between model used in experiment analysis to determine parameter in measurement process and pyrolysis model to mathematically describe the parameter of interest.
- Use statistical approach for determining uncertainty, otherwise meet equivalency to this requirement.

1. Density

Although corrugated cardboard is porous and the cross-section is not homogeneous, it is considered a homogeneous single-layer material with relatively low bulk density to account for its porous nature. Bulk density of the virgin fuel material is measured by experiment conducted at room temperature (≈298K), weighing sample's mass and dividing mass with sample volume, which is 110 kg/m^3 for this type of corrugated cardboard.

$$\boldsymbol{\rho = 110\ kg/m^3}$$

2. Thermal Conductivity

Not measured; will be obtained via numerical optimization.

3. Specific-heat Capacity

Not measured; will be obtained via numerical optimization.

4. Absorption Coefficient

Both virgin fuel and residue solid-phase materials involved in modeling are considered as an opaque material. Therefore, the absorption coefficient is essentially infinity.

$$\kappa_{fuel} \text{ and } \kappa_{residue} \rightarrow \infty$$

5. Emissivity

Not measured; will be obtained via numerical optimization.

6. Reaction Order, Pre-exponential Factor and Activation Energy

This example case is determined to have decomposition kinetics type 2 (single peak in DTG over entire mass-loss temperature range) according to TGA experiment conducted in nitrogen atmosphere (see Figure A(D)-12). Based on this information, kinetic parameters will be obtained via a model fitting method using single heating rate TGA data or numerical optimization. Actual TGA data of a generic corrugated cardboard tested in nitrogen environment is shown below. There is less than 10% of moisture loss near 100°C, which has been excluded from the thermogram to only account for the major DTG peak occurring after 200°C. Therefore, kinetic modeling is conducted for a dry-state corrugated cardboard.

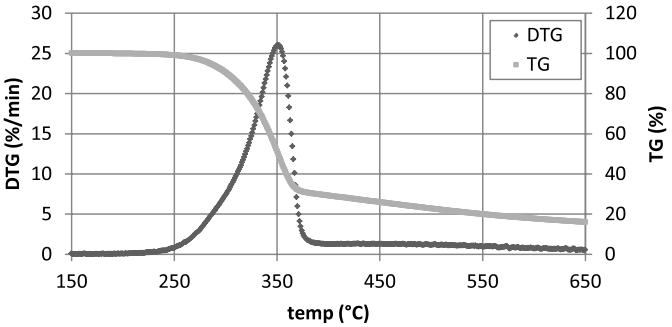

Figure A(D)-12. TGA thermogram (TG and DTG) of corrugated cardboard decomposition conducted under 20K/min heating rate and nitrogen environment

7. Heat of Reaction

Not measured; will be obtained via numerical optimization.

Summary

Among seven categories of parameters, only two have been obtained via direct measurement – fuel virgin bulk density and absorption coefficients of fuel and residue, which are shaded in the table below (see Table A(D)-4). The rest of the unknown parameters, **total of 11 parameters**, should be obtained via numerical optimization in pair with pyrolysis modeling using bench-scale experiment data or equivalent.

Table A(D)-4. Summary of necessary model parameters for simulating pyrolysis of corrugated cardboard

	No	Condense Phase	
		(*i=1, fuel*)	(*i=2, residue*)
Material Property	1	ρ_1	ρ_2
	2	k_1	k_2
	3	c_1	c_2
	4	κ_1	κ_2
Parameters for Specifying Conditions	5	ε_1	ε_2
		Heterogeneous RxN (*k=1*)	
Kinetic Parameters and Heats assuming nth order model and Arrhenius-type expression	6	n_1	
		Z_1	
		E_1	
	7	ΔH_1	

Obtain Parameters via Numerical Optimization

Run Model in Pair with Numerical Optimization

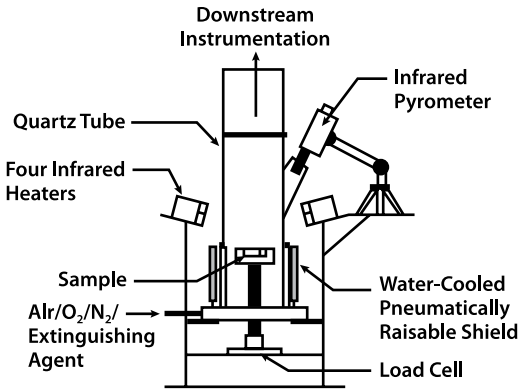

Figure A(D)-13. Schematic of the FPA

SELECT MODEL: SIMPLIFIED 1D MODEL BASED ON GPYRO

UNDERSTAND BENCH-SCALE EXPERIMENT SET-UP FOR MODELING SIMPLE CASES: DESCRIPTION REPRODUCED FROM CHAOS' PAPER[1]

A schematic of the FPA used in this study is shown in Figure A(D)-13. The present apparatus differs from that described in the ASTM standard[16] in that high-power high-density infrared heaters (Research Inc., Model 5209) are used, which can yield heat fluxes approaching 120 kW/m^2. In addition, a humidity control and delivery system[17] can control the relative humidity of the gas supply to the FPA. A flow of 100 SLM of pure nitrogen was used for all experiments (i.e., pyrolytic conditions). In the experiments, insulated circular samples[18] 9.6 cm in diameter were placed on a load cell (0-1000 g range, 0.1 g accuracy, 20 mg peak-to-peak noise), which provided a continuous record of their weight during the pyrolysis process. A water-cooled shield was used to protect the sample from exposure while the heaters stabilized at a specific heat-flux setting. A quartz tube (162 mm inner diameter) shielded the sample and gasification products from room-air entrainment. An infrared pyrometer (Heitronics KT19.81-11) was used to measure surface temperature. The wavelength range of the pyrometer is 8-10 μm, which required modification of the quartz tube used, as quartz is not transparent at these wavelengths. The pyrolysis tests performed in this study cover a heat-flux range of 20-110 kW/m^2. This ensures that both thermally thin and thick regimes are treated so that properties determined with the present approach can be applicable to practical fire conditions.

CONFIGURE MODEL CONDITIONS BASED ON UNDERSTANDING OF EXPERIMENT SET-UP

Basic assumptions are as follows:

- Instantaneous release of volatiles from solid to the gas phase
- Local thermal equilibrium between the solid and the volatiles
- No condensation of gaseous products
- No porosity effects

Further details can be found from Reference 15.

When conducting the 1D simulation for the FPA set-up, insulation at back surface is not modeled explicitly, but is included as some heat loss to the back surface. In this example case, only FPA experiment with nitrogen as purge gas will be considered; hence, there is no ignition phenomenon to be modeled.

ACQUIRE DATA SETS THAT CAN BE USED IN NUMERICAL OPTIMIZATION PROCESS IN PAIR WITH PYROLYSIS MODELING FOR OBTAINING UNKNOWN MODEL PARAMETER VALUES[iv]

1. The maximum heat-flux level of interest for this parameter estimation is 20 to 110kW/m^2, considering that estimated parameters will be used in modeling of parallel panel experiment of corrugated cardboard. Fire Propagation Apparatus (FPA) test data of triple-wall corrugated cardboard, i.e., two layers of corrugated cardboard (thickness, δ is 30 mm) impinged with effective heat fluxes (EHF) of 20 to 110 kW/m^2 is found as shown in Figure A(D)-14. Data were reproduced from Chaos' paper,[1] which are shown below for 20, 60, and 110 kW/m^2 cases for mass-loss rate (MLR) and surface temperature measurements:

[iv] To conduct simulations, unknown parameters need to be obtained via numerical optimization, for independent measurements of those parameters are cumbersome and impossible in most cases.

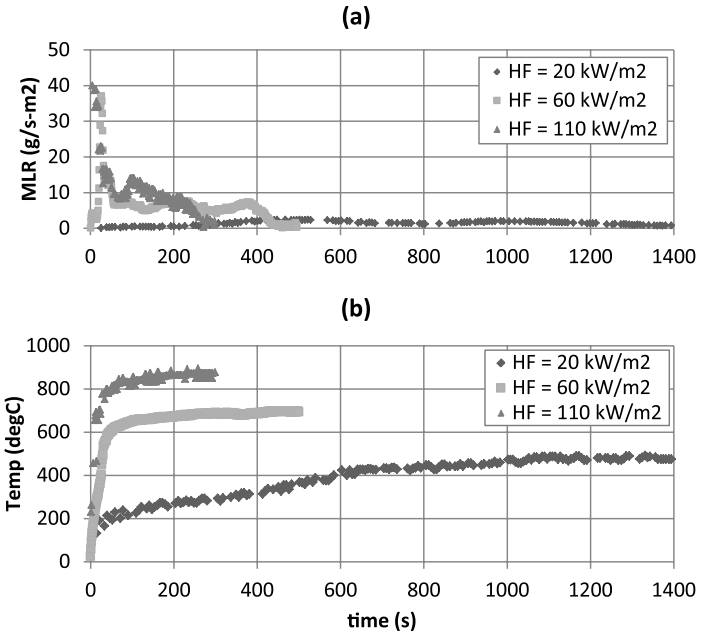

Figure A(D)-14. FPA experiment results of corrugated cardboard with applied heat flux ranging from 20 to 110 kW/m²: (a) Mass-loss rate and (b) surface-temperature measurements using pyrometer

2. Check data reproducibility by repeating identical experiments

Data is acquired from two repeating FPA tests of triple-wall corrugated cardboard under 60 kW/m² heat-flux level with nitrogen atmosphere. Uncertainty analysis will be performed later.

SELECT NUMERICAL OPTIMIZATION ROUTINE

- Genetic Algorithm (GA)
- Shuffled Complex Evolution (SCE)
- Stochastic Hill-climber (SHC)
- See Chapter 5 for more description of each optimization routine.

CONDUCT NUMERICAL OPTIMIZATION IN PAIR WITH SIMULATIONS USING EXPERIMENT DATA AS TARGETS

Numerous simulations with a simplified version of GPYRO have been used in pair with SCE algorithm to conduct numerical optimization to obtain unknown parameters. Experiment data of mass-loss rate (MLR), cumulative mass loss (CML), and surface-temperature measurements (T_s) generated with various applied heat-flux levels between 20 and 110 kW/m² have been used in the optimization process as targets (i.e., optimization is conducted for unknown parameters to match modeling outputs of interest to certain experiment data).

*Obtain Confidence Intervals for Optimized Parameters**

*Description reproduced from Chaos' paper.[1]

As part of the optimization procedure, confidence intervals (CI) were estimated for the material properties obtained. In the literature, optimization results are often reported with no CI estimates due to complexity and problem nonlinearity. This is especially the case for results obtained using evolutionary algorithms, as they lack information available through gradient-optimization methods. In this study, CIs were evaluated using asymptotic methods.[19] These are conceptually appealing and easy to implement, although they may be a poor representation of the actual CIs for highly nonlinear problems. Nevertheless, the computed CIs are useful indications of the reliability of the optimized parameters. Confidence intervals were computed **locally**, that is, at the optimum point found by the optimization scheme. At this optimum point, the standard error of the parameter estimates is approximated by a variance-covariance matrix based on the Jacobian of the model response. This matrix is then used along with the t-distribution at some desired confidence level to derive the CI. The set of equations shown below summarizes this approach:

$$\text{COV}=\frac{\|\mathbf{f}(\hat{\boldsymbol{p}})\|_2^2}{n_d-n_p}(\mathbf{J}^T\mathbf{J})^{-1};\ f(\hat{\boldsymbol{p}})=y_{\exp_i}-y_{\mathrm{mod}_i}(\hat{\boldsymbol{p}});\ i=1,\cdots,n_d$$

$$\mathbf{J}=\begin{bmatrix}\left.\frac{\partial y_{\mathrm{mod}1}(\mathbf{p})}{\partial p_1}\right|_{\hat{\boldsymbol{p}}} & \cdots & \left.\frac{\partial y_{\mathrm{mod}1}(\mathbf{p})}{\partial p_{n_p}}\right|_{\hat{\boldsymbol{p}}}\\ \vdots & \ddots & \vdots\\ \left.\frac{\partial y_{\mathrm{mod}n_d}(\mathbf{p})}{\partial p_1}\right|_{\hat{\boldsymbol{p}}} & \cdots & \left.\frac{\partial y_{\mathrm{mod}n_d}(\mathbf{p})}{\partial p_{n_p}}\right|_{\hat{\boldsymbol{p}}}\end{bmatrix}$$

$$\hat{\boldsymbol{p}}=\hat{\boldsymbol{p}}\pm t^{-1}\,(CL;\ n_d-n_p)\,\sqrt{diag[\mathbf{COV}]}$$

Where $\hat{\boldsymbol{p}}$ is the optimum parameter vector (i.e., set of material properties), n_d is the number of data points used for optimization, n_p is the number of parameters (i.e., material properties), **COV** and **J** are the covariance and Jacobian matrices, respectively, **f** is the vector of differences between model results (y_{mod}) and experimental data (y_{exp}), and t-1 is the value of the inverse t-distribution at a given confidence level (CL) and degrees of freedom (n_d–n_p). The availability of the Jacobian matrix further allows for the computation of the sensitivity of model responses to changes in input parameters (see Table A(D)-5).

Table A(D)-5. Summary of estimated optimum with confidence interval (CI) for each model parameter

	No	Condense Phase			
		i=1 fuel	Optimum ± C.I.	*i=2 residue*	Optimum ± C.I.
Material Property	**1**	ρ_1	110 kg/m^3	ρ_2	10.0 ± 6.9 kg/m^3
	2	k_1	0.65 ± 0.15 W/m^2-K	k_2	0.27 ± 0.14 W/m^2-K
	3	c_1	500 ± 40 J/kg-K	c_2	1750 ± 1240 J/kg-K
	4	κ_1	∞	κ_2	∞
Parameters for Specifying Conditions	**5**	ε_1	0.29 ± 0.02	ε_2	0.98 ± 0.13
		Heterogeneous RxN (*k=1*)		Optimum ± C.I.	
Kinetic Parameters and Heats Assuming nth order model and Arrhenius-type expression	**6**	n_1		6.51 ± 2.9	
		$\log(Z_1)$		19.1 ± 7.9 Log(/s)	
		E_1		242 ± 72 kJ/mol	
	7	$\log(\Delta H_1)$		5.95 ± 0.36 Log(J/kg)	

Parameter Estimation Results

ID				B-GA	B-SCE	B-SHC	C-GA	C-SCE	C-SHC
Parameter			Unit	Comparable Non-optimization and Optimization			Mostly Optimization		
Thermo-physical Property	i = 1 (fuel)	ρ_i	kg/m^3	110			110		
				Measurement			Measurement		
		k_i	W/m-K	0.08 ± 0.01			0.13	0.21	0.21
				Measurement			GA	SCE	SHC
		c_i	J/kg-K	2.8	2.3	0.6	2.0	2.4	1.7
				GA	SCE	SHC	GA	SCE	SHC
	i = 2 (residue)	ρ_i	kg/m^3	25	20	11	26	10	43
				GA	SCE	SHC	GA	SCE	SHC
		k_i	W/m-K	0.29	0.32	0.32	0.20	0.35	0.20
				GA	SCE	SHC	GA	SCE	SHC
		c_i	J/kg-K	1.5	1.1	0.2	1.0	0.8	2.2
				GA	SCE	SHC	GA	SCE	SHC
Optical Property	i = 1 (fuel)	κ_i	/m	10^6			10^6		
				Approximated as opaque			Approximated as opaque		
		ε_i	-	0.88 ± 0.01			0.72	0.50	0.65
				Measurement			GA	SCE	SHC
	i = 2 (residue)	κ_i	/m	10^6			10^6		
				Approximated as opaque			Approximated as opaque		
		ε_i	-	1			0.82	0.93	0.96
				Approximated			GA	SCE	SHC
Thermal-Decomposition Kinetics and Heats		n_k	-	1			3.7	3.0	2.2
				Approximated			GA	SCE	SHC
		Z_k	/s	1.1 x 10^{21}			3.9 x 10^6	9.8 x 10^{19}	6.0 x 10^{14}
				Model Fitting with single-heating-rate TGA data			GA	SCE	SHC
		E_k	J/mol	2.49 x 10^5			7.0 x 10^4	2.47 x 10^5	3.02 x 10^5
				Model Fitting with single-heating-rate TGA data			GA	SCE	SHC
		ΔH_k	kJ/kg	123	512	809	88	54	0.7
				GA	SCE	SHC	GA	SCE	SHC
Model-Dependent Parameter		h_{crz}	W/m^2-K	19	8	14	10	8	10
				GA	SCE	SHC	GA	SCE	SHC
		n_{kz}(i=1)	-	5.6	4.6	7.6	0		
				GA	SCE	SHC	Approximated		

Validation

Analyze Simulation Quality

IDENTIFY SENSITIVE PARAMETERS FOR MODEL INPUTS

For this case, total of 14 parameters are necessary due to the single-step thermal-decomposition kinetic modeling applied in this problem. Therefore, extensive sensitivity analysis is not necessary to determine sensitive parameters on model output of ineterest. However, there by Stoliarov[20] and Chaos[21] is conducted for similar cases on considering the effect of variation in material properties on the rate of burning. According to these works, it was recognized that the knowledge of parameters related to emissivity of virgin and char material and the decomposition reaction – Arrhenius pre-exponential factor, activation energy, heats, char yield – are significantly important for predicting the peak, average burning rates and surface temperatures. Based on this result, when determining the uncertainty of the model output, only these parameters will be considered for Case 2 problems, where simulation quality is analyzed by comparing the model output with its uncertainty and the experiment data with its uncertainty. Further details on sensitivity of each parameter can be found in this reference[20,21].

DETERMINE DATA AND MODEL OUTPUT UNCERTAINTY TO MAKE COMPARISON[v]

1. Conduct uncertainty analysis of data: Data is acquired from two repeating FPA tests of triple-wall corrugated cardboard under 60 kW/m^2 heat-flux level with nitrogen atmosphere.
2. Uncertainty analysis is conducted based on these two data sets. The uncertainty of MLR and surface temperature are estimated by first calculating the standard deviation of the MLR and temperature measurement of the 2 data sets at each time step. Then an average standard deviation is calculated for the time interval of interest ($0 < t < 500$s). The uncertainty is estimated as ± 2 average standard deviation. Table A(D)-6 shows the analysis results from the tests. Data were provided by FM Global. Note that these estimated uncertainties will be used for all other cases with different applied heat-flux levels assuming that these values are comparable to each other.

Table A(D)-6. Summary of estimated uncertainty in triple-wall (2 layers) corrugated cardboard FPA experiments based on 2 repeating tests at 60 kW/m^2 heat-flux level

	MLR (g/s-m^2)	T_s (K)
± 2 avg standard deviation	± 1.5	± 28

[v] Data uncertainty is accounted for here because this is required to determine the goodness of near-optimal parameter sets. Optimization targets (experiment data) should be considered with its uncertainty bounds to decide how good the match is between the targets and optimum simulations with its uncertainty.

3. Conduct uncertainty analysis of model outputs of interest – MLR and T_s
   - Baseline case was selected at simulation with EHF = 60 kW/m^2, thickness = 30 mm, and the optimum parameter set.
   - Six parameters are varied in the simulations one at a time from baseline case[vi]. See Table A(D)-7.

Table A(D)-7. Outline of 5 parameter groups – kinetic parameters, heat-of-decomposition reaction and combustion, and emissivity-of-fuel and residue – varied in uncertainty analysis using one-at-a-time method

	E1, A1	ΔH1	ρ2	ε1	ε2
Kinetic parameters	+, – –, +				
Heat of decomposition reaction		+ –			
Density of residue			+ –		
Emissivity of fuel				+ –	
Emissivity of residue					+ –

   - The effect of variation is calculated by considering the change in MLR and surface-temperature profiles from the baseline case. By varying certain parameters at one-at-a-time, average standard deviation of the two cases (altered and baseline case) are calculated as effects. Results are shown in Table A(D)-8.
   - Uncertainty in these modeling outputs (MLR and T_s) is calculated using the Law of Propagation of Uncertainty. Note that when inputs are varied to its uncertainty boundary values – minimum or maximum – the maximum effect was selected in the analysis to estimate the maximum uncertainty.

[vi] Parameter selection is based on known parameter sensitivity. Kinetic parameters are not independent; therefore, activation energy and pre-exponential factor will be considered in pair to give decomposition temperature to be at minimum and maximum in simulation. Although nth order is a kinetic parameter, this is not included in the analysis, because changing this value majorly affects the shape of the DTG peak – increase/decrease in n value results in higher/lower DTG peak and wider/narrower temperature range of decomposition, respectively.

Table A(D)-8. Comparison between experiment data from fire propagation apparatus test and modeling outputs using estimated parameter values via either measurements and numerical optimization (B-GA, B-SCE, B-SHC) or mostly numerical optimization (C-GA, C-SCE, C-SHC)

	Data	B-GA	B-SCE	B-SHC	C-GA	C-SCE	C-SHC
Peak MLR (g/m^2s)	35 ± 4	28	24	53	23	29	N/A
Avg MLR (g/m^2s)	5.7 ± 0.6	4.6	5.4	5.9	4.8	6.0	N/A
t to pMLR (s)	27 ± 1	19	13	19	4	12	N/A
Ts at 300 s (°c)	696 ± 16	685	682	684	679	679	685

COMPARE DATA WITH SIMULATION RESULTS WITH CONSIDERATION OF UNCERTAINTIES

1. TG / DTG Predictions at 10 °C/min Heating Rate Using Estimated Kinetic Parameters

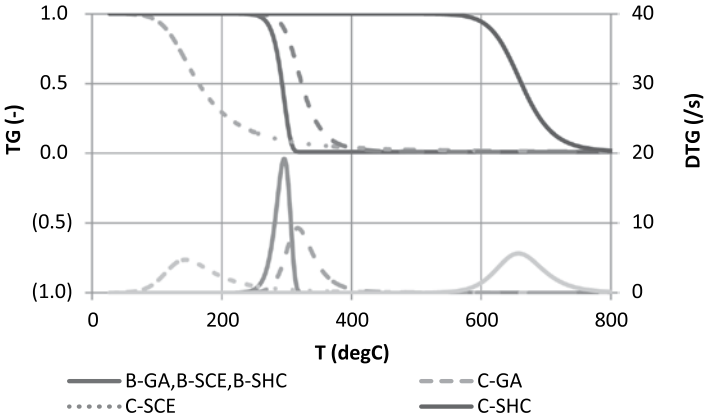

Figure A(D)-15. TG/DTG Curves at 10°C/min heating rate with different estimation results for kinetic parameters for thermal decomposition of corrugated cardboard: For better comparison, TG and DTG thermograms have been scaled to result in 100% conversion.

2. Modeling Output: Mass Loss Rate (MLR)

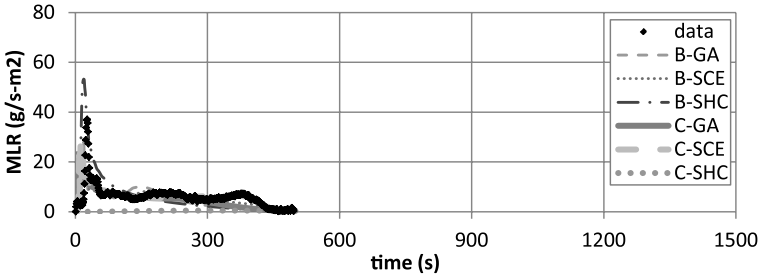

Figure A(D)-16. Mass-loss rate (MLR) comparisons for corrugated cardboard between actual MLR from experiment (data) and modeled MLR (B-GA, B-SCE, B-SHC, C-GA, C-SCE, C-SHC) at applied heat flux of 60 kW/m². Note that data shown were used to estimate model-parameter values via numerical optimization using GA, SCE or SHC routines.

3. Modeling Output: Surface Temperature (T_{surf})

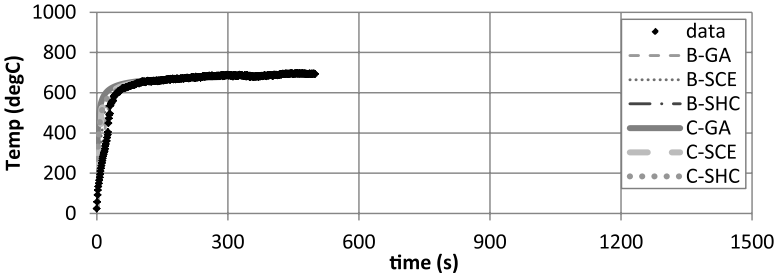

Figure A(D)-17. Surface temperature (T_{surf}) comparisons for corrugated cardboard between actual T_{surf} from experiment (data) and modeled T_{surf} (B-GA, B-SCE, B-SHC, C-GA, C-SCE, C-SHC) at applied heat flux of 60 kW/m². Note that data shown were used to estimate model-parameter values via numerical optimization using GA, SCE or SHC routines.

Validate simulation quality upon extrapolation

1. Modeling Output: Mass Loss Rate (MLR)

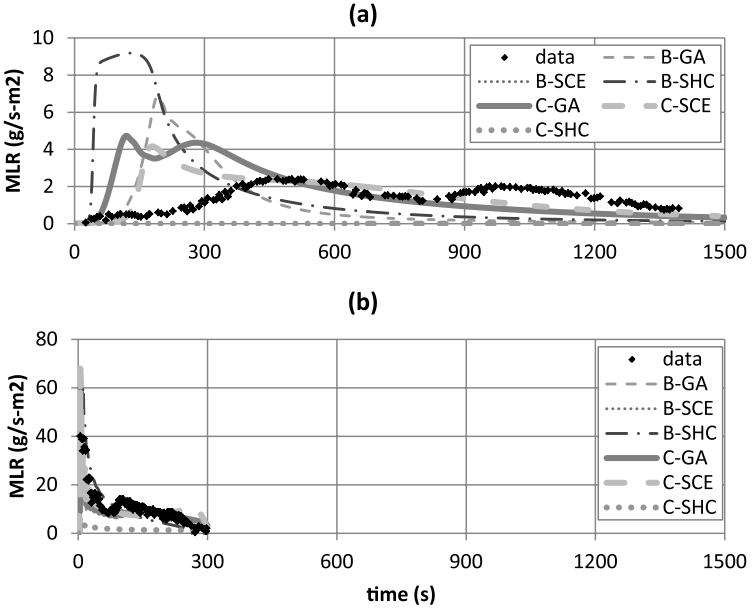

Figure A(D)-18. Mass-loss rate (MLR) comparisons for corrugated cardboard between actual MLR from experiment (data) and modeled MLR (B-GA, B-SCE, B-SHC, C-GA, C-SCE, C-SHC) at applied heat flux of (a) 20 and (b) 110 kW/m². Note that data shown were not included in the model-parameter-estimation process; hence, these two cases are considered as extrapolation cases.

2. Modeling Output: Surface Temperature (T_{surf})

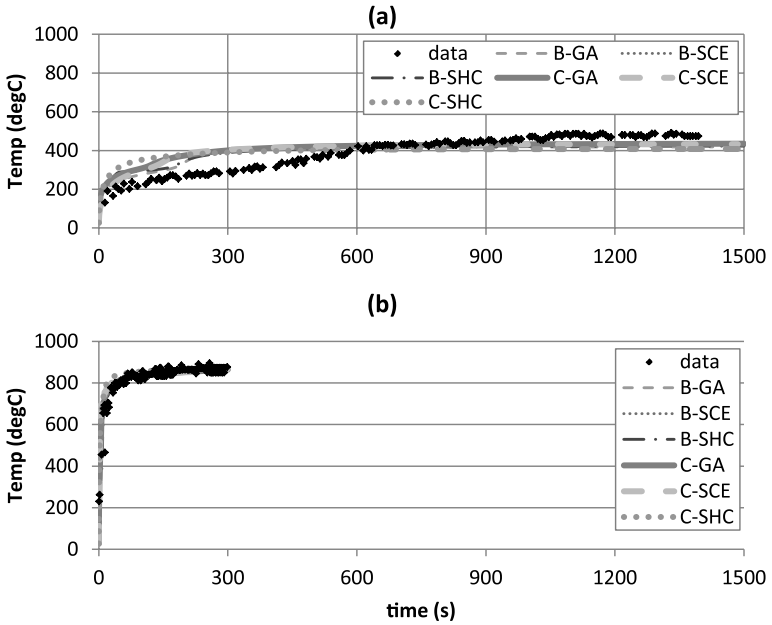

Figure A(D)-19. Surface temperature (T_{surf}) comparisons for corrugated cardboard between actual T_{surf} from experiment (data) and modeled T_{surf} (B-GA, B-SCE, B-SHC, C-GA, C-SCE, C-SHC) at applied heat flux of (a) 20 and (b) 110 kW/m². Note that data shown were not included in the model-parameter-estimation process; hence, these two cases are considered as extrapolation cases.

Commentary

General Comments

- TG/DTG
  - When kinetic modeling is conducted independently using TGA data (B-GA, B-BSE, B-SHC), the DTG peak exist near 300°C.
  - Among GA, SCE and SHC, optimization of SCE of kinetic parameters as part of other unknown parameter estimation is closest to actual TGA data (B-GA, B-SCE, B-SHC), followed by GA and SHC.
  - Optimization of SHC of kinetic parameters along with other unknown parameter estimation is considered as unsuccessful, for decomposition temperature is excessively high (see mass-loss rate optimization and extrapolation results)
- Comparison between Data and Computed Modeling Outputs
  - Generally, better agreement between data and modeling outputs is found when kinetic parameters are estimated through a separate process using TGA data (B-GA, B-BSE, B-SHC) than numerical optimization along with estimating other unknowns together (C-GA, C-SCE, C-SHC).

- None of the modeled peak MLRs are in quantitative agreement with data.
- Avg MLR of B-SCE, B-SHC and C-SCE are in good agreement with data.
- None of the modeled time-to-peak MLRs are in quantitative agreement with data.
- Surface temperatures at 300 s of B-GA, B-SCE, B-SHC and C-SHC are in good agreement with data.

- MLR
  - Optimization at HF = 60 kW/m^2: Although the peak may be off for some cases, generally good agreement exists between experiment data and all modeling results, considering the trend, except for that of C-SHC, indicating that optimization of C-SHC – optimizing for all unknowns using SHC – was unsuccessful. Oscillation in the MLR curve is due to the inhomogeneity of sample, corrugated cardboard, which is not captured in modeling due to the homogeneous assumption made when solving the problem.
  - Extrapolation at HF = 20 kW/m^2: Poor agreement exists between experiment data and all modeling results. None of the modeling cases is able to capture the slow increase in mass-loss rate in the earlier times after exposure to heating source.
  - Extrapolation at HF = 110 kW/m^2: Good agreement exists between experiment data and all modeling results, except for C-SHC case.
- Surface Temperature
  - Optimization at HF = 60 kW/m^2: Generally good agreement exists between experiment data and all modeling results considering the trend, even for that of C-SHC. Also, when thermal conductivity of the sample at its virgin state was independently measured and that value was used, modeling was able to capture the slow increase in surface temperature up until 400°C followed by a jump up to ~550°C.
  - Extrapolation at HF = 20 kW/m^2: Poor agreement exists between experiment data and all modeling results. None of the modeling cases is able to capture the slow increase in surface temperature in the earlier times after exposure to heating source.
  - Extrapolation at HF = 110 kW/m^2: Good agreement exists between experiment data and all modeling results, including C-SHC case.

Limitation in Modeling

- When considering limitation of the parameters in modeling corrugated cardboard, the modeler should take into account the applicability of the parameters and their associated uncertainties. For example, any assumptions used when determining a parameter value via experiment direct or indirect measurements can be utilized to understand when the parameter value becomes inappropriate. For this example of pyrolysis modeling of corrugated cardboard, most consideration can be given to the parameters related to decomposition kinetics.

- As shown in the below figure of corrugated cardboard decomposed in TGA at 20 K/min under nitrogen and air atmosphere, the simplified kinetic modeling using one-step decomposition mechanism is only true for a "dry" sample tested in nitrogen. Clearly, for decomposition of a "dry" sample in air results in two distinct DTG peaks. Therefore, the effect of the simplification (one-step) made to kinetic modeling should be addressed when discussing large-scale simulation quality of parallel panel experiment using the optimized parameter set from this exercise.

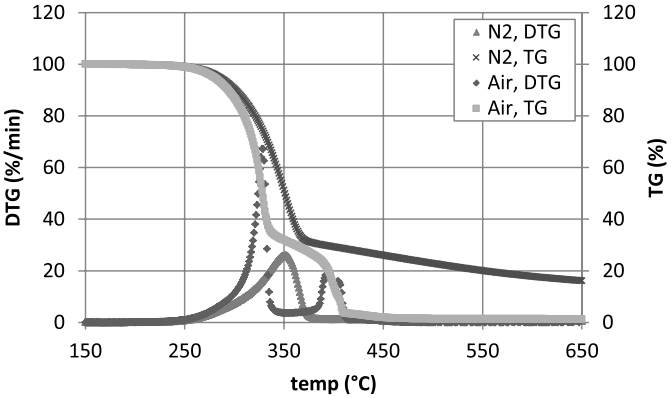

Figure A(D)-20. TGA thermograms of corrugated cardboard decomposition conducted under constant heating rate of 20 °C/min and 2 different environments – nitrogen and air

Example 5.3 Modeling Modified Acrylic FRP Composite

An example case is shown for a fiberglass-reinforced polymer (FRP) composite with modified acrylic resin with high-charring inorganic fire-retardant additive. Most of the approach and reference values of the input parameters for this simulation were obtained from Kim and Dembsey's work.[22]

Modified acrylic resin (MA) is essentially unsaturated polyester (UPE) with Methacrylic Acid (MMA) replacing most of the styrene monomers. Flame-retarded resin with MA is manufactured by adding a filler-type inorganic additive (A) as an additive, where its loading versus resin is MA:A = 0.38:0.62 by weight. Typical inorganic additives are hydrates such as alumina trihydroxide (ATH) or magnesium hydroxide, antimony trioxide, borax, chalk, silica, etc.[23] Because this additive was known to give a high-charring effect, A was categorized with typical hydroxides used as flame-retardant fillers. These hydroxides works as a flame retardant by resulting in an endothermic dehydration reaction that produces oxides and water.[24,25] The water produced by this reaction vaporizes, which is an endothermic reaction, and the vapor dilutes the gaseous phase. The oxides remain in the char layer, which adds an insulative effect. This flame retardant is added with a relatively large amount (50 to 65%) comparing to other types of additives. By adding a significant amount of an inorganic flame retardant, the polymer becomes more brittle. Because this is an inorganic additive, inserting this material into the polymer system by 50 to 65 wt% of its original polymer reduces the available fuel within the condensed phase. In addition to this effect, usually the additive has a higher heat capacity compared to the base polymer; hence, the flame retarded polymers with these types of hydroxides require more energy to increase the body temperature to its pyrolysis level. According to the product description, this resin with the flame-retardant additive is formulated to be Class I per ASTM E 84[26] (flame spread index < 20 and smoke developed < 225).
→ Propose two parallel reactions for MA and A thermal decomposition.

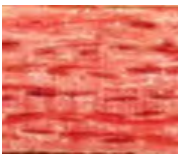

Figure A(D)-21. Cross-section of FRP composite with modified-acrylic resin with high-charring inorganic additive

Composite panels were fabricated by vacuum bagging for a relatively high-glass-content composite (31 ± 2 wt% of glass, thickness of 8.8 ± 0.6 mm) using two different types of fiberglass mats that were wetted with resin (see Figure A(D)-21 for cross-section of composite). The two types of fiberglass (E-glass) used in the composite are a chopped-strand mat and a glass-roving woven mat with an area density of 25 g/m^2 and 880 g/m^2, respectively. The chopped-strand mat is thinner and more porous than the woven mat. The laminate schedule (provided by the manufacturer) is

chopped-strand mat and roving alternating three times with another chopped-strand mat layer at the end. Visual inspection of a polished cross-section of the composite slab is consistent with this laminate schedule, but with polymer-resin layers between each fiberglass layer. The chopped-strand mat layer is difficult to identify in the cross section, perhaps because more resin is soaked into this layer than the roving layer. The roving layer is observed as a prominent glass layer possibly because the resin is absorbed only at the fiberglass layer surfaces, leaving the interior with primarily glass.
→ Apply effective homogeneous single layer of resin, additive and fiberglass mixture.

Note that for this example, one approach will be used to estimate model parameters – mostly optimization method denoted as Approach GA, SCE, or SHC. For optimization routines, Genetic Algorithm (GA), Shuffled Complex Evolution (SCE) or Stochastic Hill-climber (SHC) is applied.

Measure Parameters

When conducting parameter estimation via independent experiments, consider the following:

- Check consistency between model used in experiment analysis and pyrolysis model.
- Use statistical approach for determining uncertainty; otherwise, meet equivalency to this requirement.

1. Density

Although this FRP composite is porous, due to the nature of the fiberglass and lamination, and therefore the cross-section is not homogeneous, it is considered as an effective homogeneous single-layer material with relatively low bulk density to account for its porous nature. Bulk density of the composite is measured by experiment conducted at room temperature (≈298K), weighing the sample's mass and dividing mass with sample volume, which is 1900 kg/m^3. This density is a mixture of resin (MA), additive (A), and fiberglass (G).

$$\boldsymbol{\rho_{bulk} = 1900\ kg/m^3}$$

Also, the resin-with-additive and resin-only sample cured free of fiberglass has been provided by the fabricator. Using this material, the density of resin and additive has been obtained using measurements (ρ_{MA+A} and ρ_{MA}) and the following correlation (ρ_{MA}):

$$\bar{\rho} = \left(\sum \frac{Y_i}{\rho_i}\right)^{-1}$$

$$\boldsymbol{\rho_{MA+A} = 1700\ kg/m^3}$$

$$\boldsymbol{\rho_{MA} = 1200\ kg/m^3}$$

$$\boldsymbol{\rho_{A} = 2300\ kg/m^3}$$

The density of residue can be found from kinetic modeling, where the weight-loss fraction is estimated for each decomposition reaction.

Density of the fiberglass has been provided by the manufacturer as below:

$$\boldsymbol{\rho_{G} = 2600\ kg/m^3}$$

2. Thermal Conductivity

Not measured; will be obtained via numerical optimization. However, from literature research, adding inorganic high-charring additives such as hydroxides is known to increase the overall thermal conductivity of the cured resin with additive. Therefore, one can note that the estimated thermal conductivity of the additive, A, should be greater than that of the resin, MA.

3. Specific-heat Capacity

Not measured; will be obtained via numerical optimization.

4. Absorption Coefficient

Based on visual observation of the composite, every condense-phase material involved in modeling is considered as an opaque material. Therefore, the absorption coefficient is essentially infinity.

$$\kappa \rightarrow \infty$$

5. Emissivity

Not measured; will be obtained via numerical optimization.

6. Reaction Order, Pre-exponential Factor and Activation Energy

This example case is determined to have decomposition kinetics type 3 (two major peaks – decomposition of resin and additive, respectively – overlapping in DTG over entire mass-loss temperature range) according to TGA and DSC experiments conducted in nitrogen atmosphere. Based on this information, kinetic parameters when using Arrhenius expression and n^{th} order kinetic model – pre-exponential factor, activation energy and n – will be obtained via **Iso-conversional Method (activation energy)** and **model-fitting method (pre-exponential factor and n)**. For modeling fitting method, numerical optimization is conducted with least square method to estimate optimum values for pre-exponential factor and n for each reaction.

CONDUCT DYNAMIC THERMOGRAVIMETRIC ANALYSIS (TGA) AND DIFFERENTIAL SCANNING CALORIMETER (DSC) EXPERIMENTS IN NITROGEN

Thermogravimetic Analysis (TGA) experiments are conducted at various heating rates – 5, 20, 40, and 60°C/min – with samples sizes near 10 mg for minimal thermal resistance during heating. Temperature range used in the tests is from ambient to 800°C with nitrogen as purging gas.

TGA and DSC data of the decomposable component of the FRP composite, resin and additive cured together (MA+A), and resin only (MA) tested in nitrogen environment with a heating rate of 20°C/min are shown in Figure A(D)-22. Note that DSC data is shown with baseline correction. In the DSC thermogram, a significant endothermic peak is observed for the MA+A sample in 250 to 400°C temperature range, where this is not shown in the MA's thermogram (see green arrow in (b) in Figure A(D)-22). Based on this comparison, the modeler can assume decomposition reaction for the fire-retardant additive, A, in this temperature range followed by that of resin itself, MA, knowing that decomposition of A results in large endothermic reaction.

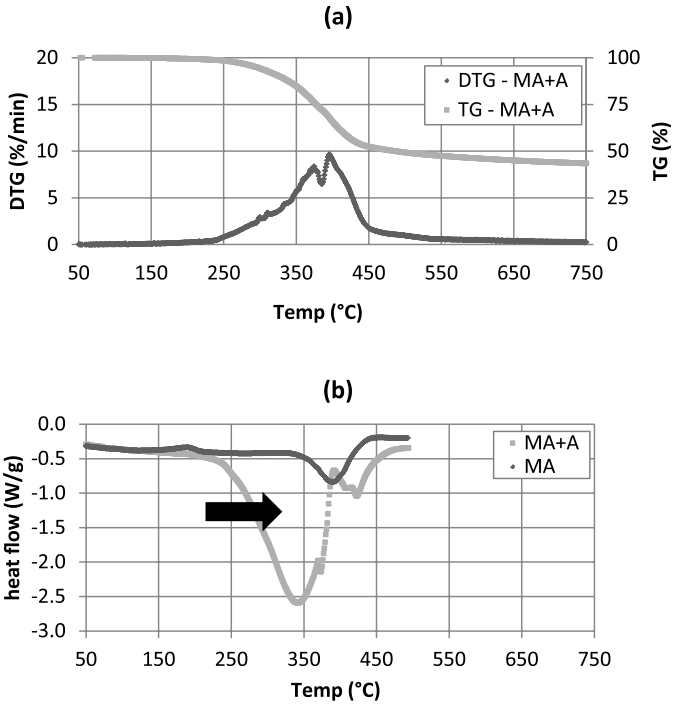

Figure A(D)-22. TGA (a) and DSC (b) thermograms of decomposition of modified-acrylic resin with high-charring additive conducted under 20K/min heating rate and nitrogen environment

CONDUCT KINETIC MODELING TO OBTAIN KINETIC PARAMETERS

1. Conduct Iso-conversional Method

Based on this method, activation energy of MA+A and MA are found for $0 < \alpha < 0.2$ (additive decomposition) and $0.1 < \alpha < 0.7$ (resin decomposition) range, respectively (see Figure A(D)-23). According to Iso-conversional Method, two-step reaction mechanism can be proposed as below:

$$\mathrm{A} \rightarrow \nu_{\mathrm{p,a}}\mathrm{A_residue} + \left(1-\nu_{\mathrm{p,a}}\right)\mathrm{gas} \qquad \text{(+A-R1)}$$

$$\mathrm{MA} \rightarrow \nu_{\mathrm{p,c}}\mathrm{MA_residue} + \left(1-\nu_{\mathrm{p,c}}\right)\mathrm{gas} \qquad \text{(R)23}$$

Estimated activation energy for these reactions are 160 ± 3 kJ/mol for decomposition of A and 183 ± 2 kJ/mol for that of MA. Note that slopes, E_a/R, are found via the least-square method. Additionally, considering the uncertainty of ±6% (magnitude of |±6% |=12%) in TG data from decomposing MA+A samples, initial weight-loss and char-oxidation reactions that are less than 5% of weight loss are ignored. They can be determined as insignificant changes.

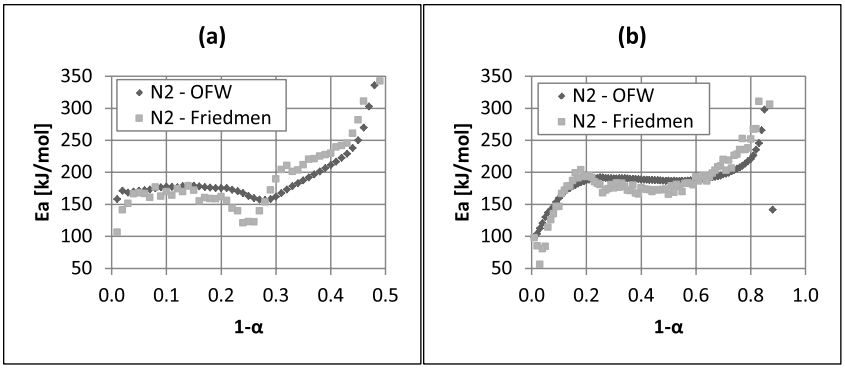

Figure A(D)-23. Estimated activation energy, E_a, with respect to conversion (1α) based on Iso-conversional Method for decomposition of modified-acrylic resin with (a) and without (b) inorganic high-charring additive

2. Conduct model-fitting method using n^{th} order reaction kinetic model (f(α))

Once the minimum number of reactions and their activation energies are estimated by conducting Iso-conversional Method, other kinetic parameters to fully mathematically describe decomposition of MA+A need to be estimated as well. This is done by conducting the model-fitting method with a kinetic model assumed. Typically a n^{th} order reaction model is used due to its flexibility in providing good fitness between the data and the model. Therefore, n^{th} order will be utilized in this example. Based on the model-fitting method, estimation of total-weight-loss fraction, pre-exponential constant, and n are conducted for each reaction (see Table A(D)-9).

Table A(D)-9. Kinetic parameters for 2-step model – decomposition of additive (+A-R) and resin (R) – for modeling modified-acrylic resin with inorganic high-charring additive

	+A-R	R
Weight Fraction	0.2	0.3
E_a (kJ/mol)	**165**	**183**
log (A (/s))	12.2	12.5
n (/)	5	1.3

Note that estimation has been done with least-square method by comparing TGA data (TG and DTG from iso-heating rate tests (see Figure A(D)-24) with kinetic modeling's output. The kinetic modeling's output is calculated by applying the Runge-Kutta 4^{th} order method (ODE solving method) to the decomposition ODE equation.

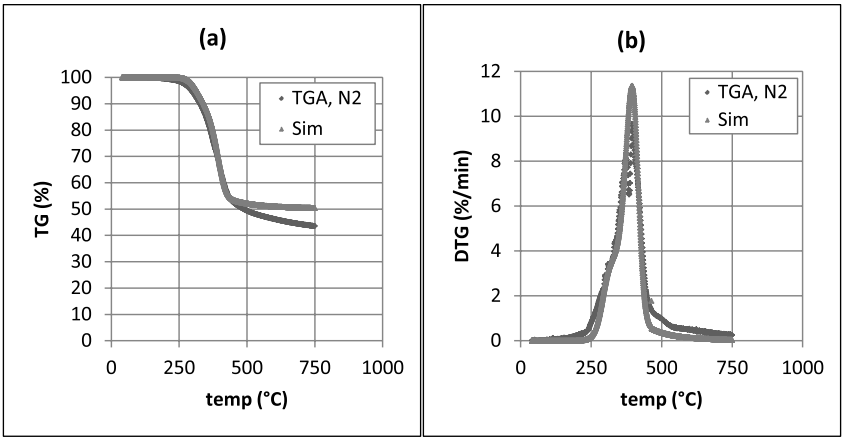

Figure A(D)-24. Comparison of TGA experiment data (TG and DTG) at 20°C/min under nitrogen atmosphere with kinetic modeling results based on model-fitting method for modified-acrylic resin with inorganic high-charring additive

$$\log A_1 = 12.2\ (\log(/s));\ E_1 = 1.65 \times 10^5\ (J/mol);\ n_1 = 5$$
$$\log A_2 = 12.5\ (\log(/s));\ E_2 = 1.83 \times 10^5\ (J/mol);\ n_2 = 1.3$$

7. Heat of Reaction

For decomposition reaction of the additive, A, three identical DSC experiments are conducted to determine heat-of-reaction: $(3.42 \pm 0.34) \times 10^6$. However, in DSC scans, when the sample is losing mass during the experiment, baseline required to sum energy over temperature range of interest is not stable; therefore, uncertainty should be higher than estimated.

$$\Delta H_1 = 3420 \pm 340\ kJ/kg$$

For decomposition reaction of the resin, MA, heat of reaction is not measured; will be obtained via numerical optimization.

Summary

Among seven categories of parameters, parameters that have been estimated via direct measurement are shaded in Table A(D)-10. The rest of the unknown parameters, a **total of 16 parameters**, should be obtained via numerical optimization in pair with pyrolysis modeling using bench-scale experiment data or equivalent.

Table A(D)-10. Summary of necessary model parameters for simulating pyrolysis of modified-arylic resin with high-charring additive (MA+A) FRP composite

	No	Condense Phase				
		i=1, A	***i=2, A_residue***	***i=3, MA***	***i=4, MA_residue***	***i=5, G***
Material Property	**1**	ρ_1	ρ_2	ρ_3	ρ_4	ρ_5
	2	k_1	k_2	k_3	k_4	k_5
	3	c_1	c_2	c_3	c_4	c_5
	4	κ_1	κ_2	κ_3	κ_4	κ_5
Parameters for Specifying Conditions	**5**	ε_1	ε_2	ε_3	ε_4	ε_5
		Heterogeneous RxN				
		k = 1, +A-R		***k = 2, R***		
Kinetic Parameters and Heats assuming n^{th} order model and Arrhenius-type expression	**6**	n_1		n_2		
		Z_1		Z_2		
		E_1		E_2		
	7	ΔH_1		ΔH_2		

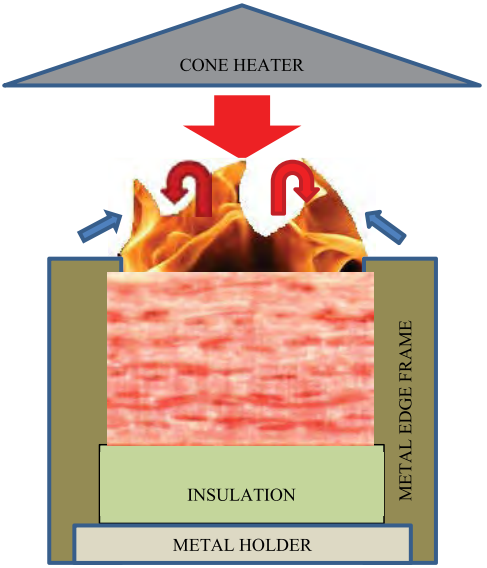

Figure A(D)-25. Simplified representation of a cone calorimeter test of FRP composite

SELECT MODEL: GPYRO

UNDERSTAND BENCH-SCALE EXPERIMENT SET-UP FOR MODELING SIMPLE CASES

A simplified representation of a cone calorimeter test of FRP composite is shown in Figure A(D)-25. The sample is placed on top of an insulation, which sits on a metal holder. Another metal frame is placed on top of the sample, insulation, and the holder. A metal edge frame is used as well.

Front Surface: As heating starts by opening the shutter to allow radiation from the cone heater to impinge on the sample surface (large red arrow), cooling also begins via natural convection (blue arrows) and re-radiation. The surface decomposes with bubbling with respect to temperature increase occurring through heat conduction and/or in-depth radiative transport. The pyrolyzates leave through the surface until complete burnoff, because this material leaves no residue. When ignition occurs as the fuel-vapor concentration above the surface exceeds its LFL (lower flammable limit), additional heat flux from the flame is introduced on the surface (red arrows). Regression of the sample surface with respect to consumption of the resin layers in pyrolysis is negligible due to limited expanding of the fiberglass layers upon heating.

Back surface: The sample is placed on top of insulation. In the experiment, an air gap of a few millimeters thickness exists between the sample and the insulation due to thermal contact. Due to the insulation, nothing leaves through the back face when 1D assumption holds for the experiment.

CONFIGURE MODEL CONDITIONS BASED ON UNDERSTANDING OF EXPERIMENT SET-UP

In the model, the phenomena discussed above are simulated as below. Basic assumptions are as follows:

- Instantaneous release of volatiles from solid to the gas phase
- Local thermal equilibrium between the solid and the volatiles
- No condensation of gaseous products
- No porosity effects

Further details can be found from the *Technical Reference*[6] and *User's Guide*[7] of GPYRO (http://code.google.com/p/gpyro).

When conducting the GPYRO simulation for the cone calorimeter set-up, the metal edge frame will be ignored, and backing is insulated. The ignition phenomenon is interpreted as the following in the simulations: at a known time-of-ignition (from experiment data), additional heat flux of 20 kW/m^2 is applied to the surface to simulate heat flux from the flame. This value is estimated from a measurement from this material pyrolyzing in the cone with a total-heat-flux gauge measuring heat flux impinging on the sample surface (see Figure A(D)-26 – test conducted at 50 kW/m^2 applied heat flux; from time-of-ignition an increase in measured heat flux is observed due to flame).

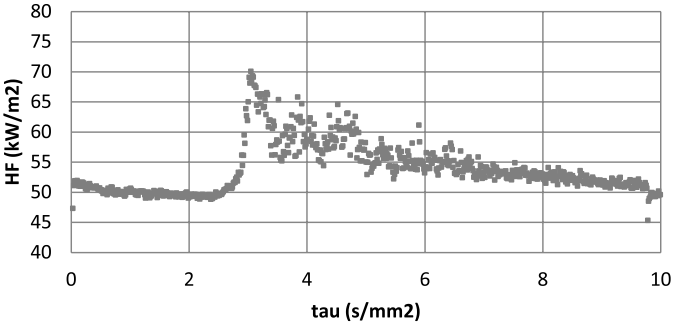

Figure A(D)-26. Heat flux measured during cone calorimeter test of modified-acrylic resin with high-charring additive (MA+A) FRP composite at external-heat-flux level of 50kW/m^2: ignition occurs near τ = 3 s/mm^2, and from this point additional heat flux impinges on the surface due to the flame.

In addition to the parameters introduced in a previous section (see Parameter Estimation Results), the model (GPYRO) has a coefficient (γ, GAMMA) that is used to model radiative heat transfer through the pores. This parameter with T^3 is a model-dependent parameter that is added as another term in the effective thermal conductivity. γ is used for porous fiberglass and decomposed solid species, which results in a more porous state due to the weight loss; therefore, more radiative heat transfer through the gas phase pores, i.e., for condense phase specie i = *2* (A_residue), *4* (MA_residue) and *5* (G).

Another set of parameters included as unknowns is the temperature-dependent terms used to describe the variation of thermal conductivity and specific-heat capacity with respect to temperature increase: $k(T)=k_0\,(T/T_r)^{n_k}$ and, $c(T)=c_0\,(T/T_r)^{n_c}$ respectively, where T_r is a reference temperature. Only properties of fiberglass are allowed to vary with respect to temperature, knowing that for high-glass-content FRP composite, glass may be a controlling factor for its fire behavior. This approach is utilized to give much flexibility during parameter estimation for fiberglass.

Therefore, the **total unknown parameters** of 16 now becomes **21,** including γ, n_k, and n_c.

ACQUIRE DATA SETS THAT CAN BE USED IN NUMERICAL OPTIMIZATION PROCESS IN PAIR WITH PYROLYSIS MODELING FOR OBTAINING UNKNOWN MODEL-PARAMETER VALUES[vii]

1. The maximum heat-flux level of interest for this parameter estimation is 25 to 75 kW/m^2.
2. Cone calorimeter (cone) test data of modified-acrylic resin with high-charring additive FRP composite (thickness, δ is 8.8 ± 0.6 mm) impinged with effective heat fluxes (EHF) of 25 to 75 kW/m^2 is obtained and are shown in Figure A(D)-27 for mass-loss rate (MLR), surface, and back face temperature measurements:
3. Check data reproducibility by repeating identical experiments: Data is acquired from three repeating cone tests of MA+A FRP composite under 50 kW/m^2 heat flux level. Uncertainty analysis will be performed later.

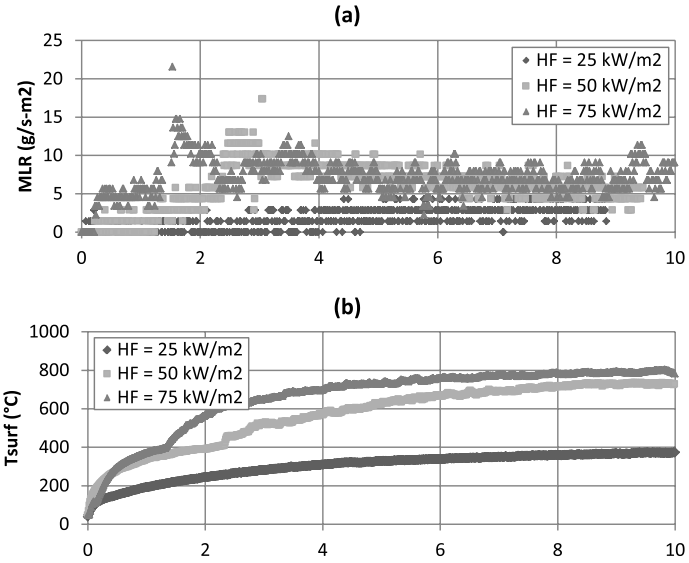

[vii] To conduct simulations, unknown parameters need to be obtained via numerical optimization, for independent measurements of those parameters are cumbersome and impossible in most cases.

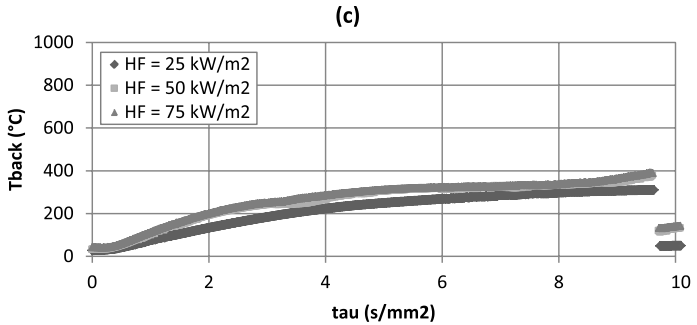

Figure A(D)-27. Cone calorimeter experiment results of modified-arylic resin with high-charring additive (MA+A) FRP composite with applied heat flux ranging from 25 to 75 kW/m²: (a) mass-loss rate and (b) surface temperature, and (c) back-surface temperature measurements

SELECT NUMERICAL OPTIMIZATION ROUTINE

The property estimation for the modified-acrylic composite is conducted by coupling a generalized pyrolysis model for slab experiments developed by Lautenberger and the Genetic Algorithms (GA) for optimization routine.[27,7] GA was developed based on the mechanics of the Darwinian survival-of-the-fittest theory.

CONDUCT NUMERICAL OPTIMIZATION IN PAIR WITH SIMULATIONS USING EXPERIMENT DATA AS TARGETS

Numerous simulations with GPYRO have been used in pair with GA algorithm to conduct numerical optimization to obtain unknown parameters. Experiment data of mass-loss rate (MLR), cumulative mass loss (CML), and surface and back-face temperature measurements (T_s and T_b) generated with a heat-flux level of 50 kW/m² have been used in the optimization process as targets (i.e., optimization is conducted for unknown parameters to match modeling outputs of interest to certain experiment data).

Obtain Confidence Intervals for Optimized Parameters

One possible approach for addressing the uncertainty of a numerically optimized parameter when using GA optimization is to use the near-optimal parameter sets or "best solutions" to generate a relatively large population of parameter sets (see parameter set fitness after ~ 80 generations in Figure A(D)-28). A multi-objective optimization algorithm, such as the GA applied to pyrolysis modeling, typically produces many near-optimal sets or "best solutions," which are a set of solutions that represent tradeoffs between many objective functions. Each parameter in each set can be evaluated individually to determine whether the near-optimal value of one parameter changes significantly from one set to another. Also, comparing the model outputs, such as the mass-loss rate and temperature predictions simulated with different near-optimal parameter sets, will allow the user to determine how much the simulation results vary from one set to another within the

collection of optimized parameter sets. This numerical experiment may provide insight to the sensitivity of the optimization routine to any changes in the inputs as well as to the uncertainties in the model outputs associated with the optimized parameter values.

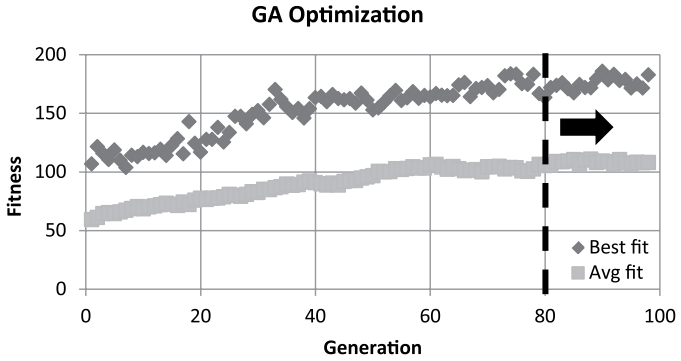

Figure A(D)-28. Increase in model output fitness to targets – mass-loss rate, cumulative mass loss, surface and back-surface temperatures – from genetic algorithm (GA) optimization for estimating unknown parameters from simulating pyrolysis of modified-acrylic resin with high-charring additive (MA+A) FRP composite

Parameter Estimation Results

ID				GA(avg)	GA(best)	SCE	SHC
Parameter			Unit	Comparable Non-optimization and Optimization			
Thermo-physical Property	i = 1 (Resin)	ρ_i	kg/m^3	1200			
				Measurement			
		k_i	W/m-K	0.23 ± 0.02	0.21	0.54	0.04
				GA	GA	SCE	SHC
		c_i	J/kg-K	1400 ± 100	2200	300	1300
				GA	GA	SCE	SHC
	i = 2 (R_residue)	ρ_i	kg/m^3	253			
				Measurement, Kinetic Modeling			
		k_i	W/m-K	0.19 ± 0.02	0.12	0.08	0.31
				GA	GA	SCE	SHC
		c_i	J/kg-K	1900 ± 200	1600	1800	1800
				GA	GA	SCE	SHC
	i = 3 (Additive)	ρ_i	kg/m^3	2300			
				Measurement			
		k_i	W/m-K	1.22 ± 0.10	1.44	0.82	2.74
				GA	GA	SCE	SHC
		c_i	J/kg-K	1200 ± 100	930	2500	2400
				GA	GA	SCE	SHC
	i = 4 (A_residue)	ρ_i	kg/m^3	1558			
				Measurement, Kinetic Modeling			
		k_i	W/m-K	0.24 ± 0.04	0.22	0.59	0.36
				GA	GA	SCE	SHC
		c_i	J/kg-K	1200 ± 100	2200	300	780
				GA	GA	SCE	SHC

	i = 5 (Glass)	ρ_i	kg/m^3	2600			
				Reference (MSDS)			
		k_i	W/m-K	0.18 ± 0.02	0.15	0.30	0.09
				GA	GA	SCE	SHC
		c_i	J/kg-K	400 ± 100	170	300	110
				GA	GA	SCE	SHC
Optical Property	i = 1 (R)	κ_i	/m	10^6			
				Approximated as Opaque			
		ε_i	-	0.84 ± 0.03	0.81	0.82	1.24
				GA	GA	SCE	SHC
	i = 2 (R_res)	κ_i	/m	10^6			
				Approximated as Opaque			
		ε_i	-	0.90 ± 0.03	0.87	1.00	0.97
				GA	GA	SCE	SHC
	i = 3 (A)	κ_i	/m	10^6			
				Approximated as Opaque			
		ε_i	-	0.81 ± 0.04	0.77	1.00	0.84
				GA	GA	SCE	SHC
	i = 4 (A_res)	κ_i	/m	10^6			
				Approximated as Opaque			
		ε_i	-	0.89 ± 0.03	0.96	1.00	0.42
				GA	GA	SCE	SHC
	i = 5 (Glass)	κ_i	/m	10^6			
				Approximated as opaque			
		ε_i	-	0.88 ± 0.02	0.90	1.00	1.41
				GA	GA	SCE	SHC
Kinetics and Heats	k = 1 R → $R_{residue}$+vap↑	n_k	-	1.3		Model Fitting with Multiple Heating Rate TGA Data	
		Z_k	/s	3.2 x 10^{12}			
		E_k	J/mol	1.83 x 10^5			
		ΔH_k	kJ/kg	(2.5 ± 0.2) x 10^3	2.0 x 10^3	2.6 x 10^3	2.6 x 10^3
				GA	GA	SCE	SHC
	k = 2 A → $A_{residue}$ + vap↑	n_k	-	5.0		Model Fitting with Multiple Heating Rate TGA Data	
		Z_k	/s	1.6 x 10^{12}			
		E_k	J/mol	1.60 x 10^5			
		ΔH_k	kJ/kg	3760 ± 1130 (30%)			
				Measurement, DSC			
Model Dependent Parameter		n_{kz} (i=5)	-	0.59 ± 0.06	0.58	0.01	0.18
				GA	GA	SCE	SHC
		n_c (i=5)	-	0.53 ± 0.06	0.37	0.88	-0.26
				GA	GA	SCE	SHC
		γ (i=2)	m	0.00348 ± 0.00134	0.00051	0.00002	0.02482
				GA	GA	SCE	SHC
		γ (i=4)	m	0.00475 ± 0.00184	0.00625	0.00001	0.05832
				GA	GA	SCE	SHC
		γ (i=5)	m	0.00769 ± 0.00225	0.00001	0.00003	-0.02453
				GA	GA	SCE	SHC

Validation

Analyze simulation quality

IDENTIFY SENSITIVE PARAMETERS FOR MODEL INPUTS[1]

Global Sensitivity Analysis (Morris Method): For this case, a total of 21 parameters are necessary. In this example case, a structured global sensitivity analysis technique is used to determine the sensitivity of input parameters used in the model. Among various global-analysis techniques, screening design is one of the simplest methods to identify important parameters.[28,29,30] Typical screening designs are one-at-a-time (OAT) experiments, where a value is changed and its impact is evaluated in turn. It is known that classical OAT experiments are less meaningful if the model of interest is affected by nonlinearities, which causes a drastically different "sensitivities" when parameter changes around the "control" scenario, depending on the chosen "control" scenarios. To address this limitation, Morris (1991) has proposed a global OAT design method, by covering the entire space in which the parameters may vary independently of the specific initial "control" scenario one may commence the experiment with. A global OAT design assumes that the model is characterized by a large number of parameters and/or is computationally expensive (regarding computational time and computational resources) to run.

Although originally the Morris Method was used for unit-less parameters, for this problem it was used for parameters with units. Because the Method allowed the user to interpret the effect of changes made in the inputs to the model outputs in terms of simulation variation observed in dimensional units (i.e., seconds for time, °C for temperature, and g/m^2-s for mass-loss rate), one was able to apply the significance level (see below) directly. This allows the user to rank the sensitivity of each parameter with a quantifiable variation.

Significance level: To identify the sensitive parameters of a model via a sensitivity analysis, there needs to be a measure to determine the sensitivity. This measure, defined as the level of significance, should be able to distinguish which effects shown in the simulation results due to changes made in the inputs are significant and which are not. A typical sensitivity analysis allows the user to rank the input parameters in terms of its sensitivity to model outputs. Defining the level of significance allows the user also to determine how many of the parameters from the top ranking should be set with caution, because those significantly affect the simulation results. The level of significance that defines the sensitivity of an input parameter should be predetermined by the user based on one's goal of conducting the simulation. When the best simulation accuracy is desired, the level of significance should be determined by the experimental uncertainty obtained by tests identical to the simulation set-up, such as the cone calorimeter tests. For example, if the ignition time has an uncertainty of +/- 20 sec. in the cone calorimeter tests, any changes in the model input that allows more than +/- 20 sec. in the model output should be considered as a "significant change." However, there are situations where low simulation accuracy is acceptable for one's simulation purposes. In these cases, the level of significance can be set by the modeler to be greater than the experimental uncertainty, and this approach results in less parameter being considered as sensitive to model outputs.

→ *In this example case, the significance level is set equal to experiment uncertainty for best simulation accuracy.*

Application: After identifying the necessary parameters for pyrolysis modeling with a model of choice and selecting the significance level, a sensitivity analysis is performed to identify sensitive input parameters to model output. To determine the region of experimentation for Morris' Method, the minimum and maximum range for each parameter is selected by the user using common sense. Four levels, P1 through P4, are used (p = {0,1/3,2/3,1}) with an increment of $\Delta = p/[2(p-1)] = 2/3$ following the guide presented by Morris. Four cases are simulated, resulting in four elementary effects for each parameter. See Table A(D)-11.

Table A(D)-11. Summary of unknown model parameters included in sensitivity analysis with searchable space defined with SA min and max: 4 levels (P1 though P4) and an increment of Δ are shown.

	No.		SA Min	SA Max	**p1**	**p2**	p3	p4	Δ
MA	1	k_1	0.05	0.50	0.05	0.20	0.35	0.50	0.30
	2	c_1	500	3500	500	1500	2500	3500	2000
	3	ε_1	0.01	1.00	0.01	0.34	0.67	1.00	0.66
MA_residue	4	k_2	0.05	0.50	0.05	0.20	0.35	0.50	0.30
	5	c_2	500	3500	500	1500	2500	3500	2000
	6	ε_2	0.01	1.00	0.01	0.34	0.67	1.00	0.66
	7	γ_2	0.001	0.100	0.001	0.034	0.067	0.100	0.066
A	8	k_3	0.50	5.00	0.50	2.00	3.50	5.00	3.00
	9	c_3	500	3500	500	1500	2500	3500	2000
	10	ε_3	0.01	1.00	0.01	0.34	0.67	1.00	0.66
A_residue	11	k_4	0.10	5.00	0.10	1.73	3.37	5.00	3.27
	12	c_4	500	3500	500	1500	2500	3500	2000
	13	ε_4	0.01	1.00	0.01	0.34	0.67	1.00	0.66
	14	γ_4	0.001	0.100	0.001	0.034	0.067	0.100	0.066
Fiberglass	15	k_5	0.05	0.50	0.05	0.20	0.35	0.50	0.30
	16	n_k	0.00	1.00	0.00	0.33	0.67	1.00	0.67
	17	c_5	500	3500	500	1500	2500	3500	2000
	18	n_c	0.00	1.00	0.00	0.33	0.67	1.00	0.67
	19	ε_5	0.01	1.00	0.01	0.34	0.67	1.00	0.66
	20	γ_5	0.001	0.100	0.001	0.034	0.067	0.100	0.066
HoR	21	ΔH_2	1.0E+05	1.0E+07	1.0E+05	3.4E+06	6.7E+06	1.0E+07	6.6E+06

To calculate an elementary effect, first a baseline case needs to be constructed. The baseline is a group of the entire parameters with their values randomly chosen from **P1 or P2**. This is because there are four levels in this analysis, and when conducting the analysis adding Δ should not exceed the region of experiment. Next, a random order should be created for each case, where this order is used to change the parameter value from its baseline by Δ one at a time. The effect of changing a parameter by Δ is evaluated by running the model and evaluating the changes made in the model output of interest. Using these four effects found from four cases for each parameter, the modeler now can calculate the mean and its standard deviation or variance of changes that occurred due to

an increase/decrease made to a single parameter value by Δ. Any parameter resulting in a significant change in model outputs when changed by Δ (i.e., a large mean and/or standard deviation/variance for changes made in the modeling outputs) are considered to be "sensitive."

The modeling outputs of interest are as follows for this example case:

- T_s at $\tau = 1$ s/mm^2
- T_s at $\tau = 3$ s/mm^2
- T_b at $\tau = 1$ s/mm^2
- T_b at $\tau = 3$ s/mm^2
- T_{surf}-ig where t_{ig} obtained from experiment data
- MLR-ig where t_{ig} obtained from experiment data
- MLRpeak

Note that kinetic parameters are not included in the sensitivity analysis because when a model-fitting method is used to determine kinetic parameters, any uncertainty in activation energy can be compensated by adjusting the pre-exponential coefficient and vice versa. Therefore, knowing the compensation effect between the estimated activation energy and pre-exponential factor, which is always accounted for in the model-fitting method, the effect of uncertainties in kinetic parameters on modeling outputs of interest is considered to be negligible.

Results: The results are shown with a sensitivity coefficient for each parameter defined as below:

$$SC \equiv \frac{\text{average mean or standard deviation of effects from 4 cases}}{\text{Significance Level}}$$

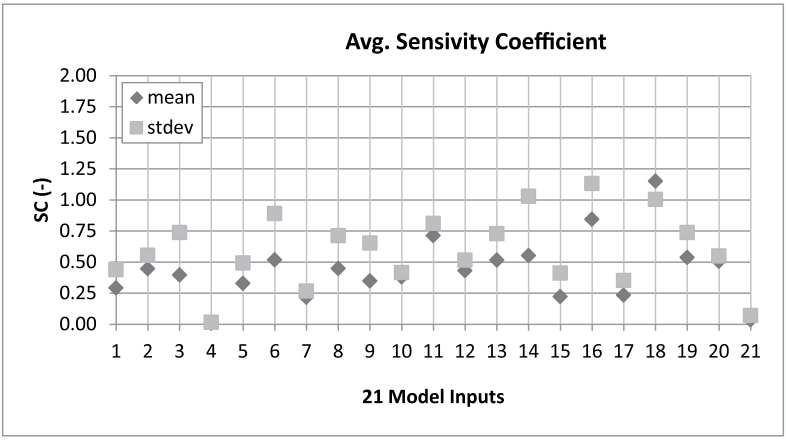

Figure A(D)-29. Sensitivity coefficient (SC) for 21 parameters included in sensitivity analysis

Based on this analysis, Δ changes made in **input parameters, 6, 11, 14, 16 and 18** results in significant changes in the modeling outputs of interest (SC ≥ 1). See Figure A(D)-29. Therefore, when conducting uncertainty analysis, these parameters will be considered to estimate the uncertainty band of modeling outputs. As noted before, the confidence interval for these parameters will be estimated from near-optimal parameter sets found from numerical optimization using GA. Note that the significance-level set as experiment uncertainty is estimated in the following section; however, it is used to calculate SC in this step.

DETERMINE DATA AND MODEL OUTPUT UNCERTAINTY TO MAKE COMPARISON[viii]

1. Conduct uncertainty analysis of data

Data is acquired from three repeating cone tests of modified-acrylic resin with inorganic high-charring additive FRP composite with relatively high glass content under 50 kW/m^2 heat flux level.

The uncertainties in the MLR and thermocouple measurements at surfaces (front and back) were quantified by comparing data from these three identical FRP composite tests. Note that normalized time, time divided by sample thickness square, i.e., τ = time/δ2, is used to remove the effect of different sample thicknesses when comparing. Because the data is transient, values at different times (τ = 1, 3, 5, and 7 s/mm^2) from each test have been used to calculate the standard deviation at each time. Then these are averaged and used to estimate uncertainty by applying Student's t distribution with a sample size of three and calculating the 95% confidence interval. See Table A(D)-12.

Table A(D)-12. Summary of estimated uncertainty in modified-acrylic resin with high-charring additive (MA+A) FRP composite cone calorimeter experiments based on 3 repeating tests at 50 kW/m² heat flux level

	MLR (g/s-m^2)	T_s (°C)	T_b (°C)
± uncertainty	± 2.2	± 67	± 14

2. Conduct uncertainty analysis of model outputs of interest – MLR, T_s and T_b

- Baseline case was selected at simulation with EHF = 50 kW/m^2, thickness = 8.7 mm, and the best optimum-parameter set.
- Five parameters that were determined to be sensitive to modeling outputs of interest are varied in the simulations one at a time from the baseline case. See Table A(D)-13 for summary.

[viii] Data uncertainty is accounted for here because this is required to determine the goodness of near-optimal parameter sets. Optimization targets (experiment data) should be considered with their uncertainty bounds to decide how good the match is between the targets and optimum simulations with their uncertainty.

Table A(D)-13. Outline of 5 parameters – MA_residue emissivity, A_residue thermal conductivity and GAMMA, fiberglass thermal conductivity, and specific heat capacity T dependent terms – varied in uncertainty analysis using one-at-a-time method

No.	Parameter	Optimum±C.I. (α=0.05, t-distribution)	ε_2	k_4	γ_4	n_k	n_c
6	MA_residue Emissivity	0.60 ± 0.04	+ –				
11	A_residue Thermal Conductivity	0.33 ± 0.11		+ –			
14	A_residue GAMMA	0.0095 ± 0.0042			+ –		
16	Fiberglass Thermal Conductivity T Dependent Term	0.30 ± 0.08				+ –	
18	Fiberglass Specific-Heat Capacity T Dependent Term	0.57 ± 0.11					+ –

- The effect of variation is calculated by considering the change in MLR, front and back-surface temperature profiles from baseline case. By varying certain parameters one at a time, standard deviation of the two cases (altered and baseline case) are calculated at each time step and 2 x the maximum standard deviation found from time interval of interest is used as effects. Results are shown in Table A(D)-14.
- Uncertainty in these modeling outputs (MLR and T_s) is calculated using the Law of Propagation of Uncertainty. Note that when inputs are varied to its uncertainty boundary values – minimum or maximum – the maximum effect was selected in the analysis to estimate the maximum uncertainty.

Table A(D)-14. Comparison between experiment data from cone calorimeter test and modeling outputs using estimated parameter values using numerical optimization (GA, SCE, SHC)

	Data	GA(avg)	GA(best)	SCE	SHC
Peak MLR (g/m^2s)	27 ± 31	10.7 ± 1.2	11.4	10.6	12.4
Avg MLR (g/m^2s)	5.8 ± 1.6	6.3 ± 1.2	6.1	6.2	8.1
t to pMLR (s)	200 ± 70	196	189	189	196
Ts at τ = 1 s/mm^2 (°c)	341 ± 54	336 ± 6	327	339	326
Ts at τ = 3 s/mm^2 (°c)	541 ± 100	496 ± 6	515	519	450
Ts at τ = 5 s/mm^2 (°c)	632 ± 9	583 ± 6	607	611	517
Tb at τ = 1 s/mm^2 (°c)	101 ± 14	111 ± 43	117	91	133
Tb at τ = 3 s/mm^2 (°c)	240 ± 23	274 ± 43	276	265	289
Tb at τ = 5 s/mm^2 (°c)	299 ± 25	302 ± 43	302	302	330

COMPARE DATA WITH SIMULATION RESULTS WITH CONSIDERATION OF UNCERTAINTIES

1. TG / DTG Predictions at 10°C/min Heating Rate Using Estimated Kinetic Parameters

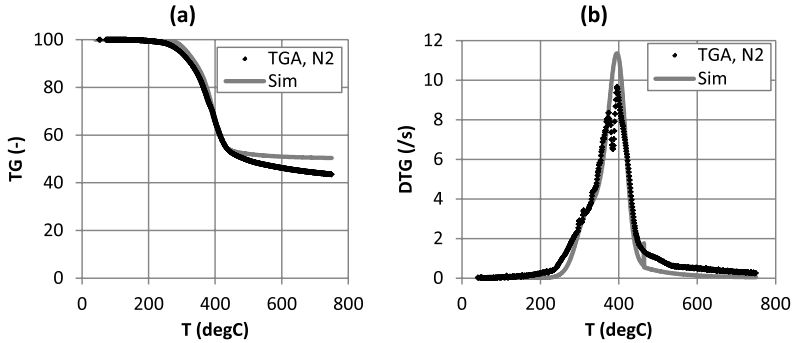

Figure A(D)-30. TG/DTG curves at 10°C/min heating rate with different estimation results for kinetic parameters for thermal decomposition of fire-retarded FRP composite: Testing of resin with additive sample (~10mg) with nitrogen purge

2. Modeling Output: Mass Loss Rate (MLR)

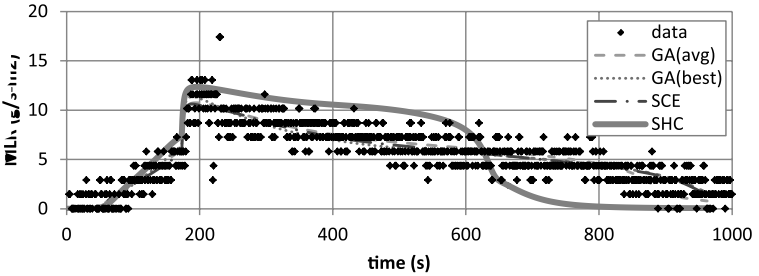

Figure A(D)-31. Mass-loss rate (MLR) comparisons for FRP composite with modified-acrylic resin with high-charring inorganic additive between actual MLR from experiment (data) and modeled MLR (GA, SCE, SHC) at applied heat flux of 50 kW/m². Note that data shown were used to estimate model-parameter values via numerical optimization using GA, SCE, or SHC routines.

3. Modeling Output: Surface Temperature (T_{surf})

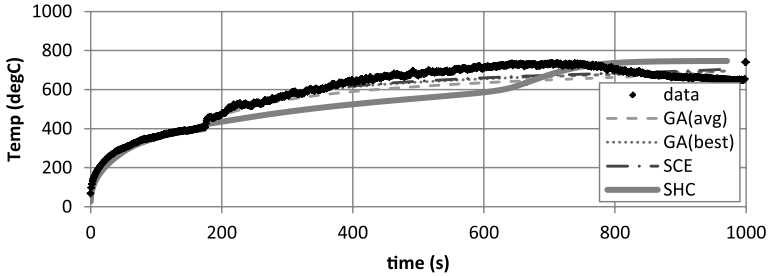

Figure A(D)-32. Surface temperature (T_{surf}) comparisons for FRP Composite with modified-acrylic resin with high-charring inorganic additive between actual T_{surf} from experiment (data) and modeled T_{surf} (GA, SCE, SHC) at applied heat flux of 50 kW/m². Note that data shown were used to estimate model-parameter values via numerical optimization using GA, SCE or SHC routines.

Validate simulation quality upon extrapolation

1. Modeling Output: Mass-Loss Rate (MLR)

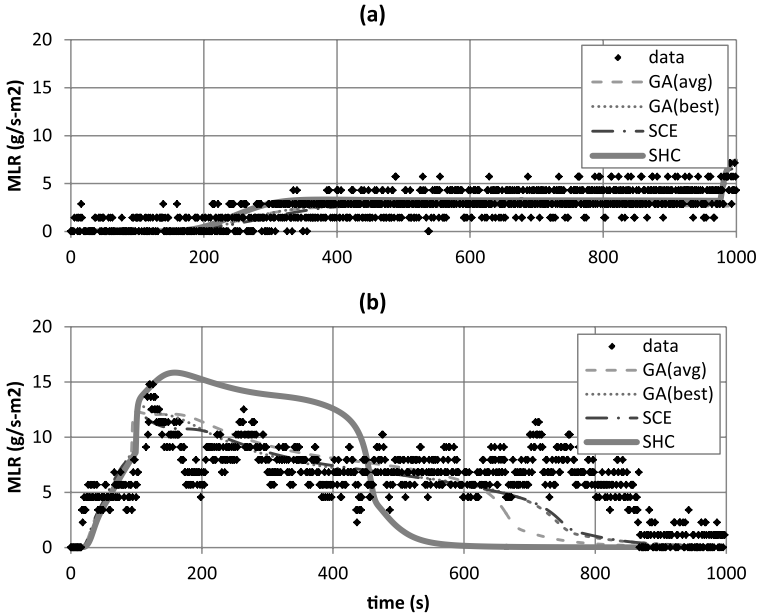

Figure A(D)-33. Mass-loss rate (MLR) comparisons for FRP composite with modified-acrylic resin with high-charring inorganic additive between actual MLR from experiment (data) and modeled MLR (GA, SCE, SHC) at applied heat flux of (a) 25 and (b) 75 kW/m². Note that data shown were not included in the model-parameter-estimation process; hence, these two cases are considered as extrapolation cases.

2. Modeling Output: Surface Temperature (T_{surf})

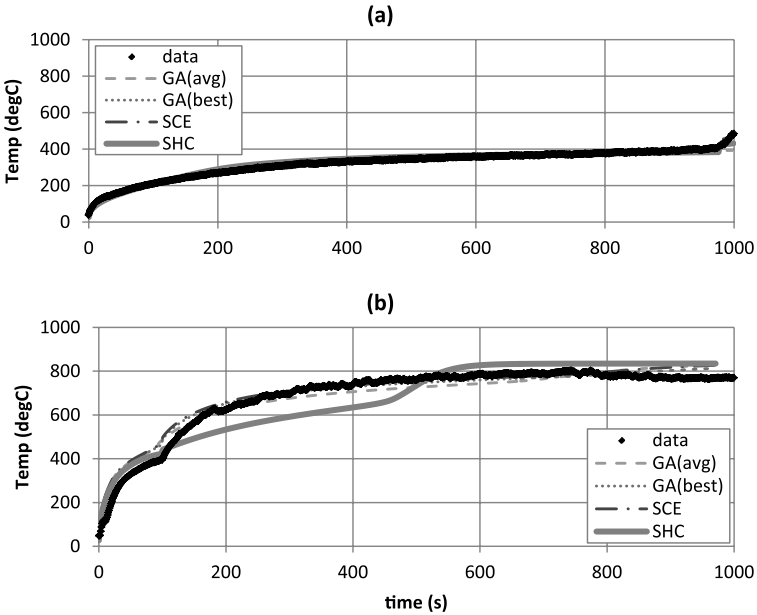

Figure A(D)-34. Surface temperature (T_{surf}) comparisons for FRP composite with modified-acrylic resin with high-charring inorganic additive between actual T_{surf} from experiment (data) and modeled T_{surf} (GA, SCE, SHC) at applied heat flux of (a) 25 and (b) 75 kW/m². Note that data shown were not included in the model-parameter-estimation process; hence, these two cases are considered as extrapolation cases.

Commentary

General Comments

- TG/DTG
  - Good agreement between simulated TG/DTG thermograms and those of actual from TGA experiment is shown when thermal decomposition kinetics is modeled using multiple heating-rate data.
  - The proposed kinetic model does not account for minor mass loss at relatively lower and higher temperature range.
- Comparison Between Data and Computed-Modeling Outputs
  - Modeled peak MLRs are all in quantitative agreement with data, considering its uncertainty.
  - Avg MLRs of modeling are in good agreement with data, except for that of SHC.
  - Modeled time-to-peak MLRs are all in quantitative agreement with data.
  - Modeled surface temperatures at earlier time (τ = 1 s/mm²) show good agreement with data, while at later times (τ = 3 and 5 s/mm²) modeling results deviate from experiment results; however, considering that there is flame interfering with data collection from surface thermocouple, uncertainty in data should probably be larger.

- Modeled back-surface temperatures at different times from GA(avg) show good agreement with data, considering the modeling uncertainty. Those from GA(best), SCE, and SHC are off by ~ 10 °C from experiment results.

- MLR
  - Optimization at HF = 50 kW/m^2: Generally good agreement exists between experiment data and all modeling results, considering the trend, except for that of SHC, indicating that optimization of SHC was close to being unsuccessful.
  - Extrapolation at HF = 25 kW/m^2: Good agreement exists between experiment data and all modeling results. All of the modeling cases are able to capture the slow increase in mass-loss rate in the earlier times after exposure to heating source and a jump near 1000 s due to ignition.
  - Extrapolation at HF = 75 kW/m^2: Good agreement exists between experiment data and all modeling results, except for SHC case. SHC's prediction is slightly higher than data and predictions from other cases; however, considering the uncertainty in the data, this falls within the acceptable bounds.
- Surface Temperature
  - Optimization at HF = 50 kW/m^2: Generally good agreement exists between experiment data and all modeling results, considering the trend, even for that of SHC. Note that after ignition (post-ignition stage) the flame interferes with data reading of thermocouple on the surface.
  - Extrapolation at HF = 25 kW/m^2: Good agreement exists between experiment data and all modeling results.
  - Extrapolation at HF = 75 kW/m^2: Good agreement exists between experiment data and all modeling results, except for the SHC case.

Limitation in Modeling

- When considering limitation of the parameters in modeling this fire-retarded FRP composite, the modeler should take into account the applicability of the parameters and their associated uncertainties. For example, any assumptions used when determining a parameter value via experiment direct or indirect measurements can be utilized to understand when the parameter value becomes inappropriate. For this example, most consideration can be given to the parameters related to decomposition kinetics. One should be cautious that these findings can cause this FRP composite to behave differently under changing conditions, which were not included in the parameter estimation process.
- First, the reaction-order-type kinetic model can be used to fit the DTG data with some degree of satisfaction for all reactions (see +A-R and R). However, the estimated reaction order is high as 5 for +A-R reaction. This indicates that the model is forced to fit the data, knowing that the reaction order of this magnitude is rare to find in the literature. Also, the DSC data confirms that the reaction-order-type model was inappropriate for +A-R as well. Although the model is giving high correlation coefficients between the data and modeling for +A-R reaction, the DSC data show that +A-R should exist from 200°C and end before

400°C, where a strong endotherm is observed. When the data is fit with a reaction-order-type kinetic model, the additive decomposition temperature range extends beyond 400°C, ending near 600°C.

- Second, the decomposition of the additive reaction is best described by a kinetic model that describes a diffusion controlled reaction (Jander's type model). The model type is reasonable, considering that the model simulates the weight loss to be slow initially with respect to temperature increase and decays relatively fast after the weight-loss rate peak. This modeling becomes suitable for an additive decomposing within a resin-polymer system resulting in a time delay due to the time necessary to degrade the polymer near the additive. Consider the additive being mixed within the resin polymer. For the additive to undergo a decomposition reaction, the degradation of the resin polymer should occur simultaneously, because the additive is aggregated within the resin. Having the additive decomposition temperature lower than that of the resin, the decomposition of the additive is delayed until the temperature is higher to allow the resin to decompose. When this model is actually applied, it provides a good estimate of the slow weight loss at the initial stage near 200°C and the temperature range for the entire reaction. Additionally, when this model is used, the modeling results for weight-loss rate after 300°C matches well with the actual DTG data together with R reaction described with a reaction-order-type kinetic model.
- Third, although kinetic modeling has been conducted to give best fitness between the modeling and the DTG data obtained over various heating rates (5 to 60°C/min), assuming that the kinetics are identical irrespective of heating rates, changes in the kinetic over four heating rates have been noticed. At lower heating rates, the portion of the sample weight consumed via MA_residue oxidation increases, where at higher heating rates it decreases. This can be explained by understanding that the MA_residue oxidation reaction is controlled by oxygen diffusion from the ambient to the condense phase. At a low heating rate, more time is available for oxygen diffusion with respect to temperature change, allowing an increase in the weight loss due to oxidation. However, when the heating rate is higher, the conditions become the opposite, and pyrolysis reaction (R) dominates. The fitness of the model to DTG data increases when this effect is accounted for in the modeling.

Example 5.4 Modeling Plywood

An example case is shown for a non-fire retarded Douglas Fir plywood. Thermal decomposition is modeled with two-step reactions – water loss and decomposition of dry plywood to char. Note that for this example, one approach will be used to estimate model parameters – a combination of non-optimization and manual optimization methods.

Measure Parameters

When conducting parameter estimation via independent experiments, consider the following:

- Check consistency between model used in experiment analysis to determine parameter in measurement process and pyrolysis model to mathematically describe the parameter of interest.
- Use statistical approach for determining uncertainty; otherwise, meet equivalency to this requirement.

1. Density

Although plywood has a laminate structure, this material is considered as a homogeneous single-layer material. Bulk density of the virgin fuel material is measured by experiment conducted at room temperature (≈298K), weighing sample's mass, and dividing mass with sample volume, which is 540 ± 10 kg/m^3.

$$\rho_{\text{wet plywood}} = 540 \text{ kg/m}^3$$

Density of water was found from literature:[31]

$$\rho_{\text{water}} = 1000 \text{ kg/m}^3$$

Based on TGA experiment, moisture content of wet plywood is estimated as 7% by weight. This information is used to estimate density of dry plywood, which is 504 kg/m^3.

$$\rho_{\text{dry plywood}} = 504 \text{ kg/m}^3$$

Also estimated based on TGA experiment, the weight loss due to thermal decomposition of dry plywood to char is 67%, resulting in:

$$\rho_{\text{char}} = 173 \text{ kg/m}^3$$

2. Thermal Conductivity

Thermal conductivity of water was found from literature:[31]

$$k_{\text{water}} = 0.6 \text{ W/m-K}$$

Thermal conductivity of dry plywood and char were estimated via manual optimization, but with its initial guess based on measurement at 20°C (ASTM C518/E1225):

$$k_{\text{initial guess}} = 0.122 \text{ W/m-K}$$

3. Specific-heat Capacity

Specific-heat capacity of water was found from literature[31]:

$$\mathbf{c_{p\ water} = 4200\ J/kg\text{-}K}$$

Specific-heat capacity of dry plywood and char were estimated via manual optimization, but with its initial guess based on measurement at 20°C (ASTM E1269):

$$\mathbf{c_{p\ initial\ guess} = 1200\ J/kg\text{-}K}$$

4. Absorption Coefficient

For simplification, solid-phase species involved in modeling are considered as an opaque material. Therefore, the absorption coefficient is essentially infinity.

$$K \rightarrow \infty$$

5. Emissivity

Emissivity of water and char are approximated as 1. Emissivity of dry plywood is measured using ASTM E903:

$$\mathbf{\varepsilon_{dry\ wood} = 0.891 \pm 0.018}$$

6. Reaction Order, Pre-exponential Factor, and Activation Energy

This example case is determined to have decomposition kinetics type 3 (two major peaks in DTG over entire mass-loss temperature range) according to TGA experiment conducted in nitrogen atmosphere. Based on this information, kinetic parameters will be obtained via the model-fitting method with four iso-heating rate TGA data conducted in air atmosphere.

7. Heat of Reaction

Heat-of-reaction for water loss is measured using DSC:

$$\mathbf{\Delta H_{water\ loss} = 2500 \pm 800}$$

Heat-of-reaction for decomposition of dry plywood to char is not measured; will be obtained via manual optimization.

Summary

Among seven categories of parameters, most have been obtained via direct measurement, which are shaded in Table A(D)-15. The rest of the unknown parameters, a **total of five parameters**, should be obtained via numerical optimization in pair with pyrolysis modeling using bench-scale experiment data or equivalent.

Table A(D)-15. Summary of necessary model parameters for simulating pyrolysis of plywood

	No	Condense Phase		
		i=1, water	*i=2, dry_plywood*	*i=3, char*
Material Property	1	ρ_1	ρ_2	ρ_3
	2	k_1	k_2	k_3
	3	c_1	c_2	c_3
	4	κ_1	κ_2	κ_3
Parameters for Specifying Conditions	5	ε_1	ε_2	ε_3
		Heterogeneous RxN		
		k = 1, water loss	***k = 2, wood decomposition***	
Kinetic Parameters and Heats assuming n^{th} order model and Arrhenius-type expression	6	n_1	n_2	
		Z_1	Z_2	
		E_1	E_2	
	7	ΔH_1	ΔH_2	

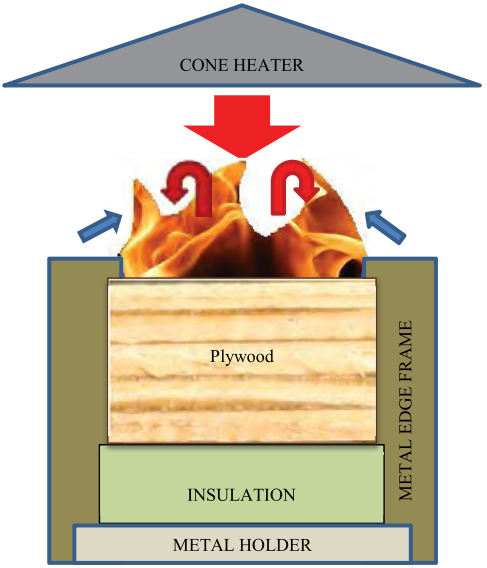

Figure A(D)-35. Simplified representation of a cone calorimeter test of plywood

SELECT MODEL: GPYRO

UNDERSTAND BENCH-SCALE EXPERIMENT SET-UP FOR MODELING SIMPLE CASES

A simplified representation of a cone calorimeter test of FRP composite is shown in Figure A(D)-35. The sample is placed on top of an insulation, which sits on a metal holder. Another metal frame is placed on top of the sample, insulation, and the holder. A metal edge frame is used as well.

CONFIGURE MODEL CONDITIONS BASED ON UNDERSTANDING OF EXPERIMENT SET-UP

In the model, the phenomena discussed above are simulated as below. Basic assumptions are as follows:

- Instantaneous release of volatiles from solid to the gas phase
- Local thermal equilibrium between the solid and the volatiles
- No condensation of gaseous products
- No porosity effects

Further details can be found from the *Technical Reference*[6] and *User's Guide*[7] of GPYRO (http://code.google.com/p/gpyro).

When conducting the GPYRO simulation for the cone calorimeter set-up, the metal edge frame will be ignored and backing is insulated. The ignition phenomenon is interpreted as the following in the simulations: at a known time-of-ignition (from experiment data), additional heat flux of 20 kW/m^2 is applied to the surface to simulate heat flux from the flame. This value is

estimated from a measurement from this material pyrolyzing in the cone with a total-heat-flux gauge measuring heat flux impinging on the sample surface. Figure A(D)-36 shows the total-heat-flux measurement from sample surface (test conducted at 50 kW/m^2 applied heat flux). From the time-of-ignition ($\tau \sim 0.1$ s/mm^2) an increase above the 50 kW/m^2 line in measured heat flux is observed due to flame. The oscillation in data in the time interval of ignition to $\tau = 1$ s/mm^2 is an artifact due to water evaporation, which had condensed near the water-cooled heat-flux gauge.

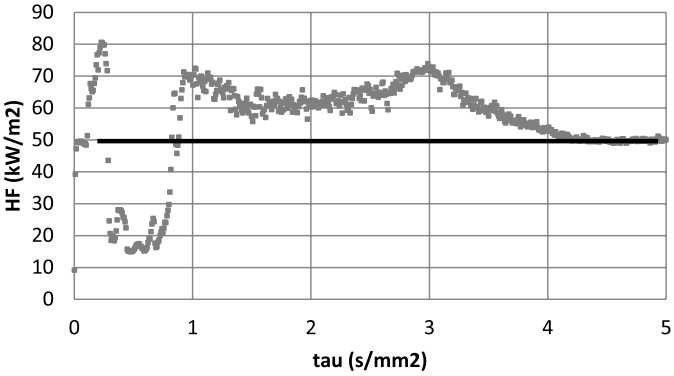

Figure A(D)-36. Total heat flux measured from plywood surface during cone calorimeter test at external-heat-flux level of 50kW/m^2: Ignition occurs before $\tau = 1$ s/mm^2 and from this point additional heat flux impinges on the surface due to the flame

For the back surface, an additional layer of insulation with known properties is modeled to simulate some heat loss through the back. The contact resistance (hcrz) between the FRP composite and the insulation is estimated as roughly 10 W/m^{2}K and that of insulation layer and ambient as 1 W/m^{2}K.

In addition to the parameters introduced in previous section (see Parameter Estimation Results), the model (GPYRO) has a coefficient (γ, GAMMA) that is used to model radiative heat transfer through the pores. This parameter with T3 is a model-dependent parameter that is added as another term in the effective thermal conductivity. γ is used for porous fiberglass and decomposed solid species, which results in a more porous state due to the weight loss; therefore, more radiative heat transfer through the gas-phase pores, i.e., for condense phase specie i = 2 (char).

Therefore, the **total unknown parameters** of five now becomes **six** including γ.

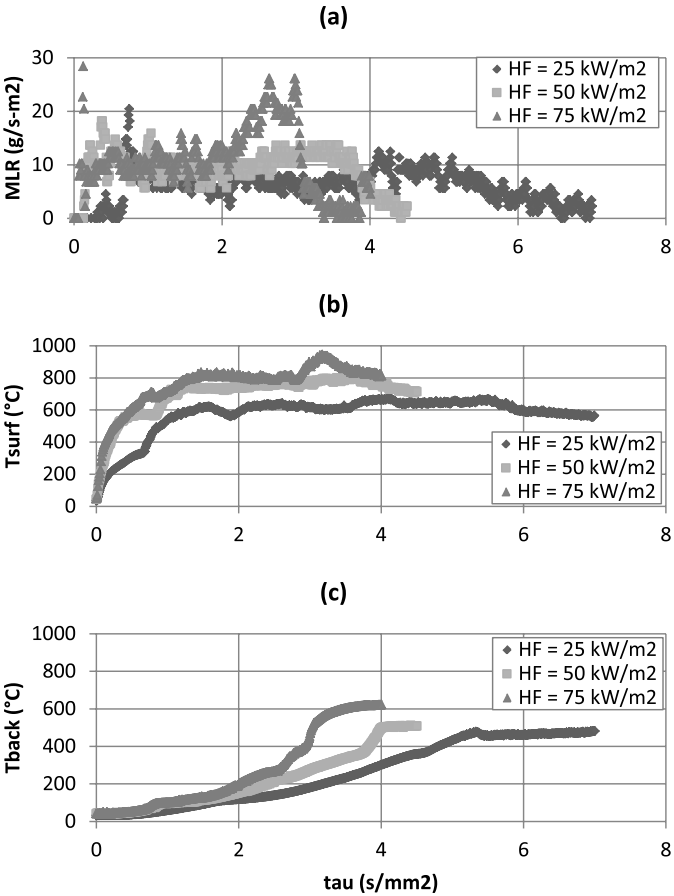

Figure A(D)-37. Cone calorimeter (cone) test data of plywood (thickness, δ is 11.1 ± 0.1 mm, density, ρ is 540 ± 10 kg/m³) impinged with effective heat fluxes (EHF) of 25 to 75 kW/m²

3. Check data reproducibility by repeating identical experiments

Data is acquired from two repeating cone tests of plywood under 50 kW/m² heat-flux level. Uncertainty analysis will be performed later.

SELECT NUMERICAL OPTIMIZATION ROUTINE

- Manual optimization
- See Chapter 5 for more description of each optimization routine.

CONDUCT NUMERICAL OPTIMIZATION IN PAIR WITH SIMULATIONS USING EXPERIMENT DATA AS TARGETS

Numerous simulations with a simplified version of GPYRO have been used in pair with manual optimization to obtain unknown parameters. Experiment data of mass-loss rate (MLR), surface-temperature measurements (T_s), and back-surface temperature measurements (T_b) generated with various applied heat-flux levels between 25 and 75 kW/m^2 have been used in the optimization process as targets (i.e., optimization is conducted for unknown parameters to match modeling outputs of interest to certain experiment data).

Obtain Confidence Intervals for Optimized Parameters

For this example case, where manual optimization is used, confidence intervals are approximated as ±10% for each optimized parameter.

Parameter Estimation Results

	Parameter		Unit	Comparable Non-optimization and Manual Optimization
Thermo-physical Property	i = 1 (water)	ρ_i	kg/m^3	1000
				Reference[31]
		k_i	W/m-K	0.6
				Reference[31]
		c_i	J/kg-K	4200
				Reference[31]
	i = 2 (dry_wood)	ρ_i	kg/m^3	504 ± 10
				Measurement
		k_i	W/m-K	0.26
				Manual Optimization with Initial Guess of 0.122 measured at 20 °C (dry_wood, ASTM C518/E1225)
		c_i	J/kg-K	2400
				Manual Optimization with Initial Guess of 1200 measured at 20 °C (dry_wood, ASTM E1269)
	i = 3 (char)	ρ_i	kg/m^3	173
				Measurement
		k_i	W/m-K	0.12
				Manual Optimization with Initial Guess of 0.122 measured at 20 °C (dry_wood, ASTM C518/E1225)
		c_i	J/kg-K	3700
				Manual Optimization with Initial Guess of 1200 measured at 20 °C (dry_wood, ASTM E1269)

Optical Property	i = 1 (water)	ε_i	-	1.00	
				Approximated	
	i = 2 (dry_wood)	κ_i	/m	10^6	
				Approximated as opaque	
		ε_i	-	0.891 ± 0.018	
				Measurement, ASTM E903	
	i = 3 (char)	κ_i	/m	10^6	
				Approximated as opaque	
		ε_i	-	1.00	
				Approximated	
Kinetics and Heats	k = 1 water → vap↑	n_k	-	5.0	Model Fitting with Multiple Heating Rate TGA Data
		Z_k	/s	2.5×10^{12}	
		E_k	J/mol	83×10^4	
		ΔH_k	kJ/kg	2500 ± 800 (30%)	
				Measurement, DSC	
	k = 2 dry_wood → char + vap↑	n_k	-	1.7	Model Fitting with Multiple Heating Rate TGA Data
		Z_k	/s	5.0×10^{16}	
		E_k	J/mol	2.10×10^5	
		ΔH_k	kJ/kg	631	
				Manual Optimization	
Model Dependent Parameter		γ (i=3)	m	0.0036	
				Manual Optimization	

Validation

Analyze Simulation Quality

IDENTIFY SENSITIVE PARAMETERS FOR MODEL INPUTS

- ε_i , $\rho_{i=2}$, ΔH_k
- Kinetic parameters are considered to be certain in this example case

DETERMINE DATA AND MODEL OUTPUT UNCERTAINTY TO MAKE COMPARISON[ix]

1. Conduct uncertainty analysis of data: Data is acquired from two repeating cone tests of plywood under 50 kW/m^2 heat-flux level.
2. The uncertainties in the MLR and thermocouple measurements on the front surface were quantified by comparing data from these two identical FRP composite tests. Note that the effect of different sample thicknesses was considered to be negligible, for sample thicknesses in two tests were 11.1 and 11.2 mm. Because the data is transient, the standard deviation at each time step was calculated. Then these are averaged and multiplied by 2 to estimate uncertainty: uncertainty in MLR, Ts and Tb are ± 3.4g/sm^2, ± 54 °C and ± 27 °C, respectively.

[ix] Data uncertainty is accounted for here because this is required to determine the goodness of near-optimal parameter sets. Optimization targets (experiment data) should be considered with its uncertainty bounds to decide how good the match is between the targets and optimum simulations with its uncertainty.

3. Assume:
   a. Uncertainties are comparable to the same sample tested at various heat flux levels
   b. Data set found above is close to the averaged curves from multiple identical tests under same conditions

4. Conduct uncertainty analysis of model outputs of interest – MLR and T_s
   - Baseline case: HF = 50 kW/m^2, thickness = 8.7 mm.
   - Sensitive parameters – density of dry_wood and char, emissivity of water, dry_wood and char, heat-of-reaction for drying process and thermal decomposition of dry_wood to char – varied one at a time from baseline to its max and min: ±10% of estimated value or uncertainty limits found from measurement experiment. Results are shown in Table A(D)-16.
   - Kinetic parameters are considered to be certain in this example.
   - Integration of uncertainty is calculated by the Law of Propagation of Uncertainty: uncertainty in model's MLR, T_s and T_b are **± 7.2g/sm^2**, **± 57 °C** and **± 157 °C** respectively.

Table A(D)-16. Comparison between experiment data from cone calorimeter test and modeling outputs using estimated parameter values via measurements and manual optimization

	Data (Based on 2 tests, uncertainty as 2 times standard deviation)	Measurements and Manual Optimization
Peak MLR (g/m2s)	19.9 ± 4.8	18.1 ± 7.2
Avg MLR (g/m2s)	6.8 ± 0.5	6.6 ± 7.2
t to pMLR (s)	81 ± 113	23
Ts at 100 s (°c)	604 ± 112	628 ± 57
Ts at 200 s (°c)	734 ± 10	670 ± 57
Ts at 300 s (°c)	732 ± 45	689 ± 57
Tb at 100 s (°c)	68 ± 20	56 ± 157
Tb at 200 s (°c)	118 ± 1	185 ± 157
Tb at 300 s (°c)	196 ± 10	291 ± 157

1. TG / DTG Predictions at 20 °C/min Heating Rate Using Estimated Kinetic Parameters

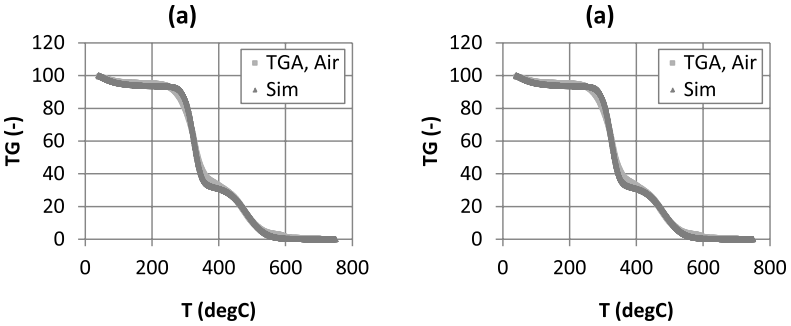

Figure A(D)-38. TG/DTG curves at 20°C/min heating rate with different estimation results for kinetic parameters for thermal decomposition of plywood: testing of plywood sample (~10mg) with air purge

2. Modeling Output: Mass Loss Rate (MLR)

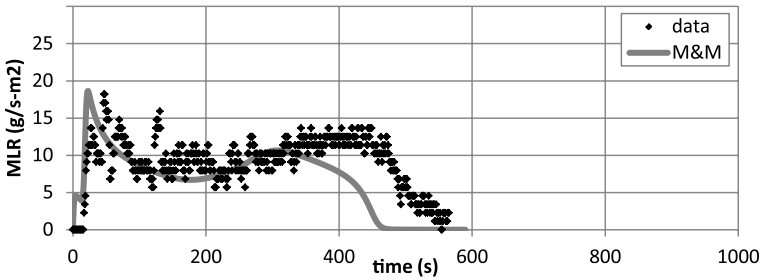

Figure A(D)-39. Mass-loss rate (MLR) comparisons for FRP composite with plywood between actual MLR from experiment (data) and modeled MLR (M&M) at applied heat flux of 50 kW/m². Note that data shown were used to estimate model parameter values via manual optimization.

3. Modeling Output: Surface Temperature (T_{surf})

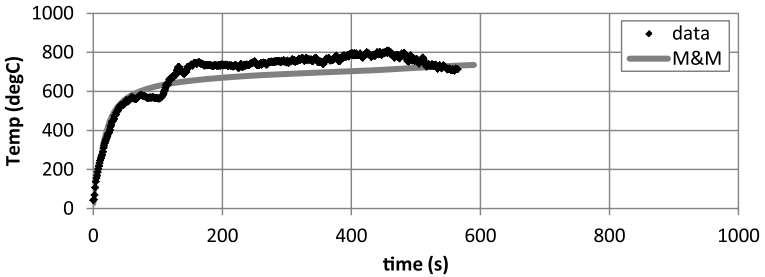

Figure A(D)-40. Surface-temperature (T_{surf}) comparisons for plywood between actual T_{surf} from experiment (data) and modeled T_{surf} (M&M) at applied heat flux of 50 kW/m². Note that data shown were used to estimate model-parameter values via manual optimization.

4. Modeling Output: Back-surface Temperature (T_{back})

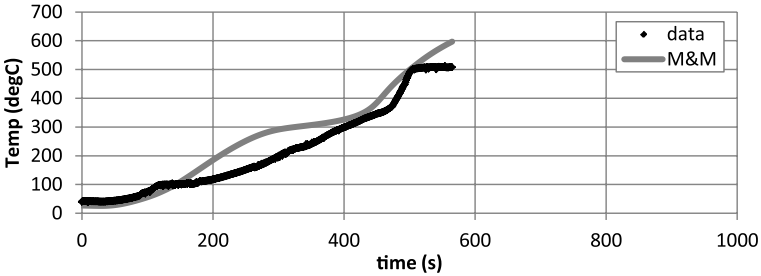

Figure A(D)-41. Back-surface temperature (T_{back}) comparisons for plywood between actual T_{back} from experiment (data) and modeled T_{back} (M&M) at applied heat flux of 50 kW/m². Note that data shown were used to estimate model-parameter values via manual optimization.

Validate simulation quality upon extrapolation

1. Modeling Output: Mass-Loss Rate (MLR)

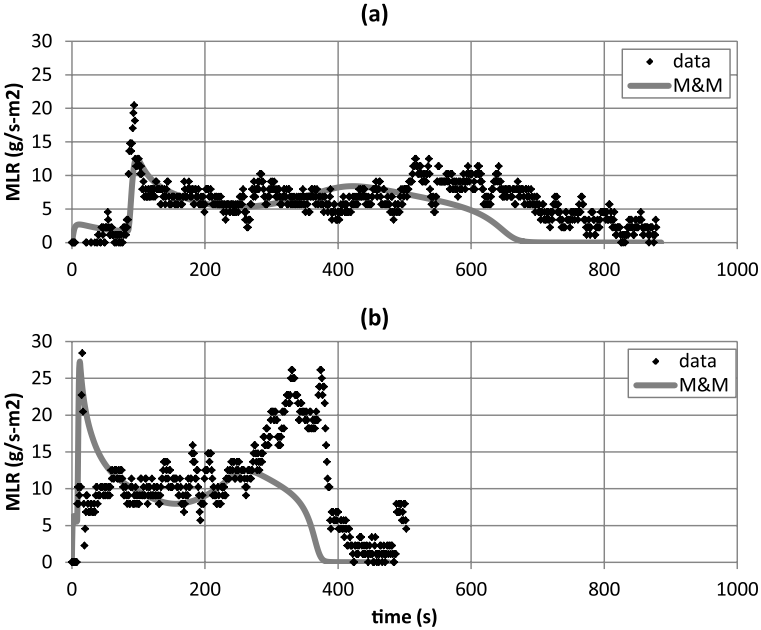

Figure A(D)-42. Mass-loss rate (MLR) comparisons for FRP composite with plywood between actual MLR from experiment (data) and modeled MLR (M&M) at applied heat flux of (a) 25 and (b) 75 kW/m². Note that data shown were not included in the model-parameter-estimation process; hence, these two cases are considered as extrapolation cases.

2. Modeling Output: Surface Temperature (T_{surf})

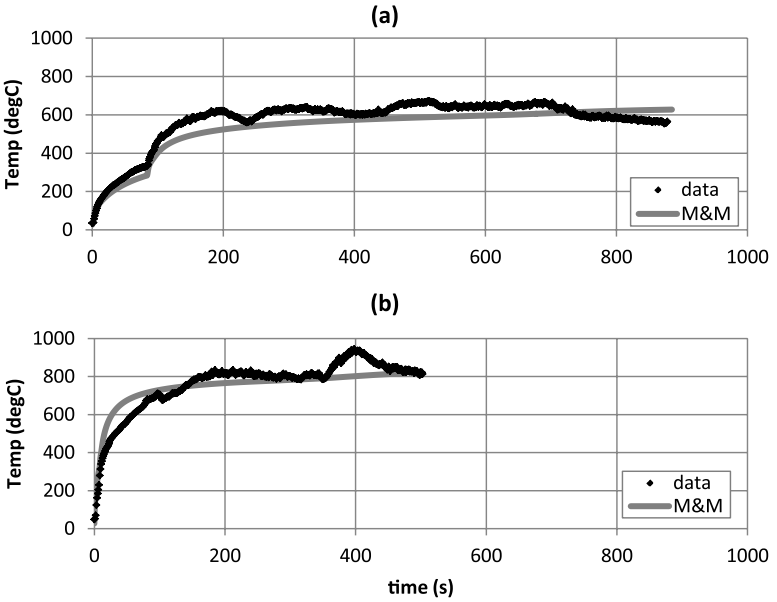

Figure A(D)-43. Surface-temperature (T_{surf}) comparisons for FRP composite with plywood between actual T_{surf} from experiment (data) and modeled T_{surf} (M&M) at applied heat flux of (a) 25 and (b) 75 kW/m^2. Note that data shown were not included in the model-parameter-estimation process; hence, these two cases are considered as extrapolation cases.

3. Modeling Output: Back-surface Temperature (T_{back})

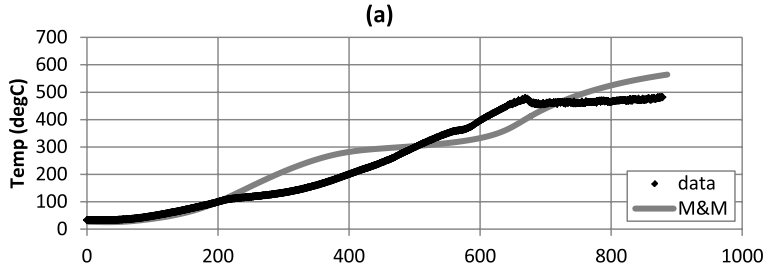

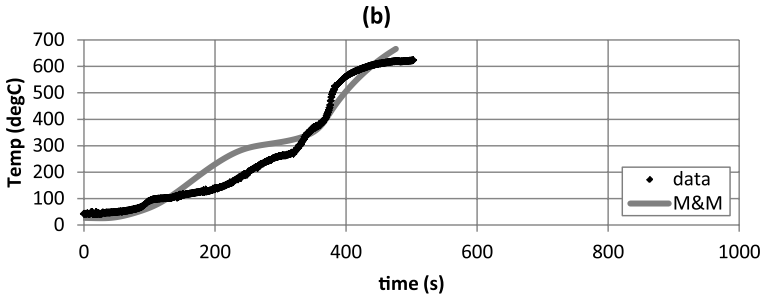

Figure A(D)-44. Back-surface temperature (T_{back}) comparisons for plywood between actual T_{back} from experiment (data) and modeled T_{back} (M&M) at applied heat flux of (a) 25 and (b) 75 kW/m². Note that data shown were not included in the model-parameter-estimation process; hence, these two cases are considered as extrapolation cases.

Commentary

General Comments

- TG/DTG
  - Good agreement between simulated TG/DTG thermograms and those of actual from TGA experiment is shown when thermal decomposition kinetics is modeled using multiple heating rate data.
  - Proposed kinetic model does not account for mass loss due to char oxidation at relatively higher temperature range (T > 400°C).
- Comparison Between Data and Computed Modeling Outputs
  - Modeled peak MLR, Avg MLR, time-to-peak MLR, and T_s, and T_b at various times are all in quantitative agreement with data, considering its uncertainty.
- MLR
  - Optimization at HF = 50 kW/m²: Generally good agreement exists between experiment data and all modeling results, considering the trend. Some deviation of modeling results from data is shown at later times, where the second peak is observed in the MLR curve. Near this region, bending of the sample toward the front surface occurs with respect to a rapid temperature increase throughout the back surface. This phenomenon is strictly a 3D behavior, which is not explicitly accounted for in current 1D model. Additionally, mass loss due to minor char oxidation at this region is speculated, for flame height becomes smaller and bending of sample may allow more oxygen to diffuse to the solid phase.
  - Extrapolation at HF = 25 kW/m²: Good agreement exists between experiment data and modeling results. Modeling is able to capture the initial mass-loss-rate peak followed by a decrease qualitatively and quantitatively. A qualitative agreement between data and modeling results exists for the second mass-loss-rate peak; however, actual sample in cone testing extends for a longer period of time (~100 s), while in modeling burnout time occurs earlier. This is probably due to excluding char oxidation in kinetic modeling.

- Extrapolation at HF = 75 kW/m^2: Good agreement exists between experiment data and modeling results, except for the second peak in mass-loss-rate curve. See above for discussion.

- Surface Temperature
  - Optimization at HF = 50 kW/m^2: Generally good agreement exists between experiment data and modeling results, considering the trend. Note that after ignition (post-ignition stage) the flame interferes with data reading of the thermocouple on surface.
  - Extrapolation at HF = 25 kW/m^2: Good agreement exists between experiment data and modeling results.
  - Extrapolation at HF = 75 kW/m^2: Good agreement exists between experiment data and modeling results.

Limitation in Modeling

- When considering limitation of the parameters in modeling this plywood, the modeler should take into account the applicability of the parameters and their associated uncertainties. For example, any assumptions used when determining a parameter value via experiment direct or indirect measurements can be utilized to understand when the parameter value becomes inappropriate. For this example, most consideration can be given to the parameters related to decomposition kinetics. One should be cautious that these findings can cause this FRP composite to behave differently under changing conditions, which were not included in the parameter estimation process.
- In this example, drying is simplified as a heterogeneous reaction (i.e., an Arrhenius Law temperature dependence evaporation rate), which occurs near 100°C, based on TGA experiment results. However, water evaporation from a wet wood is governed by transport phenomena of liquid-phase water and vapor diffusion. Additionally, typically the water travels toward the back surface during heating and re-condensation may occur, allowing the back surface to be colder. This phenomenon will not be captured in this modeling.
- Any char oxidation has been considered to be minimal in this example, considering that with a flame sheet on the material surface oxygen diffusion becomes limited. However, when analyzing the cone calorimeter results, some oxidation is speculated, for the sample loses ~4 to 6% more of the initial sample weight comparing to TGA experiment.

References

1 Stoliarov, S.I.; Crowley, S.; Lyon, R.E.; and Linteris, G.T., Prediction of the burning rates of non-charring polymers, Combustion and Flame, 156:5 (2009), 1068-1083, ISSN 0010-2180, DOI: 10.1016/j.combustflame.2008.11.010.

2 Lobo, H. and Cohen, C., Measurement of thermal conductivity of polymer melts by the line-source method. Polym Eng Sci, 30 (1990) 65-70, doi: 10.1002/pen.760300202.

3 Brandrup, J. Immergut, E.H.; Grulke, E.A.; Abe, A.; and Bloch, D.R. (Eds.), Polymer Handbook, 4th ed., John Wiley & Sons, New York, (1999).

4 Stoliarov, S.I.; and Walters, R.N., "Determination of the Heats of Gasification of Polymers Using Differential Scanning Calorimetry," *Polymer Degradation and Stability*, 93 (2008) 422-427.

5 Brandrup. J,; Immergut, E.H.; Grulke, E.A., Abe, A.; Bloch, D.R., (Eds.), Polymer Handbook. 4th ed. New York: John Wiley and Sons, (1999).

6 Lautenberger, C., Gpyro, A Generalized Pyrolysis Model for Combustible Solids, Technical Reference, Version 0.700, 19 February (2009).

7 Lautenberger, C., Gpyro, A Generalized Pyrolysis Model for Combustible Solids, Users' Guide, Version 0.700, February 19, 2009.

8 Beaulieu, P.A.; and Dembsey, N.A., "Effect of Oxygen on Flame Heat Flux in Horizontal and Vertical Orientations", *Fire Safety Journal*, 43:6 (2008), 410-428. [DOI10.1016/j.firesaf.2007.11.008].

9 ASTM Standard D 7309-07, Test Method for Determining Flammability Characteristics of Plastics and Other Solid Materials Using Microscale Combustion Calorimetry, ASTM International, West Conshohocken, PA, (2007).

10 Brandrup, J. Immergut, E.H.; Grulke, E.A.; Abe, A.; and Bloch, D.R., (Eds.), Polymer Handbook, 4th ed., John Wiley & Sons, New York, (1999).

11 Kashiwagi, T.; and Ohlemiller, T.J., "A study of oxygen effects on nonflaming transient gasification of PMMA and PE during thermal irradiation," *Proceedings of the Combustion Institute* 19 (1982) 815-823.

12 Kashiwagi T., Polymer combustion and flammability—role of the condensed phase. *Twenty-fifth Symposium (International) on Combustion*, Irvine, CA, (1994) 1423-1437.

13 Matala, A., "Estimation of Solid Phase Reaction Parameters for Fire Simulation," MS Thesis, University of Technology, Helsinki, (2008).

14 Chaos, M.; Khan, M.; Krishnamoorthy, N.; Chatterjee, P.; Wang, Y.; and Dorofeev, S.B., Experiments and Modeling of Single- and Triple-Wall Corrugated Cardboard: Effective Material Properties and Fire Behavior, In: *Fire and Materials* 2011, 12th International Conference and Exhibition, Fisherman's Wharf, San Francisco, USA, 31st January - 2nd February (2011).

15 Chaos, M.; Khan, M.M.; Krishnamoorthy, N.; de Ris, J.L.; and Dorofeev, S.B., Bench-Scale Flammability Experiments: Determination of Material Properties Using Pyrolysis Models for Use in CFD Fire Simulations. In: *Interflam 2010*, Nottingham, U.K., 5-7 July (2010).

16 ASTM Standard E 2058, Test Methods for Measurement of Synthetic Polymer Material Flammability Using a Fire Propagation Apparatus (FPA), ASTM International, West Conshohocken, PA, (2009), DOI: 10.1520/E2058-09, www.astm.org

17 Khan, M.M.; de Ris, J.L.; and Ogden, S.D., Effect of Moisture on Ignition Time of Cellulosic Materials, *Fire Safety Science* 9 (2009) 167-178.

18 de Ris, J.L.; and Khan, M.M., A Sample Holder for Determining Material Properties, *Fire and Materials* 24 (2000) 219-226.

19 Bates, D.M. & Watts, D.G. *Nonlinear Regression Analysis and Its Applications*, New York: John Wiley and Sons (2007).

20 Stoliarov, S. I.; Safronava, N.; and Lyon, R. E., The effect of variation in polymer properties on the rate of burning. *Fire and Materials*, 33 (2009) 257-271. doi: 10.1002/fam.1003.

21 Chaos, M.; Khan, M.M.; Krishnamoorthy, N.; de Ris, J.L.; and Dorofeev, S.B., Material Properties for CFD Fire Models, FM Global Open Source CFD Fire Modeling Workshop (2010), http://docs.google.com/viewer?

22 Kim, E.; Dembsey, N.A.; and Dore, C.H., "Property Estimation for Pyrolysis Modeling Applied to Flame Retarded Modified Acrylic FRP Composites", in *Proceedings of Composites & Polycon 2010*, American Composites Manufacturers Association, Mandalay Bay, Las Vegas, NV, USA, 9-11 February (2010).

23 Kulshreshtha, A.K.; and Vasile, C., Handbook of polymer blends and composites, Rapra Technology Limited, (2002).

24 Lewin, M., Synergism and Catalysis in Flame Retardancy of Polymers, *Polym. Adv. Technol.* 12 (2001) 215-222.

25 LeVan, S.L., The Chemistry of Solid Wood; Chapter 14, Chemistry of Fire Retardancy, American Chemical Society, (1984).

26 ASTM Standard E 84-05, Test Method for Surface Burning Characteristics of Building Materials, ASTM E 84-05, ASTM, 100 Barr Harbor Drive, West Conshohocken, PA, USA, (2005).

27 Lautenberger, C., "A Generalized Pyrolysis Model for Combustible Solids", Ph.D. Dissertation, Department of Mechanical Engineering, University of California, Berkeley, (2007).

28 Cacuci, D.G.; Ionescu-Bujor, M.; and Navon, I.M., *Sensitivity and Uncertainty Analysis; Theory; Volume 1*, Chapman & Hall / CRC Taylor & Francis Group, (2005).

29 Cacuci, D.G.; Ionescu-Bujor, M.; and Navon, I.M., *Sensitivity and Uncertainty Analysis; Applications to Large-Scale Systems; Volume 2*, Chapman & Hall / CRC Taylor & Francis Group, (2005).

30 Saltelli, A.; Chan, K.; and Scott, E.M., *Sensitivity Analysis*, Wiley, (2000).

31 NIST Chemistry WebBook, http://webbook.nist.gov/.

Chapter 5
Supplement – Morris' OAT Method

Supplement – Morris' OAT Method 365
References 367

Supplement – Morris' OAT Method

Morris' one-at-a-time (OAT) Method, also known as the Elementary Effect Method,[1] is one of the simplest types of a global sensitivity analysis. This method was developed for a computationally expensive model where a large number of factors are involved in the model calculations. This method is used to rank the factors from factors that have significant influence to model output to those that have negligible effect. The results from applying Morris' method allow the user to categorize the input factors into three groups – factors that have (1) negligible effect, (2) additive effects, or (3) non-linear or interaction effects on the simulation output.

A limitation of this method is that it may identify possible higher-order effects, but it only estimates for the first order effects, i.e., the method does not provide estimations for factor-interactions. Although not discussed further, there is a revised version called the new Morris method that does provide means to estimate the sensitivity of a model due to interactions between two factors known as the second order effect.[2] The basic principles of the original Morris' OAT method are discussed below.

The range of variation of each component of the vector α of parameters is standardized to the unit interval, and each component is then considered to take on p values in the set {0,1/(p–1), 2/(p–1),3/(p–1),···,1} so that the region of experimentation becomes an i-dimensional p-level grid. Selecting this region of experiment reasonably for each parameter is an important factor for a successful analysis. An elementary effect of the ith-parameter at a point α is then defined as $d_i(\alpha) \equiv \left[R(\alpha_1, \cdots, \alpha_{i-1}, \alpha_i + \Delta, \alpha_{i+1}, \cdots, \alpha_I) - R(\alpha)\right] / \Delta$, where Δ is a predetermined multiple of 1/(p–1), such that $\alpha_i + \Delta$ is still within the region of experimentation. Note that the base vector α is randomly chosen, and the model is not evaluated at this base vector. A finite distribution of F_i elementary effects for the ith parameter is obtained by sampling α from within the region of experimentation. The number of elements for each F_i is $p^{k-1}[p-\Delta(p-1)]$. For the best economy of design, p is selected as an even number and Δ is calculated by $p/[2(p-1)]$. Morris showed that applying this selection approach allows the individual input factors to have an equal probability of being selected.

The distribution F_i is then characterized by its mean and standard deviation or variance and is graphically shown in two-dimension, where the mean is the x-axis, and the standard deviation or variance is the y-axis. A high mean indicates a parameter with an important overall influence on the response; a high standard deviation or variance indicates either a parameter interacting with other parameters or a parameter whose effect is nonlinear.

Graphical representation of calculating an elementary effect for each parameter is shown in Figure A(E)-1:

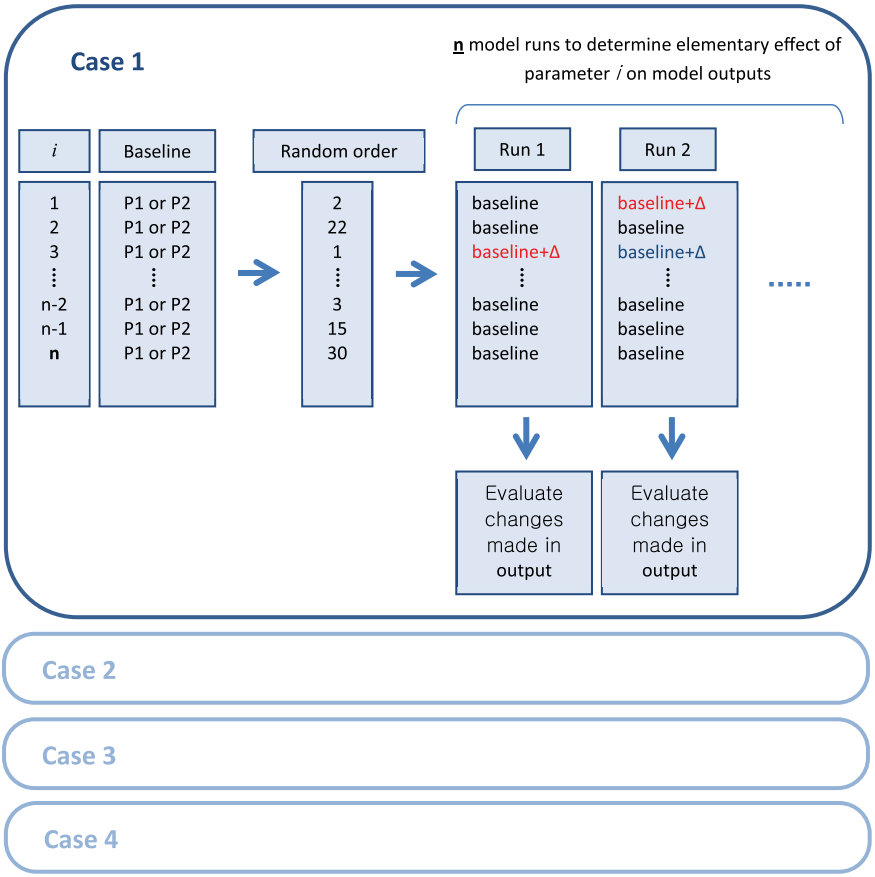

Figure A(E)-1. Schematic of Morris' OAT Method

References

1 Morris, M.D., Factorial sampling plans for preliminary computational experiments. Technometrics 33 (1991) 161-174.

2 Campolongo, F.; and Braddock, R., The use of graph theory in the sensitivity analysis of the model output: A second order screening method, Reliability Engineering and System Safety 64 (1999) 1–12, doi:10.1016/S0951-8320(02)00109-6

List of Tables

List of Tables. 369

List of Tables

Table 2-1. Example materials in Chapter 3 – empirical models: materials are either considered as a burning object or flat surface in modeling

Table 2-2. Example materials in Chapter 4 – simple analytical models: materials are either considered as thermally-thick and inert at pre-ignition with steady burning at post-ignition or thermally-thin and inert at pre-ignition with steady burning at post-ignition in modeling

Table 2-3. Example materials in Chapter 5 – Comprehensive analytical models: materials are considered to decompose with single or multiple reaction(s) with or without residue production in modeling

Table 3-1. Model parameter table: summary of model parameters required to conduct pyrolysis modeling

Table 3-2. Ignition sources specified in standard fire tests

Table 3-3. ASTM standards for measurement of time to ignition of materials exposed to specified level of incident radiant heat source in intermediate/bench-scale Calorimeter Tests

Table 3-4. Overview of example cases using empirical pyrolysis models

Table 3-5. Model parameter table for Case 1 examples

Table 3-6. Model parameter table for Case 2 examples

Table 4-1. Model Parameter table: summary of model parameters required to conduct pyrolysis modeling

Table 4-2. ASTM standards of calorimeter tests measuring ignition and burning properties of material

Table 4-3. Recommended hc values for different test apparatuses

Table 4-4. ASTM standards for measuring emissivity

Table 4-5. Overview of example cases using simple analytical pyrolysis models

Table 4-6. Model parameter table for Case 1 examples

Table 4-7. Model parameter table for Case 2 examples

Table 5-1. General governing equations for comprehensive pyrolysis models

Table 5-2. Various types of decomposition kinetics

Table 5-3. Model parameter table: summary of model parameters required to conduct pyrolysis modeling

Table 5-4. ASTM standards for measuring thermal conductivity using steady state methods

Table 5-5. ASTM standards for measuring thermal conductivity using transient methods

Table 5-6. ASTM standards for measuring specific heat capacity

Table 5-7. ASTM standards for measuring emissivity

Table 5-8. ASTM standards for thermogravimetry analysis (TGA)

Table 5-9. ASTM standard for measuring reaction enthalpies

Table 5-10. Three types of numerical optimization routines applied to comprehensive pyrolysis modeling in literature: Genetic Algorithm Shuffled Complex Evolution, and Stochastic Hill-climber

Table 5-11. Overview of example cases using comprehensive pyrolysis models

Table 5-12. Model parameter table for Case 1 examples

Table 5-13. Comparison between experiment data from cone calorimeter test and modeling outputs using estimated parameter values via either direct measurement, literature search, or approximation (A); measurements and numerical optimization (B-GA, B-SCE, B-SHC); or mostly numerical optimization (C-GA, C-SCE, C-SHC)

Table 5-14. model parameter table for Case 2 examples

Table 5-15. Comparison between experiment data from fire propagation apparatus test and modeling outputs using estimated parameter values via either measurements and numerical optimization (B-GA, B-SCE, B-SHC) or mostly numerical optimization (C-GA, C-SCE, C-SHC)

Table 5-16. Model parameter table for Case 3 examples

Table 5-17. Comparison between experiment data from cone calorimeter test and modeling outputs using estimated parameter values using numerical optimization (GA, SCE, SHC)

Table 5-18. Comparison between experiment data from cone calorimeter test and modeling outputs using estimated parameter values via measurements and manual optimization

Table A(C)-1. Ignition data from cone calorimeter tests for PMMA

Table A(C)-2. Summary of model parameter table with estimated values via direct measurements, literature search or approximation

Table A(C)-3. $\dot{q}''_{cr} / \dot{q}''_{e}$ versus $\sqrt{t_{ig}}$

Table A(C)-4. Estimation of effective heat of combustion using cone calorimeter test results at applied heat flux of 25, 50 and 75 kW/m^2

Table A(C)-5. Estimation of effective heat of gasification using cone calorimeter test results at applied heat flux of 25, 50 and 75 kW/m^2

Table A(C)-6. Summary of model parameter table with estimated values with uncertainty

Table A(C)-7. Comparison of time to ignition at different heat flux levels from actual experiment and pyrolysis modeling

Table A(C)-8. Comparison of time to ignition at different heat flux levels from actual experiment and pyrolysis modeling

Table A(C)-9. Summary of model parameter table with estimated values via direct measurements, literature search or approximation

Table A(C)-10. $\dot{q}''_{cr} / \dot{q}''_{e}$ versus $\sqrt{t_{ig}}$

Table A(C)-11. Estimation of effective heat of gasification using cone calorimeter test results at applied heat flux ranging between 25 and 75 kW/m^2

Table A(C)-12. Summary of model parameter table with estimated values with uncertainty

Table A(C)-13. Comparison of time to ignition at different heat flux levels from actual experiment and pyrolysis modeling

Table A(C)-14. Summary of model parameter table with estimated values via direct measurements, literature search or approximation

Table A(C)-15. $\dot{q}''_{cr} / \dot{q}''_{e}$ versus $\sqrt{t_{ig}}$

Table A(C)-16. Estimation of effective heat of gasification using cone calorimeter test results at applied heat flux ranging between 25 and 75 kW/m^2

Table A(C)-17. Summary of model parameter table with estimated values with uncertainty

Table A(C)-18. Comparison of time to ignition at different heat flux levels from actual experiment and pyrolysis modeling

Table A(C)-19. Ignition data from cone calorimeter tests for plywood

Table A(C)-20. Summary of model parameter table with estimated values via direct measurements, literature search or approximation

Table A(C)-21. $\dot{q}''_{cr} / \dot{q}''_{e}$ versus $\sqrt{t_{ig}}$

Table A(C)-22. Estimation of effective heat of gasification using cone calorimeter test results at applied heat flux ranging between 25 and 75 kW/m^2

Table A(C)-23. Summary of model parameter table with estimated values with uncertainty

Table A(C)-24. Comparison of time to ignition at different heat flux levels from actual experiment and pyrolysis modeling

Table A(C)-25. Ignition data from cone calorimeter tests for GRP with balsa wood core sandwich composite

Table A(C)-26. Summary of model parameter table with estimated values via direct measurements, literature search or approximation

Table A(C)-27. $\dot{q}''_{cr} / \dot{q}''_{e}$ versus $\sqrt{t_{ig}}$

Table A(C)-28. Estimation of effective heat of gasification using cone calorimeter test results at applied heat flux ranging between 30 and 90 kW/m^2

Table A(C)-29. Summary of model parameter table with estimated values with uncertainty

Table A(C)-30. Comparison of time to ignition at different heat flux levels from actual experiment and pyrolysis modeling

Table A(C)-31. Ignition data from cone calorimeter tests for thin FRP composite sheet

Table A(C)-32. Summary of model parameter table with estimated values via direct measurements, literature search or approximation

Table A(C)-33. $\dot{q}''_{cr} / \dot{q}''_{e}$ versus $\sqrt{t_{ig}}$

Table A(C)-34. Estimation of effective heat of gasification using cone calorimeter test results at applied heat flux ranging between 17 and 75 kW/m^2

Table A(C)-35. Summary of model parameter table with estimated values with uncertainty

Table A(C)-36. Comparison of time to ignition at different heat flux levels from actual experiment and pyrolysis modeling

Table A(D)-1. Summary of estimated uncertainty for each model parameter

Table A(D)-2. Summary of estimated uncertainty in PMMA Cone Calorimeter experiments based on 5 repeating tests under 49 kW/m^2 heat flux level with medium thickness sample (7.7 ~ 9.4 mm)

Table A(D)-3. Comparison between experiment data from cone calorimeter test and modeling outputs using estimated parameter values via either direct measurement, literature search, or approximation (A); measurements and numerical optimization (B-GA, B-SCE, B-SHC); or mostly numerical optimization (C-GA, C-SCE, C-SHC)

Table A(D)-4. Summary of necessary model parameters for simulating pyrolysis of Corrugated Cardboard

Table A(D)-5. Summary of estimated optimum with confidence interval (C.I.) for each model parameter

Table A(D)-6. Summary of estimated uncertainty in triple wall (2 layers) corrugated cardboard FPA experiments based on 2 repeating tests at 60 kW/m^2 heat flux level

Table A(D)-7. Outline of 5 parameter groups – kinetic parameters, heat of decomposition reaction and combustion, and emissivity of fuel and residue – varied in uncertainty analysis using one at a time method

Table A(D)-8. Comparison between experiment data from fire propagation apparatus test and modeling outputs using estimated parameter values via either measurements and numerical optimization (B-GA, B-SCE, B-SHC) or mostly numerical optimization (C-GA, C-SCE, C-SHC)

Table A(D)-9. Kinetic parameters for 2 step model – decomposition of additive (+A-R) and resin (R) – for modeling modified-acrylic resin with inorganic high-charring additive

Table A(D)-10. Summary of necessary model parameters for simulating pyrolysis of modified-acrylic resin with high-charring additive (MA+A) FRP composite

Table A(D)-11. Summary of unknown model parameters included in sensitivity analysis with searchable space defined with SA min and max: 4 levels (P1 though P4) and an increment of Δ are shown.

Table A(D)-12. Summary of estimated uncertainty in modified-acrylic resin with high-charring additive (MA+A) FRP composite cone calorimeter experiments based on 3 repeating tests at 50 kW/m^2 heat-flux level

Table A(D)-13. Outline of 5 parameters – MA_residue emissivity, A_residue thermal conductivity and GAMMA, fiberglass thermal conductivity and specific heat capacity T dependent terms – varied in uncertainty analysis using one-at-a-time method

Table A(D)-14. Comparison between experiment data from cone calorimeter test and modeling outputs using estimated parameter values using numerical optimization (GA, SCE, SHC)

Table A(D)-15. Summary of necessary model parameters for simulating pyrolysis of plywood

Table A(D)-16. Comparison between experiment data from cone calorimeter test and modeling outputs using estimated parameter values via measurements and manual optimization

List of Figures

List of Figures. 374

List of Figures

Figure 2-1. Material category: Depending on material's characteristics, material can be grouped into 4 categories and examples for each category is given.

Figure 2-2. Model selection flowchart: By examining the cross-section of material and analyzing experiment data that presents its fire behavior, modeler may determine material's virtual microstructure and appropriate pyrolysis models available for its specific use.

Figure 3-1. Flow chart of parameter estimation for empirical pyrolysis models

Figure 3-2. Effect of ignition source strength: single seat sofas tested in furniture calorimeter test with different ignition source – ignition with 59 mL gasoline poured (♦) or with 45 W butane gas flame (■)

Figure 3-3. Effect of ignition location: steel framed seat sofa mockups tested in furniture calorimeter test with different ignition location – ignition on center seat cushion (♦) or seat cushion on right side (■)

Figure 4-1. Schematic of a piloted ignition experiment

Figure 4-2. Pyrolysis modeling set-up used for thermally-thick materials

Figure 4-3. Pyrolysis modeling set-up used for thermally-thin materials

Figure 4-4. Measuring surface temperature with a thermocouple

Figure 4-5. Heat balance at the surface of a burning cone calorimeter specimen

Figure 4-6. Flow chart of parameter estimation for simple analytical pyrolysis models

Figure 4-7 Mass-loss rate (MLR) comparisons for PMMA between actual MLR from experiment (exp) and Modeled MLR (sim) at different applied heat-flux levels – (a) MLR at 25 kW/m^2; (b) MLR at 50 kW/m^2; and (c) MLR at 75 kW/m^2. Note that data shown were used to estimate model parameter values.

Figure 4-8 Mass-loss rate (MLR) comparisons for PMMA between actual MLR from experiment (exp) and modeled MLR (sim) at different applied heat-flux levels – (a) MLR at 28.4 kW/m^2; and (b) MLR at 60 kW/m^2. Note that data shown were not included in the model parameter estimation process; hence, these two cases are considered as extrapolation cases.

Figure 4-9 Mass-Loss Rate (MLR) comparisons for corrugated cardboard between actual MLR from experiment (exp) and modeled MLR (sim) at different applied heat-flux levels – (a) MLR at 25 kW/m^2; (b) MLR at 50 kW/m^2; and (c) MLR at 75 kW/m^2. Note that data shown were used to estimate model parameter values.

Figure 4-10 Mass-loss rate (MLR) comparisons for fire-retarded FRP composite between actual MLR from experiment (exp) and modeled MLR (sim) at different applied heat-flux levels – (a) MLR at 50 kW/m^2; and (b) MLR at 75 kW/m^2. Note that data shown were used to estimate model parameter values.

Figure 4-10 Mass-loss rate (MLR) comparisons for plywood between actual MLR from experiment (exp) and modeled MLR (sim) at different applied heat-flux levels – (a) MLR at 25 kW/m^2; (b) MLR at 50 kW/m^2; and (c) MLR at 75 kW/m^2. Note that data shown were used to estimate model parameter values.

Figure 4-12 Mass-loss rate (MLR) comparisons for sandwich composite – GRP skin with balsawood core – between actual MLR from experiment (exp) of the composite and modeled MLR (sim) of GRP skin at different applied heat-flux levels – (a) MLR at 35 kW/m^2; (b) MLR at 50 kW/m^2; and (c) MLR at 75 kW/m^2. Note that data shown were used to estimate model parameter values.

Figure 4-13 Mass-loss rate (MLR) comparisons for thin FRP composite between actual MLR from experiment (exp) and modeled MLR (sim) at different applied heat-flux levels – (a) MLR at 25 kW/m^2; (b) MLR at 50 kW/m^2; and (c) MLR at 75 kW/m^2. Note that data shown were used to estimate model parameter values.

Figure 5-1. Typical DTG thermogram showing single peak

Figure 5-2. Schematic of conducting Ozawa, Flynn and Wall Iso-conversional Method

Figure 5-3. Schematic of conducting Friedmen's Iso-conversional Method

Figure 5-4. Change in DTG curve with respect to changes made in n values using nth order reaction model

Figure 5-5. TG (weight loss) thermogram from TGA experiment (left) and heat flow diagram from DSC experiment (right) for decomposition of a rigid foam plastic

Figure 5-6. Melting points for a thermoplastic polymer as a function of DSC heating rates

Figure 5-7. Flow chart of parameter estimation for comprehensive pyrolysis models

Figure 5-8. Understanding manual optimization: (a) For a one-step thermal decomposition kinetics that takes place within temperature range of $T_a < T < T_b$, parameter estimation conductor may understand changing parameters related to reactant should affect fire behaviors at temperatures below T_a and changing parameters related to product should affect fire behaviors at temperatures above T_b; (b) Reducing HoR increases mass loss rate peak; (c) Reducing thermal conductivity results in wider spread between T_{surf} and T_{back}; (d) Reducing specific heat capacity results in faster increase in temperature throughout. Note that results from greater parameter value are shown in solid lines, while those from smaller value are shown in dashed lines.

Figure 5-9. Cone calorimeter test data of thick PMMA (thickness, δ ranging from 24 ~ 29 mm) impinged with effective heat fluxes (EHF) of 23, 46, and 69 kW/m^2

Figure 5-10. TG/DTG curves at 10°C/min heating rate with different estimation results for kinetic parameters for thermal decomposition of PMMA

Figure 5- 11. Mass-loss rate (MLR) comparisons for PMMA between actual MLR from experiment (data) and modeled MLR (A, B-GA, B-SCE, B-SHC, C-GA, C-SCE, C-SHC) at applied heat-flux of 46 kW/m^2. Note that data shown were used to estimate model parameter values via numerical optimization using GA, SCE or SHC routines.

Figure 5-12. Mass-loss rate (MLR) comparisons for PMMA between actual MLR from experiment (data) and modeled MLR (A, B-GA, B-SCE, B-SHC, C-GA, C-SCE, C-SHC) at applied heat flux of (a) 23 and (b) 64 kW/m^2. Note that data shown were not included in the model parameter estimation process; hence, these two cases are considered as extrapolation cases.

Figure 5-13. surface temperature (T_{surf}) comparisons for PMMA modeling using parameters estimated from different approaches – direct measurement, literature search, or approximation (A); measurement and numerical optimization (B-GA, B-SCE, B-SHC); mostly numerical optimization (C-GA, C-SCE, C-SHC) at applied heat flux of 46 kW/m^2. Note that data shown were used to estimate model parameter values via numerical optimization using GA, SCE or SHC routines.

Figure 5-14. Surface temperature (T_{surf}) comparisons for PMMA modeling using parameters estimated from different approaches – direct measurement, literature search, or approximation (A); measurement and numerical optimization (B-GA, B-SCE, B-SHC); mostly numerical optimization (C-GA, C-SCE, C-SHC) at applied heat flux of (a) 23 and (b) 64 kW/m^2. Note that data shown were not included in the model parameter estimation process; hence, these two cases are considered as extrapolation cases.

Figure 5-15. TGA thermograms of PMMA decomposition conducted under constant heating rates – 2, 5, 10 and 20K/min – and two different environments – (a) nitrogen and (b) air

Figure 5-16. Fire propagation apparatus (FPA) test data – (a) mass-loss rate; and (b) surface-temperature profile – of triple-wall corrugated cardboard, i.e., two layers of corrugated cardboard (thickness, δ is 30 mm) impinged with effective heat fluxes (EHF) of 20 to 110 kW/m^2

Figure 5-17. TG/DTG curves at 10°C/min heating rate with different estimation results for kinetic parameters for thermal decomposition of corrugated cardboard: For better comparison, TG and DTG thermograms have been scaled to result in 100% conversion.

Figure 5-18. Mass-Loss Rate (MLR) comparisons for corrugated cardboard between actual MLR from experiment (Data) and modeled MLR (B-GA, B-SCE, B-SHC, C-GA, C-SCE, C-SHC) at applied heat flux of 60 kW/m^2. Note that data shown were used to estimate model parameter values via numerical optimization using GA, SCE or SHC routines.

Figure 5-19. Mass-Loss Rate (MLR) comparisons for corrugated cardboard between actual MLR from experiment (data) and modeled MLR (B-GA, B-SCE, B-SHC, C-GA, C-SCE, C-SHC) at applied heat flux of (a) 20 and (b) 110 kW/m^2. Note that data shown were not included in the model-parameter estimation process; hence, these two cases are considered as extrapolation cases.

Figure 5-20. Surface-temperature (T_{surf}) comparisons for corrugated cardboard between actual T_{surf} from experiment (data) and modeled T_{surf} (B-GA, B-SCE, B-SHC, C-GA, C-SCE, C-SHC) at applied heat flux of 60 kW/m^2. Note that data shown were used to estimate model parameter values via numerical optimization using GA, SCE or SHC routines.

Figure 5-21. Surface Temperature (T_{surf}) comparisons for corrugated cardboard between actual T_{surf} from experiment (data) and modeled T_{surf} (B-GA, B-SCE, B-SHC, C-GA, C-SCE, C-SHC) at applied heat flux of (a) 20 and (b) 110 kW/m^2. Note that data shown were not included in the model parameter estimation process; hence, these two cases are considered as extrapolation cases.

Figure 5-22. TGA thermograms of corrugated cardboard decomposition conducted under constant heating rate of 20 °C/min and two different environments – nitrogen and air

Figure 5-23. Cross-section of FRP composite with modified acrylic resin with high-charring inorganic additive

Figure 5-24. Total heat flux measured from sample surface during cone calorimeter test

Figure 5-25. Cone calorimeter (cone) test data of modifiedacrylic resin with high-charring additive FRP composite (thickness, δ is 8.9 ± 0.2 mm, density, ρ is 1900 kg/m3) impinged with effective heat fluxes (EHF) of 25 to 75 kW/m^2

Figure 5-26. TG/DTG curves at 10°C/min heating rate with different estimation results for kinetic parameters for thermal decomposition of fire-retarded FRP composite: Testing of resin with additive sample (~10mg) with nitrogen purge

Figure 5-27. Mass-loss rate (MLR) comparisons for FRP composite with modified-acrylic resin with high-charring inorganic additive between actual MLR from experiment (data) and modeled MLR (GA, SCE, SHC) at applied heat flux of 50 kW/m^2. Note that data shown were used to estimate model parameter values via numerical optimization using GA, SCE or SHC routines.

Figure 5-28. Mass-loss rate (MLR) comparisons for FRP composite with modified-acrylic resin with high-charring inorganic additive between actual MLR from experiment (data) and modeled MLR (GA, SCE, SHC) at applied heat flux of (a) 25 and (b) 75 kW/m^2. Note that data shown were not included in the model parameter estimation process; hence, these two cases are considered as extrapolation cases.

Figure 5-29. Surface-temperature (T_{surf}) Comparisons for FRP composite with modified-acrylic resin with high-charring inorganic additive between actual T_{surf} from experiment (data) and modeled T_{surf} (GA, SCE, SHC) at applied heat flux of 50 kW/m^2. Note that data shown were used to estimate model parameter values via numerical optimization using GA, SCE or SHC routines.

Figure 5-30. Surface-temperature (T_{surf}) comparisons for FRP composite with modified-acrylic resin with high-charring inorganic additive between actual T_{surf} from experiment (data) and modeled T_{surf} (GA, SCE, SHC) at applied heat flux of (a) 25 and (b) 75 kW/m^2. Note that data shown were not included in the model parameter estimation process; hence, these two cases are considered as extrapolation cases.

Figure 5-31. Back-surface temperature (T_{back}) comparisons for FRP composite with modified-acrylic resin with high-charring inorganic additive between actual T_{back} from Experiment (Data) and Modeled T_{back} (GA, SCE, SHC) at applied heat flux of 50 kW/m^2. Note that data shown were used to estimate model parameter values via numerical optimization using GA, SCE or SHC routines.

Figure 5-32. Back-surface temperature (T_{back}) comparisons for FRP composite with modified-acrylic resin with high-charring inorganic additive between actual T_{back} from experiment (data) and modeled T_{back} (GA, SCE, SHC) at applied heat flux of (a) 25 and (b) 75 kW/m^2. Note that data shown were not included in the model parameter estimation process; hence, these two cases are considered as extrapolation cases.

Figure 5-33. Total heat flux measured from sample surface during cone calorimeter test

Figure 5-34. Cone calorimeter (cone) test data of plywood (thickness, δ is 11.1 ± 0.1 mm, density, ρ is 540 ± 10 kg/m^3) impinged with effective heat fluxes (EHF) of 25 to 75 kW/m^2

Figure 5-35. TG/DTG curves at 20°C/min heating rate with different estimation results for kinetic parameters for thermal decomposition of plywood: Testing of plywood sample (~10mg) with air purge

Figure 5-36. Mass-loss rate (MLR) comparisons for FRP composite with plywood between actual MLR from experiment (data) and modeled MLR (M&M) at applied heat flux of 50 kW/m^2. Note that data shown were used to estimate model parameter values via manual optimization.

Figure 5-37. Mass-loss rate (MLR) comparisons for FRP composite with plywood between actual MLR from experiment (data) and modeled MLR (M&M) at applied heat flux of (a) 25 and (b) 75 kW/m^2. Note that data shown were not included in the model parameter estimation process; hence, these two cases are considered as extrapolation cases.

Figure 5-38. Surface-temperature (T_{surf}) comparisons for plywood between actual T_{surf} from experiment (data) and modeled T_{surf} (M&M) at applied heat flux of 50 kW/m^2. Note that data shown were used to estimate model parameter values via manual optimization.

Figure 5-39. Surface-temperature (T_{surf}) comparisons for FRP composite with plywood between actual T_{surf} from experiment (data) and modeled T_{surf} (M&M) at applied heat flux of (a) 25 and (b) 75 kW/m^2. Note that data shown were not included in the model parameter estimation process; hence, these two cases are considered as extrapolation cases.

Figure 5-40. Back-surface temperature (T_{back}) comparisons for plywood between actual T_{back} from experiment (data) and modeled T_{back} (M&M) at applied heat flux of 50 kW/m^2. Note that data shown were used to estimate model parameter values via manual optimization.

Figure 5-41. Back-surface temperature (T_{back}) comparisons for plywood between actual T_{back} from experiment (data) and modeled T_{back} (M&M) at applied heat flux of (a) 25 and (b) 75 kW/m^2. Note that data shown were not included in the model parameter estimation process; hence, these two cases are considered as extrapolation cases.

Figure A(B)-1. Schematic of a furniture calorimeter

Figure A(B)-2. HRR curve from furniture calorimeter experiment of 4 identical tests of the same sofa mockup

Figure A(B)-3. Effect of ignition source strength: single seat sofas tested in furniture calorimeter test with different ignition source – ignition with 59 mL gasoline poured (◆) or with 45 W butane gas flame (■)

Figure A(B)-4. Effect of ignition location: steel framed seat sofa mockups tested in furniture calorimeter test with different ignition location – ignition on center seat cushion (◆) or seat cushion on right side (■)

Figure A(B)-5. Simplified representation of a cone calorimeter test of PMMA

Figure A(B)-6. MLR curve from cone calorimeter experiment of PMMA

Figure A(B)-7. Simplified representation of a cone calorimeter test of corrugated cardboard

Figure A(B)-8. MLR curve from cone calorimeter test of corrugated cardboard

Figure A(B)-9. Simplified representation of a cone calorimeter test of fire-retarded fiberglass-reinforced polymer (FRP) composite

Figure A(B)-10. MLR curve from cone calorimeter test of fire-retarded FRP composite

Figure A(B)-11. Simplified representation of a cone calorimeter test of plywood

Figure A(B)-12. MLR curve from cone calorimeter test of plywood

Figure A(C)-1. Simplified representation of a cone calorimeter test of PMMA

Figure A(C)-2. Plot of $\dot{q}''_{cr} / \dot{q}''_{e}$ versus $\sqrt{t_{ig}}$

Figure A(C)-3. Plot of steady MLR versus different applied heat-flux levels – 25, 50 and 75 kW/m^2

Figure A(C)-4. Mass-loss rate (MLR) comparisons for PMMA between actual MLR from experiment (exp) and modeled MLR (sim) at 25 kW/m^2. Note that data shown were used to estimate model parameter values.

Figure A(C)-5. Mass-loss rate (MLR) comparisons for PMMA between actual MLR from experiment (exp) and modeled MLR (sim) at 50 kW/m^2. Note that data shown were used to estimate model parameter values.

Figure A(C)-6. Mass-loss rate (MLR) comparisons for PMMA between actual MLR from experiment (exp) and modeled MLR (sim) at 75 kW/m^2. Note that data shown were used to estimate model parameter values.

Figure A(C)-7. Mass-loss rate (MLR) comparisons for PMMA between actual MLR from experiment (exp) and modeled MLR (sim) at 28.4 kW/m^2. Note that data shown were not included in the model parameter estimation process; hence, this case is considered as extrapolation case.

Figure A(C)-9. Mass-loss rate (MLR) comparisons for PMMA between actual MLR from experiment (exp) and modeled MLR (sim) at 60 kW/m^2. Note that data shown were not included in the model parameter estimation process; hence, this case is considered as extrapolation case.

Figure A(C)-10. Simplified representation of a cone calorimeter test of corrugated cardboard

Figure A(C)-11. Plot of $\dot{q}''_{cr} / \dot{q}''_{e}$ versus $\sqrt{t_{ig}}$

Figure A(C)-12. Plot of steady MLR versus different applied heat-flux levels – 25 to 75 kW/m^2

Figure A(C)-13. Mass-loss rate (MLR) comparisons for corrugated cardboard between actual MLR from experiment (exp) and modeled MLR (sim) at 25 kW/m^2. Note that data shown were used to estimate model parameter values.

Figure A(C)-14. Mass-loss rate (MLR) comparisons for corrugated cardboard between actual MLR from experiment (exp) and modeled MLR (sim) at 50 kW/m^2. Note that data shown were used to estimate model parameter values.

Figure A(C)-15. Mass-loss rate (MLR) comparisons for corrugated cardboard between actual MLR from experiment (exp) and modeled MLR (sim) at 75 kW/m^2. Note that data shown were used to estimate model parameter values.

Figure A(C)-16. Simplified representation of a cone calorimeter test of fire-retarded fiberglass-reinforced polymer (FRP) composite

Figure A(C)-17. Plot of $\dot{q}''_{cr} / \dot{q}''_{e}$ versus $\sqrt{t_{ig}}$

Figure A(C)-18. Plot of steady MLR versus different applied heat flux levels – 25 to 75 kW/m^2

Figure A(C)-19. Mass-loss rate (MLR) comparisons for fire-retarded FRP composite between actual MLR from experiment (exp) and modeled MLR (sim) at 50 kW/m^2. Note that data shown were used to estimate model parameter values.

Figure A(C)-20. Mass-loss rate (MLR) comparisons for fire-retarded FRP composite between actual MLR from experiment (exp) and modeled MLR (sim) at 75 kW/m^2. Note that data shown were used to estimate model parameter values.

Figure A(C)-21. Simplified representation of a cone calorimeter test of plywood

Figure A(C)-22. Plot of $\dot{q}''_{cr} / \dot{q}''_{e}$ versus $\sqrt{t_{ig}}$

Figure A(C)-23. Plot of steady MLR versus different applied heat -flux levels – 25 to 75 kW/m^2

Figure A(C)-24. Mass-loss rate (MLR) comparisons for plywood between actual MLR from experiment (exp) and modeled MLR (sim) at 25 kW/m^2. Note that data shown were used to estimate model parameter values.

Figure A(C)-25. Mass-loss rate (MLR) comparisons for plywood between actual MLR from experiment (exp) and modeled MLR (sim) at 50 kW/m^2. Note that data shown were used to estimate model parameter values.

Figure A(C)-26. Mass-loss rate (MLR) comparisons for plywood between actual MLR from experiment (exp) and modeled MLR (sim) at 75 kW/m^2. Note that data shown were used to estimate model parameter values.

Figure A(C)-27. Simplified representation of a cone calorimeter test of sandwich composite

Figure A(C)-28. Plot of $\dot{q}''_{cr} / \dot{q}''_{e}$ versus $\sqrt{t_{ig}}$

Figure A(C)-29. Plot of steady MLR versus different applied heat-flux levels – 25 to 75 kW/m^2

Figure A(C)-30. Mass-loss rate (MLR) comparisons for GRP with balsa wood core sandwich composite between actual MLR from experiment (exp) and modeled MLR (sim) at 25 kW/m^2. Note that data shown were used to estimate model parameter values.

Figure A(C)-31. Mass-loss rate (MLR) comparisons for GRP with balsa wood core sandwich composite between actual MLR from experiment (exp) and modeled MLR (sim) at 50 kW/m^2. Note that data shown were used to estimate model parameter values.

Figure A(C)-32. Mass-loss rate (MLR) comparisons for GRP with balsa wood core sandwich composite between actual MLR from experiment (exp) and modeled MLR (sim) at 75 kW/m^2. Note that data shown were used to estimate model parameter values.

Figure A(C)-33. Simplified representation of a cone calorimeter test of FRP composite sheet

Figure A(C)-34. Plot of $\dot{q}''_{cr} / \dot{q}''_{e}$ versus $\sqrt{t_{ig}}$

Figure A(C)-35. Plot of steady MLR versus different applied heat-flux levels – 25 to 75 kW/m^2

Figure A(C)-36. Mass-loss rate (MLR) comparisons for thin FRP composite sheet between actual MLR from experiment (exp) and modeled MLR (sim) at 25 kW/m^2. Note that data shown were used to estimate model parameter values.

Figure A(C)-37. Mass-loss rate (MLR) comparisons for thin FRP composite sheet between actual MLR from experiment (exp) and modeled MLR (sim) at 50 kW/m^2. Note that data shown were used to estimate model parameter values.

Figure A(C)-38. Mass-loss rate (MLR) comparisons for thin FRP composite sheet between actual MLR from experiment (exp) and modeled MLR (sim) at 75 kW/m^2. Note that data shown were used to estimate model parameter values.

Figure A(D)-1. Thermal conductivity of PMMA

Figure A(D)-2. Heat capacity of PMMA

Figure A(D)-3. Kinetic modeling for decomposition of PMMA under nitrogen atmosphere: Arrhenius equation with n = 1 reaction model is used.

Figure A(D)-4. Simplified representation of a cone calorimeter test of PMMA

Figure A(D)-5. Cone experiment results of PMMA with effective heat flux and thickness ranging from 23 to 69 kW/m^2 and 24 to 29 mm, respectively

Figure A(D)-6. TG/DTG curves at 10°C/min heating rate with different estimation results for kinetic parameters for thermal decomposition of PMMA

Figure A(D)-7. Mass-loss rate (MLR) comparisons for PMMA between actual MLR from experiment (data) and modeled MLR (A, B-GA, B-SCE, B-SHC, C-GA, C-SCE, C-SHC) at applied heat flux of 46 kW/m^2. Note that data shown were used to estimate model parameter values via numerical optimization using GA, SCE or SHC routines.

Figure A(D)-8. Surface-temperature (T_{surf}) comparisons for PMMA modeling using parameters estimated from different approaches – direct measurement, literature search, or approximation (A); measurement and numerical optimization (B-GA, B-SCE, B-SHC); mostly numerical optimization (C-GA, C-SCE, C-SHC) at applied heat flux of 46 kW/m^2. Note that data shown were used to estimate model parameter values via numerical optimization using GA, SCE or SHC routines.

Figure A(D)-9. Mass-loss rate (MLR) comparisons for PMMA between actual MLR from experiment (data) and modeled MLR (A, B-GA, B-SCE, B-SHC, C-GA, C-SCE, C-SHC) at applied heat flux of (a) 23 and (b) 64 kW/m^2. Note that data shown were not included in the model parameter estimation process; hence, these two cases are considered as extrapolation cases.

Figure A(D)-10. Surface-temperature (T_{surf}) comparisons for PMMA modeling using parameters estimated from different approaches – direct measurement, literature search, or approximation (A); measurement and numerical optimization (B-GA, B-SCE, B-SHC); mostly numerical optimization (C-GA, C-SCE, C-SHC) at applied heat flux of (a) 23 and (b) 64 kW/m^2. Note that data shown were not included in the model parameter estimation process; hence, these two cases are considered as extrapolation cases.

Figure A(D)-11. TGA thermograms of PMMA decomposition conducted under constant heating rates – 2, 5, 10 and 20K/min – and two different environments – (a) nitrogen and (b) air

Figure A(D)-12. TGA thermogram (TG and DTG) of corrugated cardboard decomposition conducted under 20K/min heating rate and nitrogen environment

Figure A(D)-13. Schematic of the FPA

Figure A(D)-14. FPA experiment results of corrugated cardboard with applied heat flux ranging from 20 to 110 kW/m^2: (a) mass-loss rate and (b) surface-temperature measurements using pyrometer

Figure A(D)-15. TG/DTG curves at 10°C/min heating rate with different estimation results for kinetic parameters for thermal decomposition of corrugated cardboard: For better comparison, TG and DTG thermograms have been scaled to result in 100% conversion.

Figure A(D)-16. Mass-loss rate (MLR) comparisons for corrugated cardboard between actual MLR from experiment (data) and modeled MLR (B-GA, B-SCE, B-SHC, C-GA, C-SCE, C-SHC) at applied heat flux of 60 kW/m^2. Note that data shown were used to estimate model parameter values via numerical optimization using GA, SCE or SHC routines.

Figure A(D)-17. Surface-temperature (T_{surf}) comparisons for corrugated cardboard between actual T_{surf} from experiment (data) and modeled T_{surf} (B-GA, B-SCE, B-SHC, C-GA, C-SCE, C-SHC) at applied heat flux of 60 kW/m^2. Note that data shown were used to estimate model parameter values via numerical optimization using GA, SCE or SHC routines.

Figure A(D)-18. Mass-loss rate (MLR) comparisons for corrugated cardboard between actual MLR from experiment (data) and modeled MLR (B-GA, B-SCE, B-SHC, C-GA, C-SCE, C-SHC) at applied heat flux of (a) 20 and (b) 110 kW/m^2. Note that data shown were not included in the model parameter estimation process; hence, these two cases are considered as extrapolation cases.

Figure A(D)-19. Surface-temperature (T_{surf}) comparisons for corrugated cardboard between actual T_{surf} from experiment (data) and modeled T_{surf} (B-GA, B-SCE, B-SHC, C-GA, C-SCE, C-SHC) at applied heat flux of (a) 20 and (b) 110 kW/m^2. Note that data shown were not included in the model parameter estimation process; hence, these two cases are considered as extrapolation cases.

Figure A(D)-20. TGA thermograms of corrugated cardboard decomposition conducted under constant heating rate of 20 °C/min and two different environments –nitrogen and air

Figure A(D)-21. Cross-section of FRP composite with modified-acrylic resin with high-charring inorganic additive

Figure A(D)-22. TGA (a) and DSC (b) thermograms of decomposition of modified-acrylic resin with high-charring additive conducted under 20K/min heating rate and nitrogen environment

Figure A(D)-23. Estimated activation energy, Ea, with respect to conversion (1-α) based on Iso-conversional Method for decomposition of modified-acrylic resin with (a) and without (b) inorganic high-charring additive

Figure A(D)-24. Comparison of TGA experiment data (TG and DTG) at 20°C/min under nitrogen atmosphere with kinetic modeling results based on Model-fitting Method for modified-acrylic resin with inorganic high-charring additive

Figure A(D)-25. Simplified representation of a cone calorimeter test of FRP composite

Figure A(D)-26. Heat flux measured during cone calorimeter test of modified-acrylic resin with high-charring additive (MA+A) FRP composite at external heat flux level of 50kW/m^2: Ignition occurs near τ = 3 s/mm^2 and from this point additional heat flux impinges on the surface due to the flame

Figure A(D)-27. Cone calorimeter experiment results of modified-acrylic resin with high-charring additive (MA+A) FRP composite with applied heat flux ranging from 25 to 75 kW/m^2: (a) Mass-loss rate and (b) surface-temperature and (c) back-surface-temperature measurements

Figure A(D)-28. Increase in model output fitness to targets – mass-loss rate, cumulative mass loss, surface and back-surface temperatures – from genetic algorithm (GA) optimization for estimating unknown parameters from simulating pyrolysis of modified-acrylic resin with high-charring additive (MA+A) FRP composite

Figure A(D)-29. Sensitivity coefficient (SC) for 21 parameters included in sensitivity analysis

Figure A(D)-30. TG/DTG curves at 10°C/min Heating rate with different estimation results for kinetic parameters for thermal decomposition of fire-retarded FRP composite: testing of resin with additive sample (~10mg) with nitrogen purge

Figure A(D)-31. Mass-loss rate (MLR) comparisons for FRP composite with modified-acrylic resin with high-charring inorganic additive between actual MLR from experiment (data) and modeled MLR (GA, SCE, SHC) at applied heat flux of 50 kW/m^2. Note that data shown were used to estimate model parameter values via numerical optimization using GA, SCE or SHC routines.

Figure A(D)-32. Surface-temperature (T_{surf}) comparisons for FRP composite with modified-acrylic resin with high-charring inorganic additive between actual T_{surf} from experiment (data) and modeled T_{surf} (GA, SCE, SHC) at applied heat flux of 50 kW/m^2. Note that data shown were used to estimate model parameter values via numerical optimization using GA, SCE or SHC routines.

Figure A(D)-33. Mass-loss rate (MLR) comparisons for FRP composite with modified-acrylic resin with high-charring inorganic additive between actual MLR from experiment (data) and modeled MLR (GA, SCE, SHC) at applied heat flux of (a) 25 and (b) 75 kW/m^2. Note that data shown were not included in the model parameter estimation process; hence, these two cases are considered as extrapolation cases.

Figure A(D)-34. Surface-temperature (T_{surf}) comparisons for FRP composite with modified-acrylic resin with high-charring inorganic additive between actual T_{surf} from experiment (data) and modeled T_{surf} (GA, SCE, SHC) at applied heat flux of (a) 25 and (b) 75 kW/m^2. Note that data shown were not included in the model parameter estimation process; hence, these two cases are considered as extrapolation cases.

Figure A(D)-35. Simplified representation of a cone calorimeter test of plywood

Figure A(D)-36. Total heat flux measured from plywood surface during cone calorimeter test at external heat flux level of 50kW/m^2: Ignition occurs before τ = 1 s/mm^2 and from this point additional heat flux impinges on the surface due to the flame

Figure A(D)-37. Cone calorimeter (cone) test data of plywood (thickness, δ is 11.1 ± 0.1 mm, density, ρ is 540 ± 10 kg/m^3) impinged with effective heat fluxes (EHF) of 25 to 75 kW/m^2

Figure A(D)-38. TG/DTG curves at 20°C/min heating rate with different estimation results for kinetic parameters for thermal decomposition of plywood: testing of plywood sample (~10mg) with air purge.

Figure A(D)-39. Mass-loss rate (MLR) comparisons for FRP composite with plywood between actual MLR from experiment (data) and modeled MLR (M&M) at applied heat flux of 50 kW/m^2. Note that data shown were used to estimate model parameter values via manual optimization.

Figure A(D)-40. Surface-temperature (T_{surf}) comparisons for plywood between actual T_{surf} from experiment (data) and modeled T_{surf} (M&M) at applied heat flux of 50 kW/m^2. Note that data shown were used to estimate model parameter values via manual optimization.

Figure A(D)-41. Back-surface-temperature (T_{back}) comparisons for plywood between actual T_{back} from experiment (data) and modeled T_{back} (M&M) at Applied heat flux of 50 kW/m^2. Note that data shown were used to estimate model parameter values via manual optimization.

Figure A(D)-42. Mass-loss rate (MLR) comparisons for FRP composite with plywood between actual MLR from experiment (data) and modeled MLR (M&M) at applied heat flux of (a) 25 and (b) 75 kW/m^2. Note that data shown were not included in the model parameter estimation process; hence, these two cases are considered as extrapolation cases.

Figure A(D)-43. Surface-temperature (T_{surf}) comparisons for FRP composite with plywood between actual T_{surf} from experiment (data) and modeled T_{surf} (M&M) at applied heat flux of (a) 25 and (b) 75 kW/m^2. Note that data shown were not included in the model parameter estimation process; hence, these two cases are considered as extrapolation cases.

Figure A(D)-44. Back-surface-temperature (T_{back}) comparisons for plywood between actual T_{back} from experiment (data) and modeled T_{back} (M&M) at applied heat flux of (a) 25 and (b) 75 kW/m^2. Note that data shown were not included in the model parameter estimation process; hence, these two cases are considered as extrapolation cases.